UNIVERSITY OF
KWAZULU-NATAL

ADSORPTION STUDIES FOR THE SEPARATION OF LIGHT HYDROCARBONS

Mr. Inbanathan Govender

BSc.Eng (UKZN)

Supervisor: Prof. Deresh Ramjugernath

Co-supervisors: Dr. Paramespri Naidoo and Dr. Wayne M. Nelson

Submitted in fulfilment of the academic requirements for the degree of Masters in Chemical Engineering at the University of KwaZulu-Natal.

Durban 2014

Declaration

I, Inbanathan Govender, declare that:

(i) The research reported in this dissertation, except where otherwise indicated, is my original work.

(ii) This dissertation has not been submitted for any degree or examination at any other university.

(iii) This dissertation does not contain other persons' data, pictures, graphs or other information, unless specifically acknowledged as being sourced from other persons.

(iv) This dissertation does not contain other persons' writing, unless specifically acknowledged as being sourced from other researchers. Where other written sources have been quoted, then:

a. Their words have been re-written but the general information attributed to them has been referenced;

b. Where their exact words have been used, their writing has been placed inside quotation marks, and referenced.

(v) This dissertation does not contain text, graphics or tables copied and pasted from the internet, unless specifically acknowledged, and the source being detailed in the dissertation and in the references sections.

Inbanathan Govender (Candidate) Date

As a supervisor of this candidate, I approve this dissertation for submission

Prof. Deresh Ramjugernath Date

Dr Paramespri Naidoo Date

Dr Wayne M. Nelson Date

Acknowledgements

In the compilation of this work, I have received considerable assistance from many sources. My deepest gratitude must be extended to the following people/organizations:

- My supervisors, Professor Deresh Ramjugernath, Dr Paramespri Naidoo and Dr Wayne Nelson for their invaluable guidance, assistance and wisdom.

- SASOL Ltd. for their financial assistance.

- The technical staff, Mr Leon Augustyn, Mr Ayanda Khanyile and Mr Lindinkosi Mkhize for their invaluable contribution to fabricating, commissioning and maintaining the experimental apparatus.

- Mr Matthew Lasich for assistance with the modelling aspects of this study.

- Dr Khalid Osman for assistance with the gravimetric measurements.

- My dad, Moses, my mum, Angie, my brother, Whomendren and my sister, Kobeshee for their many years of wholehearted support, encouragement and motivation.

- My extended family, friends and colleagues at the Thermodynamics Research Unit for their invaluable advice, support and friendship.

Abstract

Traditionally, the separation of ethylene from ethane is undertaken using a fractionation sequence. The distillation is performed at low temperatures and elevated pressures in conventional trayed fractionators. For economic feasibility, the separation scheme must be heat integrated to produce the low temperatures needed for separation – as low as 243 K. Low temperature distillation units are expensive to build and are typically only economically feasible for feed streams containing high amounts of ethylene.

Adsorption provides a favourable alternative to the traditional low temperature distillation process. The availability of accurately measured adsorption data over a wide range of temperatures and pressures is vital in the design of efficient separation processes. However, reproducible binary adsorption data are not readily available in the literature due largely to the uncertainties involved in measuring adsorption equilibria.

This project involved the measurement of adsorption equilibria using two techniques – the gravimetric and the volumetric technique. Particular focus was placed on the design and commissioning of a volumetric apparatus capable of measuring binary adsorption equilibria over a range of temperatures and pressures. The gravimetric apparatus is not capable of measuring multicomponent adsorption equilibria. The Thermodynamic Research Unit (TRU) has extensive capabilities in the field of phase equilibria with specialized expertise in the field of vapour liquid equilibria (VLE). The objective of this project is to develop competence in the field of adsorption equilibria by designing and commissioning new apparatus. This forms part of a larger objective to extend the capabilities of TRU. The volumetric apparatus designed and commissioned in this study uses an innovative gas mixer to prepare binary mixtures for adsorption equilibrium measurements.

The measured data were compared to literature to validate the measurement reproducibility of the apparatus and accuracy of measurement techniques used. Adsorption equilibrium data were measured for pure components and a binary system. Pure component adsorption data were measured for methane, ethane and ethylene. The binary system of ethane + ethylene was also investigated. Measurements were performed at pressures up to 15 bar, at temperatures of 298 K and 323 K, on an adsorbent zeolite 13X. The gravimetric and volumetric apparatus both showed good reliability and reproducibility. Uncertainties in temperature and pressure were 0.1 K and 4×10^{-3} bar for the gravimetric apparatus and 0.03 K and 0.002 bar for the volumetric apparatus respectively.

The measured equilibrium data were fitted to the Langmuir, Sips and Vacancy Solution Model (VSM) adsorption models. The regressed parameters were used to predict binary adsorption equilibria. The Langmuir model performed the poorest across the pressure range investigated, with an average absolute deviation (AAD) as high as 5%. The deviation however, was comparable with the experimental uncertainties reported in literature. The Sips model improved upon the Langmuir model with the VSM model generally performing the best with an AAD of approximately 1%. The Extended Langmuir, Extended Sips and VSM all provided good predictions of the binary adsorption equilibria. The Extended Langmuir model performed best with an AAD of 3%. The Extended Sips model performed marginally poorer with an AAD of 3.05%. The VSM model performed satisfactorily with an AAD of 6%, marginally higher than the reported experimental uncertainties of 5%.

Contents

List of Figures

List of Tables

Nomenclature

Symbol	Description	Default unit
a	Activity	-
A	Surface area	m^2
b	Langmuir constant	bar^{-1}
b_1	VSM parameter	bar^{-1}
c	Freundlich constant	dimensionless
G	Gibbs free energy	kJ/mol
H	Molar enthalpy	kJ/mol
h	Planks Constant	$m^2.kg/s$
k	Boltzman constant	$m^2.kg/s^2.K$
K'	Adsorption equilibrium constant	mol/g.bar
m	Mass	g
M	Molar mass	g/mol
N_0	Avogadro number	
P	Pressure	bar
P_0	Saturated vapour pressure	bar
q	Amount adsorbed	mol/g
Q	Heat of adsorption	kJ/mol
R	Universal gas constant	L.bar/mol.K
S	Molar entropy	kJ/mol.K
T	Temperature	K
V	Volume	L
V_m	Molar volume	L/mol
W	Volume of the adsorbed space	cm^3
W_0	Micropore volume	cm^3
x	Mole fraction in the adsorbate phase	-
Y	GC calibration factor	mol/μV
y	Mole fraction in the gas phase	-
α	Selectivity/separation factor	-
γ	Activity coefficient	-
δ	Area occupied by each adsorbate molecule	Å
Δ	Change in property	
δ	Standard deviation	Same unit as the data
ΔH_0	Limiting heat of adsorption	kJ/mol
ΔH_s	Isoteric heat of adsorption	kJ/mol
θ	Fractional coverage of adsorbent	-
Λ_{1v}, Λ_{v1}	VSM parameters	-
μ	Chemical potential	kJ/mol
ν	Collision frequency of gas molecules striking the surface	Collisions/s
ζ	Sticking probability	-
Ξ	Partition function	-
π	Spreading pressure	bar/m^2

ρ	Density	g/L
ϕ	Fugacity coefficient	bar/bar
ε	Potential	kJ/mol

List of Abbreviations

APTI	Air Pollution Training Institute
BCE	Before Common Era
BDDT	Brunauer, Deming and Teller
BET	Brunauer, Emmett and Teller
DR	Dubinin-Radushkevich
EoS	Equation of State
GC	Gas Chromatograph
GCMC	Grand Canonical Monte Carlo Simulation
IAST	Ideal Adsorbed Solution Model
IUPAC	International Union of Pure and Applied Chemistry
LPG	Low Pressure Gas
LSM	Lattice Solution Model
MS	Mass Spectrometer
MSB	Magnetic Suspension Balance
PSA	Pressure Swing Adsorption
PVT	Pressure, Volume and Temperature
SSTM	Simplified Statistical Thermodynamic Model
TCD	Thermal Conductivity Detector
TRU	Thermodynamics Research Unit
TSA	Temperature Swing Adsorption
UKZN	University of KwaZulu-Natal
USA	United States of America
VOC	Volatile Organic Compound
VSM	Vacancy Solution Model
IGA	Intelligent Gravimetric Analyser

1

Chapter 1: Introduction

Adsorption is a process that occurs when a gas or liquid solute accumulates on the surface of a solid (Seader and Henley, 2006). The application of adsorption and adsorption processes is documented to have begun when the Egyptians and Sumerians used charcoal (carbon) in the reduction of ores to produce bronze. The study of adsorption phenomena however, only began towards the end of the 18th century when Swedish chemist, Carl Wilhelm Scheele measured the volumes of various gases that could be adsorbed on carbon.

The last few decades have seen a number of strides made in the field of adsorption. Today, adsorption is an established industrial separation process – albeit less established than distillation. Advances have been made in developing efficient technology to effect separations while significant progress has been made in developing highly selective adsorbents (Crittenden and Thomas, 1998; Dabrowski, 2001, Rezaei and Webley, 2010). A review of commercial adsorbents is provided in Appendix A. An overview of the development of adsorption and adsorption processes is presented in Appendix B.

Industrial adsorption processes can be broadly classified into two classes – Pressure Swing Adsorption (PSA) and Temperature Swing Adsorption (TSA). The criterion for classification is the manner in which the adsorbent is regenerated. In PSA the regeneration is driven by a drop in the pressure of the adsorber. In TSA an increase in temperature drives the regeneration. TSA grew prominent toward the end of the first quarter of the 20th century; however, since then, developments in adsorbents have propelled PSA to the forefront of adsorption technology (Ruthven, 1984).

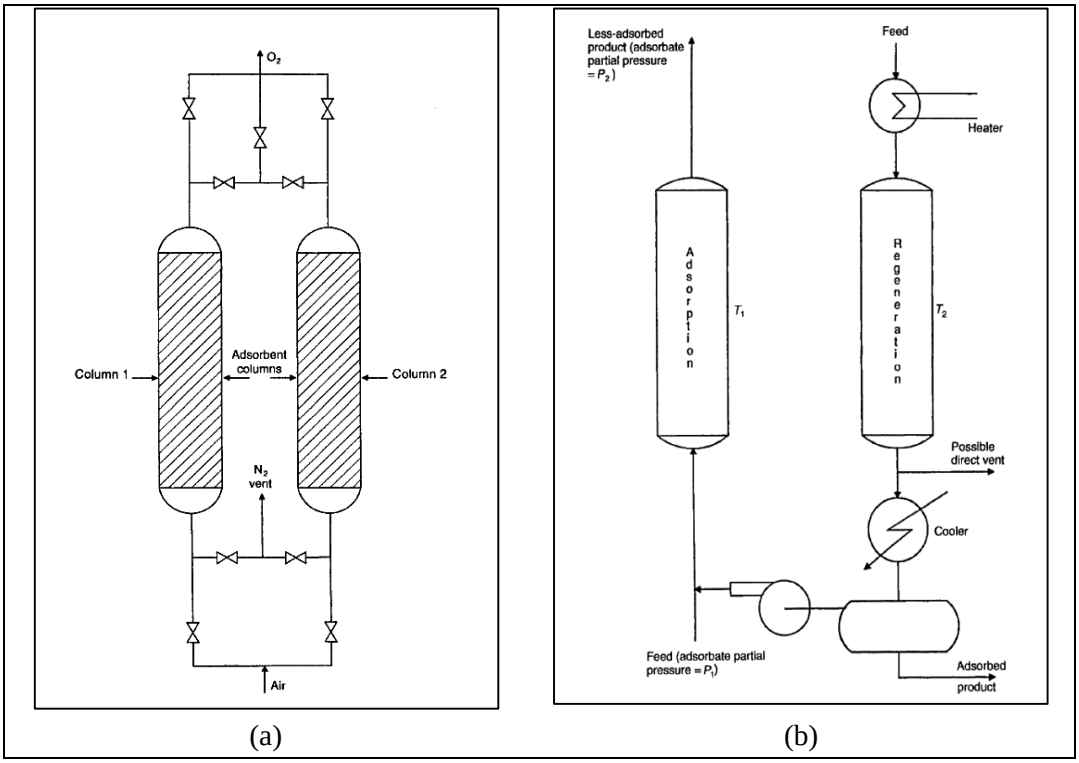

Figure 1 - 1: Basic PSA (a) and TSA (b) separation processes (Ruthven, 1984; Crittenden and Thomas, 1998).

A basic PSA process uses two beds that operate 180° out of phase with each other. The process is carried out in four steps. In the example in Figure 1 - 1, air is separated into nitrogen and oxygen. In the first step, column 1 is pressurized using the feed or product. In the second step, adsorption is undertaken in the pressurized bed (column 1). In the last two steps, the bed undergoes counter-current depressurisation and is then purged with a fraction of the product. Whilst column 1 is undergoing depressurisation, column 2 is pressurised using the produced oxygen or the air feed and then used to undertake adsorption. In this way, the PSA process allows for fast separation to be achieved with a total cycle amounting to a few minutes or even seconds (Ruthven, 1984; Crittenden and Thomas, 1998).

A basic TSA process consists of four steps as well. However, in TSA, simply increasing the temperature is not enough to regenerate the adsorbent (unlike PSA where a drop in pressure is sufficient). In the first step, adsorption onto the regenerated solid is undertaken at T_1. In the second step the temperature of the bed is increased to T_2 by passing hot feed or steam through it. The third step may be combined with the second. In this step the adsorbent is regenerated at T_2 using a purge fluid. In the final step, the bed is cooled to T_1 using cold feed or a purge fluid (Crittenden and Thomas, 1998).

Adsorption offers a number of advantages and is applicable to a wide range of separation requirements. The technique offers high selectivity, high (adsorbent) capacity as well as the ability to separate components at low partial pressures. Adsorption may be used as a bulk separation process or for purification, depending on feed concentrations (Ruthven, 2004; Seader and Henley, 2006). A brief outline of some applications is presented in Table 1 - 1.

Table 1 - 1: Applications of adsorption processes. Typical adsorbents for each of the processes are listed (Dabrowski, 2001).

Separation	Adsorbent used
Gas bulk separations	
n-paraffins from iso-paraffins, aromatics, olefins	Zeolites
N_2 from air	Zeolites
O_2 from air	Carbon molecular sieve
H_2 from CO, CH_4 , CO_2 , N_2 , NH_3	Zeolites, activated carbons
Acetone from vent streams	Activated carbon
C_2H_4 from vent streams	Activated carbon
Gas purification	
H_2O from olefin-containing cracked gas, natural gas, Silica, alumina, air, synthesis gas	Zeolites
CO_2 from C_2H_4 , natural gas	Zeolites
Organics from vent streams	Activated carbon
Sulphur compounds from natural gas, hydrogen, liquefied petroleum gas	Zeolites
Solvents from air	Activated carbon, zeolites
Odours from air	Activated carbon
NO_x from N_2	Zeolites, carbons
SO_2 from vent streams	Zeolites, carbons

Adsorption provides an attractive alternative to other separation techniques; in particular, adsorption is ever increasing in its competitiveness with distillation. In chemical systems comprising close boiling components, separation using distillation may be very difficult, and costly, to achieve. The developments made in adsorption technology and adsorbent science have made such separations not only possible, but economical as well (Ruthven, 1984; Yang, 1987, Bao et al., 2011). The attractiveness of adsorption is fuelled further by the increasing cost of energy and tighter emission control legislation.

Fundamental to the design of adsorption processes is the measurement of adsorption equilibria. These measurements are typically undertaken isothermally and are referred to as *adsorption isotherms*. An adsorption isotherm is the equilibrium relationship between the amount of fluid adsorbed and the pressure or concentration in the bulk fluid phase (Dabrowski, 2001). A major stumbling block in the development of adsorption technology has been the complexity of adsorption phenomena (Danner and Choi, 1978). In practice, adsorption processes involve mixture adsorption (coadsorption) over a range of pressures and temperatures with varying concentrations. However, pure component adsorption data is readily available (Reich et al., 1980). Predictions based on pure component isotherms are often unreliable and only seem applicable to mixtures of nearly identical molecules e.g. n/iso-paraffins (Keller et al., 1999).

This study investigated the use of adsorption techniques in the separation of the ethane/ethylene system. Olefin/paraffin separations are one the most important processes in the chemical and petrochemical industries. High purity ethylene is required for the production of plastics, rubbers and films. Ethylene is typically produced by steam cracking ethane, resulting in a product stream

containing un-cracked ethane. A means to separate the ethane/ethylene mixture is investigated in this study.

Selection of the proper adsorbent with adequate capacity and high selectivity is an important step in the design of an adsorption process. A number of adsorbents have been evaluated for their applicability to olefin/paraffin separations. The majority of these studies however, have focused on the measurement of pure component isotherms. Among the adsorbents investigated, zeolites 5A and 13X along with activated carbons have been shown to be the most effective.

Mofarahi and Salehi (2013) performed binary measurements for the adsorption of ethane and ethylene on zeolite 5A at temperatures between 283 K and 325 K, at pressures up to 9.5 bar. The equilibrium gas composition, however, was not measured but rather calculated using an EoS. Pakseresht et al. (2002) and Nam et al. (2005) investigated the use of the same adsorbent for the adsorption of methane, ethane and ethylene at temperatures between 293 K and 313 K, and at pressures up to 20 bar.

A number of studies have investigated the use of zeolite 13X for the separation of the propane/propylene system. The adsorbent has proven to be an effective adsorbent in this regard (Bao et al., 2011). Studies have also investigated the use of zeolite 13X for the separation of the ethane/ethylene system – the system investigated in this study. A review of the literature for this system is presented in Table 3 - 1. Activated carbon has also been investigated as a suitable adsorbent for the separation of light hydrocarbons. A select review of the literature is presented in Table 3 - 1. Studies into the use of silica, zeolite 4A and Metal Organic Frameworks (MOF) as a suitable adsorbent for the separation of these systems have shown promising results (Abdul-Rehman et al., 1990; Yun et al., 2002; Romero-Pérez et al., 2010; Bao et al., 2011).

Various experimental techniques have been proposed for the measurement of adsorption isotherms. Keller et al. (1999) reviewed the more prominent techniques. Measurement of coadsorption isotherms is often tedious and time consuming. This has resulted in a gap in the literature with binary equilibria not featuring as prominently as pure component equilibria.

The overall aim of the project was to develop competence in the area of gas adsorption in the Thermodynamics Research Unit (TRU) at UKZN. This project ambitiously involved the design, construction and commissioning of a new experimental apparatus capable of performing adsorption measurements for both pure components and gas mixtures using a volumetric technique. The TRU recently procured an Intelligent Gravimetric Analyser (IGA) (Osman, 2014). The IGA uses a gravimetric technique, and is capable of measuring adsorption data with high accuracy from vacuum to high pressures. Unfortunately, the IGA-001 is limited to measurement of pure gases only. The pure component volumetric measurements, undertaken using the developed volumetric apparatus, were compared to the gravimetric measurements, undertaken using the IGA, to investigate the effects of adsorbent sample size and adsorption cell volume on adsorption capacity.

2

Chapter 2: Adsorption Equilibria Fundamentals

Adsorption is an exothermic process that occurs when a gas or liquid accumulates on the surface of a solid. Gas-solid adsorption occurs as a result of a concentration difference between the bulk gas phase and the gas near the adsorbent. The process is driven by the difference between gas-gas intermolecular interactions in the bulk phase and gas-solid intermolecular interactions near the solid surface (Mersmann, 2003).

2.1. Adsorption Steps

Adsorption is a three step process shown in Figure 2 - 1. The first step involves the transfer of gas molecules from the bulk phase to the surface of the adsorbent. In the second step the gas molecules diffuse into the macropores, mesopores and micropores of the adsorbent. In the third step, the gas molecules adsorb to the surface in the pore. The gas molecules are held on the surface by attractive forces creating a layer. In binary adsorption, the composition of this layer is determined by the affinity of the components for the adsorbent (Von and Sherman, 2004).

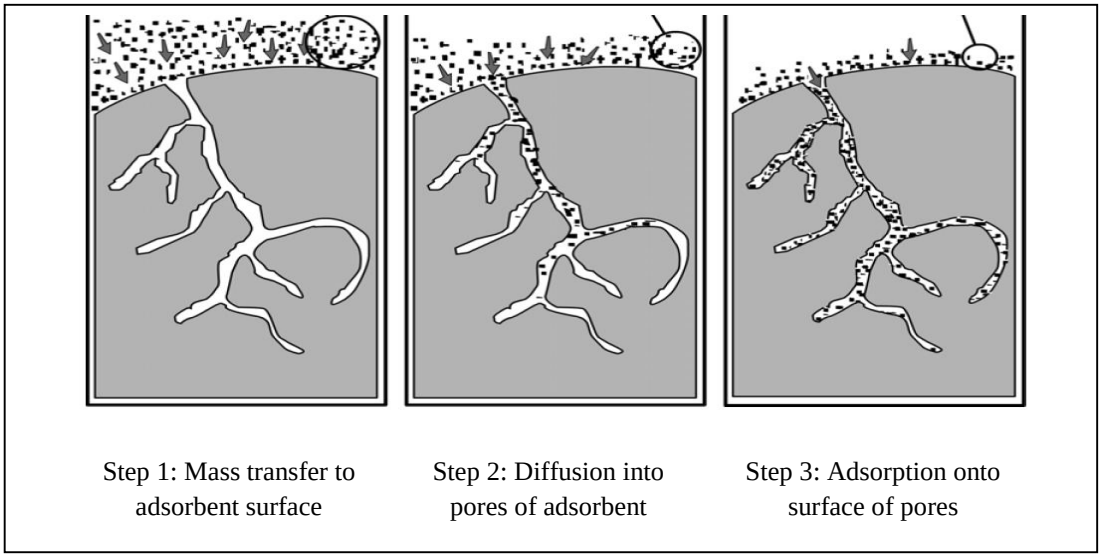

Figure 2 - 1: Adsorption steps (APTI, 1999).

Adsorbents are highly porous materials. Some adsorbents may have a specific area of up to 1300 m^2/g. According to the International Union of Pure and Applied Chemistry (IUPAC), the pores are classified according to diameter, *d* as: macropores ($d > 500$ Å), mesopores (20 Å $< d < 500$ Å) and micropores ($d < 20$ Å) (Yang, 1987). Most of the adsorption occurs in the micropores as it accounts for a large percentage of the available surface area (ATPI, 1999).

2.2. Forces of Adsorption

The phenomenon of adsorption is broadly classified into two types: physical adsorption termed *physisorption*, and chemical adsorption termed *chemisorption*. The classification is based on the strength with which the gas molecules bond to the adsorbent (Yang, 1987).

Physisorption is characterised by van der Waals and electrostatic interactions between the gas molecules and the solid surface. The van der Waals contribution is always present while the electrostatic contributions are significant only when an adsorbent with an ionic structure, such as zeolites, is used. These forces are much weaker than those prevalent in chemisorption, thus making physisorption reversible and an attractive separation technique (Ruthven, 1984).

Physisorption can occur in three ways: orientation, dispersion or induction. In polar molecules, the attraction is caused by the orientation effect. The negative charge of one molecule is attracted to the positive charge of another. In non-polar molecules, adsorption occurs due to the dispersion effect which is caused by fluctuating dipoles that are a result of momentary changes in electron distribution. The attraction between a polar molecule and a non-polar molecule is caused by the induction effect. A molecule with a permanent dipole induces a polarity into a non-polar molecule when they come into close contact (APTI, 1999).

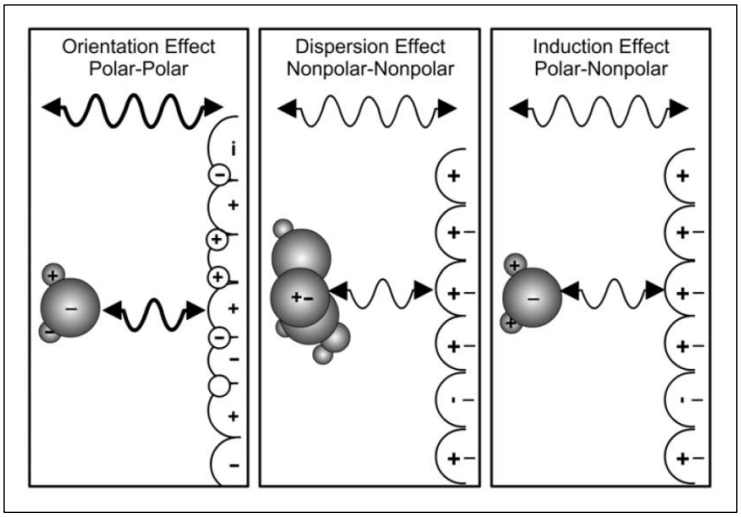

Figure 2 - 2: Physical forces causing adsorption (APTI, 1999).

Chemisorption is characterised by the occurrence of a chemical reaction between the fluid and the adsorbent. As mentioned, all adsorption processes are exothermic, liberating heat (heat of adsorption). The heat of adsorption in a chemisorption process is typically orders of magnitude greater than the heat of adsorption prevalent in physisorption. Molecules chemisorbed are very difficult, and in cases, impossible to remove from the adsorbent. Unlike in physisorption, in chemisorption multiple layers of adsorbate cannot be formed on the adsorbent surface. Instead, a monolayer forms on the adsorbent. Chemisorption is a highly selective process; physisorption is a more general phenomenon. In separation processes, physisorption is preferred (ATPI, 1999).

2.3. Selectivity

For an economic separation process, an adsorbent with high selectivity, capacity and longevity is required. The selectivity may depend on differences in either equilibrium or kinetics, but most adsorption processes in industry depend on equilibrium selectivity. A separation factor, α_{ij} is thus defined for a binary system:

$$\alpha_{12} = \frac{x_1/x_2}{y_1/y_2} \qquad (2 - 1)$$

where *1* and *2* refer to the two components separated with *x* representing the adsorbate phase composition and *y* the adsorptive (bulk gas) phase composition. The separation factor is analogous to the relative volatility encountered in distillation. A degree of control over the selectivity of the adsorbent may be achieved. Control of the equilibrium selectivity is achieved by changing the chemical nature of the surface of the adsorbent and by adjusting the pore size.

2.4. Thermodynamics of Adsorption

Ruthven (1984) performed a rigorous treatment of the thermodynamics of adsorption equilibria. An extensive thermodynamic analysis is required as a precursor to the development of adsorption models. Models based on a thermodynamic approach are presented in the next chapter.

A general assumption is made when a thermodynamic approach to adsorption equilibria is taken. It is assumed that the adsorbed layer can be treated as a distinguishable phase (Ruthven, 1984). The adsorbate phase may be defined in two ways. In the first case, the solid adsorbent and the adsorbed gas molecules are viewed as a single phase. This approach is often taken when modelling chemisorption. The alternate case, taken when modelling physisorption, considers the adsorbent to be chemically inert. The thermodynamic and geometric properties of the adsorbent are considered independent of temperature, pressure and composition of the gas. In this case, the adsorbed gas molecules are treated as a distinct phase. A detailed derivation of the applicable thermodynamic relationships is presented in Appendix C. The pertinent relations applicable to gas-solid adsorption are presented in this Chapter.

2.4.1. Criterion for Equilibrium

The condition for equilibrium- using chemical potential μ- may be written as follows:

$$\mu_s = \mu_g \qquad (2 - 2)$$

Subscripts *s* and *g* represent the adsorbed phased and gas phase respectively. The relation is still applicable when adsorption occurs from the liquid phase as the chemical potential at equilibrium in all three phases must be equal.

2.4.2. Isoteric Heat of Adsorption

The isoteric heat of adsorption is the term given to the change of enthalpy that occurs when adsorption takes place. By definition it is the difference in enthalpy between the adsorptive and adsorbed phase. Gas-solid adsorption is an exothermic process. If there is negligible difference in the heat capacity of the gas in the adsorptive and adsorbed phases, the isoteric heat of adsorption ΔH_s is given by:

$$ln\,P = constant - \frac{\Delta H_s}{RT} \qquad (2 - 3)$$

The isoteric heat of adsorption is determined by generating a plot of ln P vs. 1/T with the slope providing the required property, only valid for constant ΔHs within a selected temperature range. This is analogous to the Clausius-Clapeyron equation used to determine heat of vapourization..

2.4.3. Partial Molar Entropy

The partial molar entropy of the adsorbed phase, $\overline{S_s}$ is determined from the isoteric heat of adsorption, pressure and temperature measurements:

$$\overline{S_s} = S_g^0 + \frac{\overline{H_s} - H_g}{T} - R\,ln\frac{P}{P^0} \qquad (2 - 4)$$

where S_g^0 is the molar entropy of the vapour in the standard state at pressure P^0 and H represents the enthalpy.

2.4.4. Adsorption Equilibrium Constant

It is often convenient to define an adsorption equilibrium constant when measuring adsorption equilibria. The full derivation is provided in Appendix C. The resulting thermodynamic relationship relating the chemical potential, μ and equilibrium constant, K is presented as:

$$\mu_s - \mu_g^0 = RT\,ln\,K \qquad (2 - 5)$$

where $\mu^0{}_g$ is the chemical potential at reference pressure P^0

If the standard state is chosen as an infinitely dilute ideal adsorbed phase, Eq. (2 - 5) simply reduces to Henry's Law in the low coverage limit.

$$\lim_{P\to 0}\frac{q}{P} = \frac{K a_s^0}{P^0} \equiv K' \qquad (2 - 6)$$

The temperature dependence of the Henry's constant, K' follows the van't Hoff equation:

$$\lim_{P\to 0}\frac{q}{P} = K_0' e^{\frac{-\Delta H_0}{RT}} \qquad (2 - 7)$$

where $(-\Delta H_0)$ is the limiting heat of adsorption at zero coverage. $(-\Delta H_0)$ is a positive quantity, *K'* therefore reduces with an increase in temperature. This is true because the Gibbs free energy of the system, *G* must decrease for adsorption to occur. From the relation for *G*:

$$\Delta G = \Delta H - T\Delta S \qquad (2 - 8)$$

The entropy change of the system at equilibrium, ΔS is negative due to the decrease in degrees of freedom. From Eq. (2 - 8) it follows that ΔH must also be negative. The quantity $(-\Delta H_0)$ is thus positive.

The simplest model for describing adsorption equilibria, Henry's Law follows directly from the derivations made in this chapter and Appendix C and is written as follows:

$$q = K'P \qquad (2 - 9)$$

3

Chapter 3: Analysis, Modelling and Prediction of Adsorption Equilibria

Most adsorption problems in practice involve the separation of mixtures over a range of temperatures and pressures. To solve these problems, the engineer requires multi-component adsorption equilibrium data (Reich et al., 1980). Often, however, only pure component adsorption data over a limited range of pressures and temperatures is available in the literature. This is due largely to the relative ease with which pure component data is measured. It is therefore desirable to predict adsorption equilibria using the limited data from literature. In the case of pure component modelling, the range of data is extended and intermediate points are determined. In the case of multi-component adsorption equilibria, models are used to predict the behaviour using pure component isotherms.

3.1. Pure Gas Isotherms

Much of the published work on adsorption equilibria reports pure component adsorption equilibria. For pure components, adsorption isotherms have been classified into five shapes as discussed by Brunauer and co-workers (Yang, 1987).

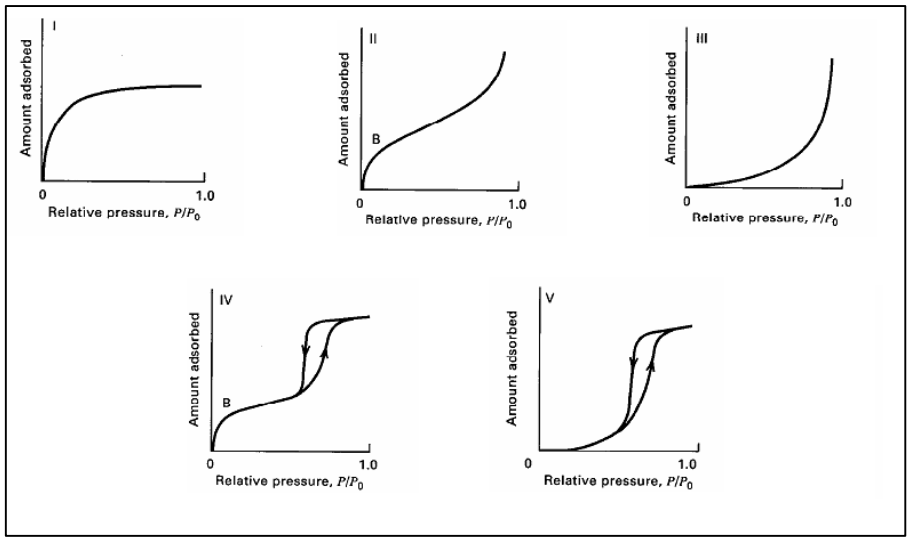

Figure 3 - 1: The five types of adsorption isotherms according to the Brunauer, Demmin and Teller (BDDT) classification (Yang, 1987).

Type I isotherms are the simplest and most common and corresponds to unimolecular adsorption (Seader and Henley, 2006). In type I isotherms, adsorption is limited to the completion of a single layer of gas on the adsorbent. This type applies to gases above their critical temperature. Type I isotherms are observed for the adsorption of gases on microporous solids whose pore sizes are not much larger than the molecular diameter of the gas (Crittenden and Thomas, 1998).

Type II isotherms are associated with multi-molecular adsorption of the Brunauer, Emmett and Teller (BET) type for gases lower than their critical temperature and pressures lower than, but approaching saturation pressure. As the adsorbate approaches saturation pressure, the adsorbent displays a higher capacity for adsorption. Adsorbents with a wide pore size distribution form type II isotherms; condensation occurs within the larger pores. The point of inflection on the curve indicates the completion of a monolayer after which successive layers are adsorbed. The heat of adsorption for the first layer is greater than that for succeeding layers. Heat of adsorption for the succeeding layers is assumed to be equal to the heat of condensation (Crittenden and Thomas, 1998; Seader and Henley, 2006). Types I and II are desirable isotherms as they exhibit strong adsorption.

Type III isotherms show a steady increase in adsorption capacity as the pressure is increased. However, at low pressures, the extent of adsorption is too low, hence, type III isotherms are undesirable (Seader and Henley, 2006).

The equilibrium vapour pressure in a pore or capillary is reduced by the effect of surface tension. Hence, liquid adsorbate condenses at a vapour pressure lower than the saturated vapour pressure. This phenomenon is described as capillary condensation. Types IV and V are capillary condensation versions of types II and III respectively. Hysteresis is observed on the plot. The upward branch is due to simultaneous multimolecular adsorption and capillary condensation at higher pressures. The downward branch, at lower pressures, exhibits only capillary condensation. The capillary condensation region is undesired as the selectivity of the adsorbent is reduced, or even lost (Crittenden and Thomas, 1998; Mersmann, 2003; Seader and Henley, 2006).

There are 3 approaches to developing isotherm models for pure gas adsorption (Yang, 1987). The adsorption models presented in this chapter can all be derived using the thermodynamic approach discussed in Chapter 2; however the Langmuir-type models are derived from a kinetic approach offering the advantage of a more intuitive understanding of the model development. The more rigorous aspects of the thermodynamic derivations are discussed elsewhere (Ruthven, 1984).

1. *Langmuir Approach*: The Langmuir approach assumes the adsorption system is in dynamic equilibrium. The rate of evaporation (desorption) is equal to the rate of condensation (adsorption). To date, the Langmuir approach remains the most useful approach for data correlation (Ruthven, 1984).

2. *Gibbs Approach*: The Gibbs approach makes use of the Gibbs adsorption isotherm (Yang, 1987). The isotherm is derived using a classical thermodynamics approach:

$$-Ad\pi + nd\mu = 0 \qquad (3 - 1)$$

   where, A, π and μ represents the adsorbent surface area, the spreading pressure and the equilibrium chemical potential respectively. Eq. (3 - 1) is integrated to yield the desired adsorption isotherm.

3. *Potential Theory*: In potential theory the adsorption system is viewed as a gradual concentration of gas molecules toward the solid surface due to a potential field. A relation exists between the potential field, ε and the volume above the solid surface.

3.1.1. Langmuir Approach

3.1.1.1. Langmuir Model

The model describes adsorption equilibria well in the low to moderate coverage region and is popular when type I isotherms are to be modelled (Kaul, 1984). It is based on the following assumptions:

1. Molecules are adsorbed at a fixed number of localized sites.
2. Each site can hold only one molecule.
3. No interaction takes place between molecules adsorbed on neighbouring sites.
4. The energy of adsorption is constant over all sites, i.e. the surface is homogenous.

The Langmuir model is derived based on the concept of dynamic equilibrium between the rates of adsorption and desorption. The sites already occupied are not available for adsorption; hence the rate of adsorption per unit surface area is given by:

$$r_A = \xi \nu (1 - \theta) \qquad (3 - 2)$$

where r_A, ξ, ν, θ represent the rate of adsorption of the gas, the sticking probability of the gas, the collision frequency of the gas molecules striking the adsorbent surface and the fractional coverage respectively (Yang, 1987). The sticking probability is the probability that gas molecules are trapped on the surface of the adsorbent. The fractional coverage is given by:

$$\theta = \frac{q}{q^{\infty}} \qquad (3 - 3)$$

where q and q^{∞} is the amount of gas adsorbed and the saturation limit respectively. The fractional coverage is also defined as the number of sites occupied over the number of sites available for adsorption.

From the kinetic theory of gases, ν is given by (Yang, 1987):

$$\nu = \frac{P}{\sqrt{2\pi m k T}} \qquad (3 - 4)$$

The rate of desorption for a physisorbed species may be written:

$$r_D = k_D \theta \, exp\left(-E_d / RT\right) = k_D \theta \, exp\left(-Q / RT\right) \qquad (3 - 5)$$

where k_D and E_d are the desorption rate constant and the activation energy for desorption respectively (Yang, 1987).

At equilibrium, the rates of adsorption and desorption are equal, resulting in the Langmuir model (Yang, 1987):

$$\theta = \frac{q}{q^{\infty}} = \frac{bP}{1 + bP} \qquad (3 - 6)$$

Written with q as the subject:

$$q = \frac{bq^{\infty}P}{1 + bP} \qquad (3 - 7)$$

where (Yang, 1987):

$$b = \frac{\xi}{k_D\sqrt{2\pi mkT}} exp\left({}^{Q}/_{RT}\right) \qquad (3 - 8)$$

At low pressure, the Langmuir isotherm reduces to Henry's Law (Mersmann, 2003).

$$\theta = bP \qquad (3 - 9)$$

As is seen from Eq. (3 - 8), the value of b decreases as temperature increases, hence physical adsorption is an exothermic process.

3.1.1.2. Freundlich Model

For many systems, the heat of adsorption decreases with an increasing extent of adsorption. If this trend is logarithmic, it implies that adsorption sites are distributed exponentially. The Freundlich model is based on this assumption and is written as (Crittenden and Thomas, 1998; Mersmann, 2003):

$$q = kP^{c} \qquad (3 - 10)$$

When c = 1, Eq. (3 -10) reduces to Henry's Law. The parameter c is however, often less than 1. For very small values of c, the isotherm approaches a so called *rectangular isotherm*. For these isotherms, pressure or concentration must be reduced to extremely low values for adsorption to occur. The Freundlich model is often used to model adsorption of hydrocarbons on activated carbon (Duong, 1998).

3.1.1.3. Langmuir-Freundlich Model (Sips Model)

The Langmuir-Freundlich model was developed for the case of dissociative adsorption, i.e. each molecule occupies d sites (where d is the inverse of c). The resulting isotherm is a three parameter empirical model. It is superior for predicting adsorption over a wider range of temperature and pressure when the Langmuir and Freundlich models fail. The model has been shown to predict pure component adsorption equilibria of ethane, ethylene, propane and propylene on activated carbon well in the temperature range 310 K – 478 K. The isotherm is given by (Yang, 1987):

$$q = \frac{bq^{\infty}P^{c}}{1 + bP^{c}} \qquad (3 - 11)$$

The Freundlich model has a continuing increase in the amount adsorbed with increasing pressure. The Langmuir-Freundlich model improves upon this by providing a finite limit for the amount adsorbed at sufficiently high pressures. The parameter c also accounts for the heterogeneity in the system. A low magnitude in the c parameter indicates a more heterogeneous system.

3.1.2. Gibbs Approach

If the adsorbate is treated as a 2 dimensional microscopic entity, the fundamental equations in classical thermodynamics may be applied (Yang, 1987). Applying the Gibbs free energy equation to the surface of the adsorbate (Yang, 1987):

$$dG = -SdT + \mu dn + Ad\pi \qquad (3\text{ -}12)$$

The third term on the right hand side of Eq. (3 -12) is analogous to the traditional *PdV* term in the Gibbs free energy equation.

The Gibbs-Duhem relation is given by (Yang, 1987):

$$SdT - Ad\pi + nd\mu = 0 \qquad (3\text{ -}13)$$

For a constant temperature, Eq. (3 -13) becomes:

$$-Ad\pi + nd\mu = 0 \qquad (3\text{ -}14)$$

Assuming ideal gas behaviour, and equilibrium conditions, one obtains:

$$\left(\frac{d\pi}{d\ ln\ P}\right)_T = \frac{n}{A}RT \qquad (3\ 15)$$

Eq. (3 ***15)*** is used in conjunction with an EoS to obtain the isotherm model.

For adsorption on solid surfaces, the adsorbed species is treated as a 2D film governed by a 2D EoS relating *π-A-T*. However, *π* cannot be measured for an adsorbate on a solid surface and the EoS is assumed. The simplest model developed using the Gibbs approach is derived from the ideal gas law (Yang, 1987):

$$\pi\delta = RT \qquad (3\text{ -}16)$$

Combining Eqs. (3 ***15)*** and (3 -16) results in Henry's Law.

A later development of the Gibbs approach is the vacancy solution model. The model was developed to be applied readily to more than one adsorbate.

Vacancy Solution Model (VSM)

The surface of the adsorbent is considered to consist of a vacancy, *v* and an adsorbed species, *1*. The bulk vacancy solution is assumed to be very dilute.

The chemical potential for *v* in the adsorbed phase is given by (Yang, 1987):

$$\mu = \mu_0 + RT\ ln\ \gamma x + \pi\delta \qquad (3\text{ -}17)$$

In the gas phase, the last two terms of Eq. (3 -17) fall away. Equating the chemical potential of both phases:

$$\pi = -\frac{RT}{\delta_v} ln\, \gamma_v x_v \qquad (3\text{ -}18)$$

γ_v is determined using an activity coefficient model. Suwanayuen and Danner (1980) used the Wilson equation (Yang, 1987).

$$ln\, \gamma_v = -ln(x_v + \Lambda_{v1} x_1) - x_1 \left[\frac{\Lambda_{1v}}{x_1 + \Lambda_{1v} x_v} - \frac{\Lambda_{v1}}{x_v + \Lambda_{v1} x_1}\right] \qquad (3\text{ -}19)$$

Combining Eqs. (3 -18) and (3 -19), Eq. (3 15) is integrated to give the VSM Model

$$P = \left[\frac{q^{\infty}}{b_1}\frac{\theta}{1-\theta}\right]\left[\Lambda_{1v}\frac{1-(1-\Lambda_{v1})\theta}{\Lambda_{1v}+(1-\Lambda_{1v})\theta}\right] exp\left[-\frac{\Lambda_{v1}(1-\Lambda_{v1})\theta}{1-(1-\Lambda_{v1})\theta} - \frac{(1-\Lambda_{1v})\theta}{\Lambda_{1v}+(1-\Lambda_{1v})\theta}\right] \qquad (3\text{ -}20)$$

b_1 is defined such that it agrees with Henry's Law at low pressures (Yang, 1987).

$$b_1 = \lim_{P\to 0}\left(\frac{q}{P}\right) \qquad (3\text{ -}21)$$

If isothermal data are available, the four parameters that make up the model, Λ_{1v}, Λ_{v1}, q^{∞} and b_1 are determined using non-linear regression. The pairwise interaction constants Λ_{1v} and Λ_{v1} are highly correlated. The product ($\Lambda_{1v}\times\Lambda_{v1}$) is approximately equal to 1~1 (Duong, 1998).

3.1.3. Potential Theory

Models based on potential theory are typically used to model adsorption by capillary condensation. As such, it has been used to model adsorption on activated carbon and zeolites (Yang, 1987). The adsorption mechanism present in these microporous adsorbents is termed micropore filling (Yang, 1987). In these solids, the proximity of the micropore walls to each other provides an enhanced adsorption potential within the micropores. Polanyi (1914) developed a concept to represent this potential, ε. He represented the surface force field by equipotential contours above the surface of the adsorbent. The space between each of the contours corresponds to a definite adsorbed volume. The cumulative volume of the adsorbed space may be written (Yang, 1987):

$$W = f(\varepsilon) \qquad (3\text{ -}22)$$

In potential theory, the above function, although unspecified, characterises a particular gas-solid system and is referred to as the characteristic curve. The adsorption potential is defined as the change in free energy accompanying the compression of one mole of gas from the equilibrium partial pressure P to the saturated vapour pressure P_o at the temperature of adsorption T. The adsorption potential, by definition, is independent of temperature; hence the characteristic curve

is independent of temperature. Using potential theory, it is possible to predict adsorption at different temperatures for the same gas-solid system once the characteristic curve is obtained for a single temperature. Hence for one mole of ideal gas (Yang, 1987):

$$\varepsilon = \int_{P}^{P_0} V dP = RT\, ln \frac{P}{P_0} \qquad (3\text{ -}23)$$

For an ideal gas, the volume of the adsorbed space is given by (Yang, 1987):

$$W = nV_m \qquad (3\text{ -}24)$$

The characteristic curve is generated by plotting *nVm vs. RTln (P_0/P)*. Other forms of the characteristic curve have been proposed (Yang, 1987). Dubinin postulated semi-empirical functions to define the characteristic curve. For microporous adsorbents, such as activated carbon, he proposed the following (Duong, 1998):

$$W = W_0 exp\left(-k\frac{\varepsilon^2}{\beta^2}\right) \qquad (3\text{ -}25)$$

Eq. (3 -25) is often referred to as the Dubinin-Radushkevich (D-R) equation.

In cases where it is not possible to assume ideal gas behaviour, fugacity is used in Eq. (3 -23) instead of pressure. The potential theory approach is useful for engineering design; however it does suffer three major disadvantages (Ruthven, 1984):

1. In the low concentration limit, the expression for the characteristic curve does not reduce to Henry's law. This is a requirement for thermodynamic consistency. This shortfall is however, not as important in the high concentration region.
2. There is appreciable uncertainty in the methods used to estimate molar volume of the adsorbed phase.
3. The assumption of a temperature-independent characteristic curve is often unrealistic, particularly when polar sorbates are used.

3.2. Gas Mixture Models

Most adsorption systems involve more than one component hence models used to correlate gas mixture adsorption are crucial to the design of industrial separation processes. The measurement of binary adsorption equilibria is often tedious work. For this reason, models that are capable of predicting binary equilibria from pure component isotherms are required. As is the case with pure gas isotherms, there are 3 approaches to developing models for gas mixture isotherms.

3.2.1. Langmuir Approach

3.2.1.1. Extended Langmuir Model

The Langmuir isotherm for pure gas adsorption can be readily extended to a binary system. The derivation for a binary system follows.

For a gas mixture, the assumptions outlined for pure component adsorption apply. The system is defined as containing partial pressures P_1 and P_2 in equilibrium with coverage θ_1 and θ_2 on the surface respectively. The rates of adsorption and desorption of species *1* is given by (Yang, 1987):

$$r_{A_1} = \alpha_1 v_1 (1 - \theta_1 - \theta_2) \qquad (3\text{-}26)$$

$$r_{D_1} = k_D \theta_1 \qquad (3\text{-}27)$$

At equilibrium, the rate of adsorption is equal to the rate of desorption, giving:

$$\theta_1 = \frac{b_1 P_1 (1 - \theta_2)}{1 + b_1 P_1} \qquad (3\text{-}28)$$

A similar equation is derived for component 2 and substituted in Eq. (3 -28):

$$\theta_1 = \frac{b_1 P_1}{1 + b_1 P_1 + b_2 P_2} \qquad (3\text{-}29)$$

Extended to an N-component mixture:

$$\theta_1 = \frac{b_i P_i}{1 + \sum_j^N b_j P_j} \qquad (3\text{-}30)$$

where the definition of *b* is provided in Eq. (3 - 8)

If it is assumed that each species in the mixture maintains its own molecular area (the amount covered by one molecule that is not influenced by other species on the surface of the adsorbent), the amount adsorbed is given by (Yang, 1987):

$$q_i = \frac{b_i q_i^{\infty} P_i}{1 + \sum_j^N b_j P_j} \qquad (3\text{-}31)$$

Thermodynamic consistency requires $q_1^{\infty} = q_2^{\infty}$, however when adsorption of molecules of different sizes occur, this assumption is often unrealistic. The use of different values for q_i^{∞} is allowed using the extended Langmuir isotherm. However, this must be done with caution. For these systems, the monolayer capacity is given by (Ruthven, 1984):

$$\frac{1}{q^{\infty}} = \frac{x_1}{q_1^{\infty}} + \frac{x_2}{q_2^{\infty}} \qquad (3\text{-}32)$$

The *Extended Langmuir Model* has been shown to correlate binary equilibrium data for CO_2/CO and O_2/CO systems on silica gel very well (Ruthven, 1984). In another study the model was used to correlate binary data for a CO_2/CO system on activated carbon and showed good results (Crittenden and Thomas, 1998).

3.2.1.2. Extended Langmuir-Freundlich (Sips) Model

In as much the same way as the Langmuir isotherm is extended to mixtures, the Sips model is extended to N-component mixtures:

$$q_i = \frac{b_i q_i^{\infty} P_i^{c_i}}{1 + \sum_j^N b_j P_j^{c_j}} \qquad (3\text{-}33)$$

The extended Langmuir-Freundlich isotherm was determined to work well for the adsorption of non-polar, binary mixtures on molecular sieves (Seader and Henley, 2006). The model also works well when correlating the binary adsorption data of simple gases on molecular sieve adsorbents and is used extensively in adsorption process design (Ruthven, 1984).

The extensions to the Langmuir and Langmuir – Freundlich models for multi-component mixtures have been shown to be thermodynamically inconsistent (Kaul, 1984). The models are used purely as emperical models and have no theoretical foundation. However, the models do provide a good fit to adsorption data and may be used with caution (Mersmann, 2003).

3.2.2. Gibbs Approach

Vacancy Solution Model

The vacancy solution model is readily extended to n-component mixtures. Accounting for the vacancy, the system requires *N+1* equations to be completely defined. The model has widespread application as it is based on only the most general assumptions concerning the nature of the adsorbed phase (Ruthven, 1984).

The VSM isotherm for a pure component is given by:

$$P = \left[\frac{q^{\infty}}{b_1}\frac{\theta}{1-\theta}\right]\left[\Lambda_{1v}\frac{1-(1-\Lambda_{v1})\theta}{\Lambda_{1v}+(1-\Lambda_{1v})\theta}\right] exp\left[-\frac{\Lambda_{v1}(1-\Lambda_{v1})\theta}{1-(1-\Lambda_{v1})\theta} - \frac{(1-\Lambda_{1v})\theta}{\Lambda_{1v}+(1-\Lambda_{1v})\theta}\right] \qquad (3\text{-}34)$$

The activity coefficients for *i* and *v* are given by:

$$\ln \gamma_k = 1 - \ln\left[\sum_j x_j \Lambda_{kj}\right] - \sum_i \left[\frac{x_i \Lambda_{ik}}{\sum_j x_j \Lambda_{ij}}\right] \qquad (3\text{-}35)$$

For the i^{th} component, the following expressions for chemical potential are written (Crittenden and Thomas, 1998):

$$\mu_i^g = \mu_{i_0}^g + RT\, ln(\phi_i y_i P) \qquad (3\text{-}36)$$

$$\mu_i^s = \mu_{i_0}^s + RT + ln(\gamma_i^s x_i^s) + \pi\delta \qquad (3\text{-}37)$$

At equilibrium $\mu_i^g = \mu_i^s$:

$$\mu_{i_0}^g + RT\, ln(\phi_i y_i P) = \mu_{i_0}^s + RT + ln(\gamma_i^s x_i^s) + \pi\delta_i$$
$$ln\left(\frac{\phi_i y_i P}{\gamma_i^s x_i^s}\right) = \frac{\mu_{i_0}^s - \mu_{i_0}^g}{RT} + \frac{\pi\delta_i}{RT} \qquad (3\text{ -}38)$$
$$\frac{\phi_i y_i P}{\gamma_i^s x_i^s} = exp\left(\frac{\mu_{i_0}^s - \mu_{i_0}^g}{RT}\right) exp\left(\frac{\pi\delta_i}{RT}\right)$$

Cochran et al. (1985) showed that:

$$\gamma_i^s = f(x_i^s, x_v^s) \qquad (3\text{ -}39)$$

The following relationships are also presented (Cochran et al., 1985):

$$x_i^s = \frac{q_t x_i}{q_t^\infty} \qquad (3\text{ -}40)$$
$$x_v^s = 1 - \frac{q_t}{q_t^\infty} \qquad (3\text{ -}41)$$

Assuming the same standard state for both chemical potentials, and using the relationships presented above (Yang, 1987):

$$\phi_i y_i P = \gamma_i x_i q_t \frac{q_i^\infty \Lambda_{iv}}{q_t^\infty b_i} exp(\Lambda_{vi} - 1) exp\left(\frac{\pi\delta_i}{RT}\right) \qquad (3\text{ -}42)$$

where:

$$q_t^\infty = \sum_i^N x_i q_i^\infty \qquad (3\text{ -}43)$$

$$-\frac{\pi\delta_i}{RT} = \left[1 + \frac{q_t^\infty - q_i^\infty}{q_t}\right] ln\, \gamma_v x_v \qquad i \neq v \qquad (3\text{ -}44)$$

Eq. (3 -34) to Eq. (3 -44) provides a complete set of equations that may be used to predict binary adsorption equilibria from pure component isotherms. The adsorbate-surface interaction parameters Λ_{iv} and Λ_{vi} are empirical constants obtained from pure component adsorption data. The interaction parameters between species in the adsorbate, Λ_{ij} and Λ_{ji}, can be estimated using (Yang, 1987):

$$\Lambda_{ij} = \frac{q_i^\infty}{q_j^\infty} exp\left(-\frac{\lambda_{ij} - \lambda_{ii}}{RT}\right) \qquad (3\text{ -}45)$$

where:

$$\lambda_{ii} = \frac{2}{z}(\Delta H_s + RT) \qquad (3\text{ -}46)$$

and

$$\lambda_{ij} = \sqrt{\lambda_{ii}\lambda_{jj}} \qquad (3\text{ -}47)$$

z is the coordination number of the molecule in the adsorbate and is evaluated empirically. For zeolites, *z* is typically assumed to be 3 (Suwanayuen and Danner, 1980). For adsorbates that are similar in nature: $\Lambda_{ij} = \Lambda_{ji} = 1$. The VSM model has been applied with good results to a number of systems. The model provides good predictions for the adsorption of binary mixtures on activated carbon and zeolites (Suwanayuen and Danner, 1980; Danner and Hyun, 1982) and is able to predict azeotropic behaviour which other models cannot (Yang, 1987).

3.2.3. Potential Theory

Extended Dubinin-Radushkevich Model

The D-R isotherm presented in Eq. (3 -25) is readily extended for mixed gas adsorption (Yang, 1987):

$$n_t = \sum n_i = \frac{W_0}{\sum x_i V_{mi}} exp\left[\frac{-kT^2}{(\sum x_i \beta_i)^2}\left(\sum x_i \, ln\frac{P_{0_i}}{P_i}\right)^2\right] \qquad (3\text{ -}48)$$

where:

$$\sum x_i = 1 \qquad (3\text{ -}49)$$

Eqs. (3 -48) and (3 -49) are not sufficient for solving n_t and n_i. For a binary system the following additional relationship developed by Lewis et al. (1950) is used to fully describe the system (Yang, 1987):

$$\frac{q_1}{q_1^0} + \frac{q_2}{q_2^0} = 1 \qquad (3\text{ -}50)$$

or

$$\frac{x_1}{q_1^0} + \frac{x_2}{q_2^0} = \frac{1}{q_t} \qquad (3\text{ -}51)$$

Eqs. (3 -48) to (3 -51) have been used to predict binary adsorption below the critical temperature with good results. The model requires a good representation of the pure gas adsorption using the D-R isotherm. The Lewis relationship must hold. This relation agrees well with experimental data for light hydrocarbon mixtures on activated carbon (Yang, 1987).

The models presented in this chapter are by no means a complete summary of the models used to describe adsorption equilibria. A review of the models most commonly used in the literature to regress and predict adsorption equilibria is presented in Table 3 - 1.

The models presented in this chapter are those that are most commonly used in the literature. Appendix D expands upon the models presented in this chapter. The reader is referred to the works of Ruthven (1984), Yang (1987), and Crittenden and Thomas (1998) for further reading on the remaining models appearing in the table that follows.

Table 3 - 1: A review of the models used to regress and predict adsorption equilibria. $T_{isotherm}$ and *P range* indicate the isothermal temperature and pressure range at which the models were applied. The Brunauer–Emmett–Teller (BET), Dubinin-Polanyi, Dubinin-Radushkevich (DR), Ideal Adsorbed Solution Theory (IAST), Langmuir, Lattice Solution Model (LSM), Simplified Statistical Thermodynamics Model (SSTM), Sips and Vacancy Solution Model (VSM) are among the models used in the literature. Grand Canonical Monte Carlo (GCMC) Simulation has also been used.

Reference	Adsorbent	Pure Gas Adsorption				Binary Gas Adsorption			
		Gas	$T_{isotherm}$ (K)	P range (bar)	Model	System	$T_{isotherm}$ (K)	P range (bar)	Model
Danner and Choi (1978)	Molecular Sieve 13X	Ethane Ethylene	298.15 323.15	0 - 1.38	VSM	Ethane/ethylene			2-D Gas Model IAST LSM SSTM
Reich et al. (1980)	Activated Carbon	Carbon Dioxide Ethane Ethylene Methane	212.7 260.2 301.4	0.01 - 35	Dubinin-Polanyi Theory	Methane/ethane Methane/ethylene Ethane/ethylene	212.7 260.2 301.4	1 - 20	Dubinin-Polanyi Theory
Danner and Hyun (1982)	Molecular Sieve 13X	Carbon Dioxide Ethane Ethylene Isobutane	298.15 325.15 373.15	0 – 1.378	Langmuir SSTM VSM	Ethylene/carbon dioxide Isobutane/ethane Isobutane/ethylene	298.15 325.15 373.15	1.378	IAST SSTM VSM
Kaul (1987)	Molecular Sieve 13X	Ethane Ethylene	323.15 373.15 423.15	0 – 5.5	VSM	Ethane/ethylene	323.15 423.15	0 - 1.38	
	Kureha Beads (Activated Carbon)	Ethane Ethylene Methane Propane	301.4 212.7	0 - 5.5					

Costa et al. (1991)	Molecular Sieve 13X	Ethylene Propylene Carbon Dioxide	279 293 308	0 - 1	Langmuir Prausnitz BET				
Pakseresht et al. (2002)	5A Zeolite	Carbon Dioxide Carbon Monoxide Ethane Ethylene	303 373 573	0 - 10	Langmuir Sips				
Yun et al. (2002)	MCM 41	Ethane Methane	264.75 303.15 373.15	0 - 35	GCMC Simulation	Ethane/methane	264.75	0 -35	IAST GCMC Simulation
Choi et al. (2003)	Activated Carbon	Ethane Ethylene Hydrogen Methane Nitrogen	293.15 303.15 313.15	0 - 20	Sips				
Al-Muhtaseb et al. (2007)	BDH Activated Carbon	Ethane	313.15 323.15 333.15	0 - 5	Langmuir DR				
		Methane	303.15 313.15						
		Nitrogen	323.15 333.15	0 - 8					
Al-Muhtaseb (2010)	Date Pits (Activated Carbon)	Ethane Ethylene Methane Nitrogen	303.15 318.15 333.15	0 – 7.58	Langmuir				

4

Chapter 4: A Review of the Techniques and Equipment used in the Measurement of Adsorption Equilibria

The volumetric and gravimetric techniques for the measurement of adsorption equilibria are the most widely applied techniques. Other techniques include the volumetric-gravimetric and the oscillometric techniques. A detailed review of the volumetric and gravimetric techniques is provided in this chapter. The volumetric-gravimetric and oscillometric techniques are discussed briefly. The theoretical framework required in the measurement of adsorption equilibria is also presented. The selection of the technique and the experimental apparatus for measurements can greatly influence the accuracy and efficiency with which experiments can be performed.

4.1. Experimental Theory

Despite being the most widely used techniques for the measurement of adsorption equilibria, neither the volumetric technique nor the gravimetric technique allows the determination of the mass being adsorbed without introducing a model assumption. The assumptions relate to defining the phase boundary for the adsorbed phase. The assumptions form the basis for the development of working equations for the calculation of adsorption isotherms. The equations presented in this study are based on work by Keller et al. (1999) and Cavenati et al. (2004).

Consider a closed vessel of volume V^t containing a porous solid of mass m^{ad} and a binary gas adsorptive with component masses m_i^g. Defining the mass of component *i* adsorbed as m_i^a, the following balance is written:

$$m_i^t = m_i^g + m_i^a \qquad (4 - 1)$$

The mass balance however does not yield any tangible results as the terms on the right hand side are not clearly defined and cannot be obtained by experimental procedures. To overcome this, the concept of *volume of a porous solid* V^{ad} was introduced (Gibbs, 1876). The mass of component *i* in the adsorptive is defined by:

$$m_{G_i}^g = \rho_i^g \left(V^t - V^{ad}\right) \qquad (4 - 2)$$

Eq. (4 - 2) is an expression of the *Gibbs Excess Mass* of adsorption where ρ_i^g is the partial density of component *i* in the adsorptive far away from the adsorptive/adsorbate boundary.

The Gibbs excess mass, first introduced by J.W. Gibbs in 1876, is based on three assumptions, namely:

1. The gas fills all of the space within the equilibrium cell except V^{ad}.

2. Gas molecules in the adsorptive do not interact with the adsorbent.
3. The volume, V^{ad} is inaccessible to the adsorptive and does not depend on particle size.

Introducing an auxiliary partial density, the total mass of component *i* is given by:

$$m_i^t = \rho_i^t \left(V^t - V^{ad}\right) \qquad (4 - 3)$$

The Gibbs excess mass is widely used in adsorption calculations, however it must be noted that the measurement of V^{ad} has a strong coupling to the measurement procedure.

Combining Eqs. (4 - 2) and (4 - 3), we arrive at an expression for the Gibbs excess mass for the adsorbate phase.

$$\begin{aligned} m_{G_i}^a &= m_i^t - m_{G_i}^g \\ &= \left(\rho_i^t - \rho_i^g\right)\left(V^t - V^{ad}\right) \end{aligned} \qquad (4 - 4)$$

A shortfall of the Gibbs excess mass is the change of volume of the adsorbate phase. To overcome this, a new quantity V^{as} is introduced. V^{as} is the volume of the solid adsorbent plus the volume of gas adsorbed.

Eq. (4 - 2) then becomes:

$$m_i^g = \rho_i^g (V^t - V^{as}) \qquad (4 - 5)$$

Combining Eqs. (4 - 1), (4 - 3) and (4 - 5), the absolute mass adsorbed is given by:

$$\begin{aligned} m_i^a &= m_i^t - m_i^g \\ &= m_{G_i}^a + \rho_i^g \left(V^{as} - V^{ad}\right) \geq m_{G_i}^a \end{aligned} \qquad (4 - 6)$$

From Eq. (4 - 6), the volume of the adsorbed phase is given by:

$$V^a = V^{as} - V^{ad} \qquad (4 - 7)$$

Re-writing Eq. (4 - 6)

$$m_i^a = m_{G_i}^a + \rho_i^g V^a \qquad (4 - 8)$$

The difference between the absolute mass adsorbed and the experimentally determined Gibbs excess mass, $\rho_i^g V^a$, is often negligible, especially at low gas pressure.

Typically the volume, V^{ad}, is approximated using helium. It is assumed that helium is neither adsorbed nor absorbed. Argon has also been used to determine the volume of the adsorbent (Keller et al., 1999). The volume is calculated as follows:

$$V_{He}^{ad} = V^t - \frac{m_{He}^t}{\rho_{He}^g} \qquad (4 - 9)$$

The volume of the adsorbent/adsorbate system is given by:

$$V^{as} = V_{He}^{ad} + \sum_i^N \frac{m_i^a}{\rho_{i_0}^L} \qquad (4 - 10)$$

From Eqs. (4 - 9) and (4 -10), the volume of the adsorbed phase is given by:

$$V^a = \sum_i^N \frac{m_i^a}{\rho_{i_0}^L} \qquad (4 - 11)$$

where ρ_{i0}^{L} is the density of pure component *i* in a liquid reference state.

Statistical molecular models used to predict and simulate adsorption equilibria will generally lead to the absolute mass of gas adsorbed and not the Gibbs excess mass as described in this chapter. However, the volumetric and gravimetric technique cannot be used to experimentally determine the absolute mass adsorbed. Instead, the techniques yield a so called *reduced mass of adsorption* (Keller et al. 1999):

$$\Omega_i = m_i^a - \rho_i^g V^{as} \qquad (4 - 12)$$

$$\Omega_i = m_{G_i}^a - \rho_i^g V^{ad} \qquad (4 - 13)$$

Using Eqs. (4 -12) and (4 -13), either the absolute mass adsorbed, $m^a{}_{i,}$ or the Gibbs excess mass, $m^a{}_{Gi}$ may be obtained upon introducing a model to determine V^{as} or V^{ad}.

4.2. Experimental Techniques and Equipment

4.2.1. The Volumetric Technique

The volumetric technique for the measurement of multi-component adsorption equilibria is the most widely applied technique. It provides high flexibility, good accuracy and the added benefit of low cost when compared to the other techniques (Ahmed et al., 2012). The volumetric method is most often of the static type allowing the adsorbate to equilibrate with the adsorbent in a closed system (Kaul, 1987). The technique has been favoured by researchers since the 1950's (Ray and Box, 1950) and is as popular today (Ahmed et al., 2012).

A known amount of gas, determined using PVT relations, is prepared in a storage vessel with volume V_{SV} and expanded into an adsorption chamber with volume V_{AC}. This method of preparing the gas in a storage vessel is preferred by most researchers (Keller et al., 1999). The gas is partly adsorbed onto the adsorbent with mass m^{ad} causing a decrease in pressure. The decrease in pressure is caused by molecules leaving the gas phase and attaching to the solid resulting in fewer gas-gas interactions. Equilibrium is achieved when the pressure in the adsorption chamber

stabilises. This pressure is recorded for the isotherm. For binary gas mixtures, a gas sample is removed from the adsorption chamber for analysis via gas chromatography resulting in molar concentrations y_i^g.

The volume of both the storage vessel V_{SV} and the adsorption chamber V_{AC} is calculated by filling the vessels with a known mass of fluid and using its density at experimental conditions to calculate the vessel volume. The volume of the adsorbent V^{ad} must also be known. The adsorbent volume is most often calculated using selected inert gases. These gases are chosen as they do not adsorb appreciably – if at all - onto the solid. A known mass of gas is expanded into the adsorption chamber with the adsorbent present. The pressure and temperature is measured and the volume of gas in the presence of the adsorbent is calculated. The volume determined using the inert gas is the volume of the equilibrium gas phase V^g.

Whence the volume available for the equilibrium gas is known, the adsorption measurements are undertaken. An Equation of State (EoS) is used to calculate the mass of equilibrium gas present in the adsorptive phase m_i^g in the adsorption chamber when undertaking measurements. This is possible as the volume available in the adsorption chamber V^g is known once the adsorbent volume V^{ad} is measured. The difference in mass of gas discharged from the storage vessel and the amount calculated in the adsorption chamber at equilibrium is the amount of gas adsorbed m_i^a. The working equations needed to determine the relevant quantities are presented below. The apparatus of Keller et al. (1999) is used as an illustration.

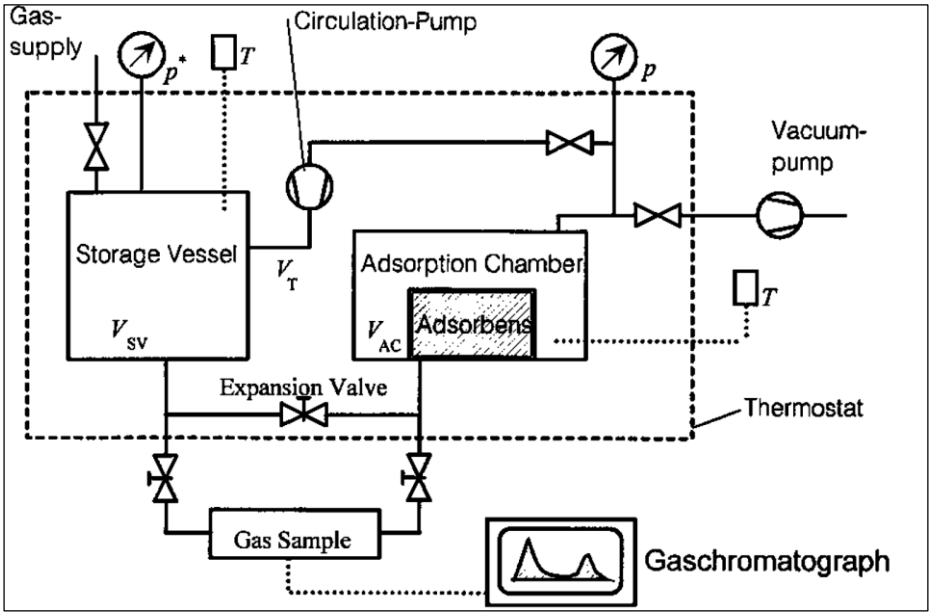

Figure 4 - 1: Schematic of the volumetric apparatus of Keller et al. (1999).

The total volume of the system is given by:

$$V^t = V_{SV} + V_{AC} + V_T \qquad (4\text{-}14)$$

where V_T is the volume of tubes and fittings used in the apparatus.

The total mass of gas in the adsorptive is:

$$m^g = \rho^g (V^t - V^V) \qquad (4\text{-}15)$$

The density of the adsorptive is determined using a thermal EoS:

$$\rho^g = \frac{PM^g}{ZRT} \qquad (4\text{-}16)$$

where M^g for a gas mixture is given by:

$$M^g = \sum_i^N M_i y_i \qquad (4\text{-}17)$$

The Peng-Robinson Equation of State (PREoS) was used to determine compressibility. The PREoS is given by (Poling et al., 2001):

$$P = \frac{RT}{V-b} - \frac{a(T)}{V(V+b)+b(V-b)} \qquad (4\text{-}18)$$

where:

$$a(T) = a(T_c)\alpha \qquad (4\text{-}19)$$

$$a(T_c) = 0.457235\frac{(RT_c)^2}{P_c} \qquad (4\text{-}20)$$

$$\alpha(T) = \left[1 + \kappa\left(1 - \sqrt{\frac{T}{T_c}}\right)\right]^2 \qquad (4\text{-}21)$$

$$\kappa = 0.37464 + 1.54226\omega - 0.26992\omega^2 \qquad (4\text{-}22)$$

$$b = 0.077796\frac{RT_c}{P_c} \qquad (4\text{-}23)$$

Eqn. (4 -18) is re-written in terms of the compressibility factor and is given as:

$$Z^3 - (1-B)Z^2 + (A - 3B - 2B^2)\mathrm{Z} - (AB - B^2 - B^3) = 0 \qquad (4\text{-}24)$$

where:

$$A = \frac{aP}{R^2T^2} \qquad (4\text{ -}25)$$

$$B = \frac{bP}{RT} \qquad (4\text{ -}26)$$

Equation (4 -24) yields one or three roots depending on the number of phases in the systems. For a two-phase region the smallest positive root corresponds to the compressibility factor of the liquid while the largest root corresponds to that of the vapour.

The PREoS, being a cubic EoS, offers the advantage of being readily extended to mixtures. The one-fluid mixing rules of van der Waals assumes that the "EoS for the mixture is the same as that for a hypothetical 'pure' fluid whose characteristic constants *a (T)* and *b* depend on composition" (Naidoo, 2004).

$$a_m = \sum_i^n \sum_j^n y_i y_j a_{ij} \qquad (4\text{ -}27)$$

where:

$$a_{ij} = \sqrt{a_i a_j}\left(1 - k_{ij}\right) \qquad (4\text{ -}28)$$

$$b_m = \sum_i^n \sum_j^n y_i y_j b_{ij} \qquad (4\text{ -}29)$$

where:

$$b_{ij} = \frac{1}{2}\left(b_i + b_j\right)\left(1 - l_{ij}\right) \qquad (4\text{ -}30)$$

where k_{ij} and l_{ij} are the binary interaction parameters. In the case of non-polar mixtures, l_{ij} is set equal to 0; k_{ij} is fitted to experimental data.

For a binary mixture of ethane and ethylene at a pressure of 1.377 bar and a temperature of 303.42 K, Eqs. (4 -27) – (4 -30) are reduced. The binary interaction parameter, k_{ij} was determined to be $8.9\text{x}10^{-3}$, using AspenPlus V8.0.

$$a_m = y_1^2 a_1 + 2y_1 y_2 \sqrt{a_1 a_2} \times 8.9 \times 10^{-3} + y_2^2 a_2 \qquad (4\text{ -}31)$$

$$b_m = y_1 b_1 + y_2 b_2 \qquad (4\text{ -}32)$$

The parameters – a_m and b_m – are then substituted into the PREoS to determine compressibility of the mixture.

The volume V^V introduced in Eq. (4 -15) represents the void volume inaccessible to the adsorptive molecules. This may be the volume of the solid adsorbent, V^{ad} or the volume of the adsorbent/adsorbate system, V^{as}.

Multiplying Eq. (4 -15) with the mass fraction of the adsorptive and combining with Eq. (4 - 1), the mass of component *i* adsorbed is:

$$m_i^a = \Omega_i + \rho_i^g V^V \qquad (4\text{ -}33)$$

where Ω_i is interpreted as the reduced mass adsorbed with the reduction due to the void volume, V^v. A model is required to determine V^v which is then used to determine $m_i{}^a$. Typically, there are two methods for determining V^V.

- V^V is taken to be the adsorbent volume V^{ad} approximated by the helium volume $V_{He}{}^{ad}$. Eq. (4 -33) then yields the Gibbs excess mass of adsorption:

  $$m_{G_i}^a = \Omega_i + \rho_i^g V_{He}^{ad} \qquad (4\text{ -}34)$$

  Ω_i is calculated using the following auxiliary relation:

  $$\Omega_i = m_i^t - \rho_i^g V^t \qquad (4\text{ -}35)$$

- V^V is taken to be the volume of the combined adsorbent/adsorbate system V^{as} approximated by the helium volume $V_{He}{}^{as}$.

  $$V^V = V^{as} \cong V_{He}^{ad} + \sum_i^N \frac{m_i^a}{\rho_{i_0}^L} \qquad (4\text{ -}36)$$

  Eqs. (4 -33) and (4 -36) are combined to yield a system of N linear equations for the absolute masses of all components adsorbed:

  $$m_i^a = m_i^t - \rho_i^g \left[V^t - V_{He}^{ad} - \sum_k^N \frac{m_k^a}{\rho_{k_0}^L} \right] \qquad (4\text{ -}37)$$

Table 4 - 1: Comparison of the volumetric technique and its uncertainties. The reader is referred to Appendix C for further details on the equipment listed.

Reference	Storage Cell	Equilibrium Cell	Recirculation	Temperature		Absolute Pressure		q
	Volume/mL	Volume/mL		Range/ K	Uncertainty/ K	Max/ bar	Uncertainty/ bar	Uncertainty
Reich et al. (1980)	5000	70		70 - 350	0.1	100	0.017	0.15mmol/g
Kaul (1987)	-	variable volume	Yes	283 - 866	1	69	0.07	5%
Ghosh et al. (1993)	1000	1000	No	298 (range not provided)	0.1	206		
Pakseresht et al. (2002)	999.5	188.5	Yes	303 - 673	0.1	15	0.01	
Yun et al. (2002)			No	263 - 274	0.02	33	0.017	0.2%(pure) 1.5% (binary)
Choi et al. (2003)	522.73±1	521.61±1	No	293 - 313	0.02	20	0.1	
Saha et al. (2011)	76.38 (used at high gas pressure)	80.27	No	255 - 353	0.1	120	0.2	
Lee et al. (2013)	642.6±0.3	411.4±0.2	No		0.1	180	0.72	5%

A storage cell is typically used in a static volumetric setup. The cell as the name suggests, is used to prepare and store the gas before the adsorption step. Storage cell volumes range from a mere 20 mL (Ahmed et al., 2012) to 5 L (Reich et al., 1980) depending on the operating range and capacity of the adsorption apparatus. More importantly however, the storage vessel is used in the preparation of gas mixtures in the measurement of mixed gas adsorption. A sample is removed from the storage vessel to determine if the right composition is achieved (Ghosh et al., 1993). In cases where a storage cell was not used (Costa et al., 1981; Kaul, 1987; Yun et al., 2002), a dynamic approach was applied. The storage cell is placed in a bath (Ghosh et al., 1993; Choi et al., 2003; Al-Muhtaseb et al., 2007; Saha et al,. 2011; Ahmed et al., 2012) or may be operated under atmospheric conditions (Pakseresht et al., 2002).

The equilibrium cell used in the measurement of adsorption data is placed in a bath to maintain isothermal conditions. A liquid bath is most commonly used, however electrical heaters (Pakseresht et al., 2002), ovens (Al-Muhtaseb et al., 2007) and sand baths (Kaul, 1987) have been used. When a static approach is used, equilibrium is indicated by constancy in the pressure. In the case of the dynamic approach, gas samples are periodically removed and analysed. Equilibrium is indicated by constancy in composition.

A significant drawback with the volumetric approach is the slow attainment of equilibrium. This is attributed to the diffusion resistance present in the adsorbent. Equilibrium may take several days to achieve (Yang, 1987). However, use of a recirculation pump can significantly reduce the time to reach equilibrium.

Accurate measurement of pressure and temperature are pivotal to the volumetric approach. The measurements are necessary to determine the amount of gas adsorbed. Temperature was measured with accuracy as low as 1 K (Kaul, 1987) and as high as 0.01 K (Choi et al., 2003). Accurate pressure measurement and control is important in measuring adsorption data. A fine control valve is usually installed between the storage cell and the equilibrium cell to facilitate this.

4.2.1. Gravimetric Technique

The gravimetric technique for the measurement of adsorption equilibria works on the principle of a change in mass of the adsorbent during adsorption. The technique is second only to the volumetric technique with respect to widespread application and utilization among researchers.

A typical gravimetric apparatus consists of a microbalance holding a sample of adsorbent with mass m^{ad} and a kentlage (counterweight) within an adsorption chamber of volume V_{AC}. The sample is typically suspended through an electromagnet. A gas circulation pump is sometimes used; however, this is not always the case. Apparatus capable of measuring binary equilibria is fitted with the required composition analysis equipment, typically a gas chromatograph (GC) or mass spectrometer (MS).

A gas mixture of known composition or pure component gas is expanded in the adsorption chamber where it is partially adsorbed. Equilibrium is achieved when the mass of the sample within the adsorption chamber is constant. In addition, equilibrium is also indicated by constancy in the temperature and pressure of the equilibrium gas present in the adsorption chamber. Gravimetric measurements, like volumetric measurements can be undertaken in both static and dynamic configurations. In the case of binary measurements, a sample is removed for composition analysis once equilibrium is reached.

The working equations needed to determine the relevant quantities are presented. The apparatus of Keller et al. (1999) is used as an illustration.

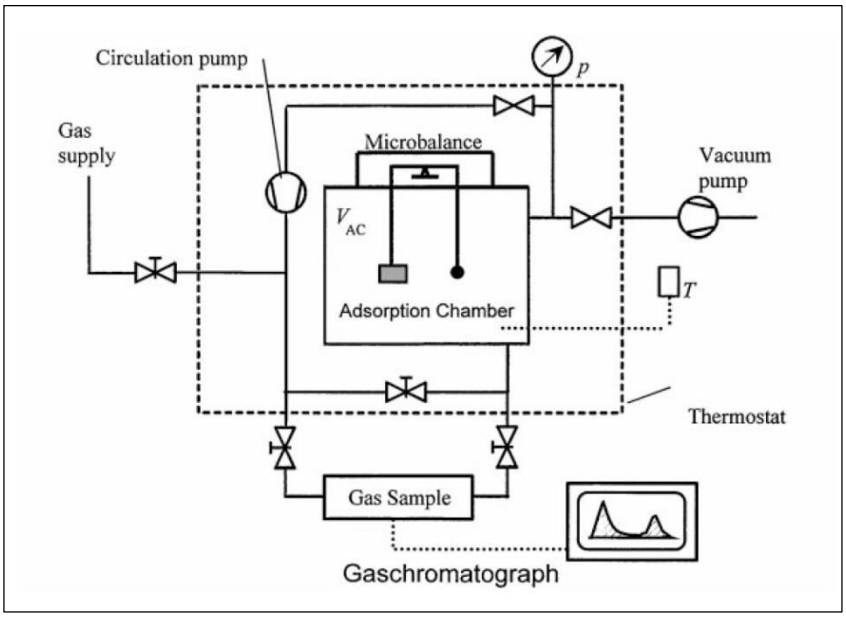

Figure 4 - 2: Schematic of the gravimetric apparatus of Keller et al. (1999).

The total volume of the system is given by:

$$V^t = V_{AC} + V_T + V_{MB} \qquad (4\text{ -}38)$$

where V_T is the volume of tubes and fittings used in the apparatus and V_{MB} is the internal volume of the microbalance.

The total mass of gas in the adsorptive is:

$$m^g = \rho^g (V^t - V^V) \qquad (4\text{ -}39)$$

The gravimetric technique yields the reduced mass adsorbed:

$$\Omega_{MB} = m^a - \rho^g V^V \qquad (4\text{ -}40)$$

Combining the overall mass balance

$$m^t = m^g + m^a \qquad (4\text{ -}41)$$

with Eq. (4 -39), the total mass of gas charged to the system – in terms of density and microbalance measurements is given by:

$$m^t = \rho^g V^V + \Omega_{MB} \qquad (4\text{ -}42)$$

The mass of component *i* adsorbed is thus given by:

$$m_i^a = \Omega_{MB_i} + \rho_i^g V^V \qquad (4\text{ -}43)$$

For component *i*, the reduced mass adsorbed is given by:

$$\Omega_{MB_i} = \left(w_i^0 - w_i\right)\rho_i^g V^t + w_i^0 \Omega_{MB} \qquad (4\text{ -}44)$$

where w_i^0 and w_i are the initial and equilibrium mass concentrations of component *i* in the adsorptive.

Combining Eqs. (4 -43) and (4 -44) and introducing a model assumption for the void volume V^V, the absolute mass adsorbed is obtained using:

$$m_i^a = \Omega_{MB_i} + \rho_i^g \left(V_{He}^{ad} + \sum_k^N \frac{m_k^a}{\rho_{k_0}^L} \right) \qquad (4\text{ -}45)$$

The main advantage of the gravimetric technique is that it only requires a small sample of adsorbent to undertake measurements. Often however, the technique cannot be used to undertake measurements with corrosive gases. In such cases, magnetic suspension balances are used (Dreisbach, 2002).

4.2.2. Volumetric-Gravimetric Technique

The volumetric-gravimetric technique is useful when measuring co-adsorption equilibria of binary gas mixtures. This method does not require the use of a GC or mass spectrometer. The method works for mixtures comprising non-isomeric components. The technique has a drawback in that it does not provide accurate measurement of systems with dilute mixtures.

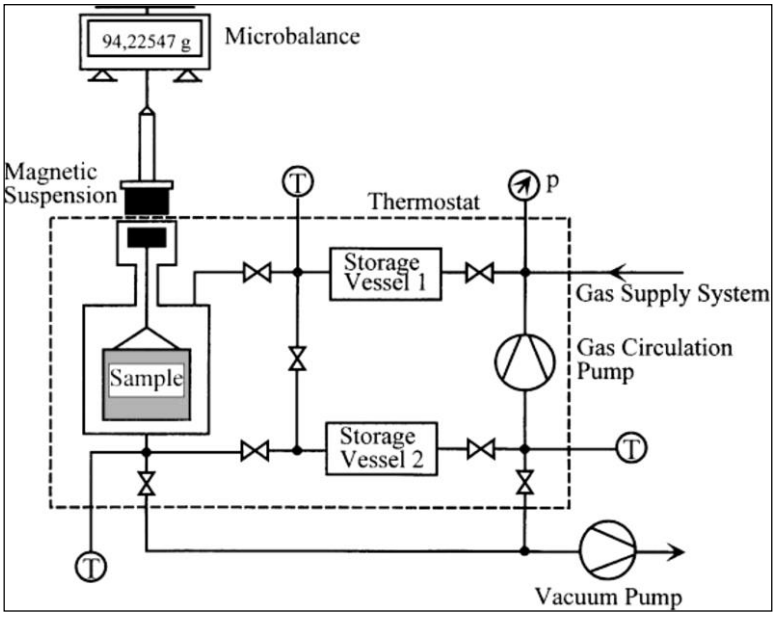

Figure 4 - 3: Schematic of the volumetric-gravimetric apparatus of Keller et al. (1999).

The apparatus of Keller et al. (1999) includes a magnetic suspension similar to that used in the gravimetric apparatus (Keller et al., 1999). The magnetic suspension is decoupled from the adsorption chamber allowing measurements of corrosive gases. The binary gas mixture is prepared by mixing pure components of mass m_1 and m_2 filled in storage vessel 1 and storage vessel 2 respectively. The vessels have a volume of V_1 and V_2 respectively. The pure components are mixed using a recirculating pump and expanded into the adsorption chamber. The amount of each component adsorbed is measured by the change of mass of adsorbent and a thermal EoS.

4.2.3. Oscillometric Technique

This technique works on the principle of frequency of oscillations. The amount of gas adsorbed is determined by observing the frequency of oscillations of the sorbent system (Keller, 1999).

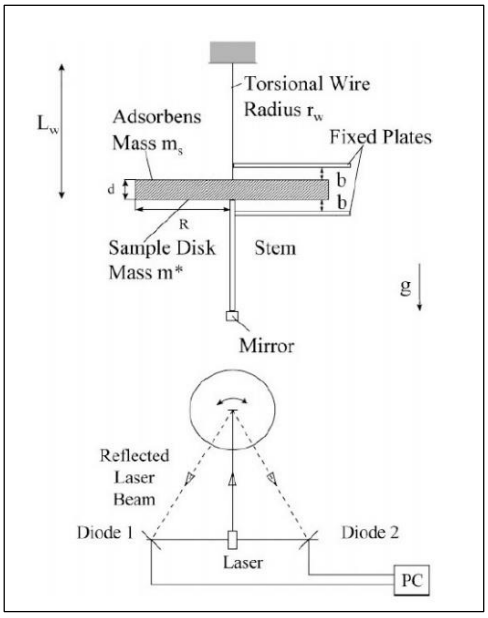

Figure 4 - 4: Schematic of the oscillometric apparatus of Keller et al. (1999).

The apparatus of Keller et al. (1999) operates in the following manner: the adsorbent is placed on a rotating disc inside the adsorption cell. The speed of rotation is measured using a laser, as gas is adsorbed onto the disc, the rotation speed changes and is measured using the laser. The laser is reflected onto a detector allowing the measurement of the change in angular frequency. When using the oscillometric technique, the volume of the adsorbent is not required. This is advantageous.

Table 4 - 2: Comparison of adsorption measurement techniques (Keller et al., 1999).

Technique/Method	Advantages	Disadvantages
Volumetric	Cost effective	Uncertainty in volume of adsorbent
	Well established	Uncertainty when measuring mass of gas using PVT relations
	Literature readily available for comparisons to be drawn	
Gravimetric	Relatively small amounts of adsorbent are required	High cost of high precision suspension balance
	Uncertainty in PVT relations avoided	Not very effective for dilute mixtures
	Volume of adsorbent need not be known	
Volumetric-Gravimetric	GC or MS not required	Combined disadvantages of both volumetric and gravimetric techniques
Oscillometric	Volume of adsorbent need not be known	Still some difficulty in interpreting measured data
	PVT relations not required	

5

Chapter 5: Experimental Equipment and Procedure

Adsorption measurements were undertaken using the volumetric and gravimetric techniques. Volumetric measurements were undertaken using an apparatus designed and commissioned as part of this study. Gravimetric measurements were undertaken using an Intelligent Gravimetric Analyser (IGA). The experimental equipment and techniques used are presented in this chapter.

5.1. Volumetric Apparatus

The review presented in Chapter 4 gives an outline of the parts or constituents required in a volumetric apparatus. The apparatus designed and commissioned in this study, together with auxiliary equipment, for the measurement adsorption equilibria for pure component and binary mixtures, comprises the following:

- An equilibrium cell with a volume of approximately 375 mL and a maximum operating pressure of 20 bar at a maximum temperature of 425 K.
- A storage cell with a volume of approximately 987 mL and a maximum operating pressure of 100 bar at a maximum temperature of 373 K.
- A mixing cell with a volume of approximately 723 mL and a maximum operating pressure of 50 bar at a maximum temperature of 373 K.
- Instrumentation and fittings including temperature and pressure sensors along with data acquisition systems.
- Composition analyses equipment
- A high precision Ohaus Explorer mass balance with a capacity of 6100 g and a readability of 0.01 g. The balance was calibrated by Trilab support (SANAS approved) with an uncertainty of 0.07 g.

Figure 5 - 1: Volumetric apparatus developed in this study.

5.1.1. Apparatus

5.1.1.1. Equilibrium Cell

The equilibrium cell developed for this study is of the static type. The cell has an internal volume of 375 mL when empty. The volume of cells used in previous studies varies from approximately 20 mL (Ahmed et al., 2012) to approximately 1000 mL (Ghosh et al., 1993) depending on the capacity of the equipment and sensitivity of the instrumentation. The equilibrium cell was fabricated for a previous study undertaken by Rice (2010). It is constructed from stainless steel and is designed to operate at pressures up to 20 bar at a maximum temperature of 425 K. The original cell had to be modified to suit the requirements of this study. The original design used a self-forming gasket to seal the top of the cell. This type of seal is impractical when the cell needs to be opened periodically. This seal was hence not feasible as the cell had to be opened each time the adsorbent was loaded and unloaded, requiring a new self-forming seal each time. In addition to the expensive/cost of replacing this seal, the time required for the seal to set would add to the downtime of the apparatus. It was decided to rather use a Viton® O-ring to seal the vessel and replace this each time the cell was opened – if needed.

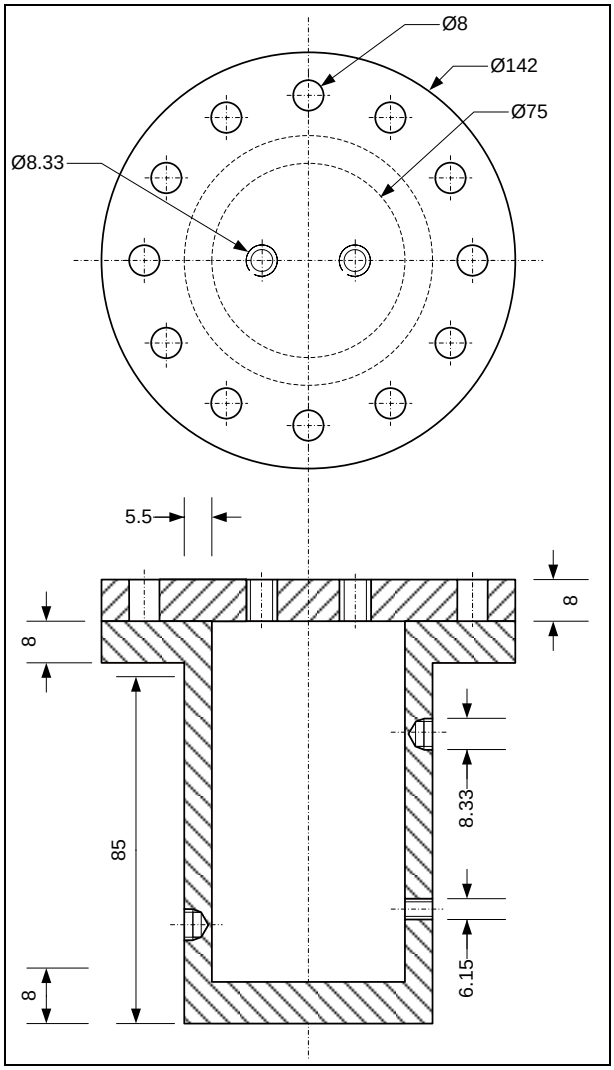

Figure 5 - 2: Schematic of the equilibrium cell (dimensions in millimetres).

The original cell had two 8.33 mm holes drilled through the wall for insertion of the Pt100 (SS) probes. However, this method of fitting the Pt100's to the equipment is now rarely applied in the design of the equipment in the TRU laboratories. In the previous configuration, the probes were fitted with a nut and ferrule and then fitted onto the equilibrium cell using an appropriate fitting. This method of measurement is advantageous as the temperature of the fluid is directly measured. It does however have two distinct disadvantages. The drilling of through holes on the wall of the cells introduces the potential for leaks in both the compression and NPT fittings. In addition, the ferrule crimping down on the Pt100 housing could potentially damage the probe. As the holes were already drilled into the wall of the cell there was nothing that could be done to avoid potential leaks at the NPT end of the fitting. Potential leaks at the compression end however were eliminated by specially fabricating plugs for the Pt100 to be fit into. The plugs are fabricated in such a way that the Pt100 is not in direct contact with the fluid phase. The assumption is made that at equilibrium the temperature of the fluid within the cell and the cell itself are exactly the same.

The analysis of the composition of the equilibrium sample was done on-line. 6 port switching valves were used to remove a sample from the mixing vessel and equilibrium cell. The sampling configuration will be discussed in detail in a later section.

5.1.1.2. The Storage Cell

The storage vessel is used to determine the amount of gas charged to the equilibrium cell for adsorption. The amount of gas charged to the equilibrium cell is determined by measuring the change in pressure of the gas in the storage vessel. Together with volume and temperature measurements, the number of moles of gas charged to the equilibrium cell is determined. The storage cell is constructed from stainless steel 316L and has a volume of 987 mL with an uncertainty of 1 mL. The cell is designed to operate at pressures up to 100 bar at a maximum temperature of 373 K. A thermal press design was used as opposed to a flanged-end design since there was no need to open the storage cell. A schematic of the cell is presented in Figure 5 - 3.

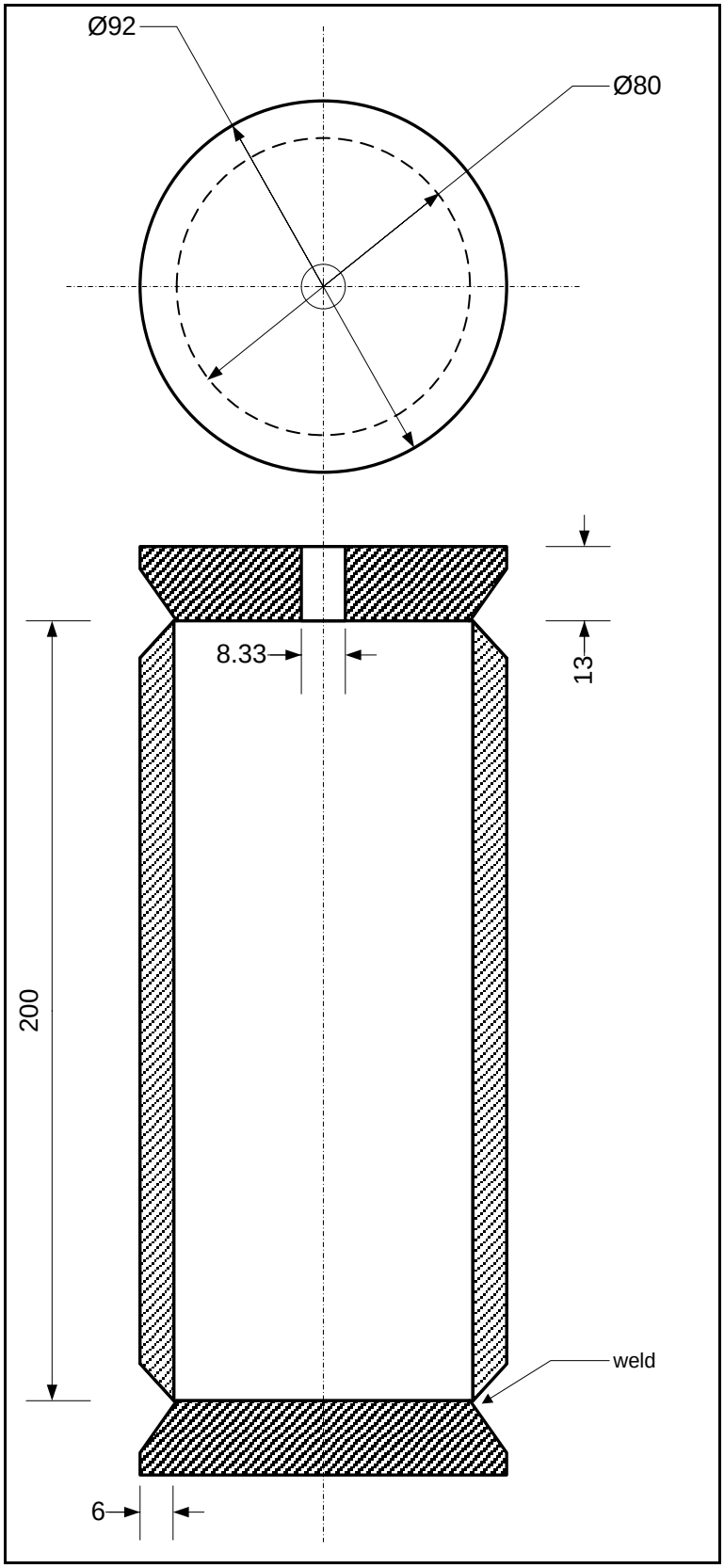

Figure 5 - 3: A schematic of the storage cell (dimensions in millimetres).

5.1.1.3. The Gas Mixing Cell

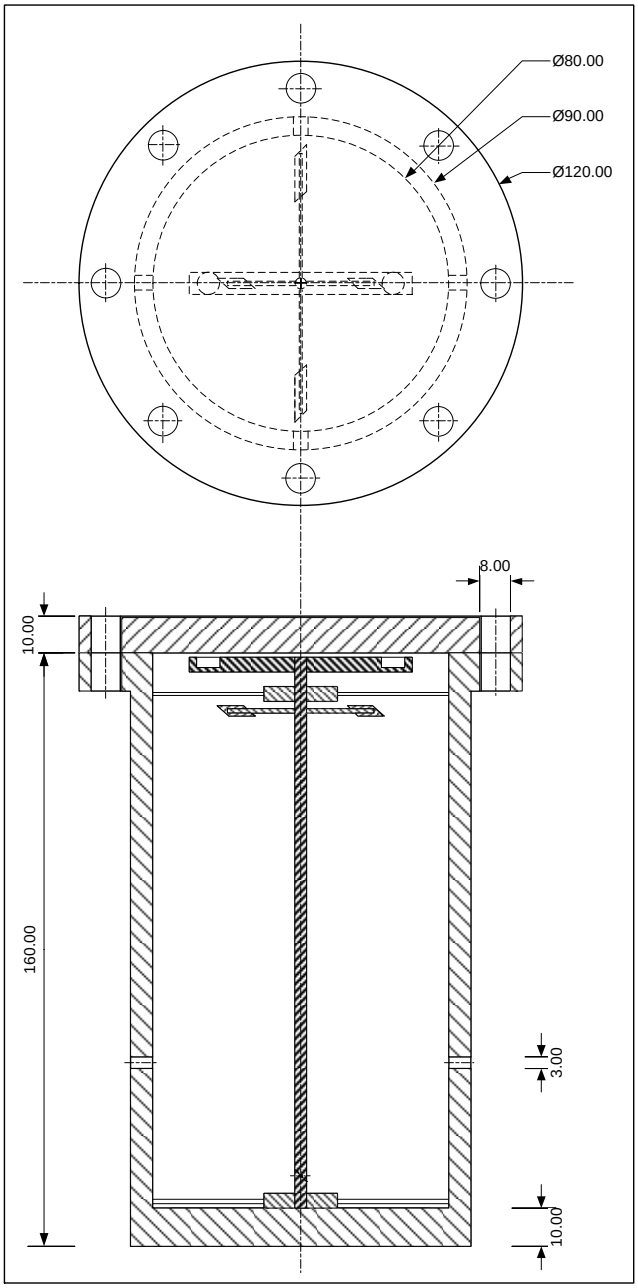

Figure 5 - 4: The mixing cell used to prepare binary mixtures (dimensions in mm)

The binary mixtures were prepared gravimetrically using an impellor type gas mixer. The mixer is constructed from 316L stainless steel and is designed to operate at pressures up to 50 bar at a maximum temperature of 373 K. Mixing of the gases in the cell is achieved by driving a shaft fitted with impellors using magnetic coupling as shown in Figure 5 - 5.

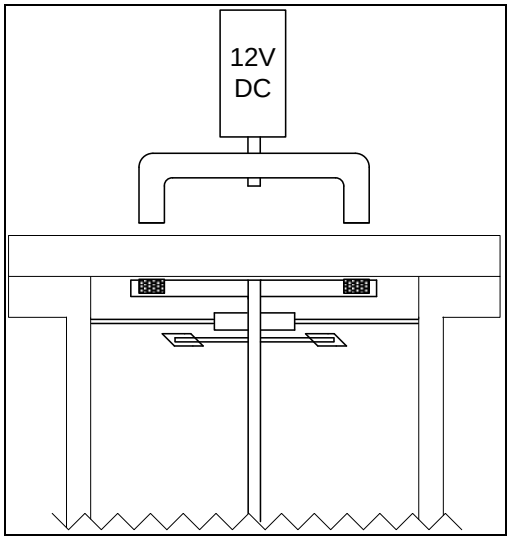

Figure 5 - 5: Magnetic coupling configuration of the mixing cell.

A horseshoe magnet – constructed from alcino – is attached to a 12V DC motor and held above the mixing cell. The motor is powered using a GP 30-5 DC power supply. The horseshoe couples with two neodymium magnets inside the mixing cell. The neodymium magnets are housed in a stainless steel bar, placed a distance apart equal to the diameter of the horseshoe. The stainless steel bar is attached to the shaft that facilitates mixing. To hold the mixing shaft and to allow for ease of motion, two ball bearings are installed along the length of the shaft. The bearings are held in place by metal rods that push against the interior wall of the cell.

The mixing shaft is fitted with two pairs of mixing blades – at the top and bottom of the mixing cell. The pairs are positioned such that when at rest they are at 90° to each other when viewed from the top of the cell. The mixing blades are attached to the mixing shaft using stainless steel rods with one end of the rod welded to the mixing shaft and the other to the end of the pedal. The pedals are at 45° to the horizontal plane. The pair of pedals at the top of the mixer is closer to the centre than those at the bottom. The varied diameter as well as the 45° angle of the pedals promotes increased turbulence within the mixer. The gas mixer used in this study was designed and fabricated by Dr Wayne Nelson and Mr Leon Augustyn.

A schematic of the volumetric apparatus is presented in Figure 5 - 7. The experimental technique used is explained in the next section.

5.1.1.4. Pressure, Temperature, Mass and Composition Measurements

5.1.1.4.1. Pressure

The pressure of the storage/mixing cell and the equilibrium cell were measured using WIKA D-10-P transducers. The transducer ranges were 0-100 bar and 0-25 bar respectively. The accuracy of the transducers is 0.05% of the span as quoted by the manufacturer. Pressure data acquisition was undertaken using RS232 communication and *EasyCom* software provided by WIKA. An *Edwards Rotary Vane 3* (RV3) vacuum pump was used to achieve a vacuum as high as 2×10^{-3} mbar in the system. Calibration of the pressure transducers along with the uncertainties are discussed in Section 5.1.2.2.

5.1.1.4.2. Temperature

Temperature was measured using Pt100 probes (1/10 DIN) supplied by WIKA. Two probes were fitted on the equilibrium cell, at the base and top, to ensure isothermal conditions were maintained and temperature gradients, if present, were measured. A single Pt100 was fitted to the storage cell and the mixing cell. The Pt100 probes have an operating range of 73 K - 673 K as stated by the manufacturer. They were calibrated from 293 K up to 373 K for this study. The probes are have a resolution of 0.01 K. Temperature data were acquired using a *PICO PT104 Data Logger* (24-bit ADC).

A bath containing a solution of water and ethylene glycol (97%) was used to maintain isothermal conditions of the equilibrium cell. The bath was equipped with a Polyscience heater and circulator (Model 7306). A Polyscience chiller unit (Model 070885) was used to maintain temperatures below 303 K.

A second bath was used to maintain isothermal conditions of the storage cell and the mixing cell. The bath was equipped with a Polyscience heater and circulator (Model 7306). Both baths used in this study have a capacity of 20 L. Calibration of the Pt100 probes along with the uncertainties are discussed in Section 5.1.2.2.

5.1.1.4.3. Composition

The composition analysis was undertaken using a Shimadzu 2010 Gas Chromatograph. The GC is equipped with a Flame Ionisation Detector (FID). A FID was selected as the components are all hydrocarbons and a high sensitivity was required. A *GS GasPro* capillary column was fitted to the GC. GC settings are provided in Table 5 - 1. Calibration of the FID is discussed in Section 5.1.2.

Gas samples from the equilibrium cell were flushed to the GC using a combination of a 2-position 6-port switching valve and a 2 position 4-way crossover valve. The 6 port valve was manufactured by VALCO and supplied by Anatech. The 4-way valve was supplied by Swagelok and fitted with a ball orifice to avoid cross-flow when switching. The mixing cell and equilibrium cell were both fitted with the configuration shown in Figure 5 - 6. This method of sampling was chosen as it allowed a small sample of gas to be removed at sub atmospheric and high pressure without disturbing the equilibrium conditions. A sample loop was constructed to trap the gas sample for analysis. The loop has a volume of 100 μL. The 4-way valve was used to ensure the GC received a constant supply of carrier gas, helium in this study.

The configuration, shown in Figure 5 - 6 was operated in three modes: evacuating, sampling and flushing. In the evacuating mode, the sample loop (a piece of tubing attached to ports 3 and 6) was evacuated in preparation for sample withdrawal. The lines connecting the 6-port valve to the 4-way valve were also evacuated. Gas from the equilibrium cell flowed through the 6-port valve via ports 1 and 2. Helium was supplied to the configuration via port 4 of the 4-way valves and was sent to the GC via port 3. This ensured a constant supply of helium to the GC through all modes of operation. In sampling mode, the equilibrium gas flowed through the sample loop. This was achieved by switching the position of the 6-port valve (as indicated on the diagram). The vacuum created in the sample loop during the evacuating step forced a sample of gas into the sample loop. The valve position was switched once the sample was obtained, trapping the gas in the sample loop. The position of the 4-way valve was then changed to carry the equilibrium sample to the GC for analysis. The three step technique was repeated several times to ensure a representative sample was used for analysis.

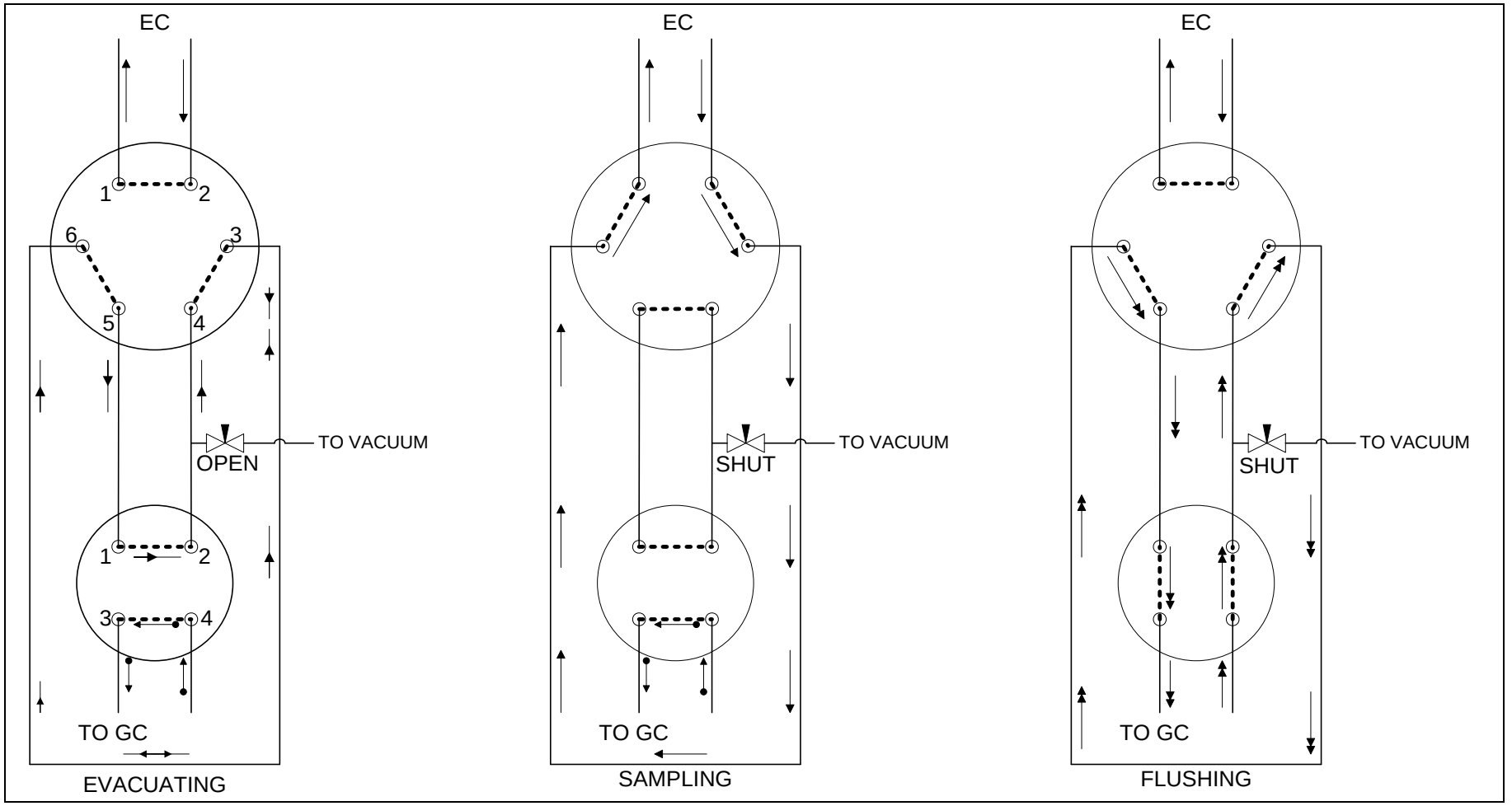

Figure 5 - 6: Sampling configuration used to analyse binary samples. Gas samples from the equilibrium cell were flushed to the GC using a combination of a 2-position 6-port switching valve and a 2 position 4-way crossover valve.

5.1.1.5. Valves, Fittings and Tubing

All the valves, tubing and fittings used in this study were manufactured and supplied by *Swagelok* with the exception of the 6 port valves that were manufactured by *VICI* and supplied by *Anatech Instruments*. With the exception of the tubing used for removing a sample for composition analysis and pressure measurement, all tubing used in this study has an outer diameter (OD) of 3.175 mm or 1/8th in. and an internal diameter (ID) of 1.753 mm with a maximum operating pressure of 586 bar at a maximum operating temperature of 310 K. The tubing used for composition analysis and pressure measurements has and OD of 1.588 mm or 1/16th in. and an ID of 0.876 mm with a maximum operating pressure of 558 bar at a maximum operating temperature of 310 K. All tubing used is stainless steel.

The two-way (V3, V9 and V10) and three-way (V8, V13) ball valves used, shown in Figure 5 - 7 have a maximum operating pressure of 172 bar at a maximum operating temperature of 421 K. The four-way cross-over ball (V7 and V12) valves have a maximum operating pressure of 172 bar at maximum operating temperature of 338 K. The needle valves (V4 and V5) used have a maximum operating pressure of 236 bar at a maximum operating temperature of 505 K. All gas bottles were fitted with high pressure double stage gas regulators (V1 and V2) supplied by *Swagelok*. T-pieces, union crosses and other fittings were supplied by *Swagelok*.

The connection points (CP1, CP2 and CP3) in Figure 5 - 7 indicate quick connection points. A braided house was used to link the connection points. The quick connectors have maximum operating pressure of 206 bar at a maximum operating temperature of 310 K. The stems, bodies and braided hose were all supplied by *Swagelok*.

All ratings listed were as quoted by the manufacturer.

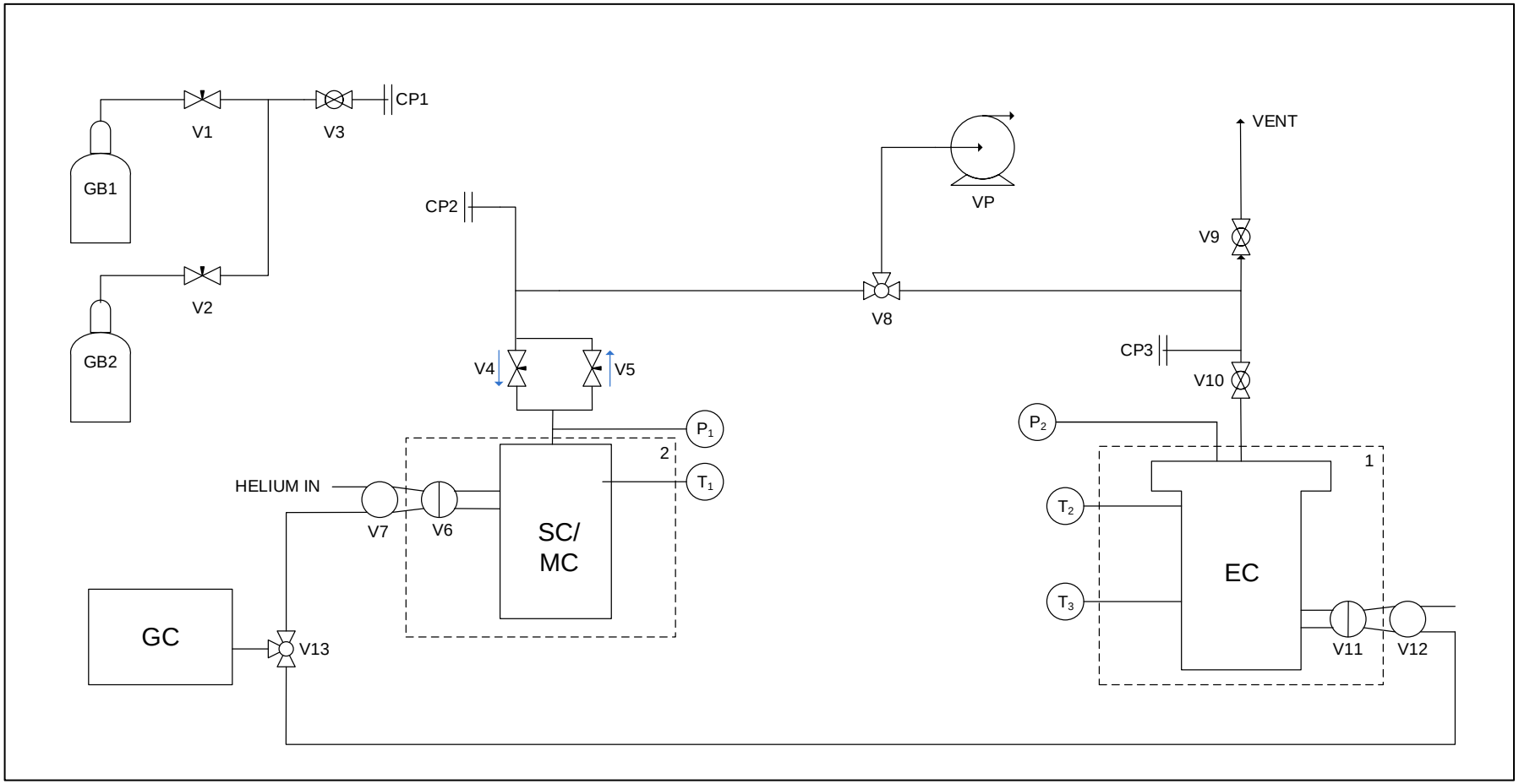

Figure 5 - 7: Experimental setup of the volumetric apparatus. CP, connection point; EC, equilibrium cell; GB, gas bottle; GC, gas chromatograph; MC, mixing cell; P, pressure indicator; SC, storage cell; T, temperature indicator; V, valve; VP, vacuum pump.

5.1.2. Volumetric Experimental Method

The volumetric apparatus was commissioned as part of this study. Commissioning of apparatus for the purpose of measuring gas-solid adsorption equilibria via the volumetric technique involved leak testing of the equipment; calibration of pressure, temperature and composition measurement devices; and undertaking vapour pressure measurements.

5.1.2.1. Leak Testing

Gas leaks are a considerable concern in the development of static apparatus. Leaks not only lead to erroneous results, but also pose a safety hazard in the case of hazardous gases. Leak testing was undertaken using three different techniques. The first and most simple technique involved charging the system with an inert gas at 20 bar. All valves and fittings were sprayed with Snoop®. In the event of a leak, the liquid formed bubbles at the leaking joint. The leaking joint or fitting was tightened or replaced if necessary. The second part involved maintaining the system under pressure at isothermal conditions. The cells were once again charged with an inert gas and observed for any change in pressure over 24 hours. A change less than the uncertainty in pressure was considered acceptable. The third technique involved charging the cell with helium and using a *Restek Electronic Leak Detector* to detect any points of leakage. Once the apparatus was determined to be gas tight at the design pressure, calibrations were undertaken.

5.1.2.2. Calibrations

5.1.2.2.1. Temperature

Temperature calibrations were undertaken using a standard Pt100 probe calibrated by WIKA. The probe is fitted to a WIKA CTB 9100 temperature calibration unit. The standard has an uncertainty of 0.03 K. The three probes used in this study were immersed in a silicon bath together with the standard. The bath temperature was ramped in 10 K increments from 293 K to 373 K then decreased in 10 K steps within the same range. The temperature was then increased again in the same increments. The temperature reading from the standard (referred to as T_{actual}) and the temperature reading from the probes used in this study (referred to as $T_{measured}$) were compared and fitted with a straight line correlation. The difference between the temperatures calculated using the model and the temperature measured using the standard is defined as ΔT in the figures below. The calibration curves showed a very strong linear trend, indicated by a correlation index (R^2) of unity, with no hysteresis observed.

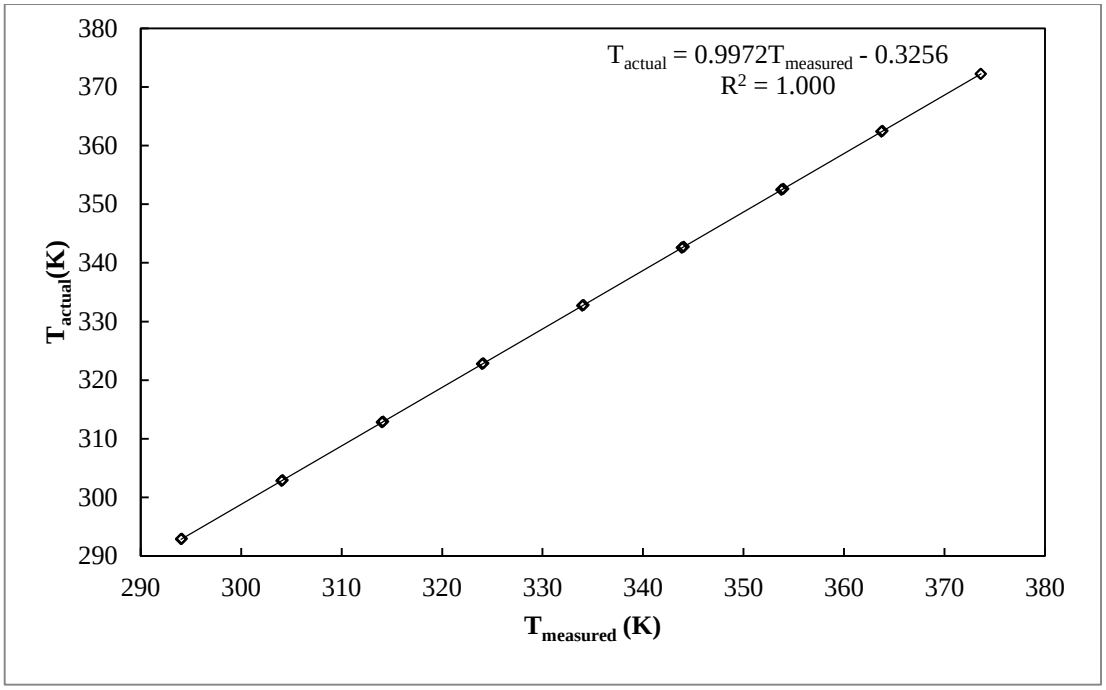

Figure 5 - 8: Temperature calibration curve for probe 1. The temperature reading from the standard, T_{actual} and the temperature reading from the probe used in this study, $T_{measured}$ were compared and fitted with a straight line correlation.

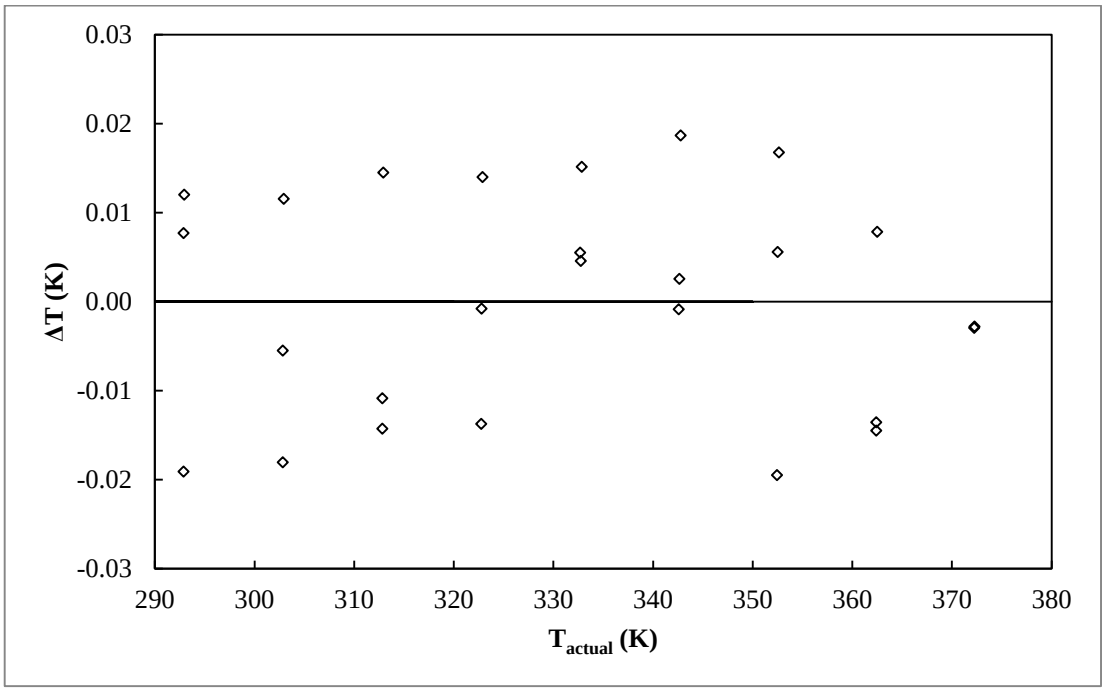

Figure 5 - 9: Temperature deviations for probe 1. ΔT is defined as the difference between the temperature calculated using the straight line correlation, determined from the calibration, and the temperature measured using the standard, T_{actual}.

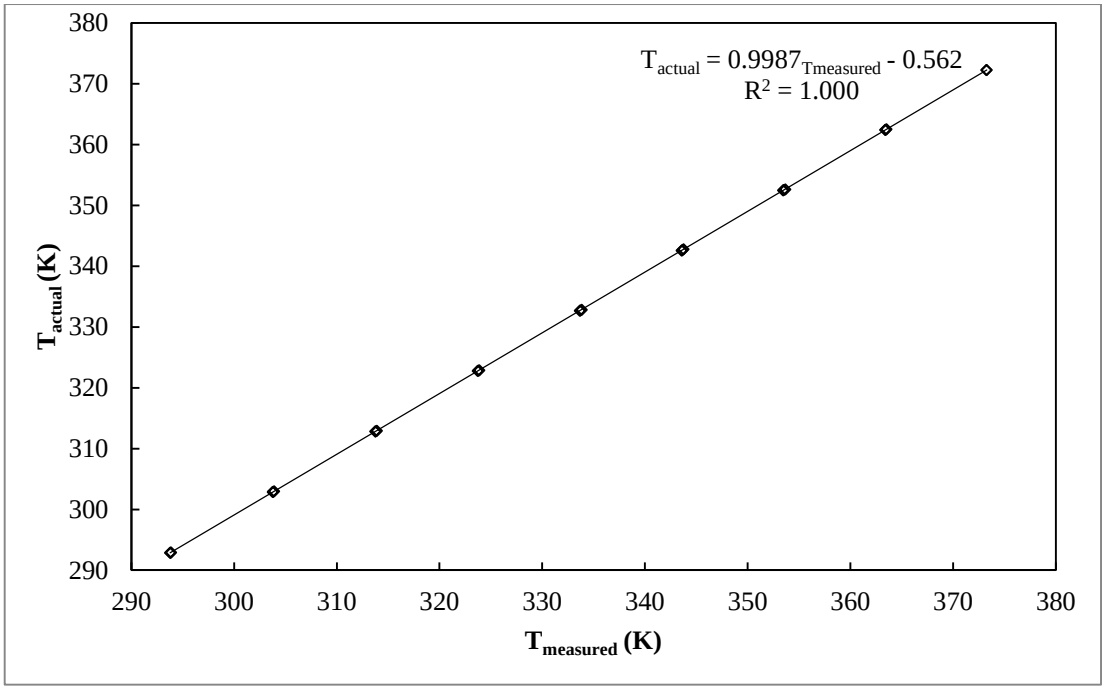

Figure 5 - 10: Temperature calibration curve for probe 2. The temperature reading from the standard, T_{actual} and the temperature reading from the probe used in this study, $T_{measured}$ were compared and fitted with a straight line correlation.

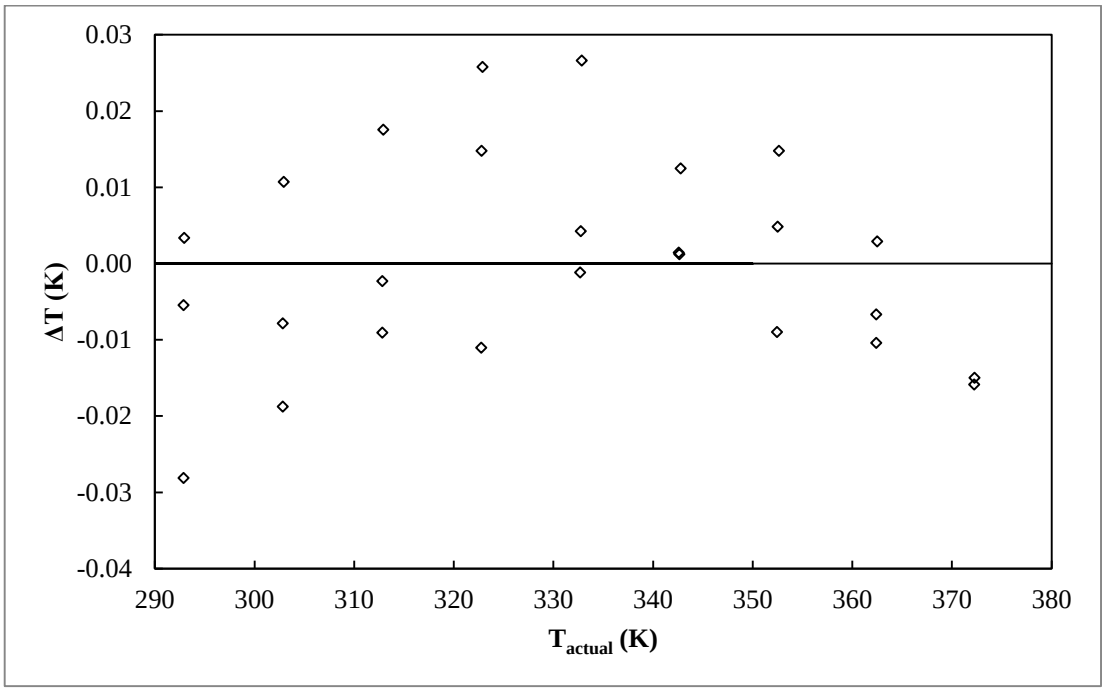

Figure 5 - 11: Temperature deviations for probe 2. ΔT is defined as the difference between the temperature calculated using the straight line correlation, determined from the calibration, and the temperature measured using the standard, T_{actual}.

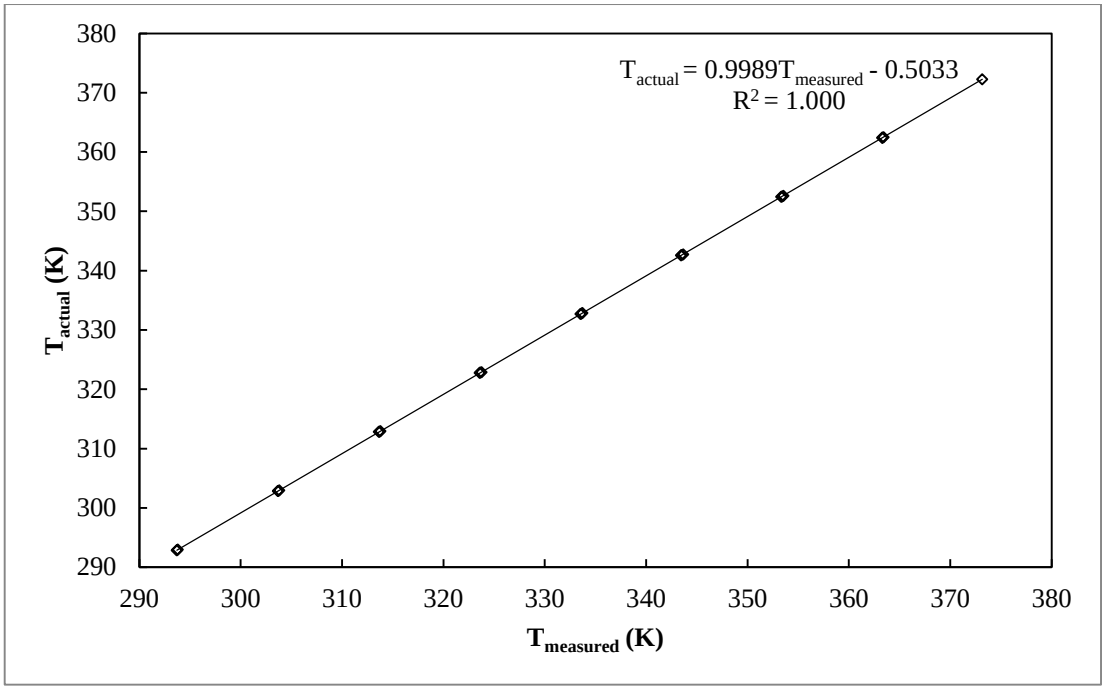

Figure 5 - 12: Temperature calibration curve for probe 3. The temperature reading from the standard, T_{actual} and the temperature reading from the probe used in this study, $T_{measured}$ were compared and fitted with a straight line correlation.

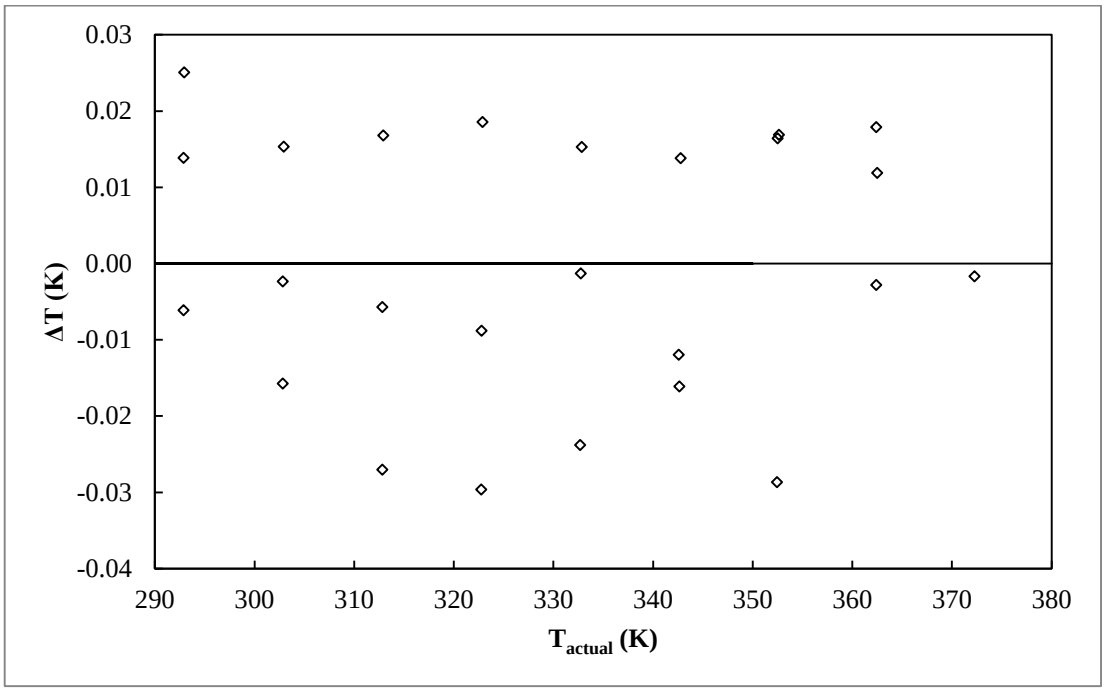

Figure 5 - 13: Temperature deviations for probe 3. ΔT is defined as the difference between the temperature calculated using the straight line correlation, determined from the calibration, and the temperature measured using the standard, T_{actual}.

Uncertainty from calibration

The uncertainty for temperature was determined using the methods outlined in Appendix G. The combined standard uncertainty is given by:

$$u_c(T) = \pm\sqrt{u_{rep}(T)^2 + u_{calib}(T)^2 + u_{grad}(T)^2} \qquad (5 - 1)$$

where

$$u_{calib}(T) = \pm\sqrt{u_{poly}(T)^2 + u_{st}(T)^2} \qquad (5 - 2)$$

Of concern here is the u_{calib} term. The repeatability and gradient contributions are discussed later. u_{poly} is determined using the calibration plots presented. All 3 residual plots were evaluated collectively and u_{poly} was taken as the maximum residual value of the 3 plots i.e. 0.04 K. The second term, u_{st}, is the uncertainty introduced by the standard. The standard has an uncertainty of 0.03 K. Using a rectangular distribution for u_{poly} and u_{st}, the uncertainty for the temperature calibration is thus 0.03 K. The overall uncertainties are discussed in Section 6.2. and Appendix G.

5.1.2.2.2. Pressure

Pressure calibrations were undertaken using two pressure standards. A standard 0-250 bar (gauge) pressure transducer as well as a standard 0-16 bar (absolute) pressure transducer were used. Both standards were calibrated by WIKA. Both standard transducers were fitted to the WIKA CPH 6000 digital calibrator multimeter. The standards have an uncertainty of 0.02 bar and 0.002 bar respectively. P_1 was calibrated in the range 0-100 bar using the 0-250 bar standard. P_2 was calibrated in the range 0-15 bar using the 0-16 bar standard and in the range 10-20 bar using the 0-250 bar standard. The overlapping calibration range was intentionally chosen to ensure linearity of the transducer across the combined calibration range. The cell was pressurised using nitrogen. The pressure reading from the standard (referred to as P_{actual}) and the pressure reading from the D-10-P used in this study (referred to as $P_{measured}$) were compared and plotted against each other. Adjustments for barometric pressure were made when using the 0-16 bar standard. Measured data were fitted with a straight line correlation as well as a quadratic equation correlation. The model that provided the better fit is presented. The equation of the respective fits is referred to as the model. The difference between the pressure calculated using the model and the pressure measured using the standard is defined as ΔP in the figures that follow.

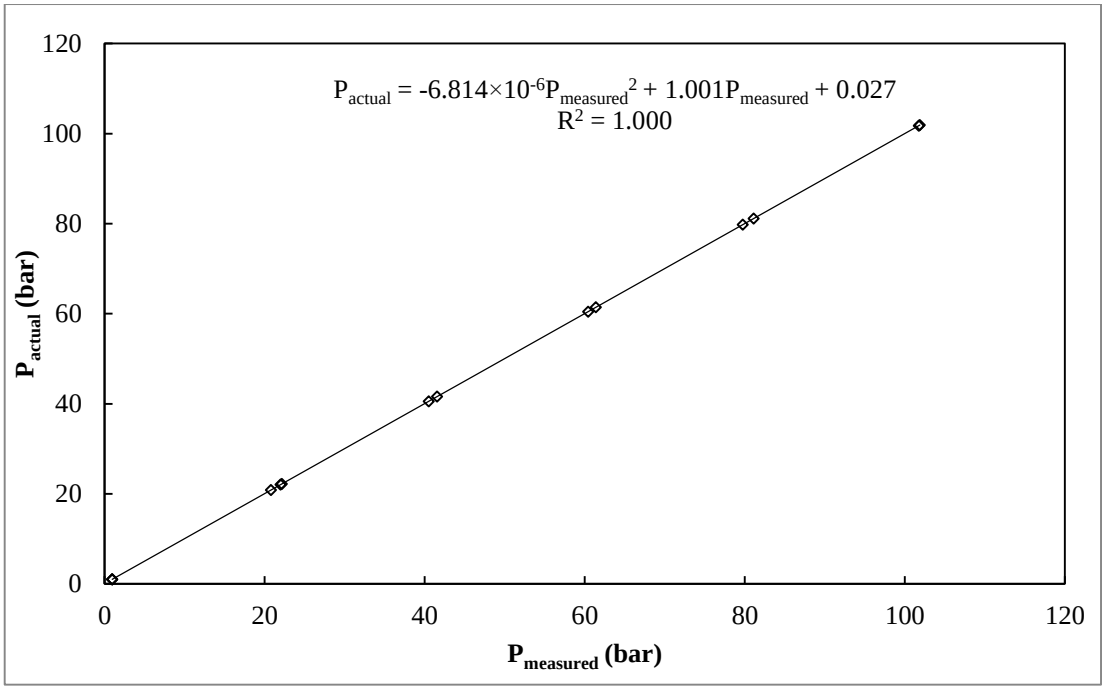

Figure 5 - 14: Pressure calibration curve (2nd Order) for transducer 1. The pressure reading from the standard, P_{actual} and the pressure reading from the transducer used in this study, $P_{measured}$ were compared and fitted with a quadratic correlation.

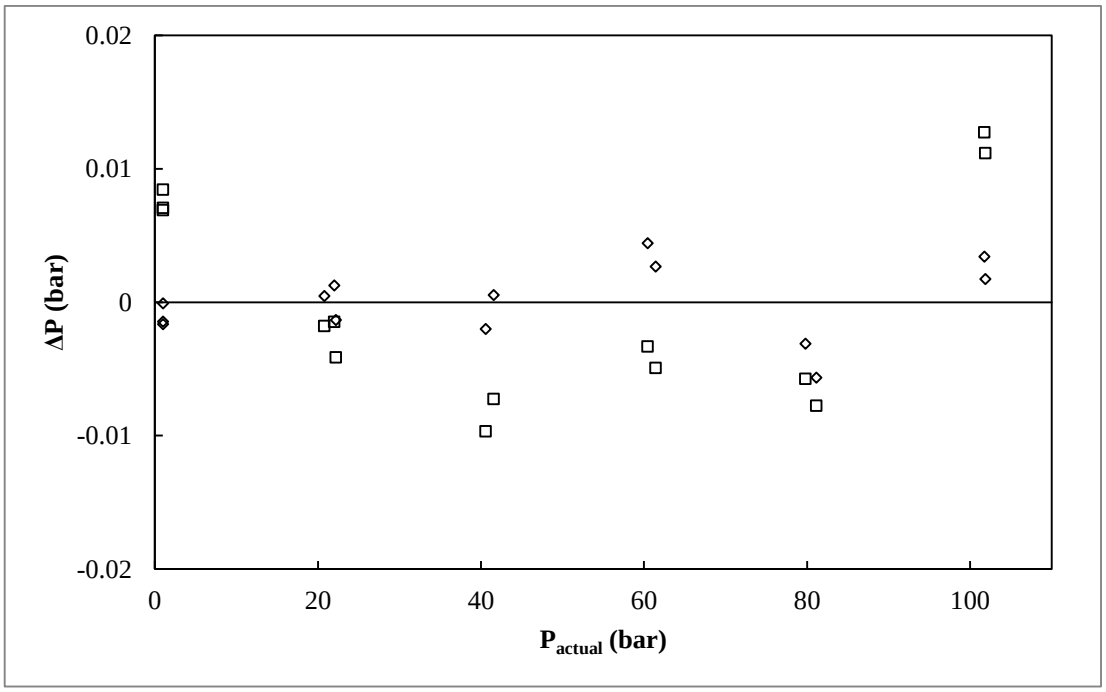

Figure 5 - 15: Pressure residuals for transducer 1; 1st order (□), 2nd order (◊). ΔP is defined as the difference between the pressure calculated using the straight line or quadratic correlation, determined from the calibration, and the pressure measured using the standard, P_{actual}.

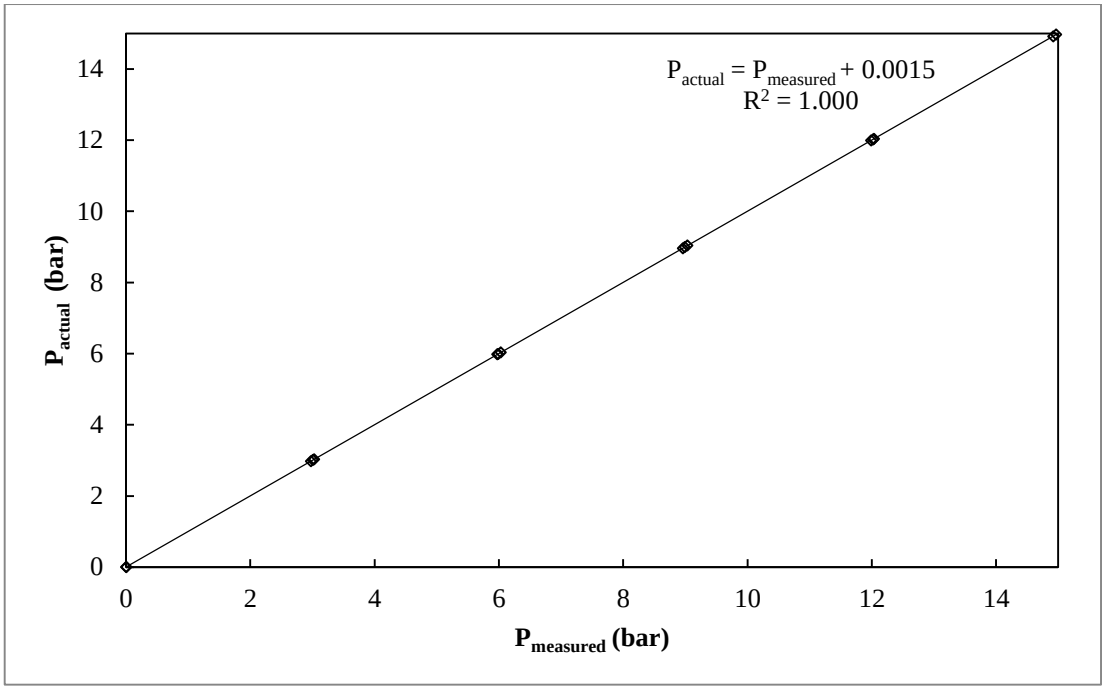

Figure 5 - 16: Pressure Calibration Curve for transducer 2 in the range 0-15 bar. The pressure reading from the standard, P_{actual} and the pressure reading from the transducer used in this study, $P_{measured}$ were compared and fitted with a straight line correlation.

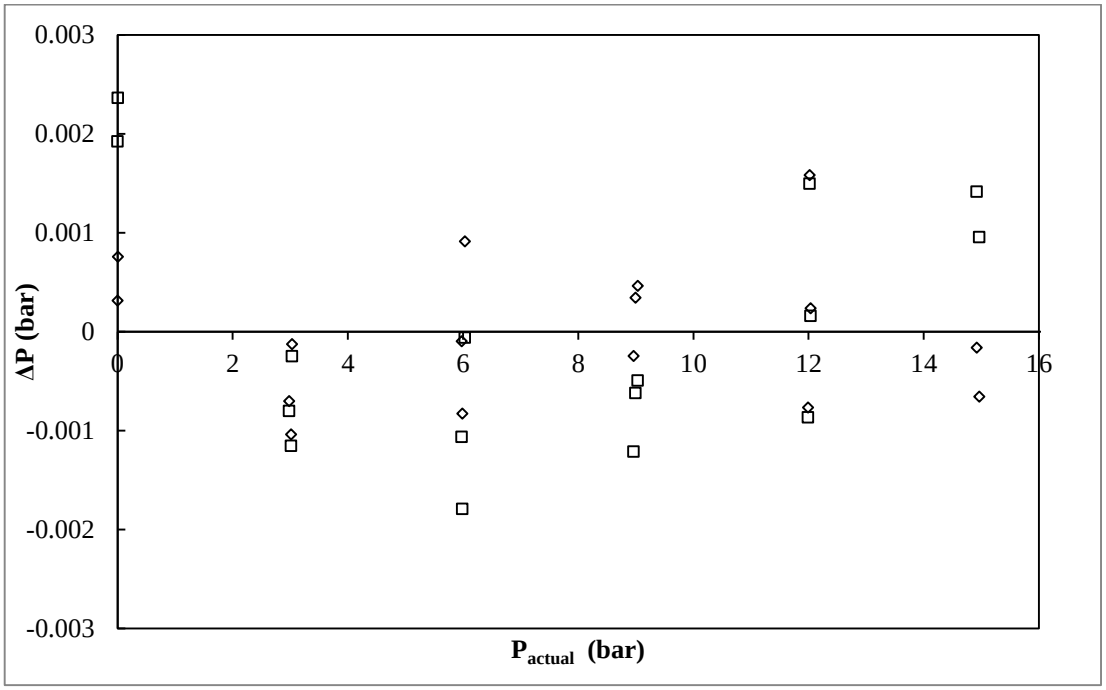

Figure 5 - 17: Pressure residuals for transducer 2 in the range 0-15 bar; 1st order (□), 2nd order (◊). ΔP is defined as the difference between the pressure calculated using the straight line correlation, determined from the calibration, and the pressure measured using the standard, P_{actual}.

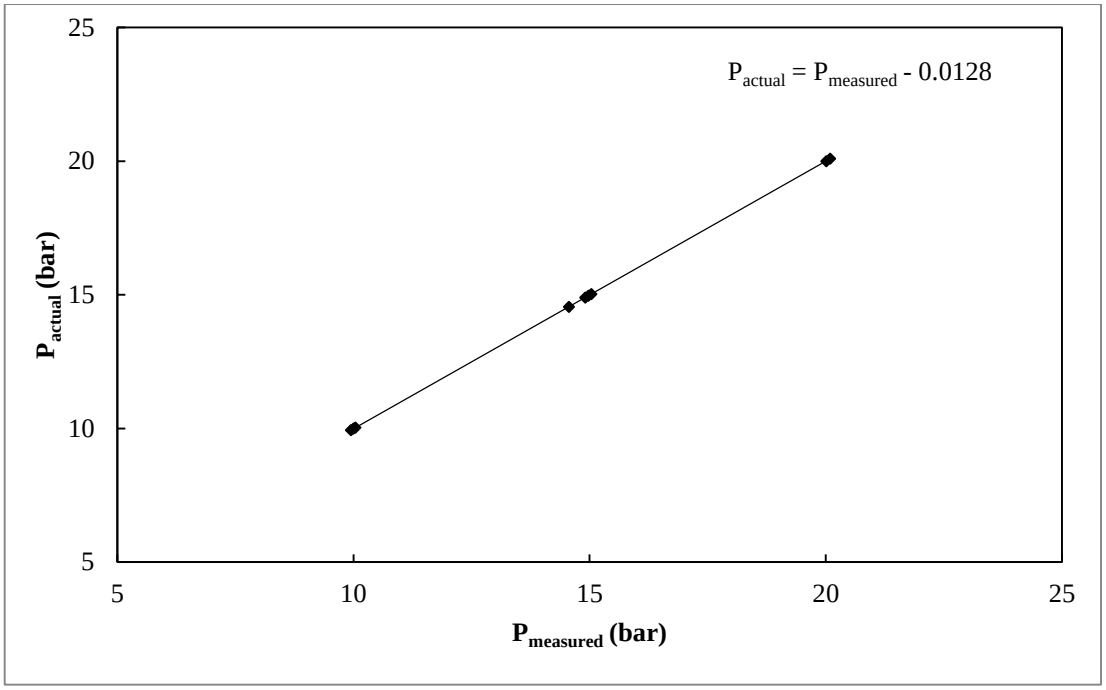

Figure 5 - 18: Pressure Calibration Curve for transducer 2 in the range 10-25 bar. The pressure reading from the standard, P_{actual} and the pressure reading from the transducer used in this study, $P_{measured}$ were compared and fitted with a straight line correlation.

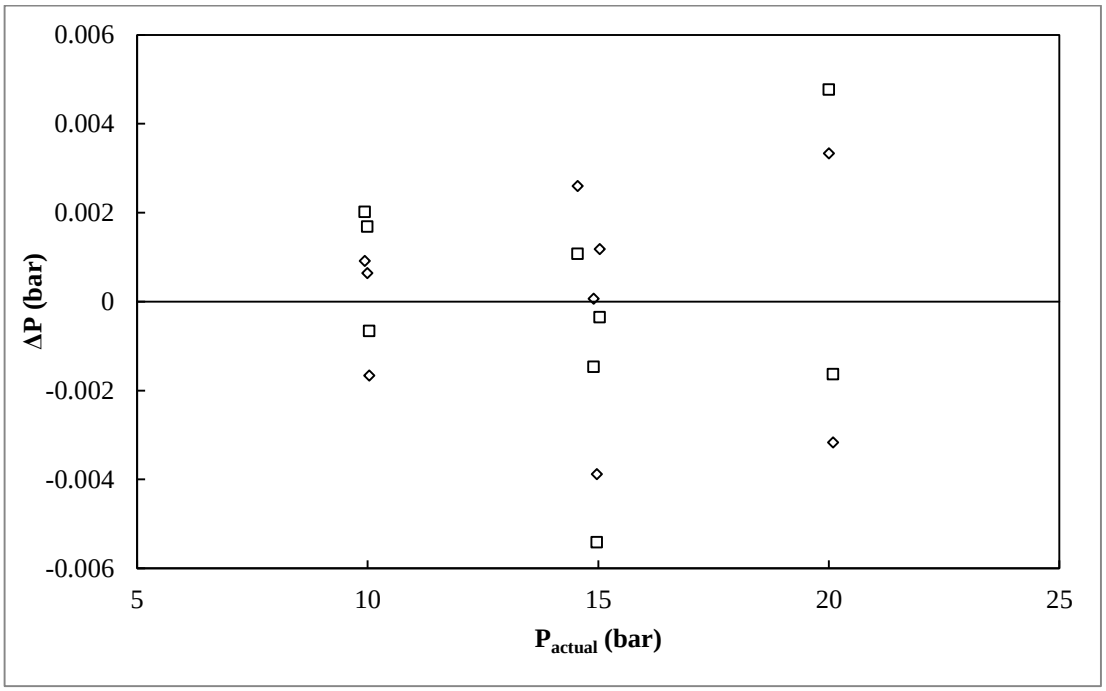

Figure 5 - 19: Pressure residuals for transducer 2 in the range 10-20 bar; 1st order (□), 2nd order (◊).*ΔP* is defined as the difference between the pressure calculated using the straight line correlation, determined from the calibration, and the pressure measured using the standard, P_{actual}.

The second order polynomial was selected as the model for P_1. The quadratic model provided a better fit as determined from the maximum residual indicated in the figure above. Linear models were selected for both calibration ranges for P_2. The quadratic models offered negligible improvement on the linear models as indicated in the residual plots.

Uncertainty in pressure calibration

Similarly to the calculation for temperature, of concern in this section is the uncertainty introduced by the calibration, given by:

$$u_{calib}(P) = \pm\sqrt{u_{poly}(P)^2 + u_{st}(P)^2} \qquad (5 - 3)$$

From the residual plots, u_{poly} for transducer 1 is 0.01; for transducer 2 the residuals are 0.003 and 0.006 for the ranges 0-15 bar and 10-20 bar respectively. The standard (0-16 bar) has an uncertainty of 0.002 bar. The uncertainty for the pressure calibration is thus 0.006 bar for transducer 1 and 0.002 bar for transducer 2 in the range 0-15 bar. The overall uncertainties are presented in Section 6.2.

5.1.2.2.3. Gas Chromatograph

Calibration of the gas chromatograph (GC) entailed calibration of the flame ionisation detector (FID). The FID produces peaks proportional to the amount of sample passing through the column at its retention time. The area obtained from integration of these peaks is related to the number of moles passing through the column by way of calibration

The detector was calibrated using the *area ratio method* as detailed in Raal and Mühlbauer (1998). The technique is typically used when calibrating the GC detector with liquid samples. However, in this study the use of a gas mixer enabled the preparation of gas mixtures with known composition. Standard mixtures were prepared gravimetrically using the Ohaus Explorer Pro EP6102 mass balance over the composition range and analysed. Samples were prepared by charging varying amounts of ethane and ethylene to the mixing cell. The gases were mixed for an hour. Ethane and ethylene have similar densities allowing a relatively short mixing time. A 100 μL sample of the binary mixture was removed from the gas mixer using a gas-tight syringe for analysis.

The sample injected into the GC yields 2 peaks with area ratio A_i/A_j. In the area ratio method method, Raal and Mühlbauer (1998) define a response factor, F_i as a proportionality constant between the number of moles of any component *i* passing the detector, n_i and its peak area, A_i.

$$n_i = F_i A_i \qquad (5 - 4)$$

Applying this technique for a binary system:

$$\frac{n_1}{n_2} = \left(\frac{F_1}{F_2}\right)\left(\frac{A_1}{A_2}\right) = \frac{y_1}{y_2} \qquad (5 - 5)$$

In practice, mole ratios (n_1/n_2) are more linearly proportional to area ratios (A_1/A_2) than number of moles n_1 to peak area A_1 in the presence of another component. The slope in each case is

determined using least squares linear regression. A smaller deviation is observed in the case of area ratios. In this study, response factor ratios were used with the limiting condition that at $y_i = 0, A_i = 0$. To validate this method of calibration curve, (y_1/y_2) *vs.* (A_1/A_2) was shown to pass through the origin thereby satisfying the aforementioned condition.
Five binary mixtures of ethane and ethylene were prepared and analysed. Mixtures were prepared using the gas mixer. The mixer was first evauated then charged with ethane and the mass recorded. Ethylene was then charged to the cell and the mass of the total gas present in the cell was measured. The amount of ethylene charged was determined by difference.

To reduce the uncertainties arising from the gravimetric measurements, the mixer was charged with as much gas as possible. For a binary mixture of 20% ethane at 25 bar present in the gas mixer at ambient temperature, this translates to approximately 5.7 g of ethane. The balance has an uncertainty of 0.07 g. for compositions below 25%, the uncertainty exceeded the exceptable value.

For each of the 5 mixtures, a minimum of 5 samples was analysed using the GC. The known compositions of the mixture, determined gravimetrically, were used to determine the concentration ratio, shown on the y-axis in the figure below. The area ratio shown on the axis was determined using the areas under the response peak for each gas.

Table 5 - 1: GC Settings used for calibration of ethane-ethylene system

GC Settings	
Capillary column	GS-GasPro
Column dimensions (L×I.D.)	30 m x 0.32 mm
Oven temperature (K)	308.15
Detector type	FID
Detector temperature (K)	523
Carrier gas	Helium
Carrier linear velocity (cm/s)	20

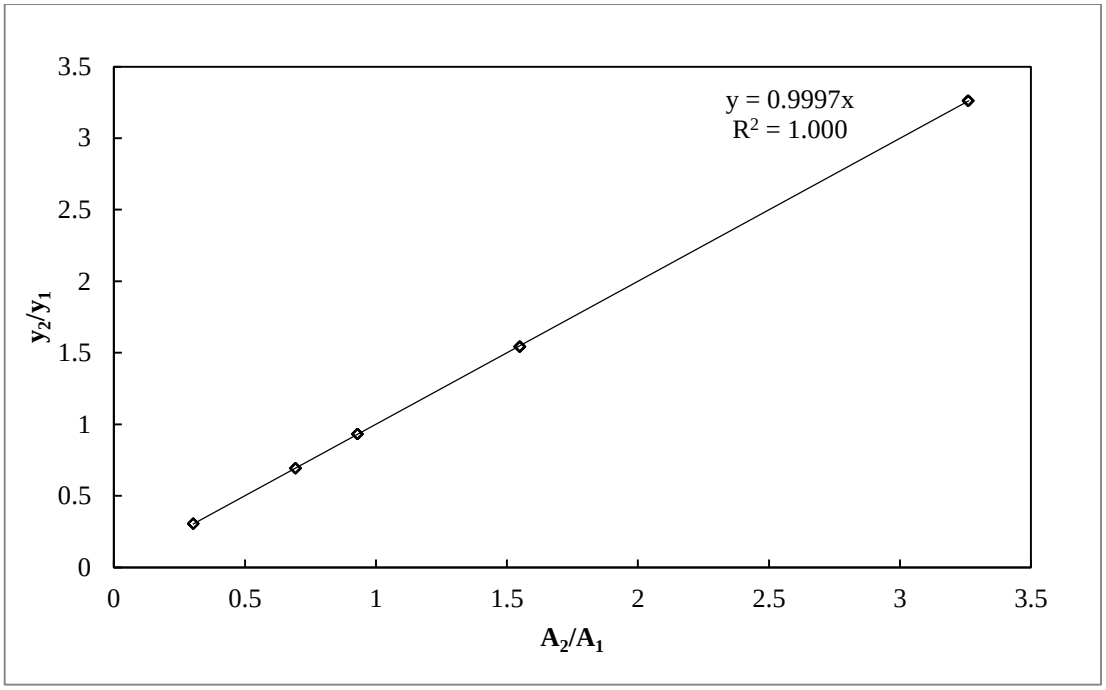

Figure 5 - 20: FID calibration curve for the ethane (1)/ethylene (2) system. The ratio of the known compositions of both components (y_2/y_1) is compared to the ratio of their GC peak areas (A_2/A_1).

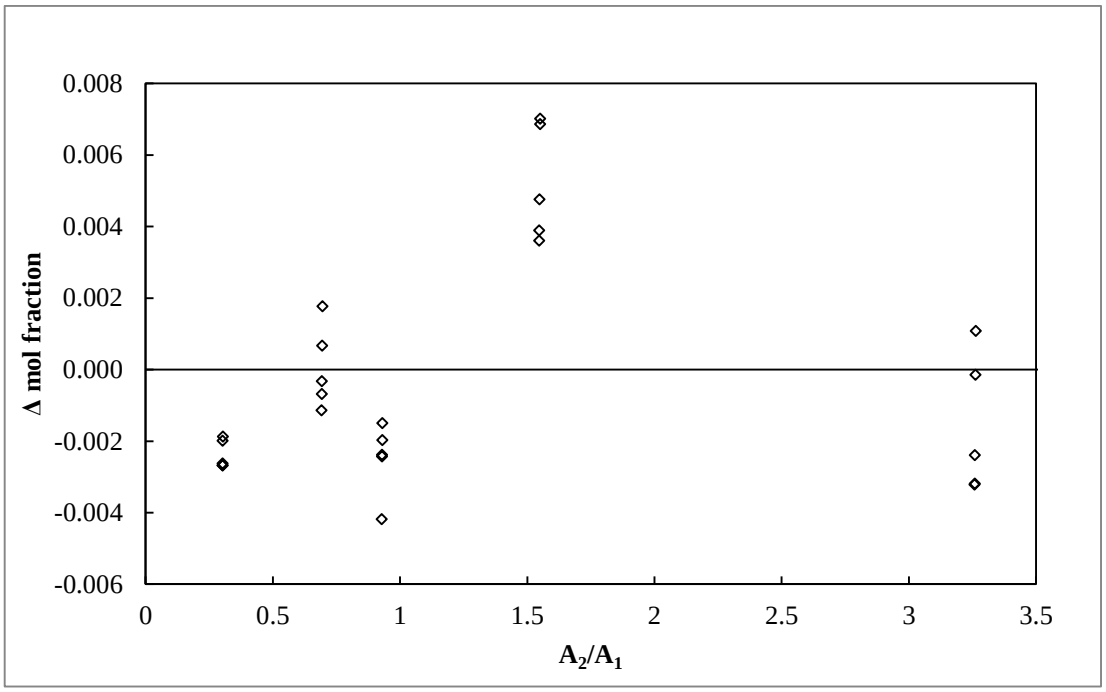

Figure 5 - 21: Residual plot for the FID calibration of the ethane (1)/ethylene (2) system. *Δ mol fraction is* defined as the difference between the composition ratio y_2/y_1 calculated using the straight line correlation, determined from the calibration, and the composition ratio determined experimentally.

Uncertainty in composition calibration

The standard uncertainty resulting from calibration is given by:

$$u_{calib}(y_i) = \pm\sqrt{u_{balance}(y_i)^2 + u_{poly}(y_i)^2} \qquad (5 - 6)$$

The uncertainty arising from the polynomial is taken as the maximum residual between the calculated (using the calibration polynomial) and true composition. The uncertainty contribution of the mass balance for a binary system is given by:

$$u_{balance}(y_i) = y_1 y_2 \sqrt{\left(\frac{u(m_1)}{m_1}\right)^2 + \left(\frac{u(m_2)}{m_2}\right)^2} \qquad (5 - 7)$$

where: $u(m_1) = u(m_2) = 0.07\ g$

The gravimetric results for each of the mixtures are presented below along with the uncertainty from the balance.

Table 5 - 2: Calibration Results for the system of ethane (1)-ethylene (2)

run	**1**		**2**		**3**		**4**		**5**	
species	1	2	1	2	1	2	1	2	1	2
m (g)	6.33	19.26	10.55	15.19	13.65	11.87	15.93	10.30	20.86	5.94
n (mol)	0.211	0.687	0.351	0.541	0.454	0.423	0.530	0.367	0.694	0.212
y (%)	23.5	76.5	39.3	60.7	51.8	48.2	59.1	40.9	76.6	23.4

From the residuals plot, the uncertainty from the calibration polynomial is 0.007 mole fraction. Applying Eq. (5 - 6) u_{calib} is thus 0.007 mole fraction.

GC calibration of systems involving gases is typically undertaken using the *direct injection method* (Raal and Mühlbauer, 1998). However in this study the *area ratio method* (Raal and Mühlbauer, 1998) was used instead. This was due to poor peak area reproducibility using direct injection of pure component gas. However, the area ratios for a binary mixture were reproducible. Poor peak reproducibility using the direct injection technique indicates a difference in the number of moles passing through the column with each injection. Temperature, pressure and volume variations could result in varying number of moles. Gas pressure in the syringe before injection is assumed to be atmospheric pressure. It is assumed that the gas in the syringe, regardless of the withdrawal pressure from the cylinder escapes through the needle until the gas in the syringe is at atmospheric pressure. As it is very difficult, if not impossible, to exactly measure the gas pressure within the syringe before injection, this assumption is the best way forward. Temperature variations within the syringe may occur due to operator handling. Heat from the hand may warm up the syringe thus raising the temperature of the gas from the assumed room temperature. Perhaps the largest constributor to poor peak area reproducibility is variation in volume. Dead volume in the syringe, gas adsorption/absorption on the walls of the syringe and manufacturer imperfections could all result in a volume different to that indicated on the syringe

being injected into the GC. Thus, when applicable, the *area ratio method* (Raal and Mühlbauer, 1998) is considered a superior method of calibration.

5.1.2.3. Vapour Pressure Measurements

Vapour pressure measurements were undertaken to verify the temperature and pressure calibrations of the instrumentation fitted to the equilibrium cell. The experimental data were compared to literature to check the calibrations. The procedure used to measure vapour pressure is outlined.

Prior to undertaking the vapour pressure measurements, the equilibrium cell was evacuated at the maximum measurement temperature for a period of 12 hours. This was done to remove any air that may have absorbed/adsorbed onto the Viton O-ring used to seal the equilibrium cell. The evacuation was followed by a flushing step, where the chemical used to undertake vapour pressure measurements was used to flush the system several times. The system was evacuated after each flushing stage.

The chemicals for which vapour pressure measurements were undertaken are gases at ambient conditions. To obtain a liquid phase, the equilibrium cell was cooled to 278 K before charging it with the gas. As it was not possible to view the contents of the equilibrium cell, an alternative method was used to determine the presence of a liquid phase. The equilibrium cell was charged for 30 seconds with a feed pressure of 10 bar (propylene) and 6 bar (R134a). The vapour pressure within the cell was recorded (P_0). A small amount of gas was vented from the equilibrium cell (a quick open-shut movement of the valve) causing a drop in the pressure to P_1. In the presence of a liquid, the pressure in the cell should return to a reading close to P_0 (the presence of volatile impurities results in a slightly lower pressure reading), P_2. See Figure 5 - 22.

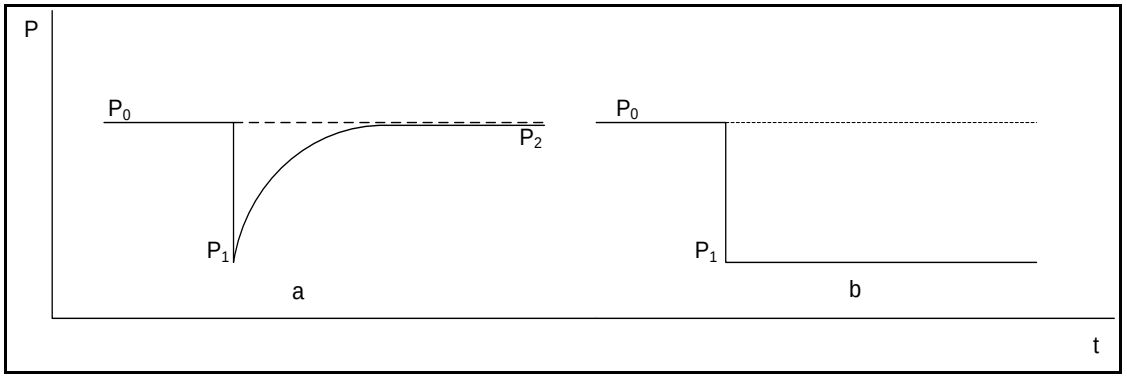

Figure 5 - 22: Illustration of the method used to determine presence of a liquid phase during vapour pressure measurements; the presence of liquid is shown by a on the left, the figure on the right indicates no liquid phase present.

The purity of both chemicals used was checked using a gas chromatograph. Both chemicals contained impurities that were more volatile. The impurities were removed by venting off at 323 K- the maximum temperature in the vapour pressure measurement range investigated in this study. Measurements were undertaken between 293 K and 323 K in 5 K increments. Degassing was undertaken as follows. A small amount of gas was vented from the equilibrium cell. The pressure of the vapour was measured before and after venting, once the vapour phase built up. This procedure of venting and recording the pressure was repeated until the pressure readings were the same before and after the vent i.e. $P_n = P_{n-1}$.

Table 5 - 3: Analysis of chemicals used for vapour pressure measurements.

	Propylene	**R134a**
Quoted purity (%)	99.5	-
GC Peak Area (%)	99.7	99.6
GC Analysis		
Packed column	Restek 5% Krytox CBK-B	Poropak Q 80/100 mesh
Column dimensions (L× I.D.)	3 m x 2 mm	4 m x 3.17 mm
Column temperature (K)	318.15	473.15
Detector type	TCD	TCD
Detector temperature (K)	473.15	498.15
Carrier gas	Helium	
Carrier flow rate (mL/min)	20	30

Experimentally obtained data were compared to literature data. The *Extended Antoine Equation* was used in this study to calculate vapour pressure as a function of temperature using literature data. The equation is given by (Poling et al., 2001):

$$log\, P_{vap} = A - \frac{B}{T + C - 273.15} + 0.43429x^n + Ex^8 + Fx^{12} \qquad (5 - 8)$$

where:

$$x = \frac{T - t_0 - 273.15}{T_c} \qquad (5 - 9)$$

Table 5 - 4: Extended Antoine parameters and limits (Poling et al., 2001).

	Propylene	**R134a**
A	3.95606	4.11874
B	789.62	850.881
C	247.58	232.99
T_c (K)	365.57	374.26
t_0	-41	-20
n	2.67417	2.39793
E	22.13	31.124
F	-199.34	2784.8
P_{min} (bar)	1.74	2.44
T_{min} (K)	238.15	268.15
P_{max} (bar)	44.67	39.69
T_{max} (K)	363.15	373.15

5.1.2.4. Adsorbent preparation and loading

Adsorption measurements were carried out using Zeolite 13X that were generously donated by CECA S.A. A BET surface area analysis was carried out using a Micromeritics TriStar II Surface Area and Porosity Analyser with TriStar II 3020 v1.03 software. The adsorbent has a surface area of 524±10 m^2/g and a pore volume of 0.420±0.008 cm^3/g. The loading procedure of Loughlin et al. (1990) and Choi et al. (2003) informed the loading process used in this study. A sample of the zeolites was loaded into a glass flask that was then held under vacuum, approximately 0.002 bar, and immersed in an ethylene glycol bath at a temperature of 373 K. This was done for 24 hours to remove moisture from the air that would have adsorbed onto the zeolite. The mass of the empty flask under vacuum was measured prior to loading the adsorbent. After the 24 hour period, the mass of the flask with dry adsorbent was measured. The zeolite was then transferred to the equilibrium cell. The cell was maintained at a temperature of 373 K under vacuum, approximately 0.002 bar, for a further 24 hours to remove any moisture adsorbed during the transfer process. A single sample of 94.90 g was used for all the adsorption measurements.

5.1.2.5. System Volume

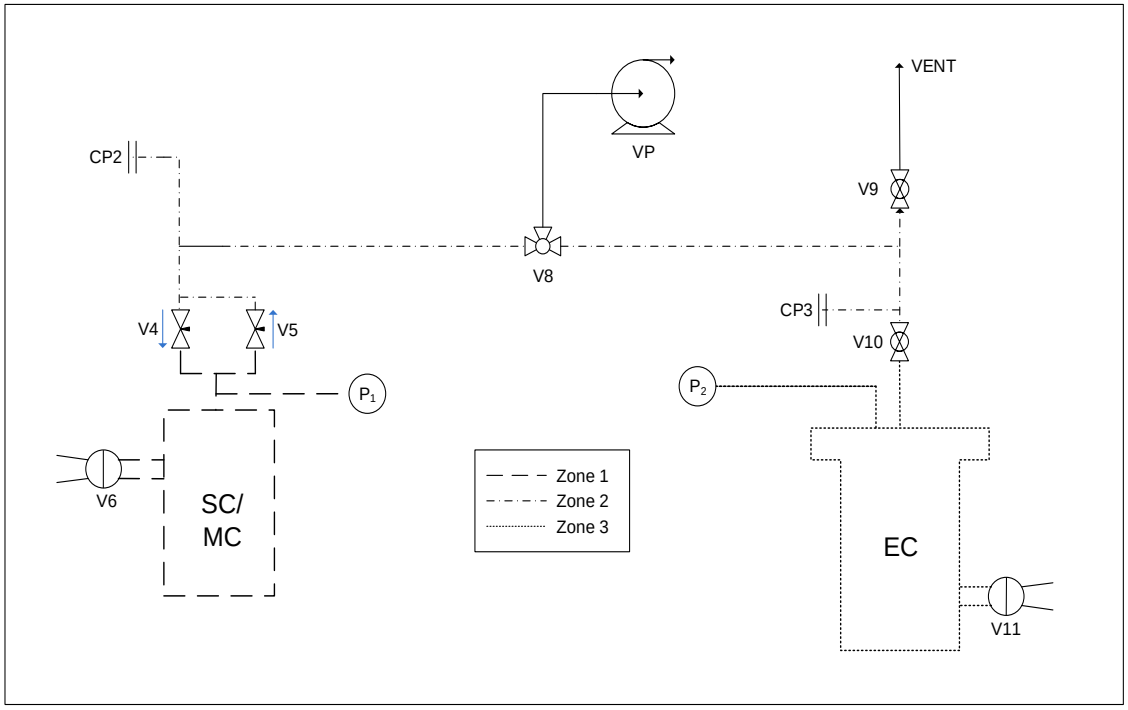

Figure 5 - 23: Schematic detailing different areas of the volumetric apparatus for which volume measurements were undertaken. EC, equilibrium cell; GB, gas bottle; GC, gas chromatograph; MC, mixing cell; P, pressure indicator; SC, storage cell; T, temperature indicator; V, valve; VP, vacuum pump.

The volumetric technique requires the volume of the system to be known prior to commencing with the equilibrium measurements. The experimental set-up was divided into three zones when determining the volume of the system, shown in Figure 5 - 23. The storage cell and its immediate fill lines (including the line to the pressure transducer) was labelled zone 1. The fill lines between the storage cell and equilibrium cell was labelled zone 2 and the equilibrium space (with the adsorbent present in the cell) was labelled zone 3.

The volume of zone 1 was determined using mass and density measurements of water. The storage cell was charged to capacity with ordinary tap water at ambient conditions and weighed. The mass of the empty cell was recorded prior to the charging; hence the mass of water was calculated by difference. The density of the water at experimental conditions was measured using an Anton Paar DMA 5000 Density Meter. Mass measurements were undertaken using an Ohaus Explorer mass balance. This procedure was carried out 5 times. The volume of the cell is 987 ± 1 cm^3.

The volume of zones 2 and 3 was determined using helium displacement. It was assumed that helium does not adsorb appreciably onto the zeolite. The storage cell was charged with a known amount of helium (determined using PVT measurements). The helium was expanded into zones 2 and 3 using a fine control needle valve (V5) to the desired pressure. The number of moles charged to zones 2 and 3 was equal to the number of moles that left zone 1. As the number of moles present in zones 2 and 3 was now known, together with the temperature and pressure, the collective volume was obtained using an EoS. To determine them individually, zone 3 was isolated from zone 2 which was evacuated. The helium in zone 3 was then expanded into zone 2, causing a drop in the pressure (PI_2). The volumes were thus calculated individually. When charged with 94.90 g of zeolite 13X, the equilibrium space has a volume of 290.35 mL.

5.1.2.6. Equilibrium Adsorption Measurements

The purity of the gases used to perform adsorption measurements were verified using a gas chromatograph. A Shimadzu GC 2014 fitted with a capillary column and Flame Ionisation Detector (FID) was used. The results are presented in Table 5 - 5. Ethane and ethylene were supplied by *Air Products South Africa* and *Afrox* respectively.

Table 5 - 5: Analysis of chemicals used for adsorption measurements.

	Ethane	**Ethylene**
Quoted purity (%)	99.99	>99.9
GC Peak Area (%)	99.99	99.98
GC Analysis		
Capillary column	GS-GasPro	GS-GasPro
Column dimensions (L×I.D.)	30 m x 0.32 mm	30 m x 0.32 mm
Column temperature (K)	308.15	308.15
Detector type	FID	FID
Detector temperature (K)	523	523
Carrier gas	Helium	
Carrier linear velocity (cm/s)	20	20

5.1.2.6.1. Pure Gas Isotherms

The technique used to measure the adsorption isotherms is similar to that used to determine the apparatus volume. After completion of the volume measurements (above), the adsorbent was regenerated at a temperature of 373 K under vacuum, approximately 0.002 bar, for 24 hours. The bath was then set to the measurement temperature (either 298 K or 323 K). Pure gas is charged to the storage cell from the gas cylinder. Ethane and ethylene were used for pure component measurements. The change in pressure of the gas in the storage cell was used to determine the number of moles charged to the storage cell.

The gas was then expanded into the equilibrium cell until the desired pressure was reached. A fine control needle valve was used to control the pressure of the equilibrium cell. The system was allowed to reach equilibrium- indicated by a stable pressure reading. Equilibrium was typically reached in 3 to 5 hours. During the process of adsorption a pressure drop occurred as gas molecules left the adsorptive phase and entered the adsorbent.

At equilibrium the pressure and temperature of the gas within the equilibrium cell was recorded. The mass of gas charged to the equilibrium cell was determined from the change in pressure of the gas in the storage cell. The PREoS was used to determine the mass of gas present in the gas phase in the equilibrium cell at equilibrium. The amount of gas adsorbed was calculated by difference.

5.1.2.6.2. Binary Isotherms

For a binary system, the measurement technique is more complicated. The introduction of a new component to the system introduces an additional degree of freedom. Hence another variable must be fixed. It was decided to fix the equilibrium pressure of the system. Thus the binary adsorption equilibria were measured isothermally and isobarically. Binary gas mixtures were prepared in the mixing cell and charged to the equilibrium cell. The charging procedure for the binary system differs from the pure component measurements. To ensure isobaric conditions, the following procedure is followed. The gas mixture is charged to the equilibrium cell to the desired equilibrium set point, $P^{SP}_{eq.}$ Due to the gas adsorbing, the equilibrium pressure will drop to P^{2}_{eq} (see Figure 5 - 24). More gas is then charged to the equilibrium cell to the desired equilibrium set point, P^{SP}_{eq}. However, this time the drop in equilibrium will be less pronounced. The process of adding more gas and waiting for the attainment of equilibrium is repeated until the drop in pressure is no longer appreciable and the set point, P^{SP}_{eq} is achieved.

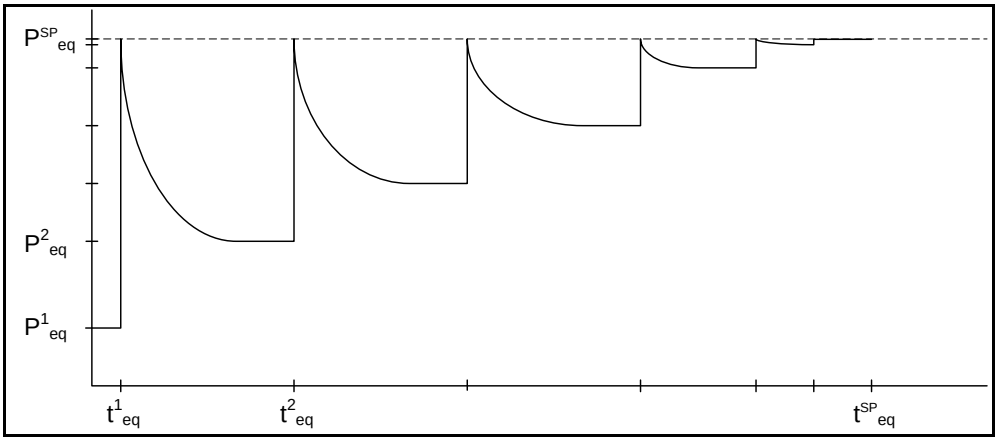

Figure 5 - 24: Illustration of technique used to charge binary gas mixtures to the equilibrium cell.

The attainment of a single binary adsorption data point took approximately 12 hours. This was due to the nature of the measurements – isobaric. This is of course, not accounting for the regeneration between experiments. The time-consuming nature of the measurement of isobaric, isothermal binary adsorption equilibria has already been mentioned, and was illustrated in this study. For this reason, only one binary system was measured.

5.1.2.6.3. Regeneration and Venting

The same sample of adsorbent was used to undertake all measurements. The zeolite was regenerated at a temperature of 373 K for 24 hours under vacuum, approximately 0.002 bar.

5.1.3. Operability and Safety of the Volumetric Apparatus

The volumetric experimental technique was designed with a strong emphasis on safety and operability. Safety precautions were taken to protect the researcher as well as the apparatus. Some of these aspects are:

- All valves and fittings selected have a pressure and temperature rating considerably higher than the operating conditions (20 bar and 373 K) of the apparatus. The system was designed with a +50% safety factor.
- The pressure transducers used had a 200% over-pressure safety feature.
- A vent valve was installed (V9) to release the gas in the event of pressure build-up in the apparatus. The apparatus was housed in an extraction unit.
- The tanks of the flammable gases used in this study viz, methane, ethane, ethylene, propylene and hydrogen were kitted with flashback arrestors.

The start-up, operation and shut-down of the volumetric apparatus is a routine process. A detailed procedure is provided for the measurement of vapour pressure, adsorbent volume as well equilibrium adsorption measurements.

Vapour Pressure Measurement

See Figure 5 - 7

1. Bath 2 was set to 323 K and it was ensured that all the valves of the apparatus were closed.
2. Connection Point 1 (CP1) was connected to CP3.
3. Valves V8 and V10 were opened to evacuate the equilibrium cell.
4. The evacuation was undertaken for 12 hours, upon which valves V8 and V10 were closed.
5. Bath 2 was set to 278 K.
6. Valves V1 and V3 were opened.
7. Valve V10 was opened for a period of 5 seconds to fill the equilibrium cell. Valves V1, V3 and V8 were then closed.
8. The equilibrium cell contents was vented under an extraction unit by opening valves V9 and V10.
9. Valve V9 was closed and V7 was opened to evacuate the equilibrium cell. The equilibrium cell was held under vacuum for a minimum of ten minutes. Valve V7 was closed.
10. Steps 7-9 were repeated a further 4 times to flush the system of any impurities that may have been present.
11. The equilibrium cell was then charged by opening valves V1 and V3 and the V8 for a period of 30 seconds. At 278K propylene and R134a liquefied upon entering the equilibrium cell. Valves V1, V3 and V8 were closed.
12. Bath 2 was set to 323 K.

13. Valve V9 was opened. V10 was then opened for a second or less to vent the volatile impurities that were present in the propylene and R134a. This step was repeated several times to remove the volatile impurities.
14. Upon removing the volatile impurities and achieving equilibrium (indicated by a constancy in pressure), the temperature (T_2, T_3) and pressure (P_2) of the equilibrium cell was recorded.
15. The temperature of bath 2 was decreased in 5 K decrements. P_2, T_2, T_3 was recorded each time upon achieving equilibrium. .
16. Step 15 was repeated until a final set point of 298 K was reached.

Adsorbent Volume Measurement

See Figure 5 - 7

1. The water bath (1) and ethylene glycol bath (2) were set to 303 K and 298 K respectively.
2. It was ensured that all the valves of the apparatus were closed. The adsorbent was weighed and charged to the equilibrium cell. The equilibrium cell was held under vacuum at 373 K for 24 hours before commencing with the adsorbent volume measurement.
3. Connection Point 1 (CP1) was connected to CP2.
4. The storage cell and fill lines were evacuated by opening/closing valves V3, V5 and V8.
5. Helium was charged to the storage cell by opening valves V1 and V3. The needle valve, V4 was used to control the amount of the helium charged to the storage cell. Valves V1, V3 and V4 were closed once the set point was reached.
6. CP2 was disconnected from CP1 and connected to CP3.
7. Valve V8 was opened to evacuate all fill lines. The equilibrium cell, having undergone a 24 hour evacuation, did not need to be evacuated again. Valve V8 was closed.
8. The initial temperature and pressure of the storage cell (T^i_1,P^i_1) and equilibrium cell(T^i_2, T^i_3, P^i_2) was recorded.
9. Valve V10 was opened to charge the equilibrium cell with helium. The needle valve V5 was used to charge the equilibrium cell to the desired pressure (P^f_2). V10 was closed upon charging the equilibrium cell.
10. Upon achieving equilibrium, the final temperature and pressure of the storage cell (T^f_1,P^f_1) and equilibrium cell(T^f_2, T^f_3, P^f_2) was recorded.
11. The amount of gas charged to the equilibrium cell from the storage cell was determined using:

$$n_{charged} = \frac{P_1^i V_1}{Z_1^i R T_1^i} - \frac{P_1^f V_1}{Z_1^f R T_1^f} \qquad (5\text{-}10)$$

The temperature readings recorded at the top and bottom of the cell are averaged, and given by T^f_γ. The volume of the equilibrium cell charged with adsorbent is thus:

$$V_2 = \frac{Z_2^f n_{charged} R T_\gamma^f}{P_2^f} \qquad (5\text{-}11)$$

Equilibrium Adsorption Measurement

See Figure 5 - 7

Pure Gas Isotherms

The procedure for measuring pure gas adsorption was similar to that used to measure the volume of the equilibrium cell. The following procedure was followed:

1. Both baths were set to the desired temperatures and all the valves were inspected and confirmed to be closed.
2. CP1 was connected to CP2.
3. Valves V3, V5 and V8 were opened to evacuate the storage cell and fill lines and closed upon completion of the evacuation step.
4. Ethane/Ethylene was charged to the storage cell by opening valves V1 and V3. The needle valve, V4 was used to control the amount of the helium charged to the storage cell. Valves V1, V3 and V4 were closed once the set point was reached.
5. CP2 was disconnected from CP1 and connected to CP3.
6. Valve V8 was opened to evacuate all fill lines. The equilibrium cell, having undergone a 24 hour evacuation, did not need to be evacuated again. Valve V8 was closed.
7. The initial temperature and pressure of the storage cell (T^i_1, P^i_1) and equilibrium cell(T^i_2, T^i_3, P^i_2) was recorded.
8. Valve V10 was opened to charge the equilibrium cell with ethane/ethylene. The needle valve V5 was used to charge the equilibrium cell to the desired pressure. V10 was closed upon charging the equilibrium cell.
9. Upon achieving equilibrium, the final temperature and pressure of the storage cell (T^f_1, P^f_1) and equilibrium cell(T^f_2, T^f_3, P^f_2) was recorded.
10. The amount of gas charged to the equilibrium cell from the storage cell was determined using:

$$n_{charged} = \frac{P_1^i V_1}{Z_1^i R T_1^i} - \frac{P_1^f V_1}{Z_1^f R T_1^f} \qquad (5\text{-}12)$$

11. The volume of the equilibrium cell is known (V_2), the experimental technique has been discussed. The mass of gas adsorbed is thus given by:

$$m^a = \frac{n_{charged} MM - \rho^g \left(V^t - V_{He}^{ad}\right)}{1 - \frac{\rho^g}{\rho_0^L}} \qquad (5\text{-}13)$$

where MM and ρ^g represents the molar mass and density of the gas being adsorbed. The liquid density of ethane and ethylene at the respective normal boiling points was used as ρ^L_0. The development of Eq. (5 -13) is discussed in Chapter 4.

Binary Isotherms

The measurement of binary gas isotherms required a gas mixture to be prepared in the mixing cell. The procedure for preparing the binary gas mixtures is presented. The rest of the measurement technique is as described for the pure component measurements with the addition of composition analysis.

Binary gas filling

1. CP1 was connected to CP2.
2. Valves V3, V5 and V8 were opened to evacuate the mixing cell and fill lines and closed upon completion of the evacuation step.
3. Valve V1 was opened to admit gas A. The needle valve, V4 was carefully controlled to fill the mixing cell with the desired amount of component A (indicated by P_A). V1 and V4 were closed when the desired amount of gas A was charged to the mixing cell.
4. Valve V8 was opened to evacuate the fill lines to the mixing cell. Valve V2 was opened to admit gas B. The needle valve, V4 was carefully controlled to fill the mixing cell with the desired amount of component B (indicated by P_B). V2, V3 and V4 were closed when the desired amount of gas B was charged to the mixing cell.
5. The gas mixer was then switched into operation. Upon achieving a homogenous binary mixture, a sample was removed from the mixing cell for composition analysis. The feed gas composition was needed to determine the amount of each component *i* adsorbed. The binary mixture was charged to the equilibrium cell using the same procedure as that of the pure component measurements.

5.2. Gravimetric Apparatus and Experimental method used in this study

5.2.1. Intelligent Gravimetric Analyser (IGA)

The IGA, constructed by Hiden Isochema Analytical Ltd, is an apparatus designed to undertake various types of sorption analysis. Analysis is undertaken by monitoring pressure, temperature and changes in mass using a high precision balance. The IGA series comprises 5 different models – each offering varying features and degrees of versatility. In this study, the IGA-001 model was used to undertake pure component adsorption measurements. A schematic of the apparatus is provided in Figure 5 - 25.

The IGA is fitted with a computer controlled microbalance and independent balance thermostat. The balance is coated with polytetraflouroethylene (PTFE) to enhance corrosion resistance. The balance has a capacity of 1 g with a measurement range of 0-100 mg. The weighing resolution is 0.1 μg with a long term stability of 1 μg. A sample of sorbent is held inside the reactor using a stainless steel container. In the case of a solid adsorbent, a stainless steel basket is used. The container is attached to the balance using a tungsten hang-down.

The IGA employs a system that ensures precise pressure control. The pressure system is computer-controlled allowing for the admittance and removal of gas with precise set-point regulation. The stainless steel gas handling system comprises a pressure transducer, pressure relief valve, manual vacuum-pressure isolation valve (PIV1) and a port for gas supply. Pressure is measured with a resolution of 1 mbar and an accuracy of 4 mbar. The system has an operating pressure of 20 bar at a maximum operating temperature of 773 K. The stainless reactor is sealed using conflat-type flanges with copper gaskets. The reader is referred to technical notes by the Kurt J. Lesker Company (2014) for additional reading on conflat flanges.

Absolute vacuum is achieved using a high vacuum turbo molecular pump. An Edwards EXT75DX pump was used in this study. The pump is capable of vacuum as high as 10^{-8} mbar. This is achieved as a result of the ultra-high vacuum manifold. The pump is manufactured with flexible stainless steel bellows for integration with the IGA gas handling system.

The IGA apparatus is fitted with two Pt100 sensors – one inside the reactor and the other on the furnace. The sensors have a measurement range of 3 to 1273 K with resolution of 0.01 K and accuracy of 0.1 K. Temperature of the reactor is maintained using either a refrigerated recirculated water bath – up to 353 K or a furnace (not shown in the figure). The furnace is capable of operating up to 773 K.

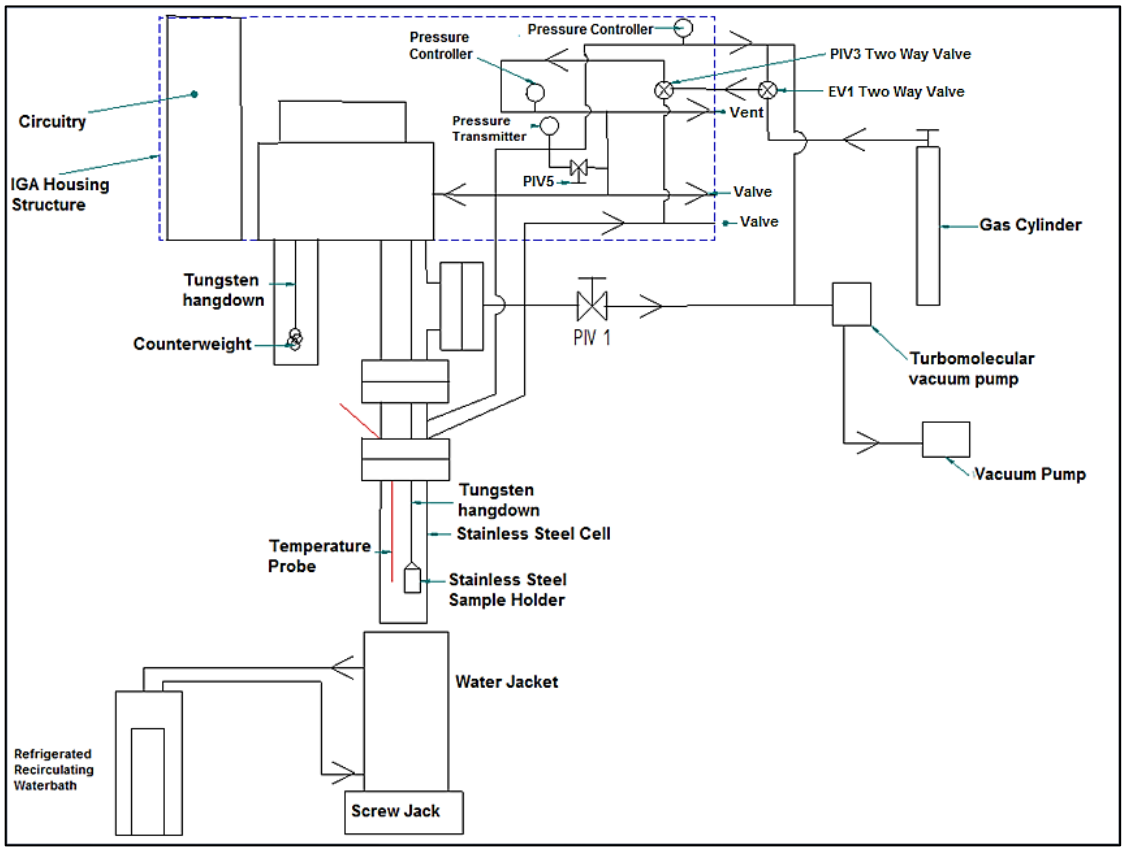

Figure 5 - 25: Schematic of the Intelligent Gravimetric Analyser (Osman, 2014).

5.2.2. Gravimetric Experimental Method

The gravimetric apparatus had been commissioned by Osman (2014) prior to the commencement of this study hence only leak testing was carried out in this study.

5.2.2.1. Leak testing and calibrations

The apparatus was checked for leaks by charging the system with 20 bar of inert gas with no sample present. The pressure control was switched off, shutting both the inlet and exhaust valve. The reactor was held under isothermal conditions using the refrigerated recirculating water bath. The system was monitored for a period of 24 hours for any drop in pressure greater than the experimental uncertainty.

5.2.2.2. Equilibrium Adsorption Measurement

The IGA apparatus is fully automated and therefore requires minimum user input. A description of the input required from the user is described. The reader is referred to the *IGA Systems User Manual* submitted in electronic format along with this dissertation for further reading.

A sample of adsorbent was loaded into the sample holder and attached to the high precision mass balance via the tungsten hang-down. The sample holder used in this study is a cone shaped basket made of stainless steel wire mesh, unlike the liquid sample holder used in the study of Osman (2014). A sample size of 78.25 mg was used in this study. The stainless steel cell was then sealed using a copper gasket.

The adsorbent was prepared by evacuating the cell at a temperature of 373 K under absolute vacuum for 24 hours and the mass of adsorbent was recorded. As was mentioned in Chapter 4, the mass of the dry adsorbent is required in this technique. Evacuation was undertaken in two stages. Firstly the pressure within the cell was reduced to 10 mbar using the vacuum pump. Secondly, an absolute vacuum of 10^{-8} mbar was drawn using the turbomolecular pump via valve PIV1.

Upon the completion of regeneration, the furnace was replaced with the refrigerated recirculated water bath (water jacket in the schematic). All measurements were undertaken using the water bath. Pure gases were charged to the system at the maximum measured isothermal pressure. Increments for pressure intervals and isothermal set points were indicated by the user. The IGA programme ensured pressure and temperature control. Upon completion of the isotherm measurement, the gas bottle was shut off and the system was evacuated. The adsorbent was regenerated in preparation for the next isothermal measurement.

5.2.3. Operability and Safety of the IGA

The IGA system design incorporates numerous safety features, these include:

- The gas handling system is fitted with a pressure relief valve and incorporates a safety interlock.
- The turbomolecular vacuum pump is fitted with a safety overpressure relief valve along with a vent port.
- The equilibrium chamber is equipped with an overpressure safety valve, indicated by ‘vent’ in Figure 5 - 25.

The reader is referred to the IGA Manual for detailed operating procedures of the apparatus.

6

Chapter 6: Experimental Results and Discussion

6.1. Vapour Pressure Measurement

Vapour pressure measurements were performed for two pure and common gases available in the laboratories. This was to verify the calibration of the sensors. The combined standard uncertainties in temperature, $u_c(T)$ and pressure, $u_c(P)$ is presented. The uncertainty in the calculated vapour pressure, u_{Pvap} determined using *The Law of Propagation of Uncertainty* is tabulated. The method for calculation is provided in Appendix G.

6.1.1. Propylene

Table 6 - 1: Vapour pressure data for propylene measured in this study.

T (K)	P_{vap} (bar)	u_{Pvap} (bar)
293.23	10.219	0.004
298.24	11.592	0.005
303.26	13.096	0.005
308.26	14.737	0.005
313.39	16.576	0.006
318.39	18.524	0.006
323.39	20.636	0.006
$u_c(P) = 0.002$ bar		
$u_c(T) = 0.03$ K		

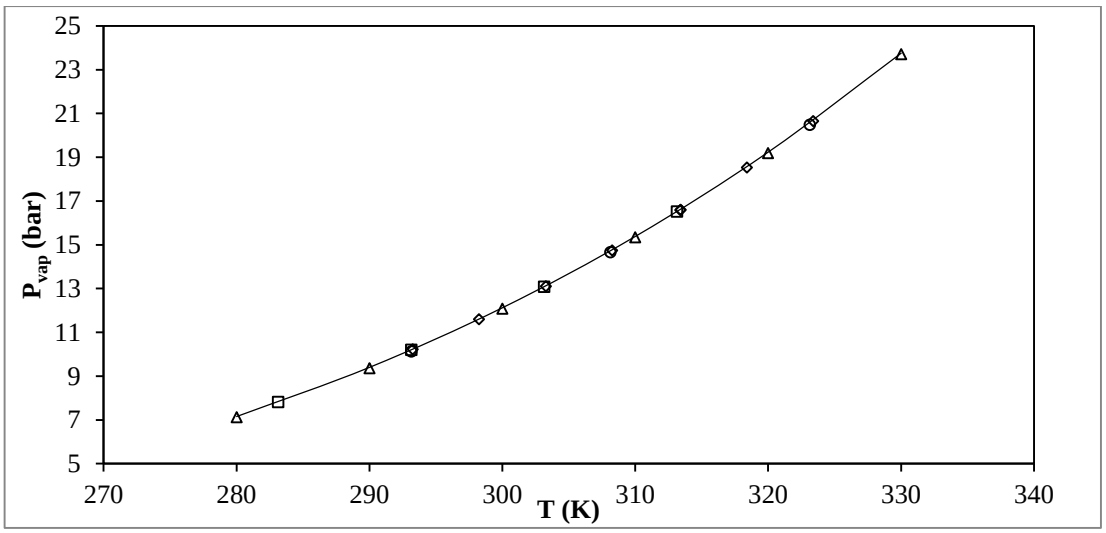

Figure 6 - 1: Vapour pressure of propylene. (◊), this study; (□), Glos et al. (2004); (Δ), Ho et al. (2005); (○), Hou and Huan (2010); (—), Extended Antoine Predictions.

The deviation of the experimental vapour pressure data for propylene from the Extended Antoine predictions is presented below. The deviations of the literature are also presented. The data measured in this study compared favourably to the literature.

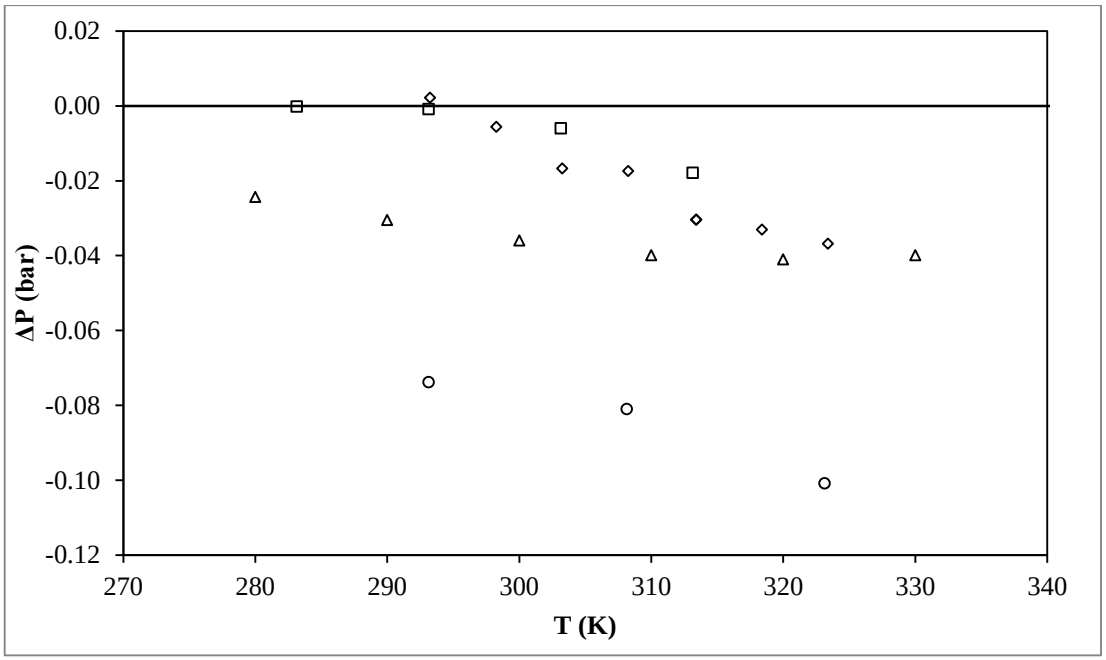

Figure 6 - 2: Deviation of experimental vapour pressure data from Extended Antoine predictions. (◊), this study; (□), Glos et al. (2004); (Δ), Ho et al. (2005); (○), Hou and Huan (2010).

6.1.2. R134a

Table 6 - 2: Vapour pressure data for R134a measured in this study.

T (K)	P (bar)	u_{Pvap} (bar)
293.40	5.792	0.005
298.41	6.727	0.005
303.42	7.774	0.004
308.43	8.942	0.004
313.43	10.239	0.004
318.44	11.669	0.004
323.24	13.154	0.003
$u_c(P) = 0.002$ bar		
$u_c(T) = 0.03$ K		

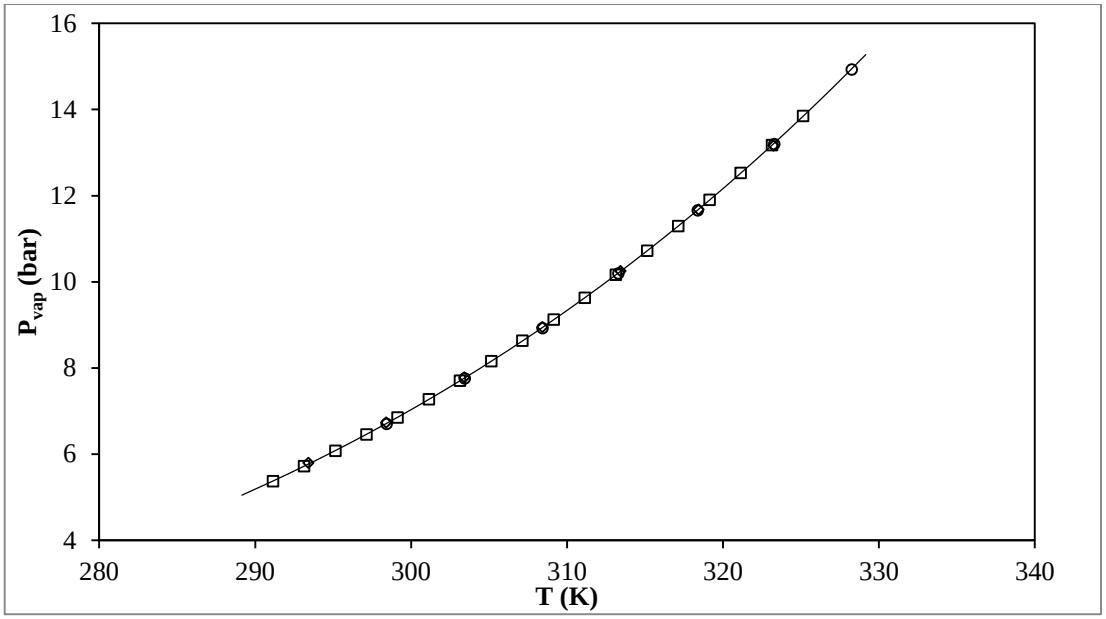

Figure 6 - 3: Vapour pressure of R134a. (◊), this study; (□), Zhu et al. (1992); (Δ), Zehioua et al. (2010a); (○), Zehouia et al. (2010b); (—), Extended Antoine calculations.

The deviation of the experimental vapour pressure data for R134a from the Extended Antoine predictions is presented below. The deviations of the literature are also presented. The data measured in this study compared favourably to the literature.

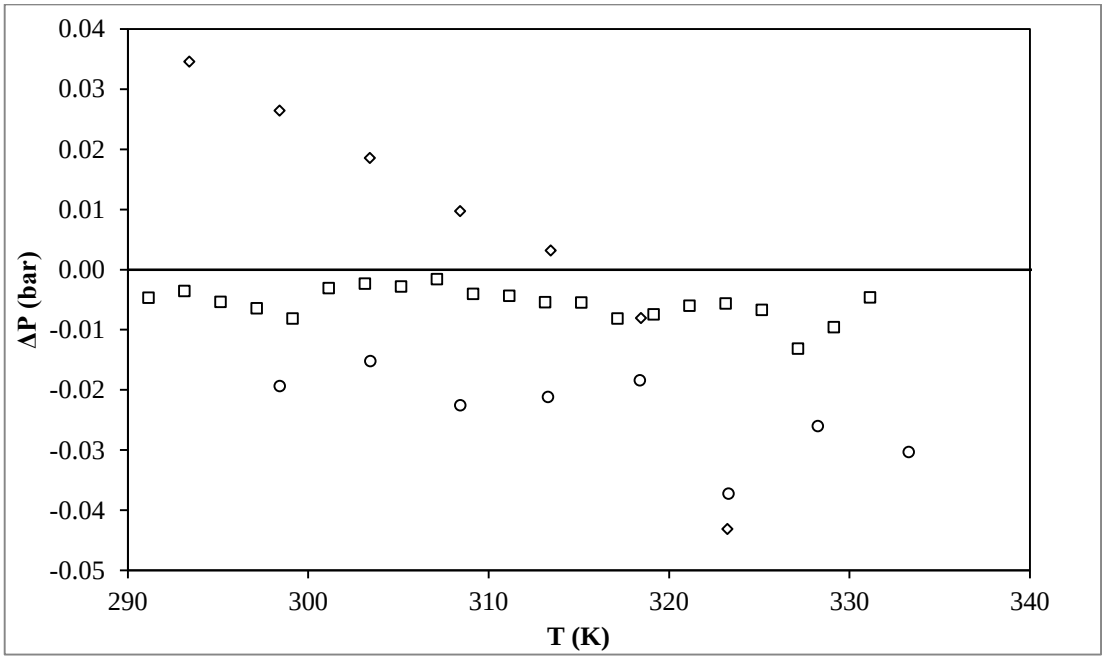

Figure 6 - 4: Deviation of experimental vapour pressure data from Extended Antoine predictions. (◊), this study; (□), Zhu et al. (1992) ;(○), Zehouia et al. (2010b).

The vapour pressure measurements undertaken showed good agreement with the literature. The uncertainties in temperature and pressure reported in this study are comparable to those found in the literature.

6.2. Adsorption Measurements

Measurements were performed using systems reported in the literature to validate the experimental technique used in this study.

Experimental Uncertainties in Pure Component Adsorption Measurements

The methods of Taylor and Kuyatt (1994) were used to determine experimental uncertainty. A detailed description is provided in Appendix G.

The experimental uncertainty in the temperature of the equilibrium cell has three contributions, namely: the uncertainty as a result of calibration, $u_{calib}\ (T)$; the uncertainty as a result of the temperature gradient within the ethylene glycol bath, $u_{grad}\ (T)$; and the uncertainty as a result of the repeatability of temperature measurements, $u_{repeat}\ (T)$. The uncertainty as a result of calibration, u_{calib} has been discussed in Chapter 5. The uncertainty as a result of calibration is 0.03 K. A temperature gradient of 0.02 K was observed in the ethylene glycol bath. Using a rectangular distribution, discussed in Appendix G, an uncertainty of 0.01 K is introduced as a result of the temperature gradient, $u_{grad}\ (T)$. The standard deviation was used as a measure of repeatability. Upon achieving equilibrium, the temperature of the equilibrium cell was recorded once every second for two minutes. The measured data were highly repeatable. The uncertainty in temperature as a result of repeatability, $u_{repeat}\ (T)$ is 10^{-4} K - two orders of magnitude smaller than $u_{calib}\ (T)$ and $u_{grad}\ (T)$. Its contribution to the total uncertainty in temperature, $u_c\ (T)$ was negligible. The combined standard uncertainty in temperature - given by Eq. (5 - 1) is thus 0.03 K.

The experimental uncertainty in the pressure of the equilibrium cell has three contributions, namely: the uncertainty as a result of calibration, $u_{calib}\ (P)$; the uncertainty as a result of the barometer used in this study, $u_{baro}\ (P)$; and the uncertainty as a result of the repeatability of pressure measurements, $u_{repeat}\ (P)$. The uncertainty as a result of calibration, u_{calib} has been discussed in Chapter 5. The uncertainty as a result of calibration is 0.002 bar. The uncertainty as a result of the barometer used in this study, $u_{baro}\ (P)$ is 0.001 bar. Barometric pressure was measured for each equilibrium point. The uncertainty in pressure as a result of repeatability, $u_{repeat}\ (P)$ is 10^{-5} bar - two orders of magnitude smaller than $u_{calib}\ (P)$ and $u_{baro}\ (P)$. Its contribution to the total uncertainty in pressure, $u_c\ (P)$ was negligible. The combined standard uncertainty in pressure is thus 0.002 bar.

A worked example for the calculation of the uncertainty in the reported data for the adsorption of ethane at a temperature of 298.13 K and a pressure of 0.194 bar using the volumetric technique is presented in Appendix G. For the most part, the experimental uncertainty in the amount adsorbed, q was less than 5% of the reported value or 0.15 mmol/g. This is comparable to the uncertainties reported by Reich et al. (1980), Kaul (1987) and Lee et al. (2013). The uncertainties in the species amount adsorbed, q, determined through the methods defined in Appendix G were appreciably high. This was expected as the amount adsorbed is not measured directly.

Using the methods outlined in Appendix G, the uncertainty in q when measured using the gravimetric technique is 10^{-5} mmol/g.

6.2.1. Pure component adsorption measurements

The adsorption measurements were performed with pure components methane, ethane and ethylene to verify the experimental techniques used in this study. For each of the pure component isotherms measured in this study – with the exception of high pressure data for ethylene on 13X - data were collected in two runs. Reproducible data are a good indication that the equipment is functioning as intended and is doing so consistently. Hysteresis was not investigated in this study as desorption points were not measured. The experimental technique (volumetric) used in this study – adding incremental amounts of gas to the equilibrium cell – is susceptible to a compounding error in the calculation of the amount of adsorbed gas. Repeatability was undertaken as a test for systematic error and yielded a negative result. Thus, the experimental technique used in this study was validated.

The data of Danner and Choi (1978), Danner and Hyun (1982) and Kaul (1987) was used to validate the experimental methods used in the low pressure range (0-1.5 bar). The data of Loughlin et al. (1990) was used to validate the experimental method used in the high pressure range (up to 15 bar).The data measured using the volumetric technique in this study showed favourable comparisons to the literature. The data measured using the gravimetric technique however, showed consistent deviation from the literature in the pressure range 0 - 1.5 bar. The experimental results in this study are presented along with the calculated uncertainties.

6.2.1.1. Low Pressure Measurements

6.2.1.1.1. Ethane + 13 X

Ethane + 13 X at 298 K

The experimental data points for the ethane isotherm at a temperature of 298 K are listed in Table 6 - 3. A graphical illustration of the experimental data is shown in Figure 6 - 5 and compares the experimental data measured in this study to literature data.

Table 6 - 3: Low pressure adsorption data for ethane on 13X at 298 K. Data measured using the volumetric technique are presented.

Volumetric						Gravimetric			
Run 1			Run 2			Run 1		Run 2	
P (bar)	q (mmol/g)	u_c (mmol/g)	P (bar)	q (mmol/g)	u_c (mmol/g)	P (bar)	q (mmol/g)	P (bar)	q (mmol/g)
0.194	1.02	0.09	0.143	0.75	0.17	0.096	0.78	0.095	0.64
0.264	1.30	0.09	0.200	1.03	0.11	0.198	1.28	0.194	1.22
0.306	1.44	0.12	0.272	1.32	0.09	0.296	1.66	0.298	1.63
0.374	1.62	0.09	0.338	1.51	0.09	0.396	1.93	0.396	1.89
0.437	1.74	0.10	0.419	1.69	0.08	0.497	2.12	0.496	2.08
0.529	1.88	0.09	0.517	1.85	0.08	0.598	2.25	0.596	2.21
0.626	1.99	0.09	0.623	1.98	0.09	0.696	2.36	0.698	2.33
0.699	2.06	0.12	0.733	2.07	0.11	0.797	2.44	0.796	2.41
0.792	2.13	0.11	0.843	2.15	0.12	0.897	2.51	0.897	2.48
0.891	2.20	0.12	0.948	2.21	0.14	0.996	2.57	0.997	2.54
0.998	2.25	0.13	1.053	2.26	0.15	1.096	2.62	1.098	2.60
1.102	2.30	0.14	1.162	2.31	0.12	1.198	2.67	1.196	2.64
1.199	2.34	0.16	1.258	2.34	0.13	1.296	2.71	1.295	2.68
1.294	2.37	0.17	1.367	2.38	0.13	1.397	2.74	1.396	2.72
1.388	2.40	0.18				1.497	2.78	1.497	2.75
$u_c(T)$ = 0.03 K						*$u_c(T)$ = 0.1 K*			
$u_c(P)$ = 0.002 bar						*$u_c(P) = 4\times10^{-3}$ bar*			
						$u_c(q) = 3.57\times10^{-5}$ mmol/g			

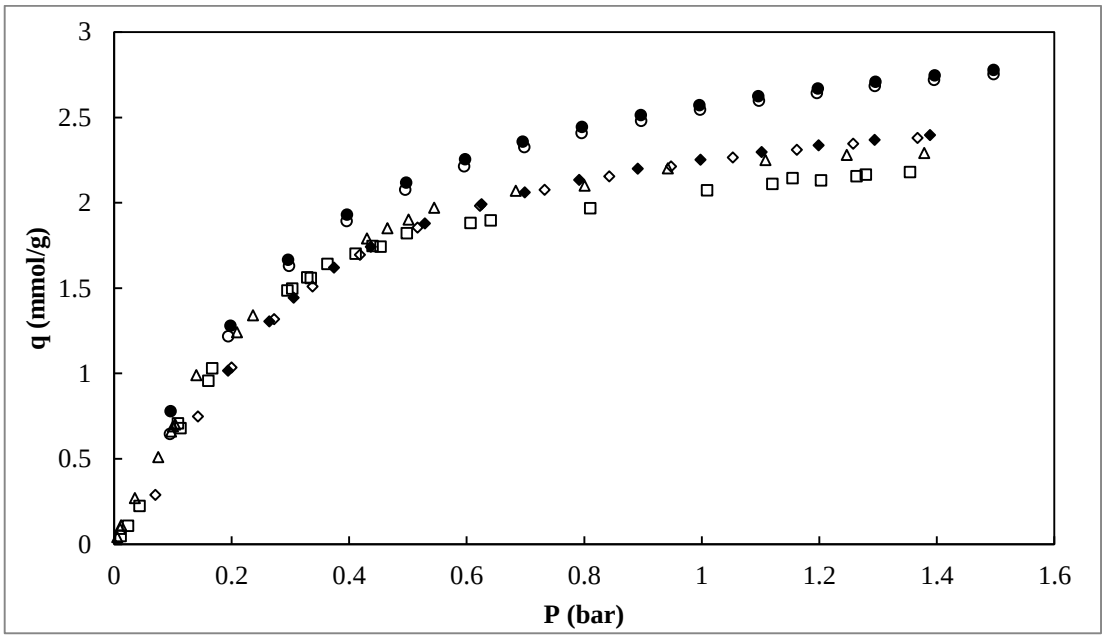

Figure 6 - 5: Low pressure adsorption isotherms for ethane on 13X at 298 K. (□), Danner and Choi (1978); (Δ), Danner and Hyun (1982); (♦), this study: volumetric run 1; (◊), this study: volumetric run 2; (●), this study: gravimetric run 1; (○), this study: gravimetric run 2.

Ethane + 13X at 323 K

The experimental data points for the ethane isotherm at a temperature of 323 K are listed in Table 6 - 4. A graphical illustration of the experimental data is shown in Figure 6 - 6 and compares the experimental data measured in this study to literature data.

Table 6 - 4: Low pressure adsorption data for ethane on 13X at 323 K. Data measured using the gravimetric technique and volumetric technique is presented.

Volumetric						**Gravimetric**			
Run 1			**Run 2**			**Run 1**		**Run 2**	
P (bar)	q (mmol/g)	u_c (mmol/g)	P (bar)	q (mmol/g)	u_c (mmol/g)	P (bar)	q (mmol/g)	P (bar)	q (mmol/g)
0.085	0.19	0.93	0.078	0.18	1.11	0.096	0.31	0.098	0.37
0.171	0.41	0.30	0.158	0.37	0.35	0.196	0.59	0.200	0.65
0.260	0.62	0.18	0.247	0.59	0.19	0.293	0.86	0.300	0.91
0.350	0.82	0.13	0.338	0.80	0.14	0.396	1.10	0.400	1.15
0.443	1.01	0.11	0.432	0.99	0.12	0.496	1.31	0.499	1.34
0.537	1.17	0.11	0.528	1.16	0.11	0.595	1.48	0.599	1.51
0.635	1.32	0.11	0.629	1.32	0.11	0.698	1.63	0.700	1.65
0.732	1.44	0.11	0.728	1.44	0.10	0.796	1.75	0.799	1.77
0.836	1.55	0.11	0.831	1.55	0.10	0.897	1.85	0.899	1.87
0.935	1.64	0.12	0.938	1.65	0.11	0.997	1.94	0.998	1.96
1.040	1.72	0.13	1.042	1.73	0.12	1.097	2.02	1.100	2.03
1.142	1.80	0.14	1.147	1.80	0.12	1.196	2.08	1.198	2.10
1.244	1.86	0.15	1.251	1.86	0.13	1.296	2.14	1.299	2.16
1.347	1.91	0.16	1.358	1.92	0.13	1.396	2.19	1.399	2.21
1.451	1.96	0.16	1.460	1.97	0.15	1.496	2.24	1.499	2.26
$u_c(T) = 0.03$ K						$u_c(T) = 0.1$ K			
$u_c(P) = 0.002$ bar						$u_c(P) = 4\times10^{-3}$ bar			
						$u_c(q) = 3.57\times10^{-5}$ mmol/g			

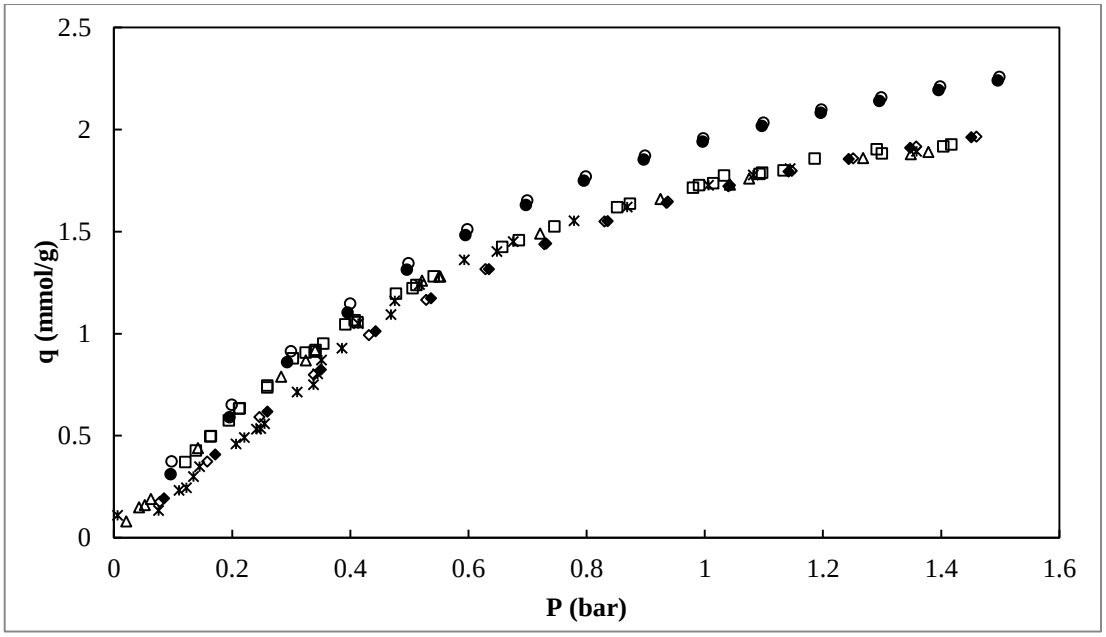

Figure 6 - 6: Low pressure adsorption isotherms for ethane on 13X at 323 K. (□), Danner and Choi (1978); (Δ), Danner and Hyun (1982); (*), Kaul (1987); (♦), this study: volumetric run 1; (◊), this study: volumetric run 2; (●), this study: gravimetric run 1; (○), this study: gravimetric run 2.

6.2.1.1.2. Ethylene + 13X

Ethylene + 13X at 298 K

The experimental data points for the ethylene isotherm at a temperature of 298 K are listed in Table 6 - 5. A graphical illustration of the experimental data is shown in Figure 6 - 7 and compares the experimental data measured in this study to literature data.

Table 6 - 5: Low pressure adsorption data for ethylene on 13X at 298 K. Data measured using the gravimetric technique and volumetric technique is presented.

Volumetric						Gravimetric	
Run 1			Run 2			Run 1	
P (bar)	q (mmol/g)	u_c (mmol/g)	P (bar)	q (mmol/g)	u_c (mmol/g)	P (bar)	q (mmol/g)
0.114	1.86	0.06	0.035	0.87	0.40	0.097	1.97
0.240	2.31	0.03	0.078	1.53	0.11	0.201	2.39
0.569	2.70	0.02	0.122	1.87	0.07	0.298	2.59
0.723	2.79	0.06	0.174	2.11	0.06	0.400	2.71
0.846	2.85	0.09	0.278	2.38	0.04	0.498	2.80
0.995	2.91	0.09	0.453	2.61	0.04	0.599	2.87
1.113	2.95	0.11	0.725	2.80	0.04	0.698	2.92
1.249	2.98	0.11	1.218	2.99	0.03	0.797	2.97
1.409	3.02	0.11				0.901	3.01
						0.998	3.05
						1.100	3.08
						1.199	3.10
						1.296	3.13
						1.398	3.15
						1.498	3.17
$u_c(T) = 0.03$ K						*$u_c(T) = 0.1$ K*	
$u_c(P) = 0.002$ bar						*$u_c(P) = 4\times10^{-3}$ bar*	
						$u_c(q) = 3.57\times10^{-5}$ mmol/g	

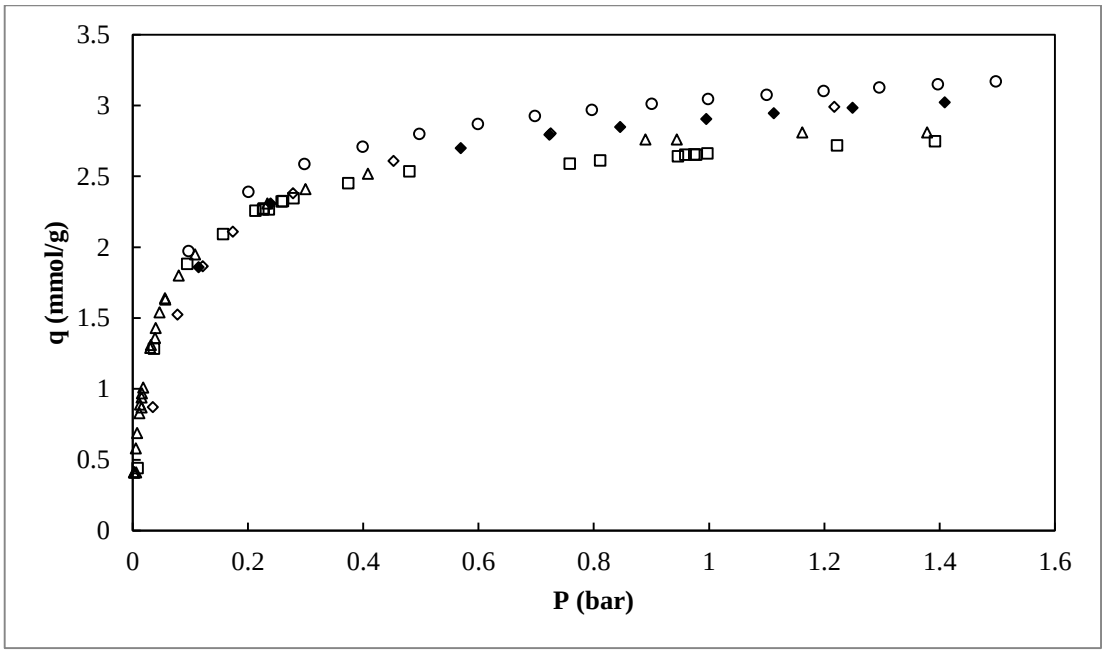

Figure 6 - 7: Low pressure adsorption isotherms for ethylene on 13X at 298 K. (□), Danner and Choi (1978); (Δ), Danner and Hyun (1982); (♦), this study: volumetric run 1; (◊), this study: volumetric run 2; (○), this study: gravimetric run 1.

Ethylene + 13X at 323 K

The experimental data points for the ethylene isotherm at a temperature of 323 K are listed in Table 6 - 6. A graphical illustration of the experimental data is shown in Figure 6 - 8 and compares the experimental data measured in this study to literature data.

Table 6 - 6: Low pressure adsorption data for ethylene on 13X at 323 K. Data measured using the gravimetric technique and volumetric technique is presented.

Volumetric						**Gravimetric**	
Run 1			**Run 2**			**Run 1**	
P (bar)	**q (mmol/g)**	**u_c (mmol/g)**	**P (bar)**	**q (mmol/g)**	**u_c (mmol/g)**	**P (bar)**	**q (mmol/g)**
0.046	0.51	0.53	0.068	0.77	0.24	0.099	1.23
0.106	0.99	0.13	0.260	1.72	0.03	0.200	1.73
0.179	1.40	0.07	0.637	2.29	0.02	0.300	2.02
0.269	1.71	0.05	1.170	2.58	0.03	0.401	2.20
0.376	1.95	0.05	1.435	2.67	0.06	0.494	2.33
0.490	2.12	0.06				0.599	2.44
0.606	2.25	0.07				0.697	2.52
0.720	2.34	0.08				0.798	2.58
0.828	2.42	0.09				0.899	2.64
0.936	2.48	0.11				0.998	2.69
1.144	2.58	0.13				1.100	2.73
1.254	2.62	0.10				1.199	2.77
1.349	2.66	0.12				1.300	2.80
1.447	2.69	0.12				1.398	2.83
						1.498	2.86
$u_c(T) = 0.03$ K						*$u_c(T) = 0.1$ K*	
$u_c(P) = 0.002$ bar						*$u_c(P) = 4\times10^{-3}$ bar*	
						$u_c(q) = 3.57\times10^{-5}$ mmol/g	

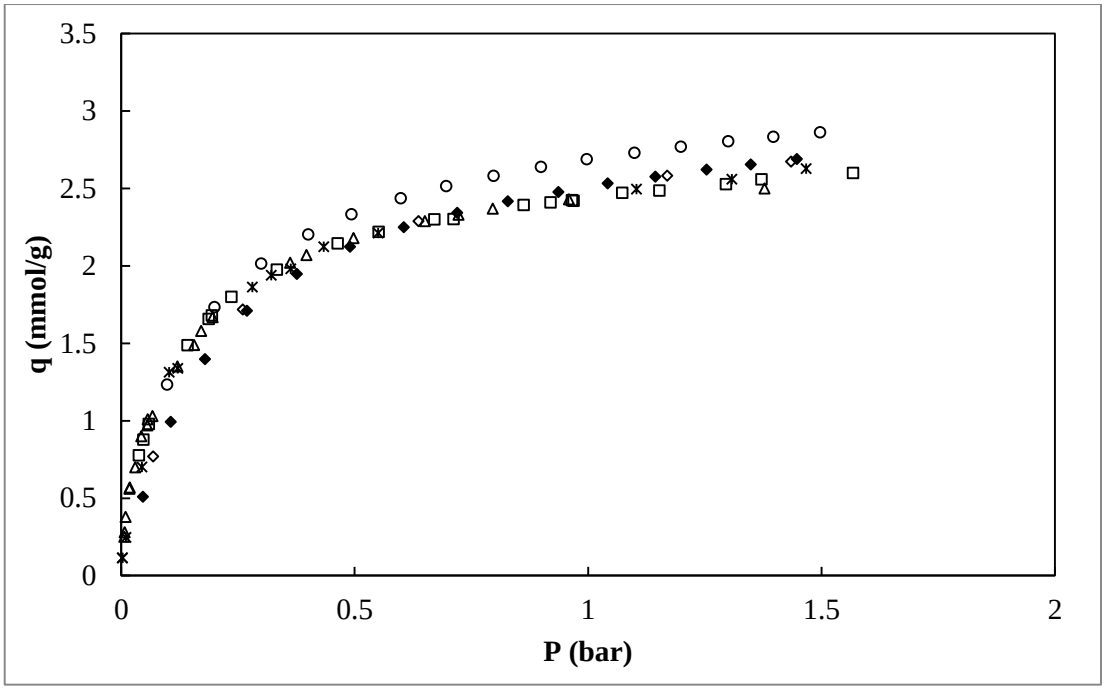

Figure 6 - 8: Low pressure adsorption isotherms for ethylene on 13X at 323 K. (□), Danner and Choi (1978); (Δ), Danner and Hyun (1982); (*), Kaul (1987); (♦), this study: volumetric run 1; (◊), this study: volumetric run 2; (○), this study: gravimetric run 1.

The data of Danner and Choi (1978) and Danner and Hyun (1982) were reported to have been measured using the same equipment and experimental technique (static volumetric). The same adsorbent, zeolite 13X, was used in both studies. The adsorbent has a specific surface area of 524 m^2/g and a specific volume of 0.3 cm^3/g. The data of Danner and Hyun (1982) showed deviation from the previous study of Danner and Choi (1978) – as high as 5%. The data measured by Danner and Hyun (1982) were considered to be in excellent agreement with the data of Danner and Choi (1978).

Kaul (1987) undertook measurements with zeolite 13X - similar to that used by Danner and Choi (1978) and Danner and Hyun (1982). The measurements in the study, however, were undertaken using a variable volume cell. The data of Kaul (1987) also showed a deviation of approximately 5% from the previously mentioned studies. The deviations in data were accepted by Kaul (1987) who reported that the variable volume cell used in the study was an accurate instrument for the measurement of adsorption of equilibria.

The adsorbent used in this study has a specific surface area identical to the one used in the mentioned studies found in the literature, viz., 524 m^2/g. The volume of the adsorbent was taken into account using helium expansion. Helium has a critical diameter of 2.0 Å, much smaller than the pore width of 13X. Helium penetrated the pores of the zeolite but did not adsorb on the zeolite. This allowed the exact calculation of the volume of adsorbent present in the equilibrium cell.

The data measured using the volumetric apparatus designed in this study showed good agreement with the literature (Danner and Choi, 1978; Danner and Hyun, 1982; Kaul, 1987) within the experimental uncertainties. The data measured using the gravimetric technique (IGA) showed greater adsorption capacity for both gases, ethane and ethylene, investigated. This increased capacity is a result of the much smaller sample size used in the gravimetric technique. The

volumetric apparatus (94.9 g) used a sample size 1000 times larger than the gravimetric apparatus (78.25 mg). The ratio of the adsorbent used to the volume of the equilibrium cell (g/mL) is 0.25 and 2×10^{-4} for the volumetric and gravimetric apparatus respectively. Comparably, the mass to volume ratio used in previous studies ranges from 0.1 (Ghosh et al., 1993) to 0.45 (Reich et al., 1980). The ratio of the mass of the adsorbent to the volume of the adsorptive gas significantly affects adsorption capacities as reported by Crittenden and Thomas (1998) and Rezaei and Webley (2010).

In the volumetric technique, the adsorbent was loaded into the equilibrium cell, forming a cylindrical bed at the bottom of the cell. In the gravimetric technique, the adsorbent was suspended inside the equilibrium cell, held in a cone shaped mesh basket. The difference in adsorbent sample sizes and arrangements within the equilibrium cell affected the hydrodynamic and dispersion characteristics of the adsorption system. The data measured with the IGA showed good repeatability; as seen in Figure 6 - 5 and Figure 6 - 6.

6.2.1.2. High Pressure Measurements

6.2.1.2.1. Methane + 13X

The experimental data points for the methane isotherm at a temperature of 300 K and 325 K are listed in Table 6 - 7. A graphical illustration of the experimental data is shown in Figure 6 - 9 and compares the experimental data measured in this study to literature data.

Table 6 - 7: High pressure adsorption data for methane on 13X at 300 K and 325 K.

T = 300 K				**T = 325 K**			
run 1		**run2**		**run 1**		**run2**	
P (bar)	q (mmol/g)	P (bar)	q (mmol/g)	P (bar)	q (mmol/g)	P (bar)	q (mmol/g)
0.997	0.51	1.000	0.53	0.999	0.31	0.997	0.31
1.998	0.90	1.998	0.93	1.998	0.56	1.999	0.57
2.999	1.22	2.999	1.26	2.999	0.80	2.999	0.80
3.998	1.49	3.997	1.52	3.999	1.01	3.998	1.01
4.998	1.71	4.999	1.74	4.999	1.20	4.999	1.21
5.999	1.89	5.999	1.93	5.999	1.36	5.997	1.37
6.998	2.05	6.998	2.08	6.998	1.50	6.996	1.52
7.999	2.18	7.999	2.22	8.000	1.63	7.997	1.65
8.998	2.30	8.998	2.34	8.999	1.75	8.996	1.77
9.999	2.41	9.997	2.44	9.999	1.85	9.994	1.87
11.001	2.50	11.000	2.54	11.000	1.94	10.994	1.96
12.000	2.58	12.000	2.62	11.998	2.03	11.994	2.05
13.001	2.66	13.002	2.70	12.999	2.11	13.000	2.13
14.087	2.74	14.001	2.78	13.998	2.18		
$u_c(T) = 0.1$ K							
$u_c(P) = 4\times10^{-3}$ bar							
$u_c(q) = 3.57\times10^{-5}$ mmol/g							

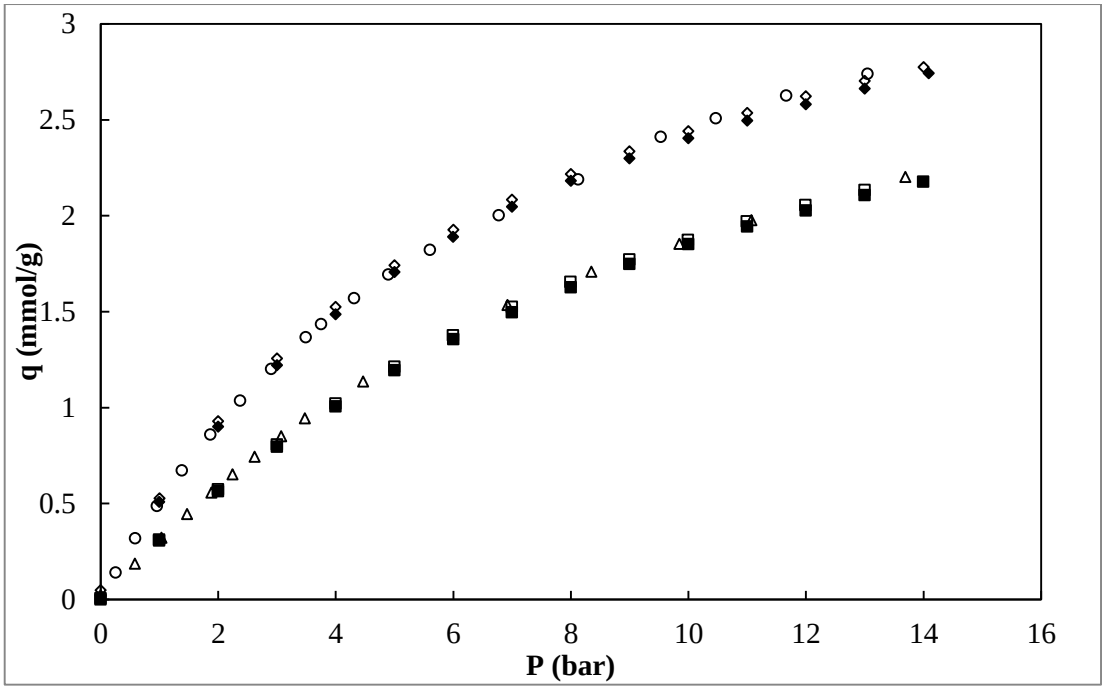

Figure 6 - 9: High pressure adsorption isotherms for methane on 13X at 300 K and 325 K. (○), Loughlin et al. (1990), 300 K; (Δ), Loughlin et al. (1990), 325 K; (♦), this study: gravimetric run 1, 300 K; (◊), this study: gravimetric run 2, 300 K; (■), this study: gravimetric run 1, 325 K; (□), this study: gravimetric run 2, 325 K.

High pressure adsorption measurements were undertaken using only the gravimetric technique due to time constraints. The IGA enabled the efficient measurement of adsorption data. High pressure adsorption data was measured to further investigate the performance of the IGA. The high pressured adsorption data were used to evaluate the performance of the adsorption models used in the high coverage area.

The data of Loughlin et al. (1990) for the adsorption of methane on 13X was used to validate the gravimetric technique used in this study in the high pressure range, up to 15 bar. Danner and Choi (1978), Danner and Hyun (1982), Kaul (1987) used the same adsorbent as Loughlin et al. (1990). The adsorption of methane has been widely investigated, driven in large part by the need for effective Carbon Capture and Storage (CCS) techniques (Yu et al., 2012). A number of adsorbents have been evaluated for the adsorption of methane. In addition to zeolite 13 X, zeolite 5A (Pakseresht et al., 2002; Nam et al., 2005) and activated carbons (Costa et al., 1981; Choi et al., 2003) have been investigated. The test system measured in this study, on zeolite 13X, adds to the literature.

The data measured using the gravimetric technique in this study showed favourable comparison to the literature data. The adsorption isotherms for methane on 13X matched the data of Loughlin et al. (1990) at both temperatures studied, 300 K and 325 K. Measurements for both isotherms were repeated to confirm reproducibility of the adsorption data obtained. The isothermal measurements for ethane at 298 K were also repeated to validate accuracy of the measured data.

6.2.1.2.2. Ethane + 13X

The experimental data points for the ethane isotherm at a temperature of 298 K and 323 K are listed in Table 6 - 8. A graphical illustration of the experimental data is shown in Figure 6 - 10. No data were found in the literature for high pressure ethane adsorption on 13X. As such, this constitutes a new system.

Table 6 - 8: High pressure adsorption data for ethane on 13X at 298 K and 323 K. The data were measured using the gravimetric technique.

T = 298 K				**T = 323 K**			
Run 1		**Run 2**		**Run 1**		**Run 2**	
P (bar)	q (mmol/g)	P (bar)	q (mmol/g)	P (bar)	q (mmol/g)	P (bar)	q (mmol/g)
0.095	0.64	0.101	0.68	0.096	0.31	0.098	0.37
0.997	2.54	0.998	2.56	0.997	1.94	0.998	1.96
1.997	2.87	1.999	2.89	1.997	2.41	2.000	2.43
2.996	3.01	2.999	3.04	2.997	2.61	2.999	2.63
3.995	3.12	3.998	3.14	3.996	2.73	3.998	2.76
4.996	3.20	5.000	3.22	4.997	2.82	4.999	2.85
5.995	3.26	5.999	3.28	5.996	2.88	5.998	2.91
6.994	3.31	6.999	3.33	6.995	2.94	6.998	2.97
7.996	3.36	8.000	3.38	7.996	2.98	7.998	3.01
8.994	3.40	8.999	3.42	8.995	3.02	8.997	3.05
9.994	3.43	9.999	3.45	9.994	3.05	9.996	3.09
10.995	3.46	11.000	3.49			10.998	3.12
11.994	3.49	12.000	3.52			11.999	3.15
12.995	3.52	13.000	3.54			12.996	3.18
13.995	3.55	13.999	3.57			14.001	3.21
$u_c(T) = 0.1\ K$							
$u_c(P) = 4\times10^{-3}\ bar$							
$u_c(q) = 3.57\times10^{-5}\ mmol/g$							

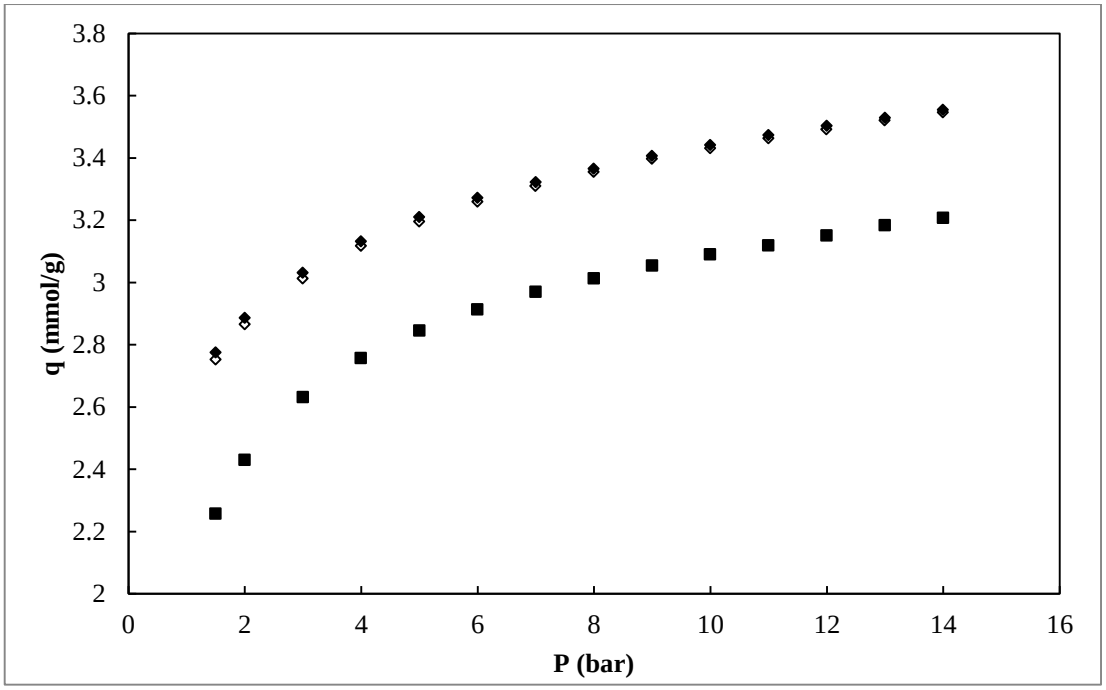

Figure 6 - 10: High pressure adsorption isotherms for ethane on 13X at 298 K and 323 K. (♦), this study: gravimetric run 1, 298 K; (◊), this study: gravimetric run 2, 298 K; (■), this study: gravimetric run 1, 323 K; (□), this study: gravimetric run 2, 323 K.

6.2.1.2.3. Ethylene + 13X

The experimental data points for the ethylene isotherm at a temperature of 298 K and 323 K are listed in Table 6 - 9. A graphical illustration of the experimental data is shown in Figure 6 - 11. No data were found in the literature for high pressure ethylene adsorption on 13X. As such, this constitutes a new system.

Table 6 - 9: High pressure adsorption data for ethylene on 13X at 298 K and 323 K. The data were measured using the gravimetric technique.

T = 298 K		T = 323 K	
P (bar)	q (mmol/g)	P (bar)	q (mmol/g)
0.098	2.05	0.099	1.23
1.000	3.11	0.998	2.69
2.001	3.32	2.000	2.98
2.999	3.43	2.998	3.12
3.997	3.51	3.997	3.22
5.000	3.57	4.999	3.29
5.999	3.61	5.999	3.34
6.999	3.65	6.999	3.39
7.999	3.68	8.000	3.43
8.999	3.71	8.999	3.46
10.000	3.73	9.996	3.49
11.000	3.76	10.998	3.52
12.002	3.78	11.998	3.55
13.000	3.80	12.996	3.57
14.000	3.81	13.999	3.59
		14.996	3.62
$u_c(T) = 0.1\ K$			
$u_c(P) = 4\times10^{-3}\ bar$			
$u_c(q) = 3.57\times10^{-5}\ mmol/g$			

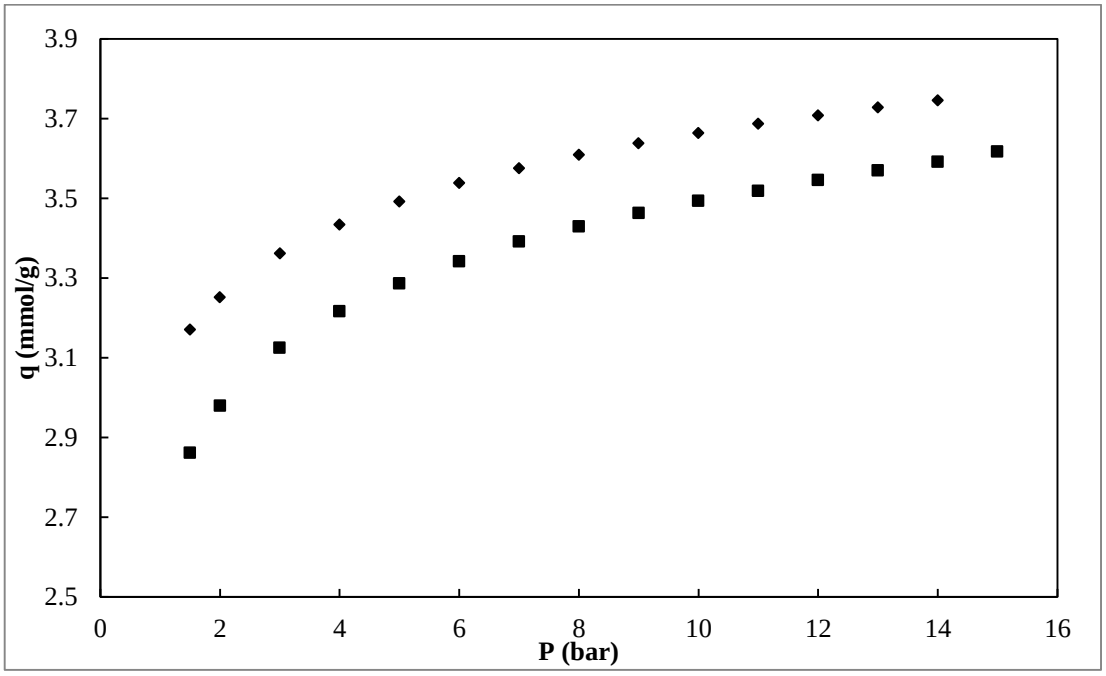

Figure 6 - 11: High pressure adsorption isotherms for ethylene on 13X at 298 K and 323 K. (◊), this study: gravimetric, 298 K; (□), this study: gravimetric, 323 K.

The isothermal data for methane indicates a significant increase in adsorption capacity with an increase in pressure within the pressure range investigated in this study (0-15 bar). The same trend is not observed for the adsorption isotherms of ethane and ethylene. An appreciable gain in adsorption capacity, *q*, was not observed for pressures beyond 4 bar. This suggests that the adsorption of ethane and ethylene should be performed at low to medium pressure in industrial applications. The additional mechanical energy requirement is not justified by appropriate increases in adsorption capacity.

The pure component isotherms obtained in this study, in accordance with the data found in literature, all exhibit Type I behaviour according to the BDDT classification discussed in Chapter 3. As expected, no hysteresis was observed. Greater adsorption capacities were observed at lower temperatures. This was expected as adsorption favours lower temperatures. The equilibrium constant describing physical adsorption follows the van't Hof equation, shown in Chapter 2.

At 298 K, the adsorption capacities for ethane and ethylene were 2.25 mmol/g at 0.988 bar and 2.91 mmol/g at 0.995 bar respectively. At 323 K the adsorption capacities were 1.72 mmol/g at 1.040 bar and 2.48 mmol/g at 0.936 bar respectively. The zeolite showed a greater affinity for ethylene at both temperatures studied. Ethylene also had a stronger attraction to the zeolite, indicated by the rectangular-like shape of the isotherms (Shi et al., 2010). In addition to the van der Waals interactions, the electrostatic contributions were also significant due to the ionic nature of the adsorbent used. The polar nature of the zeolite induced a dipole in both the ethane and ethylene molecule. Both ethane and ethylene are non-polar molecules. The greater affinity for ethylene is caused by the partial negatively charged area surrounding the double bond in the ethylene molecule, shown in Figure 6 - 12.

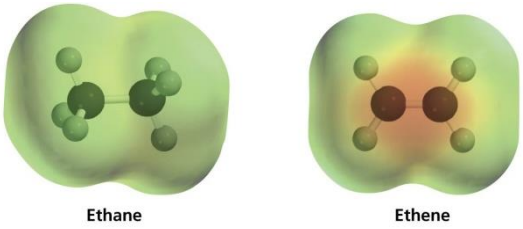

Figure 6 - 12: Electrostatic potential map for ethane and ethylene (ethene). The darker region indicates a negative charge and the lighter region indicates neutrality (Bruice, 2007).

6.2.2. Binary Measurements

The behaviour observed from the pure component measurements showed positive indications of the potential of zeolite 13X to separate a mixture of ethane and ethylene. Adsorption measurements of the binary system of ethane and ethylene were performed using the gas mixer in the experimental setup. The gas mixer replaced the storage cell used in the pure component measurements. The data were compared to the data of Danner and Choi (1978) as shown in Table 6 - 10. The measured data matched the literature well particularly in the dilute regions of the composition plot as shown in Figure 6 - 14.

Experimental Uncertainties in Binary Measurements

The experimental uncertainties in temperature and pressure have been discussed in the previous section. The experimental uncertainty in the composition of the gas phase, *y* has a single contribution – the uncertainty resulting from the calibration of the FID. The uncertainty in calibration, $u_{calib}(y)$ is 0.007 mole fraction.

The composition of the adsorbed phase, *x* and the amount of species *i* adsorbed, q_i is determined through calculation and not measured directly. The method of Taylor and Kuyatt (1994) utilising the *Root-Sum-Squared (RSS)* technique did not yield uncertainties with physical significance for *x* and q_i. Yang (1987) suggests a few percentage points would be a reasonable estimate for the uncertainty in composition. Talu (1998) gives a detailed account of the difficulties encountered in quantifying uncertainties in binary adsorption particularly for the adsorbed phase. The uncertainties in the total amount adsorbed, *q* was calculated using the methods used in the pure component measurements. Uncertainties of approximately 5% are reported; comparable to literature (Kaul, 1987; Lee et al., 2013).

Table 6 - 10: Adsorption data for the binary system of ethane/ethylene on 13X at 323 K and 1.378 bar.

ethane (1)		**ethylene (2)**		q_1 (mmol/g)	q_2 (mmol/g)	q_{total} (mmol/g)	u_c (mmol/g)
x	y	x	y				
0.915	0.989	0.085	0.011	1.70	0.16	1.86	0.13
0.847	0.975	0.153	0.025	1.59	0.29	1.87	0.12
0.691	0.924	0.309	0.076	1.34	0.60	1.93	0.12
0.598	0.886	0.402	0.114	1.18	0.79	1.98	0.12
0.453	0.804	0.547	0.196	0.94	1.13	2.07	0.11
0.422	0.776	0.578	0.224	0.89	1.22	2.11	0.10
0.249	0.611	0.751	0.389	0.56	1.70	2.26	0.10
0.176	0.500	0.824	0.500	0.41	1.93	2.34	0.10
0.092	0.305	0.908	0.695	0.23	2.25	2.48	0.10
0.010	0.043	0.990	0.957	0.03	2.61	2.64	0.09
$u_c(T) = 0.03$ K							
$u_c(P) = 0.002$ bar							
$u_c(y) = 0.007$ mole fraction							

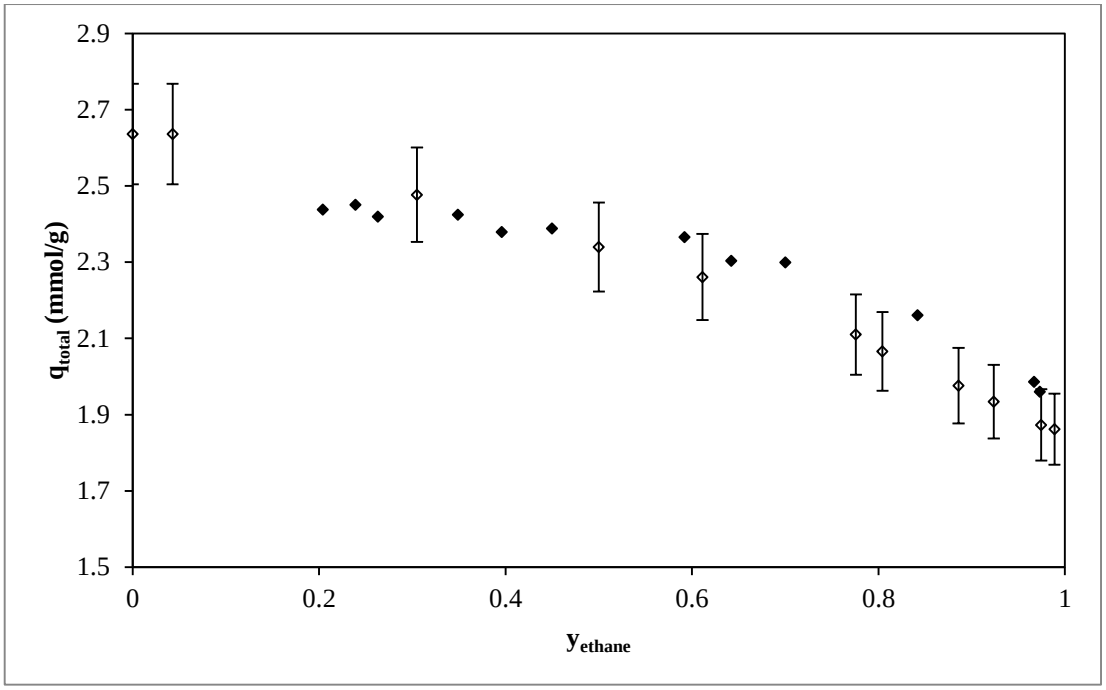

Figure 6 - 13: Adsorption data for the binary system ethane/ethylene on 13X at 323 K and 1.378 bar. (♦), Danner and Choi (1978); (◊), this study.

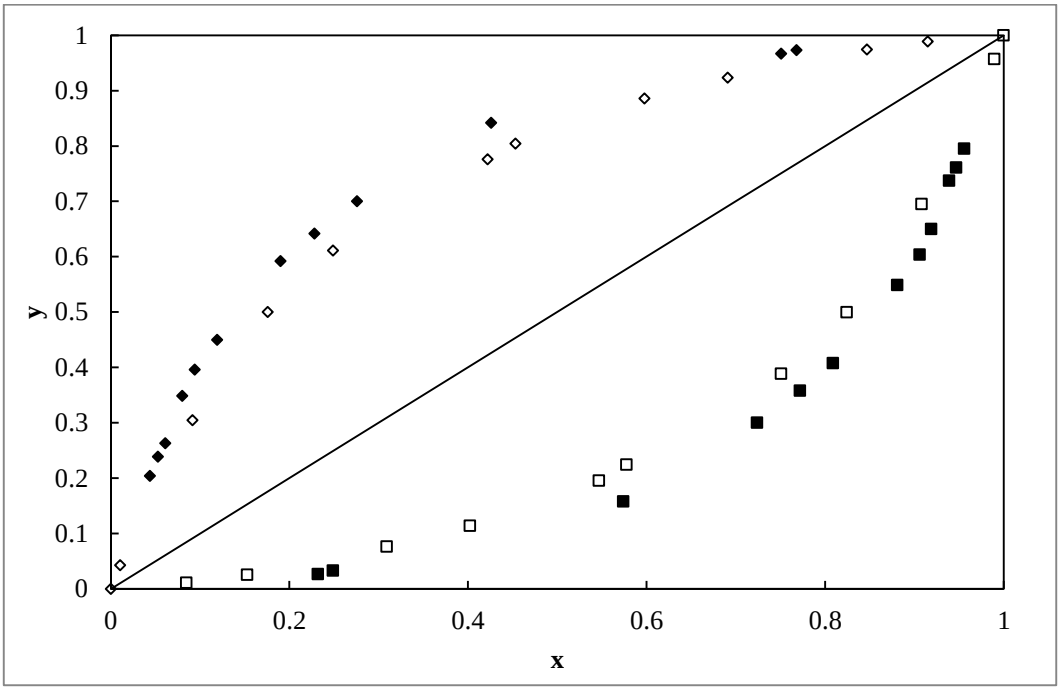

Figure 6 - 14: Adsorption data for the binary system ethane/ethylene on 13X at 323 K and 1.378 bar. (♦), Ethane – Danner and Choi (1978); (◊), Ethane this study; (■), Ethylene - Danner and Choi, 1978; (□), Ethylene – this study.

Danner and Choi (1978) did not report experimental uncertainties in their study. The data measured in this study has an experimental uncertainty of 5%. The data measured compares favourably with the literature within the experimental uncertainties shown in Figure 6 - 13. A detailed description of the sampling technique used in their study was not provided. The study of Dorfman and Danner (1975), the study in which the equipment description is provided, states merely that a sample is removed from the system and analysed using a GC. The equipment description (Figure 1) in the study of Dorfman and Danner (1975) does not indicate the use of any specialised sampling equipment. The different sampling technique used in this study may have affected the equilibrium compositions measured. This departure from the literature is presented in Figure 6 - 13. However, the deviations between the literature and this study are within the error of a few percentage points suggested by Yang (1987). The data measured in this study follow a smooth trend; the data of Danner and Choi (1978) shows considerable scatter, Figure 6 - 13. The smoothness of the data indicates good experimental technique and experimental apparatus.

The principle outcome of the binary measurements was to determine the potential of 13X to separate an ethane/ethylene mixture. The selectivity of the zeolite is presented using a separation factor α, discussed in Chapter 2.

$$\alpha_{12} = \frac{x_1/x_2}{y_1/y_2} \qquad (2.1)$$

Often, the use of adsorption as a separation technique is grouped into purification and bulk separation processes. The distinction is made based on the initial composition of the adsorbate. Initial compositions across the composition range were investigated to determine which group of separations zeolite 13X would most likely find application in.

Table 6 - 11: Separation factor, α_{12} for the ethane/ethylene system at 323K and 1.378 bar across the composition range.

Feed Composition		**Equilibrium**				**α_{12}**
		Ethane (1)		**Ethylene (2)**		
y_1	**y_2**	**x_1**	**y_1**	**x_2**	**y_2**	
0.921	0.079	0.915	0.989	0.085	0.011	0.123
0.857	0.143	0.847	0.975	0.153	0.025	0.144
0.709	0.291	0.691	0.924	0.309	0.076	0.185
0.619	0.381	0.598	0.886	0.402	0.114	0.191
0.478	0.522	0.453	0.804	0.547	0.196	0.202
0.447	0.553	0.422	0.776	0.578	0.224	0.211
0.273	0.727	0.249	0.611	0.751	0.389	0.211
0.196	0.804	0.176	0.500	0.824	0.500	0.213
0.104	0.896	0.092	0.305	0.908	0.695	0.230
0.012	0.988	0.010	0.043	0.990	0.957	0.234
$u_c(T) = 0.03$ K						
$u_c(P) = 0.002$ bar						
$u_c(y) = 0.007$ mole fraction						

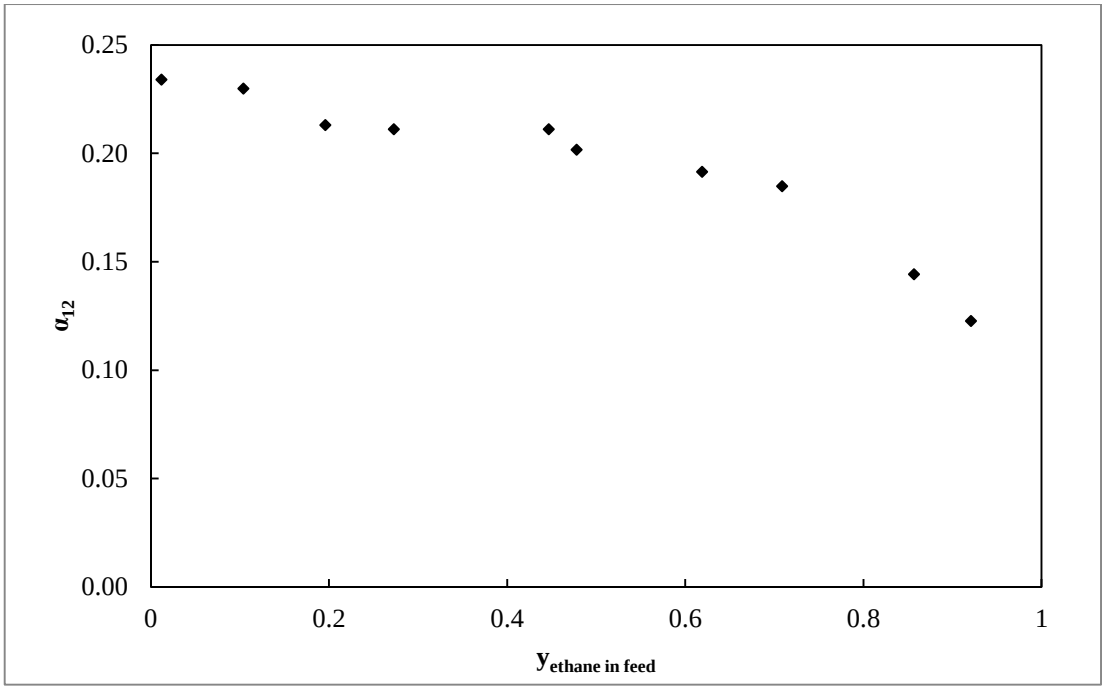

Figure 6 - 15: Separation factor, α_{12} vs. y for the binary mixture of ethane/ethylene at 323K and 1.378 bar.

The lack of binary adsorption data for the ethane/ethylene system in the literature poses a challenge when an attempt is made to benchmark the adsorbents selectivity. Mofarahi et al (2013) predicted the selectivity of zeolite 5A for ethylene. These predictions, however, are not reported at 323 K. Furthermore, the separation factor is reported as a function of equilibrium composition (α_{12} *vs.* y_1). It would prove more useful to determine selectivity as a function of initial composition, as presented in this study.

Analogous to relative volatility used in distillation, a separation factor close to unity is undesirable and indicates a difficult separation. The system of ethane and ethylene is easily separated via adsorption – as indicated by the separation factor – on zeolite 13X. Separation may be achieved across the composition range with better separation possible if the feed is rich in ethane. This trend lends itself to the use of adsorption as a purification step in a separation train, perhaps preceded by another method of separation. Danner and Choi (1978) determined that temperature had a minimal effect on the separation that could be achieved via adsorption. Unlike other separation techniques such as distillation, the use of adsorption does not require extreme operating temperatures and pressures to separate a mixture of ethane and ethylene.

To achieve a relative volatility comparable to the separation factors shown above, a distillation column at 1 bar would have to operate at 130 K (Poling et al., 2001). It is unlikely that such a column would be used in an industrial separation train. Instead, high pressure columns are used to limit extreme temperature requirements. A typical industrial column would operate at 250 K and 23 bar with over 100 trays. Cryogenic distillation alone uses an estimated 30 TWh (Terawatt hour) of energy annually, accounting for approximately 6% of the energy used in all distillation processes (Bao et al, 2011). In the early 90's, the capital costs of a world class ethylene unit exceeded $500 million; today that figure stands at approximately $750 million. A considerable amount of the capital expenditure for the plan is dedicated to the olefin/paraffin separation

(Elridge, 1993). The large capital costs associated with cryogenic distillation has fuelled research into other separation techniques, such as adsorption.

The adsorption amounts presented in this study are the *absolute* amounts adsorbed. In chapter 4, the methods to determine the *absolute* amount adsorbed from the experimentally determined *excess* amount adsorbed were discussed. In this study, the absolute amount adsorbed was not significantly greater than the excess amount adsorbed. The highest difference recorded was 0.31% for the adsorption of ethane at a pressure 1.367 bar and a temperature of 298.13 K.

7

Chapter 7: Modelling Adsorption Equilibria

7.1. Verification of the Models used for the Regression of the Measured Data

A review of the models used for correlating and predicting adsorption equilibria is presented in Chapter 3. In this study, the Langmuir Model, Langmuir-Freundlich (Sips) Model and Vacancy Solution Model (VSM) were used to model the measured data. The Langmuir model was selected as a starting point as it is an ideal model. The next model selected, the empirical Sips model, improved on the Langmuir model. As mentioned in Chapter 3, the Sips model is popular as it is able to model a wide range of equilibrium data (Malek and Farooq, 1996). Both the Langmuir and Sips models apply the Langmuir approach to modelling adsorption equilibrium data. The third model used in this study, the vacancy solution model applies the Gibbs approach. The model makes no assumption of ideality and is based on thermodynamic first principles, as discussed in Chapter 2 and Chapter 3. The potential theory approach is not used in this study. The adsorbed phase molar volume used in the potential theory approach is not very well defined. In addition the Dubinin-Radushkevich (D-R) equation is unable to correlate data at very low and very high pressures (Malek and Farooq, 1996).

Data regression was undertaken using MATLAB. A least squares technique, by way of the built-in *fminsearch* function was used. As a means of verifying the result of the *fminsearch* technique, the built in *nlinfit* and *lsqcurvefit* functions were used in the Langmuir and Sips models. The MATLAB code written for the data regression was verified by comparing the model parameters determined in this study to those reported in the literature. The Absolute Average Deviation (AAD) quantified the fit.

7.1.1. The Langmuir Model

Three data sets were used to verify the MATLAB code for the Langmuir model. The data of Pakseresht et al. (2002), Nam et al. (2005) and Tzabar et al. (2011) was used. The model equation is provided in Eq. (3 - 7).

The Langmuir model may be linearized, allowing the use of linear regression techniques to determine the model parameters. The linearized form is given by:

$$\frac{1}{q} = \frac{1}{q^{\infty} b}\frac{1}{P} + \frac{1}{q^{\infty}} \qquad (7 - 1)$$

A plot of 1/q vs. 1/P yields the required parameters. The model parameters determined in this study for data from Pakseresht et al. (2002) for the adsorption of ethylene on 5A zeolite are identical to the parameters reported by the authors. The parameters are presented in Table 7 - 1. The experimental data, along with the regressed fit is presented in Figure 7 - 1.

The simplicity of the Langmuir model, i.e., the ability to linearize the model and then solve for the model parameters using linear regression makes the model appealing. However, this method is not always reliable. The transformation of the data required for linearization can result in modifications of the error structure, introduction of error into the independent variable and alteration of weighting of data points. This may lead to differences in model parameters determined using linear and nonlinear regression (Bolster and Hornberger, 2007).

In this study, the data of Pakseresht et al. (2002) was correlated using the Langmuir model in its nonlinear form. The parameters determined using this technique for the regression is also presented in Table 7 - 1 and the model fit is presented in Figure 7 - 1.

Table 7 - 1: Model parameters and errors for the Langmuir Model for the data of Pakseresht et al. (2002) for ethylene on 5A zeolite using linear and nonlinear regression.

	T = 303 K			**T = 373 K**		
	linear		**nonlinear**	**linear**		**nonlinear**
	This study	Pakseresht et al. (2002)	This study	This study	Pakseresht et al. (2002)	This study
q^{∞}(mmol/g)	3.338	3.338	3.309	2.507	2.507	2.471
b (bar^{-1})	1.50	1.50	1.59	1.01	1.01	1.08
AAD %	1.02	1.02	1.08	1.75	1.75	1.93
$$AAD\ \% = \frac{100}{N}\sum_{i=1}^{N}\left(\frac{\left\|q_{exp} - q_{calc}\right\|}{q_{exp}}\right)_i$$						

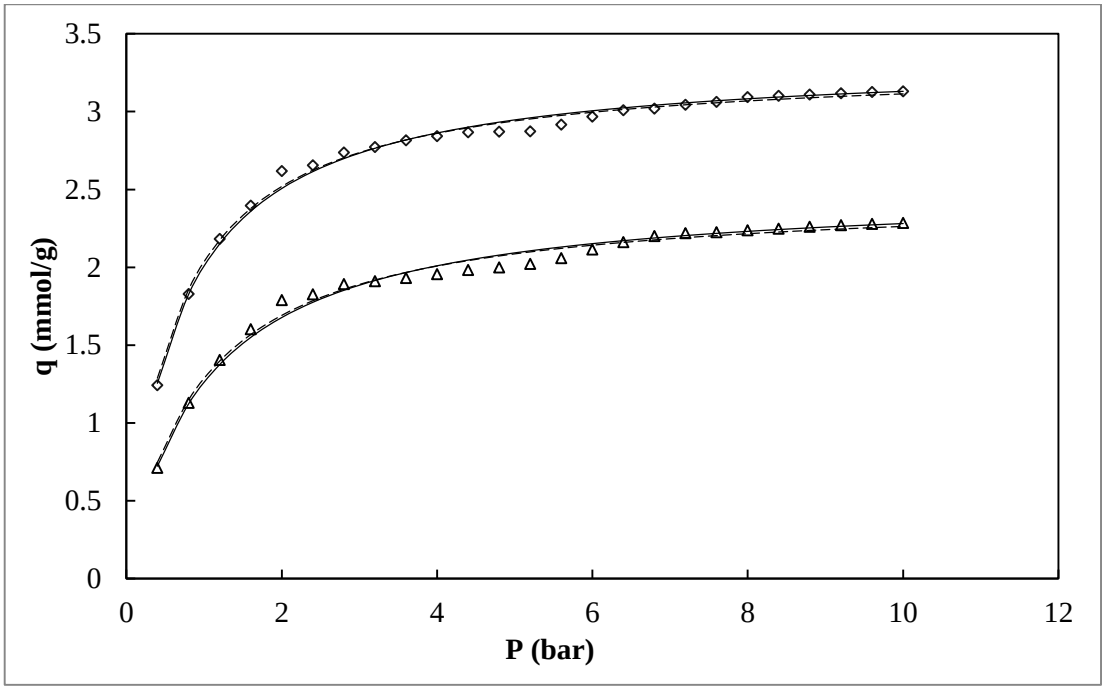

Figure 7 - 1: Equilibrium adsorption isotherms for the adsorption of ethylene on 5A zeolite (Pakseresht et al, 2002). (◊), 303 K; (Δ), 373; (—), regressed fit using linear regression; (---), regressed fit using nonlinear regression. The Langmuir model was used to perform the data regression.

The linear regression technique worked well for this data set. This is however not always the case, therefore non-linear regression is preferred.

Nonlinear regression was used to determine parameters for the Langmuir model for the data of Nam et al. (2005). The parameters determined in this study, and those reported by Nam et al. (2005) are presented in Table 7 - 2. The model data are presented in Figure 7 - 2. The parameters determined in this study are identical to those reported by Nam et al. (2005).

Table 7 - 2 Model parameters and errors for the Langmuir Model for the data of Nam et al. (2005) for ethane on 5A zeolite using nonlinear regression.

	T = 293 K		T = 303 K		T = 313 K	
	Nam et al. (2005)	**This study**	**Nam et al. (2005)**	**This study**	**Nam et al. (2005)**	**This study**
q^{∞} (mmol/g)	2.465	2.465	2.389	2.389	2.342	2.343
b (bar^{-1})	1.185	1.185	1.004	1.005	0.926	0.926
AAD %	8.60	8.60	10.11	10.11	12.86	12.86

$$AAD\ \% = \frac{100}{N}\sum_{i=1}^{N}\left(\frac{\left|q_{exp} - q_{calc}\right|}{q_{exp}}\right)_i$$

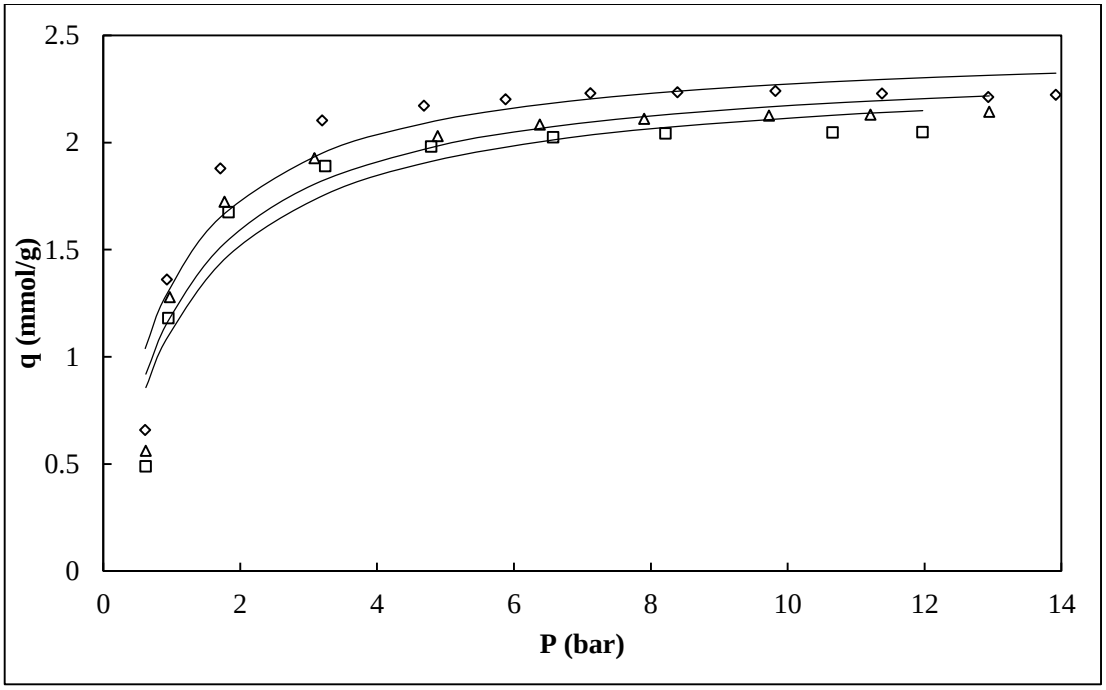

Figure 7 - 2: Equilibrium adsorption isotherms for the adsorption of ethane on activated carbon (Nam et al., 2005). The regressed parameters in this study showed no appreciable differences from the literature. (◊), 293 K; (Δ), 303 K; (□), 313 K; (–), regressed fit calculated in this study. The Langmuir model was used to perform the data regression.

The data of Tzabar et al. (2011) for the adsorption of ethane on activated carbon was correlated using the Langmuir model in its nonlinear form. The parameters regressed in this study resulted in a better fit as shown in Table 7 - 3. Tzabar et al (2011) used the Langmuir model in the linear form and this is perhaps the reason for the better fit obtained in this study.

Table 7 - 3: Model parameters and errors for the Langmuir Model for the data of Tzabar et al. (2011) for ethane on activated carbon using nonlinear regression.

	T = 293 K		T = 313 K		T = 333 K	
	Tzabar et al. (2011)	**This study**	**Tzabar et al. (2011)**	**This study**	**Tzabar et al. (2011)**	**This study**
q^{∞} (mmol/g)	5.4	5.7	5.5	5.8	5.5	5.8
b (bar^{-1})	1.550	1.332	0.763	0.660	0.469	0.395
AAD %	3.76	3.72	2.80	2.73	2.78	2.69

$$AAD\ \% = \frac{100}{N}\sum_{i=1}^{N}\left(\frac{\left|q_{exp} - q_{calc}\right|}{q_{exp}}\right)_i$$

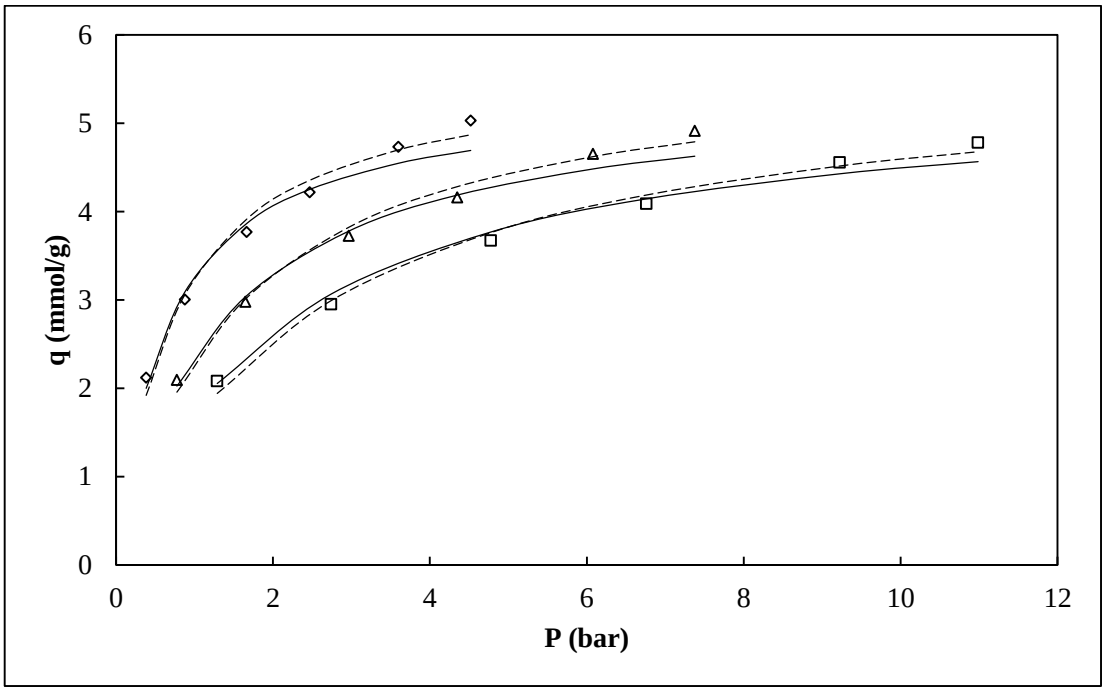

Figure 7 - 3: Equilibrium adsorption isotherms for the adsorption of ethane on activated carbon (Nam et al., 2005). The regressed parameters in this study showed a small improvement in the model fit compared to the literature. (◊), 293 K; (Δ), 313 K; (□), 333 K; (—), regressed fit using literature parameters; (---), regressed fit using parameters calculated in this study. The Langmuir model was used to perform the data regression.

7.1.2. The Sips Model

The data of Pakseresht et al. (2002) was regressed using the Sips model. The model parameters obtained in this study and those of Pakseresht et al. (2002) are presented in Table 7 - 4. The experimental data along with regressed fits are presented in Figure 7 - 4.

The parameters determined in this study, were close to, but not identical to those of Pakseresht et al. (2002). The Sips model is an empirical one and caution must be used when attaching any physical significance to model parameters. However, this difference is not appreciable as seen from Figure 7 - 4 with both sets of parameters providing a good representation of the experimental data.

The data measured at 573 K is of concern; the saturation limit, q^{∞}, of 9.558 mmol/g calculated by Pakseresht et al. (2002) was unusually high. Physical adsorption capacity is inversely proportional to temperature, see Chapter 2. The saturation limit at 573 K should be less than 2.401 mmol/g, much lower than the calculated value of 9.558 mmol/g. The same trend was observed when the data of Pakseresht et al. (2002) was regressed using the MATLAB code written in this study. However, this value is considerably lower than that of Pakseresht et al. (2002). The higher value of the saturation limit is a result of the linear trend of the data. Average absolute deviations (AAD) calculated in this study were comparable to those of Pakseresht et al. (2002). The differences in model parameters determined in this study to those of Pakseresht et al. (2002) are attributed to variations in computational algorithms used to perform the regression.

Table 7 - 4: Model parameters and errors for the Sips Model for the data of Pakseresht et al. (2002) for ethylene on 5A zeolite using linear and nonlinear regression.

	T = 373 K		T = 573 K	
	This study	**Pakseresht et al. (2002)**	**This study**	**Pakseresht et al. (2002)**
q^{∞} (mmol/g)	2.473	2.401	3.131	9.558
b (bar^{-1})	1.082	0.741	0.045	0.023
c	0.998	1.095	1.043	0.916
AAD %	1.94	1.85	1.94	1.17
$AAD\ \% = \frac{100}{N}\sum_{i=1}^{N}\left(\frac{\lvert q_{exp} - q_{calc}\rvert}{q_{exp}}\right)_i$				

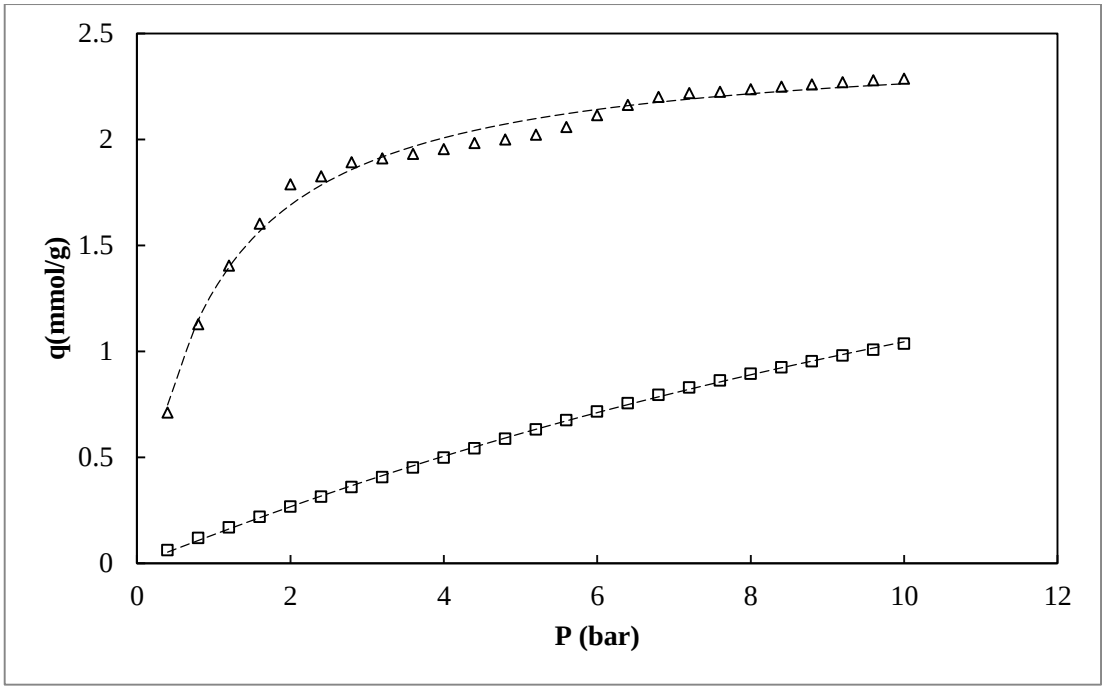

Figure 7 - 4: Equilibrium adsorption isotherms for the adsorption of ethylene on 5A zeolite (Pakseresht et al, 2002). (◊), 303 K; (Δ), 373; (□), 573K; (---), regressed fit using nonlinear regression. The Sips model was used to perform the data regression.

7.1.3. The Vacancy Solution Model (VSM)

The data of Kaul (1987) and Mofarahi and Salehi (2013) were used to verify the MATLAB code written in this study for the VSM model. The MATLAB code written to perform regression of the experimental data was significantly more complex than the Langmuir and Sips models. In Eq. (3 -20), q is implicit in the model. The technique to solve for q implicitly increased computational time significantly.

The adsorption isotherms of Kaul (1987) for ethane on activated carbon at 310.95 K and 422.05 K were used. The model parameters obtained in this study and those reported in literature are presented in Table 7 - 5. The experimental data along with model fit are presented in Figure 7 - 5.

The model parameters calculated in this study differed from those of Kaul (1987). These differences however were not substantial. The parameters determined in this study provide a better fit than those of Kaul (1987). The differences are attributed to better computational power provided by modern day computers. The exact regression technique used by Kaul is not specified. In this study, the Nelder-Mead simplex direct search method was used. The differences in parameters could be a result of the different regression methods used.

Table 7 - 5: Model parameters and errors for the VSM for the data of Kaul (1987 for ethane on activated carbon.

	T = 311 K		T = 422 K	
	Kaul (1987)	**This study**	**Kaul (1987)**	**This study**
q^{∞} (mmol/g)	6.14	6.26	4.13	4.51
b_1 (bar^{-1})	19.491	21.573	0.951	0.918
Λ_{1v}	0.175	0.274	0.524	0.454
Λ_{v1}	3.870	3.653	1.910	2.201
AAD %	7.68	3.96	6.06	2.83
$$AAD\ \% = \frac{100}{N}\sum_{i=1}^{N}\left(\frac{\left\|q_{exp} - q_{calc}\right\|}{q_{exp}}\right)_i$$				

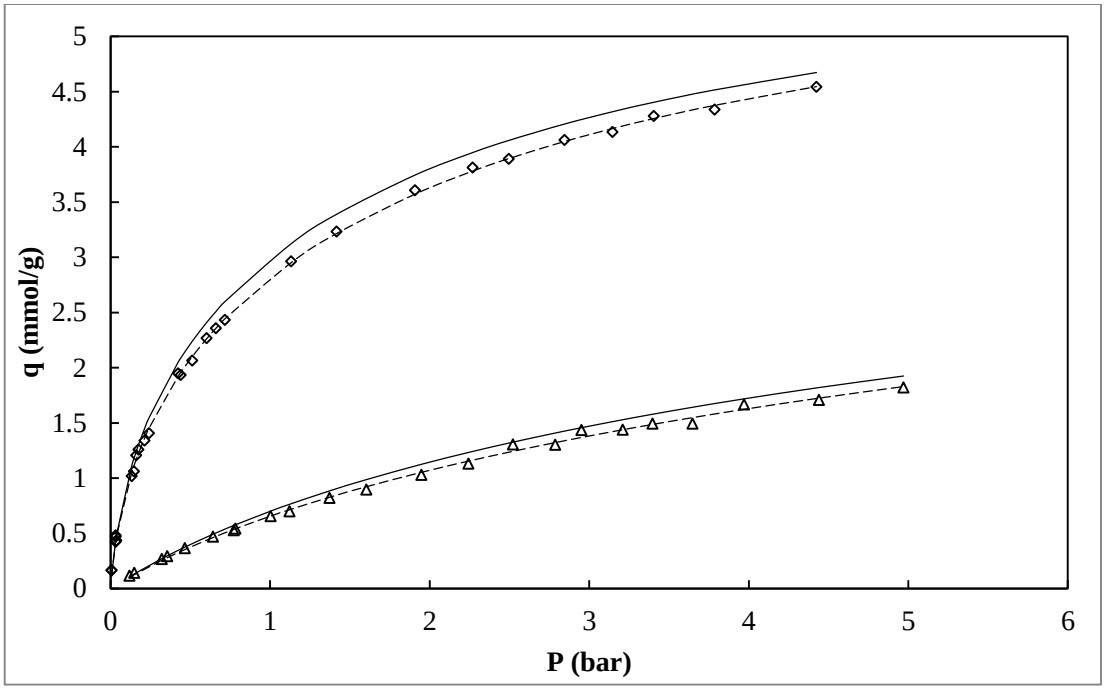

Figure 7 - 5: Equilibrium adsorption isotherms for the adsorption of ethane on activated carbon (Kaul, 1987). (◊), 311 K; (Δ), 422 K; (—), regressed fit using literature parameters; (---), regressed fit using parameters calculated in this study. The VSM model was used to perform the data regression.

The adsorption isotherms of Mofarahi and Salehi (2013) for the adsorption of ethane on zeolite 5A at 283 K, 303 K and 323 K were used to verify MATLAB code written in this study for the VSM model. The model parameters obtained in this study and those of Mofarahi and Salehi (2013) are presented in Table 7 - 6. The experimental data along with model fit are presented in Figure 7 - 6.

The model parameters regressed in this study differed from those reported by Mofarahi and Salehi (2013). With the exception of saturation limits (q^{∞}) these differences are substantial. In some instances, the difference in values being orders of magnitude higher. This is the case even when the parameters of Mofarahi and Salehi (2013) were used as initial estimates. The model used in

this study produces similar model parameters to those of Kaul et al. (1987) and produces model parameters that result in lower errors for two of the three isotherms of the data of Mofarahi and Salehi (2013). Since the model represents the system well and is shown to produce reliable results (compared with one literature source), this model was chosen to model the data measured in this study.

Table 7 - 6: Model parameters and errors for the VSM for the data of Mofarahi and Salehi (2013) for ethane on zeolite 5A.

	T = 283 K		T = 303 K		T = 323 K	
	Mofarahi and Salehi (2013)	**This study**	**Mofarahi and Salehi (2013)**	**This study**	**Mofarahi and Salehi (2013)**	**This study**
q^{∞} (mmol/g)	2.43	2.39	2.35	2.27	2.12	2.16
b_1 (bar^{-1})	17.42	11.62	11.91	8.57	5.16	5.39
Λ_{1v}	1.847	0.942	2.686	1.465	2.152	1.927
$_{v1}$	0.5412	0.85	0.4286	0.6824	0.3291	0.519
AAD %	3.07	2.98	3.54	1.95	1.29	1.36
$$AAD\ \% = \frac{100}{N}\sum_{i=1}^{N}\left(\frac{\left\lvert q_{exp} - q_{calc}\right\rvert}{q_{exp}}\right)_i$$						

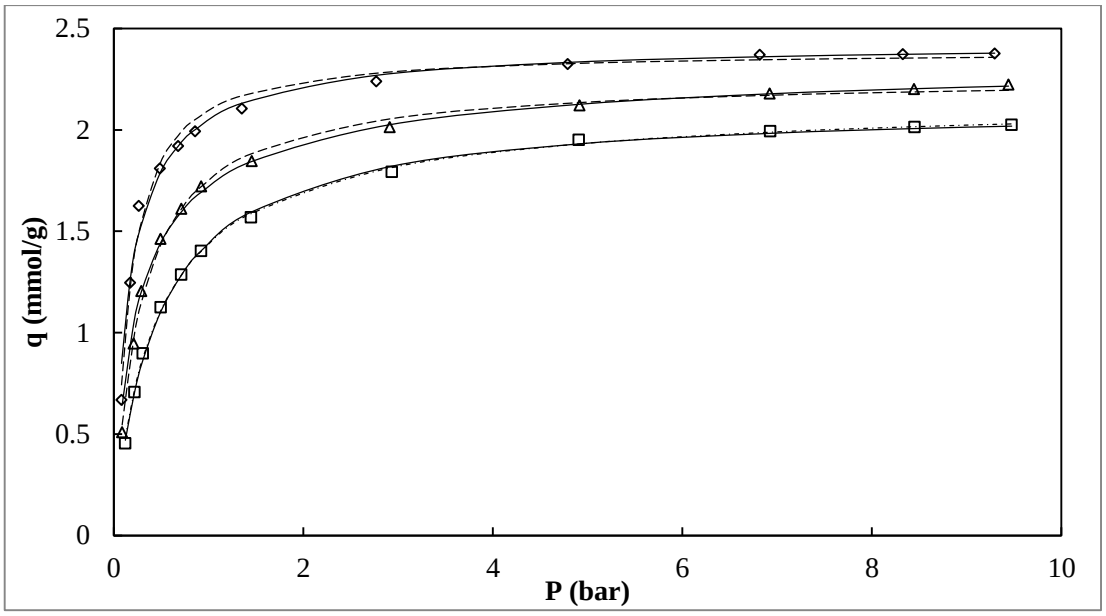

Figure 7 - 6: Equilibrium adsorption isotherms for the adsorption of ethane on zeolite 5A (Mofarahi and Salehi 2013). (◊), 283 K; (□), 323 K; (Δ), 303 K; (—), regressed fit using literature parameters; (---), regressed fit using parameters calculated in this study. The VSM model was used to perform the data regression.

7.2. Modelling of Experimental Data

The Langmuir, Sips and Vacancy Solution models were used to regress experimental pure component adsorption data and to predict binary adsorption data. The volumetric data presented in the previous chapter was regressed in the low pressure region. The gravimetric data are used to perform regression in the high pressure range (up to 15 bar). Regression of the high pressure data was undertaken to evaluate the performance of the models investigated in the high coverage area.

7.2.1. Regression of the Pure Component Data

Table 7 - 7: Model parameters and errors for the Langmuir, Sips and VSM models for adsorption data for ethane on zeolite 13X at low pressure.

	T = 298 K			T = 323 K		
Parameter	**Langmuir**	**Sips**	**VSM**	**Langmuir**	**Sips**	**VSM**
q^{∞} (mmol/g)	3.06	2.60	2.93	3.54	2.63	2.76
b (bar^{-1})	2.780	6.504	0.112	0.897	1.802	2.151
c	-	1.44	-	-	1.30	-
Λ_{1v}			0.005			0.429
Λ_{v1}			2.049			1.269
AAD %	4.71	1.10	1.77	5.03	0.78	0.21

$$AAD\ \% = \frac{100}{N}\sum_{i=1}^{N}\left(\frac{\left|q_{exp} - q_{calc}\right|}{q_{exp}}\right)_i$$

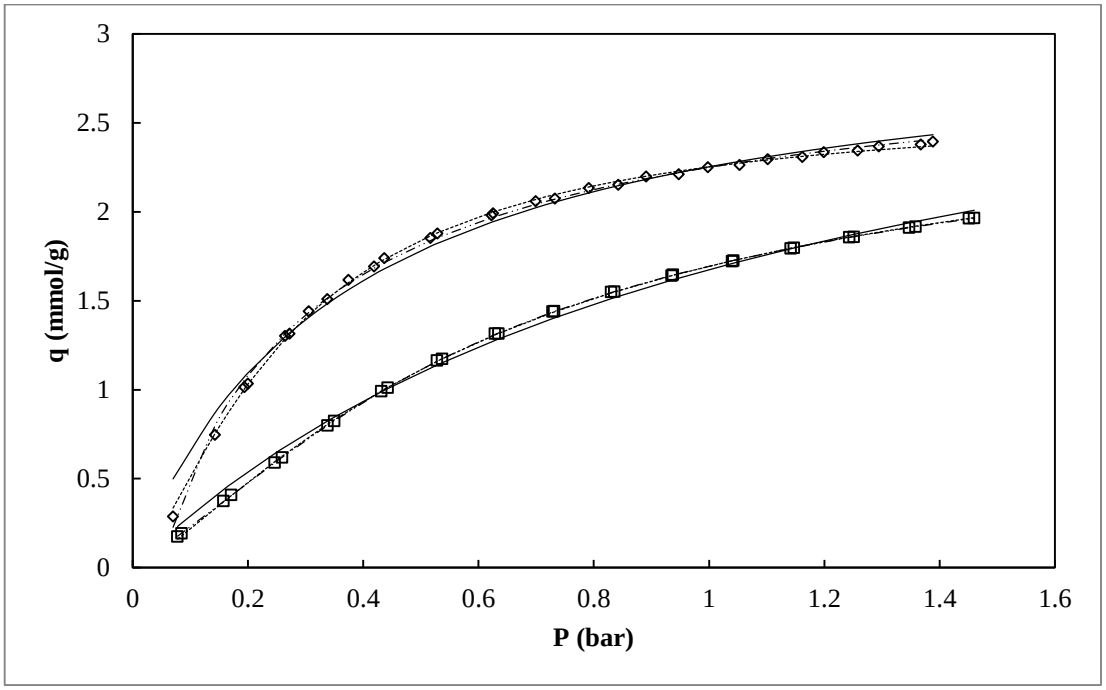

Figure 7 - 7: Experimental and model adsorption data for ethane on 13X at low pressure. (◊), 298K; (□), 323K; (—), Langmuir; (---), Sips; (—··—), VSM.

Table 7 - 8: Model parameters and errors for the Langmuir, Sips and VSM models for adsorption data for ethylene on zeolite 13X at low pressure.

	T = 298 K			T = 323 K		
Parameter	**Langmuir**	**Sips**	**VSM**	**Langmuir**	**Sips**	**VSM**
q^{∞} (mmol/g)	3.16	3.19	3.18	3.06	3.06	3.12
b (bar^{-1})	11.574	10.516	9.525	4.659	4.647	6.269
c	-	0.97	-	-	1.00	-
Λ_{1v}			6.720E-02			0.098
Λ_{v1}			2.467			2.585
AAD %	1.35	1.38	1.08	1.07	1.07	0.80
$$AAD\ \% = \frac{100}{N}\sum_{i=1}^{N}\left(\frac{\lvert q_{exp} - q_{calc}\rvert}{q_{exp}}\right)_i$$						

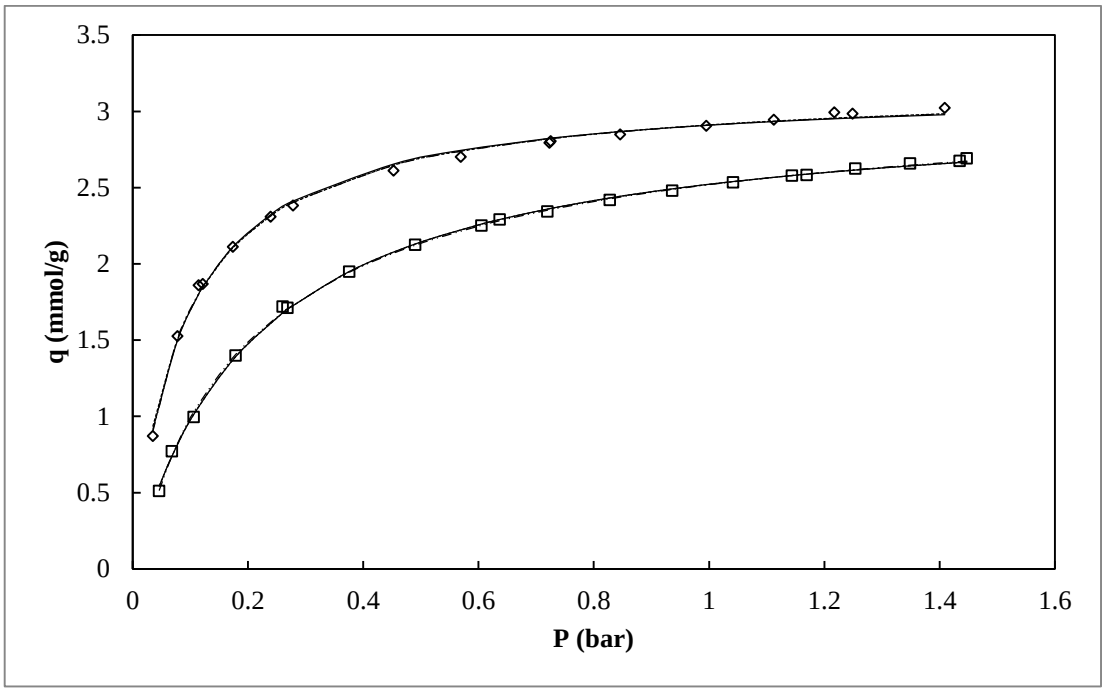

Figure 7 - 8: Experimental and model adsorption data for ethylene on 13X at low pressure. (◊), 298K; (□), 323K; (—), Langmuir; (---), Sips; (−··−), VSM.

The Langmuir model is widely used for the regression of pure component adsorption data as discussed in Chapter 3. Of the three models selected in this study, the Langmuir model produced the highest average absolute deviation (AAD), 5.03 % for ethane at 323 K. The Langmuir model overestimates the saturation limit for ethane at both temperatures investigated. However, even the worst AAD result using the Langmuir model is considerably lower than the deviations reported by Nam et al. (2005) and comparable to those reported by Tzabar et al. (2011). The AAD of 5% is comparable to the experimental uncertainties presented in Chapter 6. The regression of experimental data for ethylene using the Langmuir model produced excellent results – matching that of the Sips model.

The Sips model showed a marked improvement from the Langmuir model in the regression of data for ethane. At both temperatures studied, the Sips model returned deviations of approximately 1%, much improved from the 5% AAD produced by the Langmuir model. The improvement is expected as the Sips model has an additional parameter allowing for a much better fit to experimental data. The model however, showed no significant improvement over the Langmuir model in the regression of data for ethylene. This is attributed to the rectangular shape shown by the isotherm – discussed in Chapter 6. This is further indicated by the closeness to unity of the third model parameter, *c*.

The VSM showed improvement over the Sips models for all but one isotherm, ethane at 298 K. The improved fit is attributed to an additional parameter and the Gibbs approach used to develop the model. For ethylene at 298 K, all 3 models show deviations above 1.2 bar, indicating the regressed value for the saturation limit, q^{∞}, has been underestimated.

The model parameters determined from regression of the pure component isotherms were used to predict binary adsorption equilibria.

Table 7 - 9: Model parameters and errors for the Langmuir, Sips and VSM models for adsorption data for ethane on zeolite 13X at high pressure.

	T = 298 K			**T = 323 K**		
Parameter	**Langmuir**	**Sips**	**VSM**	**Langmuir**	**Sips**	**VSM**
q^{∞} (mmol/g)	3.64	5.44	3.63	3.34	3.86	3.29
b (bar^{-1})	1.666	0.934	1.022	1.232	1.181	1.619
c		0.26			0.53	
Λ_{1v}			0.092			0.504
Λ_{v1}			1.852			1.003
AAD %	1.07	0.19	1.13	0.83	0.17	1.19
$$AAD\ \% = \frac{100}{N}\sum_{i=1}^{N}\left(\frac{\lvert q_{exp} - q_{calc}\rvert}{q_{exp}}\right)_i$$						

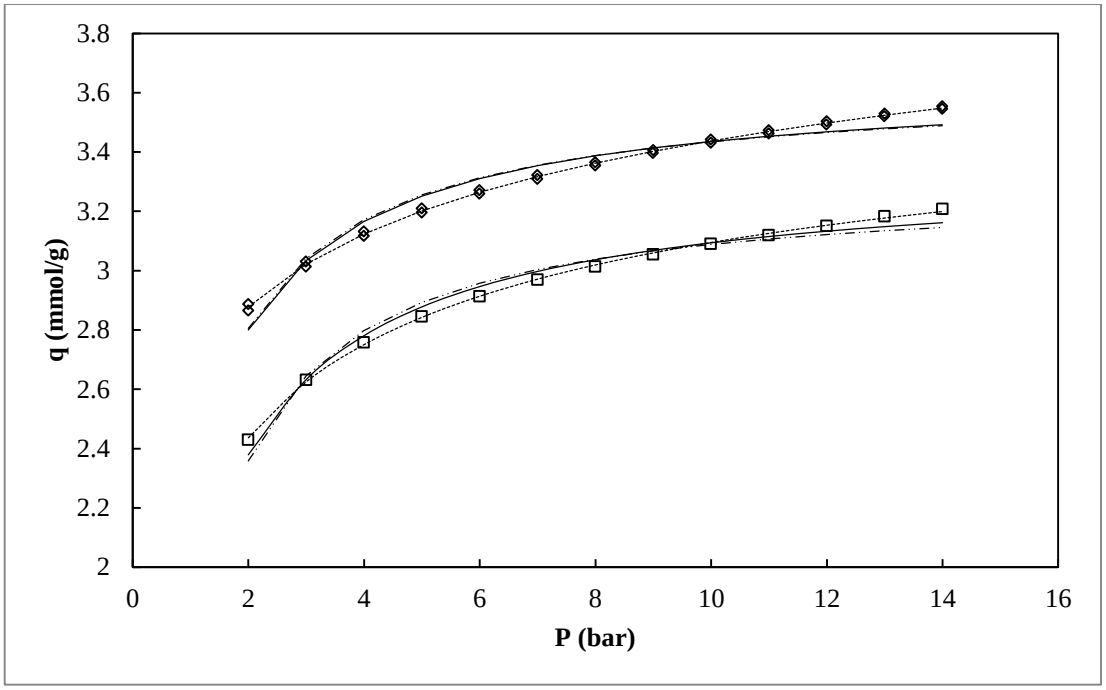

Figure 7 - 9: Experimental and model adsorption data for ethane on 13X at high pressure. (◊), 298K; (□), 323K; (—), Langmuir; (---), Sips; (−··−), VSM.

Table 7 - 10: Model parameters and errors for the Langmuir, Sips and VSM models for adsorption data for ethylene on zeolite 13X at high pressure.

	T = 298 K			T = 323 K		
Parameter	**Langmuir**	**Sips**	**VSM**	**Langmuir**	**Sips**	**VSM**
q^{∞} (mmol/g)	3.80	5.45	3.79	3.66	4.59	3.66
b (bar^{-1})	2.638	1.288	1.552	2.137	1.455	3.846
c		0.20			0.34	
Λ_{1v}			0.107			0.881
Λ_{v1}			1.683			0.755
AAD %	0.79	0.02	0.83	1.05	0.10	1.10

$$AAD\ \% = \frac{100}{N}\sum_{i=1}^{N}\left(\frac{\left|q_{exp} - q_{calc}\right|}{q_{exp}}\right)_i$$

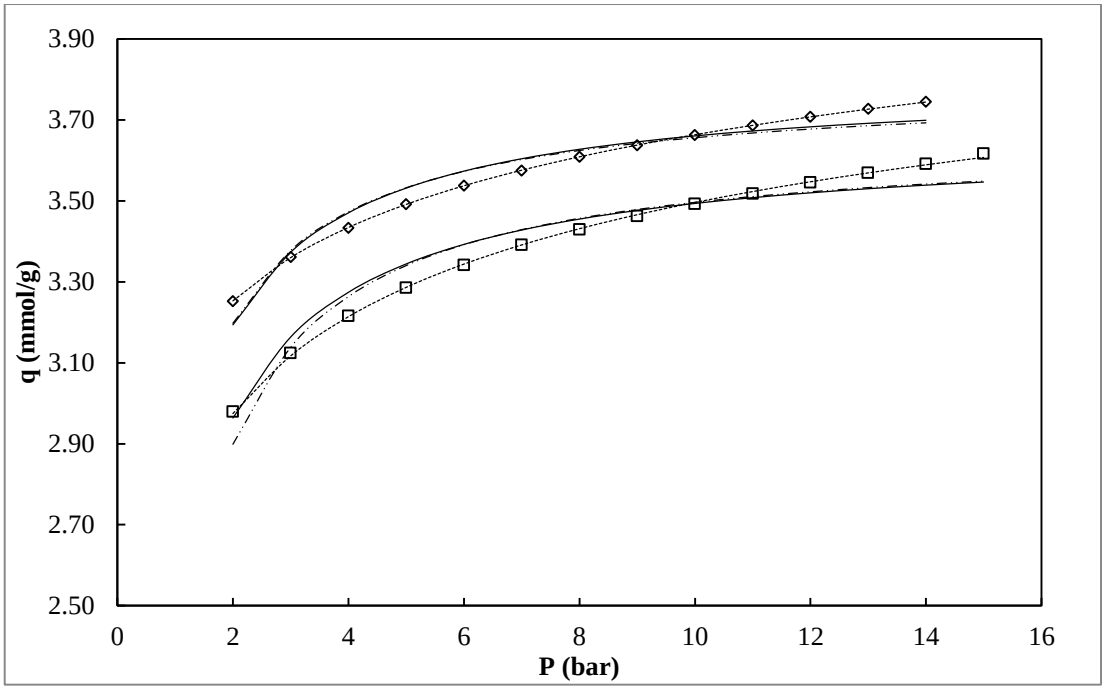

Figure 7 - 10: Experimental and model adsorption data for ethylene on 13X at high pressure. (◊), 298K; (□), 323K; (—), Langmuir; (---), Sips; (−··−), VSM.

The Langmuir and VSM models did not fit the high pressure experimental data well, for both ethane and ethylene. The Sips Model, however, provided good fits, indicated by the low AAD values, approximately 0.2 %. The parameter *c* in the Sips models returned values far from unity indicating heterogeneity.

The Langmuir model is typically used to regress adsorption data at low pressures or low coverage. As the equilibrium pressure increases, more adsorption sites are taken up by the adsorbate. The assumption of no interaction between molecules adsorbed on neighbouring sites becomes unrealistic. The Langmuir model underestimates the saturation limit for both ethane and ethylene at both temperatures studied. The predicted coverage, θ, is thus close to unity. The Langmuir model was determined to be unsuitable for application at high pressure when regressing adsorption data of ethane and ethylene on zeolite 13X.

The poor performance of the VSM model is attributed to difficulties encountered in the regression analysis. The *least squares error tolerances* used in the MATLAB code were significantly higher for the VSM model (10^{-4}) compared to the Langmuir and Sips models (10^{-9}). The higher tolerances were used out of necessity to achieve convergence of the regression analysis.

7.2.2. Prediction of the Binary Adsorption Equilibria

The three models used to regress pure component adsorption data were extended to predict binary adsorption equilibria.

7.2.2.1. The Extended Langmuir Model

The Extended Langmuir Model requires that the adsorption saturation limit for ethane and ethylene must be equal for thermodynamic consistency, viz:

$$q^{\infty}_{ethane} = q^{\infty}_{ethylene} \qquad (7 - 2)$$

This is however not the case as was shown in the data regression section. Three methods were used to predict the binary adsorption equilibria using the Extended Langmuir model. The first method used the individual saturation limits to determine the amount of ethane and ethylene adsorbed. The saturation limits determined through regression of the pure component data for ethane and ethylene, 3.54 mmol/g and 3.06 mmol/g respectively have a difference of 14%, justifying this method.

In the second method, the technique of Ruthven (1984) was used to determine a concentration-weighted saturation limit, presented in Eq. (3 -32) and repeated here for convenience:

$$\frac{1}{q^{\infty}} = \frac{x_1}{q_1^{\infty}} + \frac{x_2}{q_2^{\infty}} \qquad (3\text{-}32)$$

The concentration-weighted saturation limit was determined iteratively, as shown in Figure 7 - 11. As an initial estimate, individual saturation limits were used for ethane and ethylene, i.e. q_1^{∞} and q_2^{∞}.

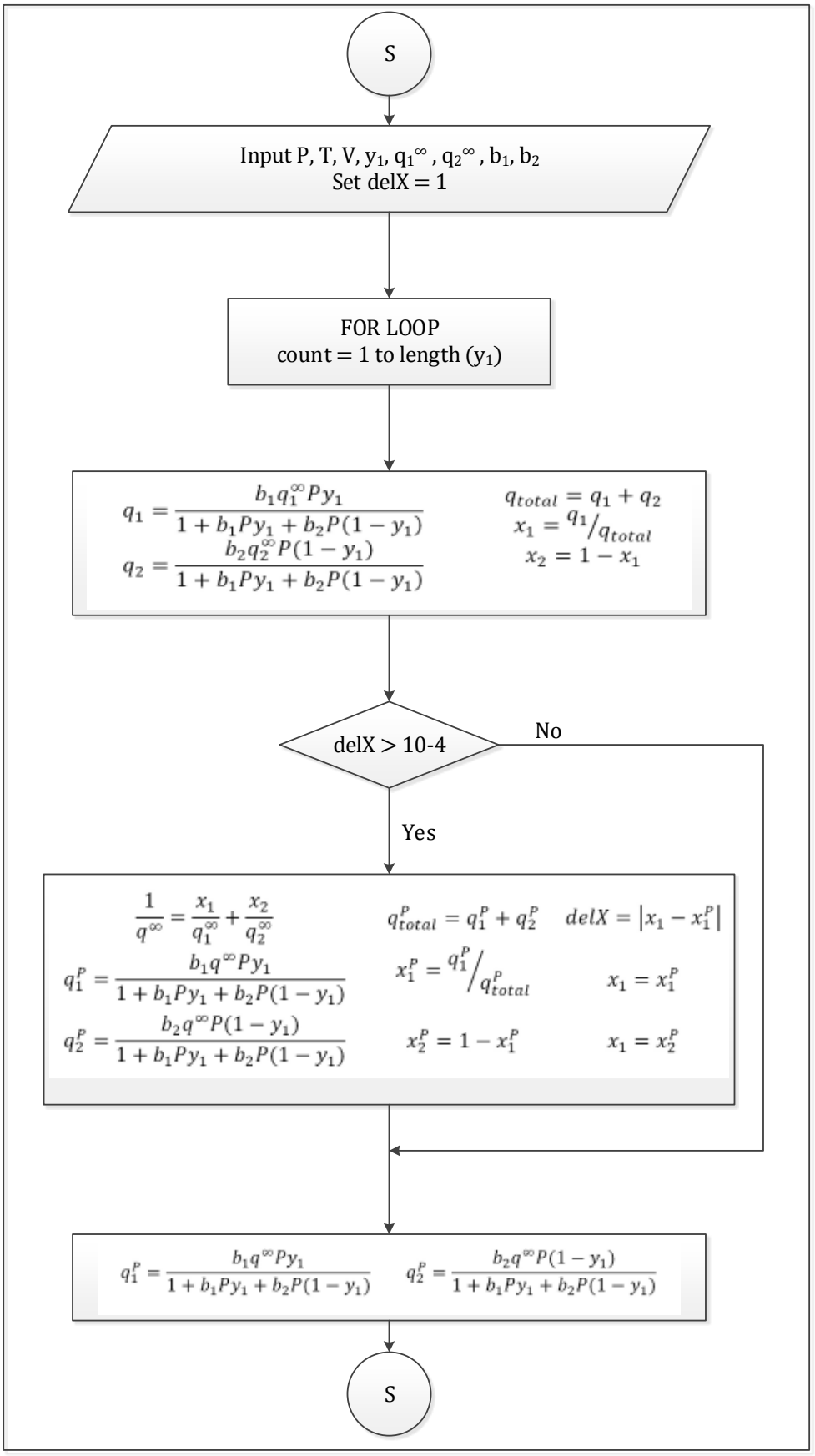

Figure 7 - 11: Flow diagram for the Extended Sips model using a concentration-weighted saturation limit.

In the third method, an average of the saturation limits for the two pure components was used, viz:

$$q^{\infty} = \frac{q_1^{\infty} + q_2^{\infty}}{2} \qquad (7 - 3)$$

This method was used since the ethane and ethylene molecules are similar in size, 4.4 Å and 4.2 Å respectively (Sigma Aldrich, 2014). Ruthven (1984) recommends an average of the saturation limits be used with caution.

Table 7 - 11: Model parameters and errors for the Extended Langmuir model for the prediction of binary adsorption equilibria of ethane + ethylene on zeolite 13X at 323 K and 1.378 bar.

	Individual saturation limits		**Concentration-weighted average saturation limit**		**Algebraic average saturation limit**	
	Ethane	**Ethylene**	**Ethane**	**Ethylene**	**Ethane**	**Ethylene**
q^{∞} (mmol/g)	3.54	3.06	Varies with concentration		3.30	
b (bar^{-1})	0.897	4.659	0.897	4.659	0.897	4.659
AAD %	6.82		2.99		7.83	
$AAD\ \% = \frac{100}{N}\sum_{i=1}^{N}\left(\frac{\lvert q_{exp} - q_{predicted}\rvert}{q_{exp}}\right)_i$						

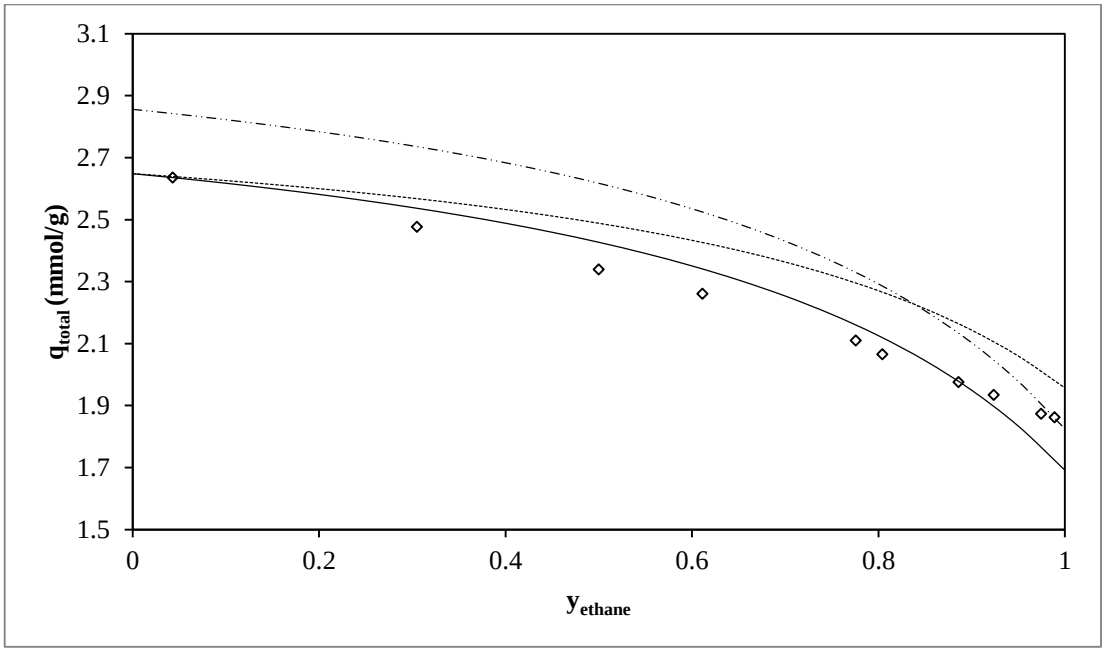

Figure 7 - 12: Experimental and predicted binary adsorption data for the ethane/ethylene binary mixture on zeolite 13X at 323 K and 1.378 bar. Predictions were performed using the Extended Langmuir model. (◊), Experimental data; (—), Extended Langmuir predictions using concentration-weighted saturation limits; (−··−), Extended Langmuir predictions using average saturation limits; (---), Extended Langmuir predictions using individual saturation limits.

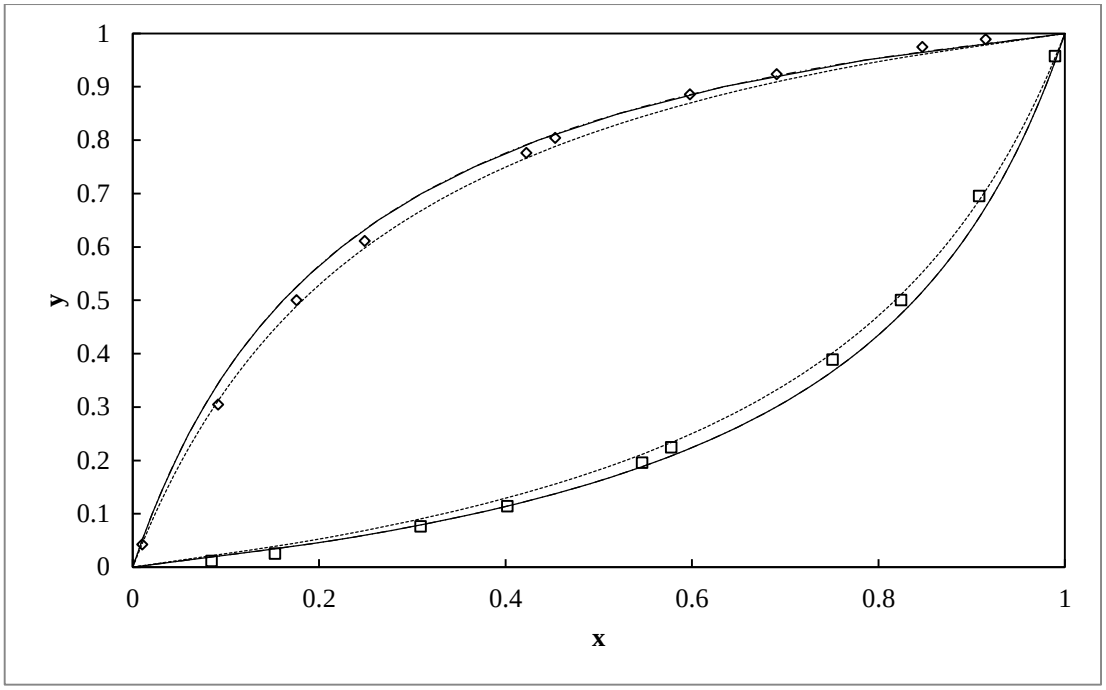

Figure 7 - 13: Experimental and predicted binary adsorption data for the ethane/ethylene binary mixture on zeolite 13X at 323 K and 1.378 bar. Predictions were performed using the Extended Langmuir model. (◊), ethane; (□), ethylene; (—), Extended Langmuir predictions using concentration-weighted saturation limits; (−··−), Extended Langmuir predictions using average saturation limits; (---), Extended Langmuir predictions using individual saturation limits.

The predictions using an average saturation limit and a concentration-weighted saturation limit appear to be identical as seen in Figure 7 - 1. However, the use of a concentration-weighted saturation limit provides better predictions as indicated in Table 7 - 11. It is not usual for a good fit on the x-y plot, Figure 7 - 13, to be obtained while there are significant deviations in the total amount adsorbed between model predictions and experimental data, Figure 7 - 12. The system of oxygen/carbon monoxide displays similar behaviour (Yang, 1987). An AAD of 3% is an acceptable result, given the experimental uncertainties discussed in Chapters 5 and 6. The predictions obtained using the individual saturation limits and an algebraic average saturation limit produced reasonable results, given the difficulty in measuring binary adsorption equilibria, however these methods must be used with caution.

7.2.2.2. The Extended Sips Model

The extended Sips model was used to predict adsorption equilibria in a manner similar to the technique used in the extended Langmuir model. Three approaches were used, viz: individual saturation limits, a concentration weighted average saturation limit and an algebraic mean for the saturation limit. The convergence criteria are the same as for the Extended Langmuir model, see Figure 7 - 11; the only difference being the model equation.

Table 7 - 12: Model parameters and errors for the Extended Sips model for the prediction of binary adsorption equilibria of ethane/ethylene on zeolite 13X at 323 K and 1.378 bar.

	Individual saturation limits		Concentration-weighted average saturation limit		Algebraic average saturation limit	
	ethane	**ethylene**	**ethane**	**ethylene**	**ethane**	**ethylene**
$\mathbf{q^{\infty}}$ **(mmol/g)**	2.63	3.06	Varies with concentration		2.85	
b ($\mathbf{bar^{-1}}$)	1.802	4.647	1.802	4.647	1.802	4.647
c	1.3	1	1.3	1	1.3	1
AAD %	3.05		6.56		11.82	
$AAD\ \% = \frac{100}{N}\sum_{i=1}^{N}\left(\frac{\lvert q_{exp} - q_{predicted}\rvert}{q_{exp}}\right)_i$						

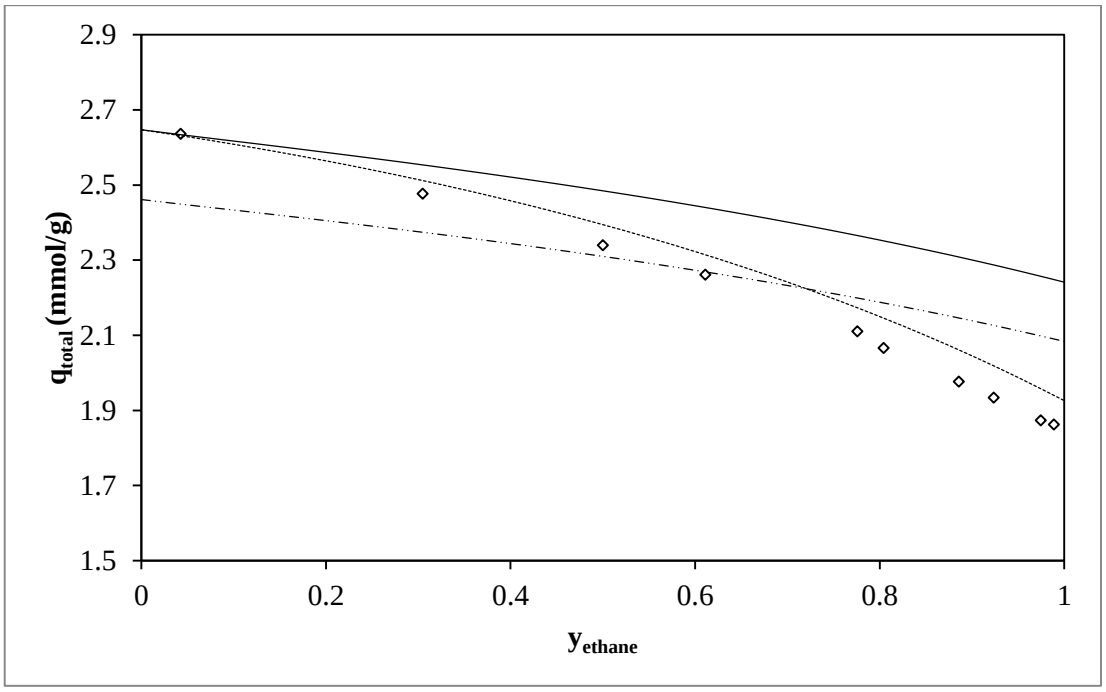

Figure 7 - 14: Experimental and predicted binary adsorption data for the ethane/ethylene binary mixture on zeolite 13X at 323 K and 1.378 bar. Predictions were performed using the Extended Sips model. (◊), Experimental data; (—), Extended Sips predictions using concentration-weighted saturation limits; (–···–), Extended Sips predictions using average saturation limits; (---), Extended Sips predictions using individual saturation limits.

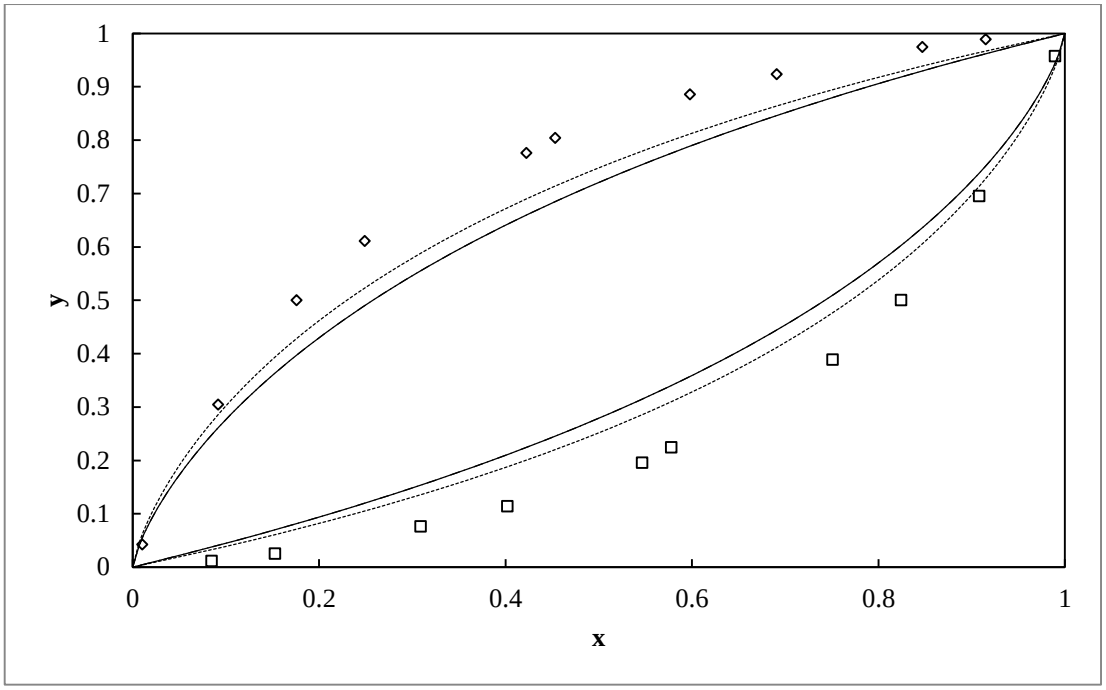

Figure 7 - 15: Experimental and predicted binary adsorption data for the ethane/ethylene binary mixture on zeolite 13X at 323 K and 1.378 bar. Predictions were performed using the Extended Sips model. (◊), ethane; (□), ethylene; (—), Extended Sips predictions using concentration-weighted saturation limits; (–··–), Extended Sips predictions using average saturation limits; (---), Extended Sips predictions using individual saturation limits.

The Extended Sips model did not perform as well as the Extended Langmuir model. This is despite performing well in the pure component regression analysis. This occurrence has also been observed by Al-Asheh et al. (2000). The best predictions were calculated using individual saturation limits. From the pure component regression, the saturation limits for ethane and ethylene are 2.63 mmol/g and 3.06 mmol/g respectively. The saturation limits have a difference of 16%. The use of an average saturation limit, both algebraic and concentration-weighted, provided poor predictions. The use of an algebraic average saturation limit provided the worst prediction, an AAD of 12%. Model deviations as high as 15% have been reported for the adsorption of hydrocarbons on zeolites (Yang, 1987).

7.2.2.3. The Vacancy Solution Model (VSM)

The VSM model provided a good model prediction of the adsorption equilibria. The assumptions made in applying the model are as follows. The adsorbate-adsorbate interactions in Eq. (3 -35) were assumed to be unity as ethane and ethylene are similar molecules. The fugacity coefficient, ϕ in Eq. (3 -42) was assumed to be unity as the model was applied at low pressure, 1.378 bar. For a given set of x_i, Eq. (3 -43) was used to calculate q_t^{∞}. Eq. (3 -35) was used to calculate the activity coefficients. Eqs. (3 -42) and (3 -44) were solved simultaneously for the gas composition and the total amount adsorbed. This was done using an iteration procedure. The following was used as the iterative condition.

$$0.999 < \sum y_i < 1.001 \qquad (7 - 4)$$

A tolerance of exactly zero, where the tolerance is defined as $|1-\Sigma y_i|$ resulted in a considerably longer computational time. The tolerance of 0.001 is well below the experimental uncertainty of 0.007 in the gas composition.

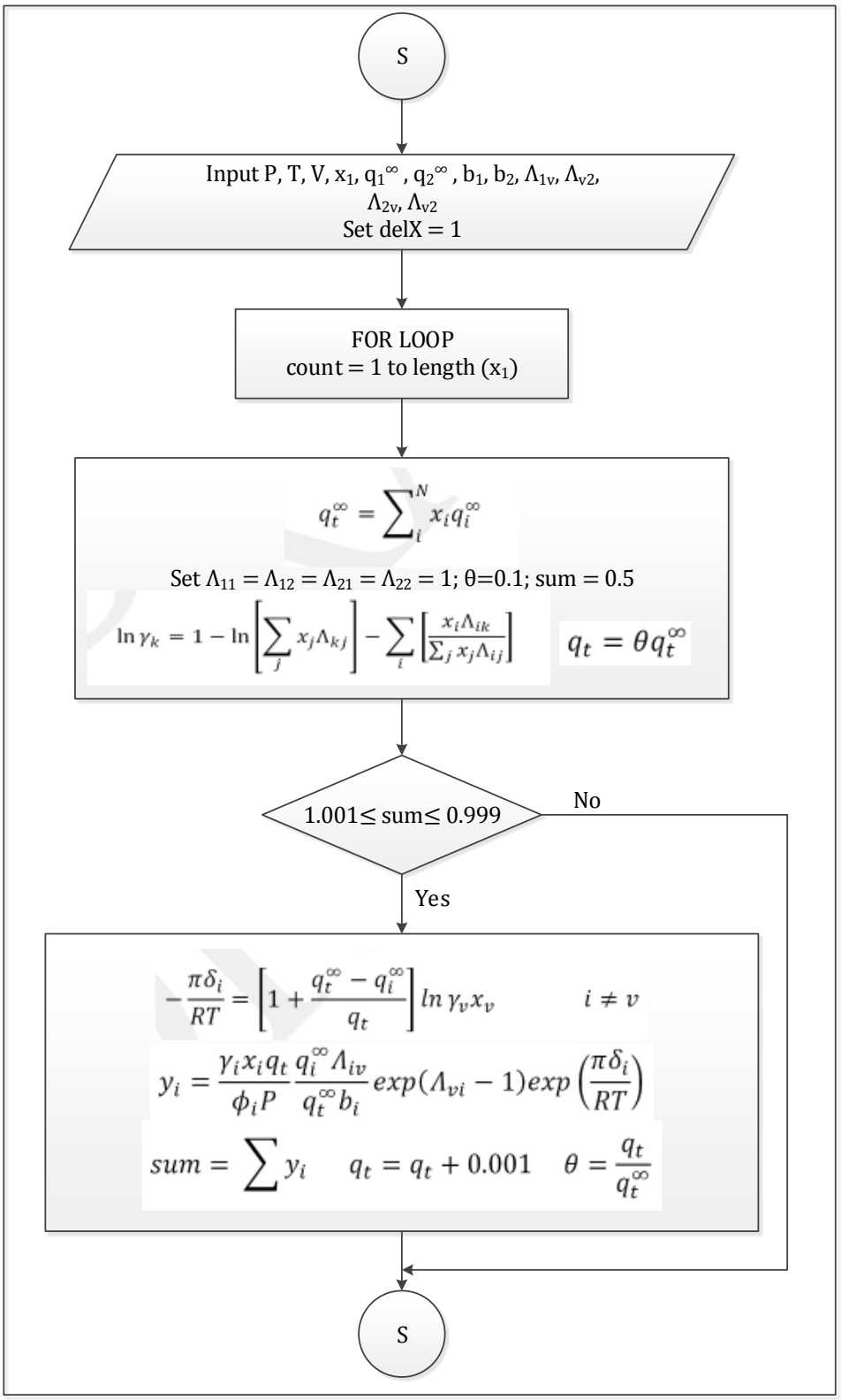

Figure 7 - 16: Flow diagram for the Extended Sips model using a concentration-weighted saturation limit.

Table 7 - 13: Model parameters and errors for the Sips model for the prediction of binary adsorption equilibria of ethane/ethylene on zeolite 13X at 323 K and 1.378 bar.

	Ethane	Ethylene
q^{∞} **(mmol/g)**	2.76	3.12
b (bar^{-1})	2.151	6.269
Λ_{1v}	0.429	0.098
Λ_{v1}	1.269	2.585
AAD %	6.10	
$AAD\ \% = \frac{100}{N}\sum_{i=1}^{N}\left(\frac{\lvert q_{exp} - q_{predicted}\rvert}{q_{exp}}\right)_i$		

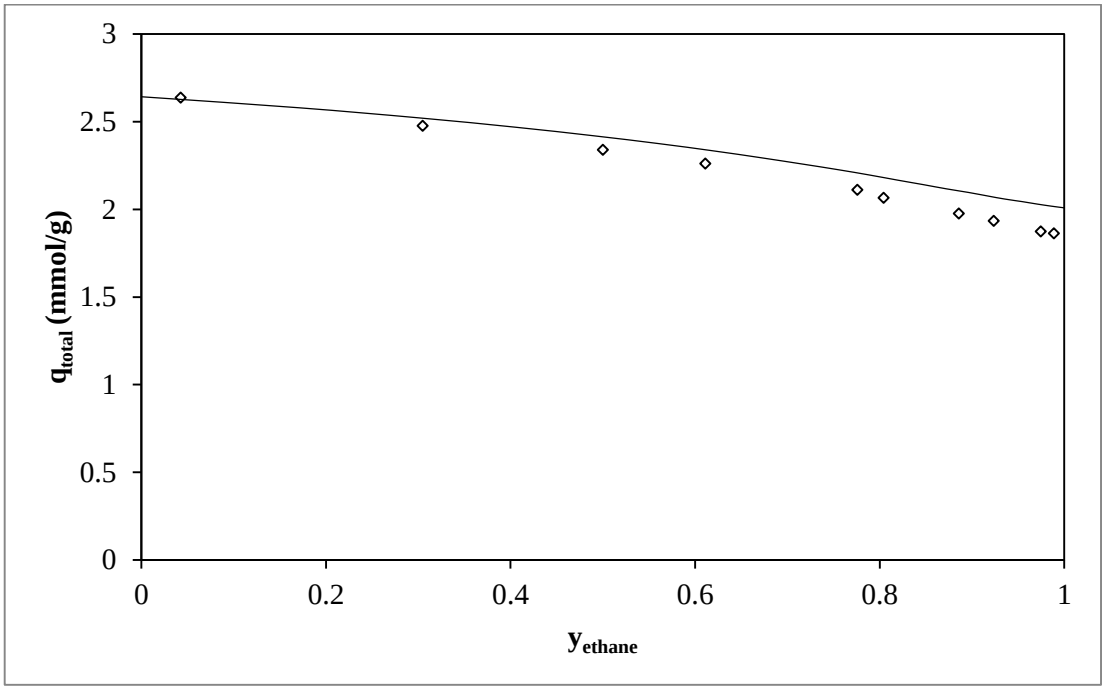

Figure 7 - 17: Experimental and predicted binary adsorption data for the ethane/ethylene binary mixture on zeolite 13X at 323 K and 1.378 bar. Predictions were performed using the VSM model. (◊), Experimental data; (—), VSM predictions.

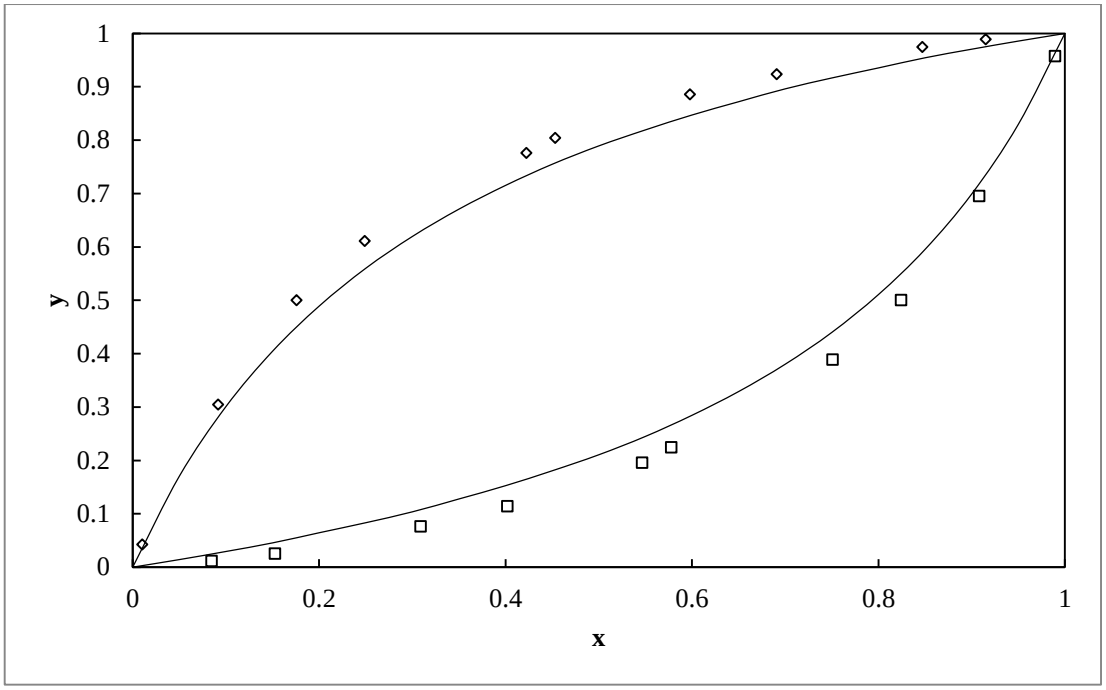

Figure 7 - 18: Experimental and predicted binary adsorption data for the ethane/ethylene binary mixture on zeolite 13X at 323 K and 1.378 bar. Predictions were performed using the VSM model. (◊), ethane; (□), ethylene; (—), VSM predictions.

8

Chapter 8: Conclusions

A volumetric apparatus and experimental technique for the measurement of adsorption equilibria was successfully developed in this study. The apparatus has a maximum operating pressure of 20 bar at a maximum operating temperature of 425 K.

Pure component adsorption isotherms were measured for ethane and ethylene on the adsorbent zeolite 13X at temperatures of 298 K and 323 K up to a pressure of 1.5 bar. The zeolite 13X showed a stronger affinity for ethylene at both temperatures studied.

Binary measurements were undertaken for the ethane/ethylene system at a temperature of 323 K and a pressure of 1.377 bar. A high selectivity was achieved for the ethane/ethylene system for all compositions studied. For an ethane rich feed (92 % ethane) a selectivity of 0.1 was determined. For an ethane lean feed (1.2% ethane) a selectivity of 0.2 was determined.

Gravimetric adsorption measurements were undertaken using the Intelligent Gravimetric Analyser (IGA). Equilibrium data were measured for methane on zeolite 13X at temperatures of 300 K and 325 K up to a pressure of 15 bar. Two new high pressure data sets were measured gravimetrically viz. pure component adsorption isotherms were measured for ethane and ethylene on 13 X at temperatures of 298 K and 323 K up to pressures of 15 bar. Comparison of the gravimetric and volumetric data indicated that the mass of the adsorbent to the volume of the adsorber affects adsorption capacity.

The experimental data were regressed using the Langmuir, Sips and VSM models. The VSM model provided the best fit for the low pressure data with average absolute deviations of approximately 1% while the Langmuir model provided the worst fit with deviations as high as 5%. These deviations are comparable with the 5% experimental uncertainties reported in this study and the literature. The Sips Model provided the best fit of the high pressure data with deviations of approximately 0.2 %.

The Extended Langmuir, Extended Sips and VSM all provided good predictions of the binary adsorption equilibria. The Extended Langmuir model performed best when a concentration-weighted saturation limit was used in the prediction with an AAD of 2.99%. The Extended Sips model performed best when individual saturation limits were used in the predictions with an AAD of 3.05%. The VSM model performed satisfactorily. The model was simplified due to the low pressure application and the similarity of the adsorbate components. An AAD of 6% is slightly higher than the 5% uncertainty reported in literature and in this study.

9

Chapter 9: Recommendations

The time taken to reach equilibrium for pure component adsorption measurements was approximately 3 to 5 hours using the volumetric technique. Equilibrium was achieved much faster using the gravimetric apparatus. The gravimetric apparatus however has a mass (of the adsorbent) to volume (of the equilibrium cell) ratio considerably smaller than the volumetric apparatus. Further studies into the effect of the mass to volume ratio will enable a better understanding of the hydrodynamics of the system assisting in achieving equilibrium faster.

The time taken to reach equilibrium for binary adsorption measurements was approximately 1 day. This was due to the small increments in which gas was added to ensure that the isobaric set-point was not overshot. Equilibrium could be achieved faster if a pressure regulation control system is used. A fully automated apparatus in addition to a recirculating pump would significantly reduce the time taken to reach equilibrium. In addition, a fully automated apparatus would require fewer user hours, improving the efficiency of the apparatus.

Several simplifying assumptions were made in applying the VSM model. It is suggested that a more rigorous form of the model be investigated to reduce the 6% average absolute deviation of model predictions from experimental data. Molecular simulations and classical density functional theory (cDFT) have found applications in adsorption equilibria. Research into the application of cDFT to the systems of ethane/13X, ethylene/13X and ethane + ethylene/13X is currently being undertaken at TRU.

Significant improvements have been made in the area of adsorbent science. The use of other adsorbents should be investigated for the separation of olefin/paraffin mixtures. Adsorbents with a higher selectivity and improved capacity should be investigated.

10

Chapter 10: References

1. Abdul-Rehman, H.B., Hasanain, M.A., Loughlin, K.F. (1990) *Quaternary, Ternary, Binary, and Pure Component Sorption on Zeolites.1. Light Alkanes on Linde S-115 Silicate at Moderate to High Pressures.* Ind. Eng. Chem. Res, 29, 1525-1535.
2. Ahmed, M.J., Mohammed, A.H.A.K., Kadhum, A.A.H. (2012) *Prediction of Multi Component Equilibrium Isotherms for Light Hydrocarbons Adsorption on 5A Zeolite.* Fluid Phase Equilibria, 313, 165-170.
3. AirGas (2011) *MSDS: Ethylene.* Accessed online at: http://www.airgas.com/documents/pdf/001022.pdf
4. Al-Asheh, S., Banat, F., Al-Omari, R., Duvnjak, Z. (2000) *Predictions of Binary Sorption Isotherms for the Sorption of Heavy Metals by Pine Bark using Single Isotherm Data.* Chemosphere. 41, 659-665.
5. Al-Muhtaseb, S.A. (2010) *Adsorption and Desorption of Nitrogen, Methane, Ethane, and Ethylene on Date-Pit Activated Carbon.* J. Chem. Eng. Data, 55, 313-319.
6. Al-Muhtaseb, S.A., Al-Rub, F.A.A., Zarooni, M.A. (2007) *Adsorption Equilibria of Nitrogen, Methane, and Ethane on BDH-Activated Carbon.* J. Chem. Eng. Data, 52, 60-65.
7. Anson, A., Lin, C.C.H., Kuznicki, T.M., Kuznicki, S.M. (2010) *Separation of Ethylene/Ethane Mixtures by Adsorption on Small-pored titanosilicate molecular sieves.*
8. Air Pollution Training Institute (APTI) (1999) *415: Control of Gaseous Emissions, Chapter 4: Adsorption.* USA.
9. Bahadur I., Osman K., Coquelet C., Naidoo P., Ramjugernath D. (2013) *Absorption of CO_2 and O_2 in Methyl Trioctyl Ammonium Bis (trifluoromethylsulfonyl) imide, 1-Butyl-3-Methyl Imidazolium Bis (trifluoromethylsulfonyl) amide, and 1-Butyl-3-Methyl Imidazolium Methyl Sulphate.* Paper currently in review, J. Phys. Chem. B.
10. Bao, Z., Alnemrat, S., Yu, L., Vasiliev, I., Ren, Q., Lu, X., Deng, S. (2011) *Adsorption of Ethane, Ethylene, Propane and Propylene on a Magnesium-Based Metal-Organic Framework.* Langmuir, 27, 13554-13562.
11. Belmabkhout, Y., Frere, M., De Welreld, G. (2004) *High-pressure Adsorption Measurements. A Comparitive Study of the Volumetric and Gravimetric Methods.* Measurment Science and Technology, 15, 848-858.
12. Bolster, C.H., Hornberger, G.M. (2007) *On the Use of Linearized Langmuir Equations.* Soil Sci. Soc. Am. J., 71, 1796-18706.
13. Bruice, P.Y. (2007) *Organic Chemistry.* 5th Edition. Pearson Prentice Hall.
14. Castrup, H. (2004) *Estimating and Combining Uncertainties*. 8th Annual ITEA Instrumentation Workshop, Lancaster.

15. Cavenati, S., Grande, C.A., Rodrigues, A.E. (2004) *Adsorption Equilibrium of Methane, Carbon Dioxide, and Nitrogen on Zeolite 13X at High Pressures.* J. Chem. Eng. Data, 49, 1095-1101.
16. Choi, B., Choi, D.K., Lee, W., Lee, B. (2003) *Adsorption Equilibria of Methane, Ethane, Ethylene, Nitrogen, and Hydrogen onto Activated Carbon.* J. Chem. Eng. Data, 48, 603-607.
17. Cochran, T.W., Kabel, R.L., Danner, R.P. (1985) *Vacancy Solution Theory of Adsorption using Flory-Huggins Activity Coefficient Equations.* AIChE Journal, 31, 268-277.
18. Costa, E., Sotelo, J.L., Calleja, G., Marron, C. (1981) *Adsorption of Binary and Ternary Hydrocarbon Gas Mixtures on Activated Carbon: Experimental Determination and Theoretical Prediction of the Ternary Equilibrium Data.* AIChE Journal, 27(1), 5-12.
19. Crittenden, B., Thomas, W.J. (1998) *Adsorption Technology and Design.* Butterworth-Heinemann.
20. Dabrowski, A. (2001) *Adsorption – from Theory to Practice.* Advances in Colloid and Interface Science, 93, 135-224.
21. Danner, R.P., Choi, E.C.F. (1987) *Mixture Adsorption Equilibria of Ethane and Ethylene on 13X Molecular Sieves.* Ind. Eng. Chem. Fundam, 17, 4, 248-253.
22. Danner, R.P., Hyun, S.H. (1982) *Equilibrium Adsorption of Ethane, Isobutane, Carbon Dioxide, and their Binary Mixtures on 13X Molecular Sieve.* J. Chem. Eng. Data, 27, 196-200.
23. Dong, Q. Chirico, R.D., Yan, X., Hong, X., Frenkel, M. (2005) *Uncertainty Reporting for Experimental Thermodynamic Properties*. J. Chem. Eng. Data, 50, 546-550.
24. Dorfman, L.R., Danner, R.P. (1975) *Equilibrium Adsorption of Nitrogen-Oxygen-Carbon Monoxide Mixtures on Molecular Sieve Type 10X*. AIChE Symposium Series. 152, 71, 30-39.
25. Dreisbach, F., Seif, R.A.H., Losch, H.A. (2002) *Gravimetric Measurement of Adsorption Equilibria of Gas Mixture CO/H_2 with a Magnetic Suspension Balance.* Chem. Eng. Technol. 25. 1060-1065.
26. Duong, D.D. (1998) *Adsorption Analysis: Equilibria and Kinetics.* London: Imperial College Press.
27. Eldridge, R.B. (1993) *Olefin/Paraffin Separation Technology: A Review.*Ind. Eng. Chem. Res., 32, 2208-2212.
28. Ellison, S., Wegscheider, W., Williams, A. (1997) *Measurement Uncertainty*. Analytical Chemistry News and Features. 607-613.
29. Felder, R.M., Rousseau, R.W. (2000) *Elementary Principles of Chemical Processes.* 3rd Edition. John Wiley and Sons, Inc.: New York.
30. Ghosh, T.K., Lin, H., Hines, A.L. (1993) *Hybrid Adsorption-Distillation Process for Separating Propane and Propylene*. Ind. Eng. Chem. Res., 32, 2390-2399.
31. Gibbs, J.W. (1876) *On the Equilibrium of Heterogenous Substances.* Trans. Conn. Acad., 3, 108-248.
32. Glos, S., Kleinrahm, R., Wagner, W. (2004) *Measurement of the (P,ρ,T) Relation of Propane, Propylene, N-Butane, and Isobutane in the Temperature Range from (95 To 340) K at Pressures up to 12 Mpa using an Accurate Two-Sinker Densimeter.* J. Chem. Thermodynamics, 36, 1037-1059.

33. Ho, Q.N., Lee, B.G., Lim, J.S., Yoo, K.S. (2005) *Measurement of Vapor-Liquid Equilibria for the Binary MixtureDifluoromethane (HFC-32) + Propylene (R-1270).* J. Chem. Eng. Data, 50, 419-424.
34. Hou, S., Duan, Y. (2010) *Measurement of Vapor-Liquid Equilibria for the Pentafluoroethane+ Propene Binary System from (263.15 to 323.15) K.* J. Chem. Eng. Data, 55, 3184-3188.
35. Jayaraman, A., Yang, R.T., Cho, S., Bhat, T.S.G., Choundary, V.N. (2002) *Adsorption of Nitrogen, Oxygen and Argon on Na-CeX Zeolites.* Adsorption, 8, 271-278.
36. Jiskoot, M.A. (2011) *Jet Mixing: A New Approach to Pipeline Conditioning.* Petro-Expo, Houston, Texas.
37. Kaul, B. K. (1987) *A modern version of volumetric apparatus for measuring gas-solid equilibrium data*. Industrial & Engineering Chemistry Research, 26 (5), 928-933.
38. Keller, J. U., Dreisbach, F., Rave, H., Staudt, R., & Tomalla, M. (1999*) Measurement of Gas Mixture Adsorption Equilibria of Natural Gas Compounds on Microporous Sorbents*.Adsorption, 5 (3), 199-214.
39. Kurt J. Lesker Company (2014) *Technical Notes 1: Flanges, Fittings and Components.* Accessed online at http://www.lesker.com/newweb/flanges/pdf/kjlced09_sec01_pages2-10_technicalnotes.pdf
40. Lee, H., Kim, H., Shi, Y., Keffer, D., Lee, C. (2013) *Competitive Adsorption of CO2/CH4 Mixtures on Dry and Wet Coal from Subcritical to Supercritical conditions.* Chem. Eng. J., 230, 93-101.
41. Lewis, W.K., Gilliland, E.R., Chertow, B., Cadogan, W.P. (1950) *Adsorption Equilibria: Hydrocarbon Gas Mixtures.* Ind. Eng. Chem., 42, 1319-1326.
42. Loughlin, K.F., Hasanain, M.A., Abdul-Rehman, H.B. (1990) *Quatenary, Ternary, Binary, and Pure Component Sorption on Zeolites.2. Light Alkanes on Linde 5A and 13X Zeolites at Moderate to High Pressures.* Ind. Eng. Chem. Res, 29, 1535-1546.
43. Malek, A., Farooq, S. (1996) *Comparison of Isotherm Models for Hydrocarbon Adsorption on Activated Carbon* AIChE Journal, 42, 3191-3201.
44. McEwen, J., Hayman, J., Yazaydin, A.O. (2013) *A Comparative Study of CO2, CH4, and N2 adsorption in ZIF-8, Zeolite-13X and BPL activated carbon.* Chemical Physics, 412, 73-76.
45. Mersmann, A. (2003) *Adsorption.* Ullman's Encyclopaedia of Industrial Chemistry. Germany: Wiley. 465-519.
46. Mofarahi, M., Salehi, S.M. (2013) *Pure and Binary Adsorption Isotherms of Ethylene and Ethane on Zeolite 5A.* Adsorption, 19, 101-110.
47. Myers, A.L., Prausnitz, J.M. (1965) *Thermodynamics of Mixed-gas Adsorption.* AIChE J., 11, 121-127.
48. Naidoo, P. (2004) *High-Pressure Vapour-Liquid Equilibrium Studies.* Thesis (PhD), University of KwaZulu-Natal, Durban.
49. Nam, G., Jeong, B., Kang, S., Lee, B., Choi, D. (2005) *Equilibrium Isotherms of CH_4, C_2H_6, C_2H_4, N_2, and H_2 on Zeolite 5A.* J. Chem. Eng. Data, 50, 72-76.
50. Nicholas, S. (2013) *Synthesis and Thermodynamic Studies of Physisorptive Energy Storage Materials.* Thesis (PhD), California Institute of Technology.
51. Osman, K. (2011) *Hiden Intelligent Gravimetric Analyser.* Thermodynamics Research Unit, School of Engineering, University of KwaZulu-Natal. Personal communication.

52. Osman, K. (2014) *Carbon Dioxide Removal from Coal Power Plants – A Review of Current Capture Techniques and an Investigation of Carbon Dioxide Adsorption using Hybrid Solvents.* Thesis (PhD). UKZN, South Africa.
53. Pakseresht, S., Kazemeini, M., Akbarnejad, M. (2002) *Equilibrium isotherms for CO, CO_2, CH_4 and C_2H_4 on the 5A molecular sieve by a simple volumetric apparatus*. Separation and Purification Technology, 28 (1), 53-60.
54. Poirier, E., Chahine, R., Tessier, A., Bose, T.K. (2005) *Gravimetric and Volumetric Approaches Adapted for Hydrogen Sorption Measurements with In Situ Conditioning on Small Sorbent Samples.* Review of Scientific Instruments, 76, 055101, 1-6.
55. Poling, B.E., Prausnitz, J.M., O'Connell, J.P. (2001) *The Properties of Gases and Liquids*. 5th Edition. McGraw-Hill: USA.
56. Purewal, J. (2010) *Hydrogen Adsorption by Alkali Metal Graphite Intercalation Compounds.* Thesis (PhD), California Institute of Technology.
57. Raal, J. D., Mühlbauer, A. L. (1998) *Phase Equilibria: Measurement and Computation*. Washington: Taylor and Francis.
58. Ray, G.C., Box, E.O. (1950) *Adsorption of Gases on Activated Charcoal*. Industrial and Engineering Chemistry, 42, 7, 1315-1318.
59. Ray, M.S. (1983) *The Separation and Purification of Gases Using Solid Adsorbents.* Separation Science and Technology, 18, 2, 95-120.
60. Reeves, S., Gonzalez R., Gasem, K.A.M., Fitzgerald, J.E., Pan, Z., Sudibandriyo, M., Robinson Jr, R.L. (2005) *Measurement and Prediction of Single-and Multi-Component Methane, Carbon Dioxide and Nitrogen Isotherms for U.S. Coals.* 2005 International Coalbed Methane Symposium.
61. Reich, R., Ziegler, W.T., Rogers, K.A. (1980) *Adsorption of Methane, Ethane, and Ethylene Gases and Their Binary and Ternary Mixtures on Carbon Dioxide on Activated Carbon at 212-301 K and Pressures to 35 Atmospheres.* Ind. Eng. Chem. Process. Des. Dev., 19, 336-344.
62. Rezaei, F., Webley, P. (2010) *Structured Adsorbents in Gas Separation Processes.* Separation and Purification Technology, 70, 234-256.
63. Rice, N.M. (2010) Research Project Proposal: *The Removal of Tetrafluoromethane from Nitrogen Trifluoride Using Adsorption and Absorption Technology*. Thermodynamics Research Unit, University of KwaZulu-Natal.
64. Romero-Pérez, A., Aguilar-Armenta, G. (2010) *Adsorption Kinetics and Equilibria of Carbon Dioxide, Ethylene, and Ethane on 4A (CECA) Zeolite.* J. Chem. Eng. Data, 55, 3625-3630.
65. Ruthven, D. M. (1984) *Principles of Adsorption and Adsorption Processes*. New York: John Wiley and Sons.
66. Saha, B.B., Jribi, S., Koyama, S., El-Sharkawy, I.I. (2011) *Carbon Dioxide Adsorption Isotherms on Activated Carbons.* J. Chem. Eng. Data, 56, 1974-1981.
67. Seader, J.D., Henley, E.J. (2006) *Separation Process Principles,* 2nd Edition, John Wiley and Sons, Inc.
68. Shi, M., Lin, C.C.H., Kuznicki, T.M., Hashisho, Z., Kuznicki, S.M. (2010) S*eparation of a Binary Mixture of Ethylene and Ethane by Adsrption on Na-ETS-10.* Chemical Engineering Science. 65, 3494-3498.
69. Shi, X., Johnson, P., Burnett, E. (2007) *Uncertainty Analysis for Vapour Pressure Measurement*. Journal of Building Physics, 500, 4, 317-336.

70. Sigma Aldrich (2014) *Technical Information Bulletin. AL-143 Mineral Adsorbents, Filter Agents and Drying Agents.* Accessed online at: http://www.sigmaaldrich.com/chemistry/chemical-synthesis/learning-center/technical-bulletins/al-1430/molecular-sieves.html
71. Smith, J.M., Van Ness, H.C., Abbott, M.M. (2005) *Introduction to Chemical Engineering Thermodynamics.* 7th Edition. McGraw-Hill: New York.
72. Soo, C. (2011) *Experimental Thermodynamic Measurements of Biofuel-related Associating Compounds and Modelling using the PC-SAFT Equation of State.* Thesis (PhD). MINES ParisTech, France.
73. Suwanayuen, S., Danner, R.P. (1980) *A Gas Adsorption Isotherm Equation based on Vacancy Solution Theory.* AIChE J., 26, 1, 68-76.
74. Taylor, B.N., Kuyatt, C.E. (1994) *Guidelines for evaluating and expressing the Uncertainty of NIST Measurement Results*. National Institute of Standards and Technology. United States Department of Commerce Technology Administration.
75. Triebe, R.W., Tezel, F.H., Khulbe, K.C. (1996) *Gas. Sep. Purif, 10, 1, 81-84.*
76. Tzabar, N., Grossman, B. (2011) *Nitrogen, Methane and Ethane Sorption on Activated Carbon.* Cryogenics, 51, 499-508.
77. Von, C.M., Sherman, J.D. (2004) *Adsorption* Kirk-Othmer Encyclopaedia of Chemical Technology. USA: Wiley. 528-663.
78. Yang, R.T. (1987) *Gas Separation by Adsorption Processes.* New York: Butterworth.
79. Younglove, B.A., Ely, J.F. (1987) *Thermophysical Properties of Fluids. II. Methane, Ethane, Propane, Isobutane, and Normal Butane.* J. Phys. Chem. Ref. Data, 16, 4, 577-798.
80. Yu, C., Huang, C., Tan, C. (2012) *A Review of CO2 Capture by Absorption and Adsorption.* Aerosol and Air Quality Research, 12, 745-769.
81. Yun, J., Duren, T., Keil, F.J., Seaton, N.A. (2002) *Adsorption of Methane, Ethane, and their Binary Mixtures on MCM-41: Experimental Evaluation of Methods for the Prediction of Adsorption Equilibrium.* Langmuir, 18, 2693-2701.
82. Zehioua, R., Coquelet, C., Meniai, A., Richon, D. (2010) *P-T-x Measurements for Some Working Fluids for an Absorption Heat Transformer: 1,1,1,2-Tetrafluoroethane (R134a) + DimethyletherDiethylene Glycol (DMEDEG) and DimethyletherTriethylene Glycol (DMETrEG).* J. Chem. Eng. Data, 55, 2769-2775.
83. Zehioua, R., Coquelet, C., Meniai, A., Richon, D. (2010b) *Isothermal Vapor-Liquid Equilibrium Data of 1, 1, 1, 2-Tetrafluoroethane (R134a) + Dimethylformamide (DMF) Working Fluids for an Absorption Heat Transformer.* J. Chem. Eng. Data, 55, 985-988.
84. Zhu, M., Fu, Y., Han, L. (1992) *Experimental Study on Vapour Pressure of HFC-134a*. J. of Thermal Science, 1, 2, 80- 85.

Appendix A: Commercial Adsorbents

The ability of porous solids to reversibly adsorb gases was recognized as early as the 18th century (Ruthven, 1984). In early applications adsorbents were used to purify process streams where only the purified component held economic value, the rest were simply removed and discarded. The removal of H_2S and mercaptans from natural gas is such an example. Activated carbon and silica gels were predominantly used for these purposes.

The application of adsorption as a means to separate process streams into two or more streams, each with valuable components was developed much later. For these separations, an adsorbent that provides a high separation factor must be selected. For these separations a class of adsorbent called 'molecular sieve' were developed. Zeolites, in particular, have enjoyed wide spread application

Currently there are 5 groups of adsorbents commercially available

- Activated Alumina
- Activated Carbon
- Carbon Molecular Sieves
- Silica Gel
- Zeolites

Activated Alumina

Activated alumina is a porous high-area form of aluminium oxide and has a great affinity for water. The adsorbent is prepared either directly from bauxite or from the monohydrate by dehydration and re-crystallization at elevated temperatures. The major use of activated alumina is in drying of industrial gases. In a well-designed adsorber, the moisture content can be reduced to below 1ppm. The adsorbent also finds applications in chromatography (Ruthven, 1984; Yang, 1987).

Activated Carbon

Activated carbon is typically prepared by thermal decomposition of carbonaceous material followed by activation at elevated temperatures. A mild oxidising gas such as CO_2 or steam is used to activate the carbon. The surface of activated carbon is generally non-polar although a slight polarity may arise from surface oxidation. Carbon adsorbents are typically hydrophobic and organophilic. Uses include adsorption of organics in the decolourization of sugar, water purification and solvent recovery (Ruthven, 1984; Yang, 1987).

Carbon Molecular Sieves

Carbon molecular sieves are a modified form of activated carbon adsorbents. Activated carbon adsorbents generally show very little selectivity in the adsorption of molecules of different sizes. By using more specialised techniques in preparing the adsorbent, such selectivity can be achieved. Carbon sieves may have pore diameters from 4 to 9 Angstroms depending on the preparation technique. Applications include air separation, cleaning of off-gases from nuclear plants and hydrogen purification (Ruthven, 1984; Yang, 1987).

Silica Gel

Silica gel is prepared by mixing a sodium silicate solution with a mineral acid such as hydrochloric or sulphuric acid. The preparation technique used impacts the pore structure of the adsorbent. Silica gel is a rigid, continuous network of spherical particles of colloidal silica. It is used predominantly for drying (Ruthven, 1984; Yang, 1987).

Zeolites

Zeolites are porous crystalline aluminosilicates. Zeolites consist of an arrangement of cage-like structures of silica oxide and aluminium oxide. The arrangement of these cage-like structures determines the adsorbent pore size. Zeolites, being crystalline have no pore size distribution. This sets Zeolites apart from other microporous adsorbents. Approximately 38 different zeolite frameworks have been identified; each exhibiting specific properties. Their applications are widespread with particular emphasis on air purification and gas separation (Ruthven, 1984; Yang, 1987).

A review of the adsorbents mentioned in Table 3-1 is provided on the next page.

Table A - 1: A review of selected adsorbents.

Reference	Adsorbent	Adsorbent Properties							Regeneration		
		Mass/ g	Shape	Dimensions/ mm	Specific surface area/ $m^2.g^{-1}$	Pore volume/ $cm^3.g^{-1}$	Bulk Density/ $g.cm^{-3}$	Particle density/ $g.cm^{-3}$	P/ Pa	T/ °C	Time/ hours
Reich et al. (1980)	BPL Activated Carbon	32.19		20/85 mesh	988 ± 15				1.3	130	1.5
Costa et al. (1981)	Activated Carbon	50	cylinder	0.83 radius 4.26 height	700		0.795	2.7	13	270	12
Danner and Hyun (1982)	Molecular Sieve 13X		pellets	1.5875	525	0.3					
Kaul (1987)	Molecular Sieve 13X		pellets	1.5875							
	Kureha Beads (Activated Carbon)		Spherical balls	0.485	800-1200						
Danner and Choi (1987)	Molecular Sieve 13X		pellets	1.5875	525	0.3				300	12
Ghosh et al. (1993)	Silica Gel	100		6x12 mesh	672		0.72	1.13	0.013	125	12
	Molecular Sieve 13X		Spherical beads	4x8 mesh	395		0.72	1.13		200	
	Ac. Carbon			6x16 mesh	874		0.6	0.8		125	
Pakseresht et al. (2002)	5A Zeolite	40	pellets	1.5875	366				670	400	16
Yun et al. (2002)	MCM 41	6.75	pellets		1023				0.27	250	2

Choi et al. (2003)	Activated Carbon		pellets	6-16 mesh	1150-1250	0.72	0.44			150	12
Al-Muhtaseb et al. (2007)	BDH Activated Carbon	78.79	granules	0.85 1.70	1220	0.534			2.7	150	2
Ahmed et al. (2012)	5A Zeolite	10						1.263	3		3
Al-Muhtaseb (2012)	Date Pit (Activated Carbon)		granules	< 200 mesh	645	0.287			2.7	150	2

Appendix B: Development of Adsorption Technology

Table B - 1: The development of adsorption technology (Dabrowski, 2001).

Date	Credit	Significance
3750BCE	**Egyptians and Sumerians**	Use of charcoal for reduction of copper, zinc and tin ores for manufacture of bronze.
1550BCE	**Egyptians**	Application of charcoal for medicinal purposes to adsorb odorous vapours from putrefactive wounds and from intestine.
460BCE	**Hippocrates and Pliny**	Introduced the use of charcoal to treat a wide range of ailments including epilepsy, chlorosis and anthrax.
1773	**Scheele**	Reported some experiments of the uptake of gases by charcoal and clays derived from various sources.
1777	**Fontana**	
1786	**Lowitz**	Used charcoal for decolourization of tartaric acid solutions as result of organic impurities uptake.
1794		Charcoal was used in the sugar industry in England as a decolourization agent of sugar syrups.
1814	**De Saussure**	Started systematic studies of adsorption of various gases by porous substances as sea-foam, cork, charcoal, and asbestos. Discovered the exothermic character of adsorption processes.
1881	**Kayser**	Introduced terms ‘adsorption’, ‘isotherm’ or ‘isotherm curve’. Developed theoretical concepts that became basic to monomolecular adsorption theory.
1879	**Chapius**	Made the first calorimetric measurements of heat generation during wetting of various carbon by liquids.
1901	**Von Ostreyko**	Set the basis for commercial development of activated carbons through processes that involve the incorporation of metallic chlorides with carbonaceous materials before carbonization and the mild oxidation of charred materials with carbon dioxide or steam at increased temperatures.
1903	**Tswet**	Discovered the phenomenon of selective adsorption. Introduced the term ‘column solid-liquid adsorption chromatography’. This discovery was not only the beginning of a new analytical technique, but also the origin of a new field of surface science .
1904	**Dewar**	Found selective adsorption of oxygen from its mixture with nitrogen, during air uptake by charcoal.
1909	**McBain**	Proposed the term ‘absorption’ to determine a much slower uptake of hydrogen by carbon than adsorption. Also proposed the term ‘sorption’ for both adsorption and absorption.

1911		The NORIT factory in Amsterdam was founded, now one of the most advanced international manufactures of active carbons.
1911		A wood distillation plant was built in Poland, initially manufacturing activated carbon solely from wood materials. World War I introduced the problem of protecting human respiratory tracts from toxic warfare agents.
1915	**Zelinsky**	Professor of Moscow University was the first to suggest and apply the use of active carbons as the adsorption medium in gas mask.
1941	**Martin and Synge**	Introduced to laboratory practice the solid-liquid partition chromatography, both in column and planar form.
1956	**Barrer and Breck**	Invented the method of zeolite synthesis. In this year the North- Breck American Linde Company started production of synthetic zeolites at a commercial scale.

Appendix C: Thermodynamics of Adsorption

A derivation of the relevant thermodynamic relationships is presented. The derivations are extracted from works by Ruthven (1984) and Yang (1987).

Isoteric Heat of Adsorption

The condition for equilibrium, using chemical potential μ may be written as:

$$\mu_s = \mu_g \qquad (C - 1)$$

where subscripts *s* and *g* represent the solid and gaseous phases respectively.

Assuming the vapour phase to be ideal:

$$\mu_s = \mu_g = \mu_g^0 + RT\, ln\frac{P}{P^0} \qquad (C - 2)$$

where $\mu^0{}_g$ is the chemical potential at reference pressure P^0

The Gibbs-Helmholtz relation is given by:

$$\frac{\partial\left[\frac{\mu}{T}\right]}{\partial T} = -\frac{\overline{H}}{T^2} \qquad (C - 3)$$

Defining adsorbed phase concentration as *q*, differentiating Eq. (C - 2) and applying Eq. (C - 3):

$$\frac{-\overline{H_s}}{T^2} = \frac{\overline{H_g^0}}{T^2} + R\left(\frac{\partial\, ln\, P}{\partial T}\right)_q \qquad (C - 4)$$

Re-arranging Eq. (C - 4) and noting for an ideal gas, the partial molar entropy $\overline{H_g^0}$ is independent of composition and identical to the molar enthalpy H_g:

$$\left(\frac{\partial\, ln\, P}{\partial T}\right)_q = \frac{H_g - \overline{H_s}}{RT^2} \qquad (C - 5)$$

The enthalpy change on adsorption, commonly referred to as the isoteric heat of adsorption ΔH_s is defined as:

$$-\Delta H_s = H_g - \overline{H_s} \qquad (C - 6)$$

Combining Eqs. (C - 5) and (C - 6)

$$\left(\frac{\partial\, ln\, P}{\partial T}\right)_q = \frac{-\Delta H_s}{RT^2} \qquad (C - 7)$$

The isoteric heat of adsorption is a function of q as seen in Eq. (C - 5). If there is negligible difference in the heat capacity of the gas in the adsorptive phase and adsorbed phase, ΔH_s is independent of T. integrating Eq. (C - 7):

$$ln\,P = constant - \frac{\Delta H_s}{RT} \qquad (C - 8)$$

Partial Molar Entropy

For an ideal vapour phase, the definition of enthalpy is given by:

$$H_g = U_g + PV = U_g + RT \qquad (C - 9)$$

The volume of the adsorbed phase is much smaller than the volume of gas in the adsorptive phase, hence:

$$\overline{U_s} \approx \overline{H_s} \qquad (C - 10)$$

Combining Eqs. (C - 6), (C - 9) and (C -10)

$$-\Delta H_s = U_g - \overline{U_s} + RT \qquad (C - 11)$$

From the definition of chemical potential:

$$\mu = \bar{H} - T\bar{S} \qquad (C - 12)$$

Combining Eqs. (C - 1), (C -12) and re-arranging:

$$\bar{S_s} - \overline{S_g} = \frac{\overline{H_s} - H_g}{T} \qquad (C - 13)$$

The partial molar entropy of the ideal vapour phase is given by:

$$\overline{S_g} = S_g^0 - R\,ln\frac{P}{P^0} \qquad (C - 14)$$

where S_g^0 is the molar entropy of the vapour in the standard state at pressure P^0

Combining Eqs. (C -13) and (C -14)

$$\bar{S_s} = S_g^0 + \frac{\overline{H_s} - H_g}{T} - R\,ln\frac{P}{P^0} \qquad (C - 15)$$

Adsorption Equilibrium Constant

For convenience, a standard state for chemical potential is defined as follows

$$\mu_s = \mu_s^0 + RT\, ln \frac{a_s}{a_s^0} \qquad (C\text{-}16)$$

where a_s is the activity of the adsorbed phase and μ_s^0 is the standard chemical potential at activity a_s^0

Combining Eqs. (C - 2) and (C -16)

$$\mu_s - \mu_g^0 = RT\, ln\left(\frac{P}{P^0}\frac{a_s^0}{a_s}\right) \qquad (C\text{-}17)$$

The adsorption equilibrium is thus defined:

$$K = \frac{P a_s^0}{P^0 a_s} \qquad (C\text{-}18)$$

Eq. (C -17) becomes:

$$\mu_s - \mu_g^0 = RT\, ln\, K \qquad (C\text{-}19)$$

If the standard state is chosen as an infinitely dilute ideal adsorbed phase, Eq. (C -18) simply reduces to Henry's Law in the low coverage limit. At higher concentrations Eq. (C -18) reduces to a definition of the activity coefficient of the adsorbed phase.

$$\lim_{P\to 0} \frac{q}{P} = \frac{K a_s^0}{P^0} \equiv K' \qquad (C\text{-}20)$$

$$\gamma = \frac{K' P}{q} \qquad (C\text{-}21)$$

The temperature dependence of K' follows the van't Hoff equation. Eq. (C -20) thus becomes:

$$\lim_{P\to 0} \frac{q}{P} = K_0' e^{\frac{-\Delta H_0}{RT}} \qquad (C\text{-}22)$$

where $-\Delta H_0$ is the limiting heat of adsorption at zero coverage.

Appendix D: Additional Models used in the Prediction of Adsorption Equilibria

Ideal Adsorbed Solution Theory (IAST)

Myers and Prausnitz (1965) considered the mixed adsorbate to be a solution in equilibrium with the gas phase. The IAST is a special case of this approach. As the mixed adsorbate is treated as a solution, the fundamental thermodynamic equations for liquids apply (Yang, 1987):

$$dU = TdS - \pi dA + \sum \mu_i dn_i \qquad (D - 1)$$

$$dG = -SdT + Ad\pi + \sum \mu_i dn_i \qquad (D - 2)$$

The adsorbed mixture is treated as a 2D phase that is not necessarily a mono layer. π plays a pivotal role in applying solution equilibria to mixture adsorption. Spreading pressure, π is related to the surface tension at a gas-liquid interface as follows (Yang, 1987):

$$\pi = \sigma^0 - \sigma \qquad (D - 3)$$

where σ^0 and σ is the surface tension of a clean surface and a monolayer covered surface respectively. Thus, π describes the lowering of the surface tension at the gas-solid interface when adsorption occurs and is defined by (Yang, 1987):

$$\pi = -\left(\frac{\partial U}{\partial A}\right)_{S,n_i} \qquad (D - 4)$$

For a gas mixture under isothermal conditions, Eq. (D - 1) reduces to:

$$Ad\pi = \sum n_i du_i \qquad (D - 5)$$

For pure gas adsorption assuming ideal gas, this becomes:

$$Ad\pi = nRTd\ ln\ P \qquad (D - 6)$$

or

$$\frac{\pi A}{RT} = \int_0^P \frac{n}{P} dP \qquad (D - 7)$$

Eq. (D - 7) can be used to calculate spreading pressure from pure gas isotherms. The intensive variables in Eq. (D - 1) are π, T and composition. Myers and Prausnitz (1965) define activity coefficients for the mixed adsorbate in the same way as for a solution.

The molar Gibbs free energy for mixing the adsorbate at constant T and π is given by (Duong, 1998):

$$g^m(T,\pi,X_i) = RT\sum X_i\, ln(\gamma_i X_i) \qquad (D - 8)$$

Equilibrium between the adsorbed phase and the gas phase requires the chemical potentials in each phase to be equal. If $P_i^0(\pi)$ is the saturated vapour pressure exerted by component i in its pure state at the same temperature and spreading pressure of the adsorbed state, then the pressure, P_i, exerted by component i in the mixture is (Crittenden and Thomas, 1998):

$$P_i = P_i^0(\pi)X_i \qquad (D - 9)$$

Eq. (D - 9) is equivalent to Raoult's law for ideal vapour-liquid systems. If the mole fraction of component i in the vapour phase is Y_i then:

$$Y_i P = P_i^0(\pi)X_i\gamma_i \qquad (D -10)$$

where γ_i is defined in Eq. (D - 8) and is unity for ideal conditions. Myers and Prausnitz (1965) define the molar area of the mixed adsorbate as follows (Yang, 1987):

$$\frac{1}{n_t} = \sum\frac{X_i}{n_i^0} + \frac{RT}{A}\sum X_i\left(\frac{\partial\, ln\,\gamma_i}{\partial\pi}\right)_{X_i} \qquad (D -11)$$

where n_i^0 is defined as the number of moles of i when adsorbed from pure gas at the same π and T as the adsorbed mixture. The number of moles of each component adsorbed is (Yang, 1987):

$$n_i = n_t X_i \qquad (D -12)$$

Eqs. (D -10) and (D -12) are used to predict mixture adsorption from pure component isotherms. Eq. (D - 7) is used to evaluate P_i^0. At high pressures, fugacity is used instead to account for non-idealities.

For an ideal solution:

$$Y_i P = P_i^0(\pi)X_i \qquad (D -13)$$

$$\frac{1}{n_t} = \sum\frac{X_i}{n_i^0} \qquad (D -14)$$

Eqs. (D - 7) and (D -12) – (D -14) form the ideal adsorbed solution theory by which mixed gas adsorption is predicted using pure gas isotherms. In this study, binary systems were investigated. A calculation procedure for a binary system is presented. The pure gas isotherms are denoted $n_1(P)$ and $n_2(P)$ for components 1 and 2 respectively. At equilibrium, the spreading pressures are equal. From Eq. (D - 7):

$$\int_0^{P_1^0} \frac{n_1}{P} dP = \int_0^{P_2^0} \frac{n_2}{P} dP \qquad (D\text{-}15)$$

For species 1:

$$PY_1 = P_1^0 X_1 \qquad (D\text{-}16)$$

For species 2:

$$PY_2 = P_2^0 X_2 = P_2^0 (1 - X_1) \qquad (D\text{-}17)$$

Eqs. (D -15), (D -16) and (D -17) define the adsorbed mixture. Eq. (D -15) can be integrated to yield an algebraic equation if the isotherm takes on a form such as the Langmuir or Freundlich or it may be solved graphically. When all compositions and pressure is known, the following equations are used to calculate n_1, n_2 and n_t:

$$\frac{1}{n_t} = \frac{X_1}{n_1(P_1^0)} + \frac{X_2}{n_2(P_2^0)} \qquad (D\text{-}18)$$

$$n_1 = n_t X_1 \qquad (D\text{-}19)$$
$$n_2 = n_t X_2 \qquad (D\text{-}20)$$

The IAST has shown good agreement with experimental data for many systems on activated carbon and zeolites. However, there have also been severe deviations. The reader is referred to the study of Yang (1987) and Duong (1998) for more on the subject.

Two-Dimensional Gas Model

An alternative approach to adsorption is to consider the adsorbed phase as a non-ideal compressed gas. If the mixing rules are applied, this approach can be extended to binary adsorption. The model is best suited for adsorption below monolayer coverage on homogenous surfaces. For submonolayer adsorption, the properties of the adsorbed phase can be described by (Yang, 1987):

$$\pi = \frac{kT}{\delta - \beta} - \frac{\alpha}{\delta^2} \qquad (D\text{-}21)$$

β is approximately equal to the molecular area at monolayer coverage. If Eq. (D -21) is combined with Eq. (3 15) the following isotherm is obtained (Yang, 1987):

$$P = \frac{K\theta}{1-\theta} exp\left[\frac{\theta}{1-\theta} - \frac{2\alpha\theta}{kT\beta}\right] \qquad (D\text{-}22)$$

For a binary mixture, the van der Waals constants are given by (Duong, 1998):

$$\beta_m = X_1\beta_1 + X_2\beta_2 \qquad (D\text{-}23)$$
$$\alpha_m = \alpha_1 X_1^2 + 2\alpha_{12} X_1 X_2 + \alpha_2 X_2^2 \qquad (D\text{-}24)$$

where:

$$\alpha_{12} = \sqrt{\alpha_1 \alpha_2} \qquad \textit{(D -25)}$$

Applying the Gibbs approach once more and assuming ideal gas, the mixed gas isotherms are (Yang, 1987):

$$ln\, PY_1 = ln\frac{X_1 K_1 \beta_1}{\delta - \beta_m} + \frac{\beta_1}{\delta - \beta_m} - \frac{2}{\delta kT}(\alpha_1 X_1 + \alpha_{12} X_2) \qquad \textit{(D -26)}$$

$$ln\, PY_2 = ln\frac{X_2 K_2 \beta_2}{\delta - \beta_m} + \frac{\beta_2}{\delta - \beta_m} - \frac{2}{\delta kT}(\alpha_2 X_2 + \alpha_{12} X_1) \qquad \textit{(D -27)}$$

where:

$$\beta_i = \frac{A}{n_i^{\infty} N_0} \qquad \textit{(D -28)}$$

If pure component isotherms are available, K, α and β can be determined for each species in the mixture. If P and Y_i are provided, Eqs. (D -26) and (D -27) can be used to solve δ and X_i. The total number of moles adsorbed is given by (Yang, 1987):

$$n_t = \frac{A}{\delta N_0} \qquad \textit{(D -29)}$$

The model has been used to predict adsorption equilibria of ethane/ethylene, propane/propylene on carbon black and ethane/ethylene on zeolite 13X which showed good results (Yang, 1987).

Simplified Statistical Thermodynamic Model (SSTM)

Zeolites have regular cage-like structure and can be treated using the statistical thermodynamic approach. This model thus applies only to zeolites. If the zeolite contains *d* identical cages each with the ability to adsorb *m* gas molecules, the grand partition function for a single cage is given by (Yang, 1987):

$$\Xi = 1 + Z_1 a + Z_2 a^2 + \cdots + Z_m a^m \qquad \textit{(D -30)}$$

where Z is the configuration integral containing s molecules given by (Yang, 1987):

$$Z_s = \frac{1}{s!}\int exp\left[\frac{-U_s(r_1, r_2, \cdots, r_s)}{kT}\right] dr_1 dr_2 \cdots dr_s \qquad \textit{(D -31)}$$

where U_s is the potential of molecules located at position vectors r_1, r_2, r_s. The integration is carried out over the entire cage volume. The activity a is given by (Yang, 1987):

$$a = \lambda \left[\frac{2\pi mkT}{h^2}\right]^{3/2} \qquad (D\text{-}32)$$

or for an ideal gas:

$$a = \frac{P}{kT} \qquad (D\text{-}33)$$

If C is defined as the number of sorbates molecules per cage (Yang, 1987):

$$C = \frac{\partial \ln \Xi}{\partial \ln a} = \frac{Z_1 a + 2Z_2 a^2 + \cdots + mZ_m a^m}{1 + Z_1 a + Z_2 a^2 \cdots Z_m a^m} \qquad (D\text{-}34)$$

The isotherm given in Eq. (D -34) is general for the statistical model. Evaluating the exact configuration integrals is often difficult; especially for large values of s. The simplifications made by Ruthven are presented (Yang, 1987).

If the gas is assumed to behave in accordance with van der Waals behaviour, Z_s is given by:

$$Z_s = \frac{z_1^s}{s!}\left(1 - \frac{sb}{v}\right)^2 exp\left(\frac{sb\iota}{vkT}\right) \qquad (D\text{-}35)$$

where b is the van der Waals co-volume, v is the cage volume and ι is a constant. Eq. (D -35) is further simplified to:

$$Z_s = \frac{z_1^s R_s}{s!} \qquad (D\text{-}36)$$

where R_s is a temperature dependant constant characteristic of the sorbate-sorbate system. For $s=1$, $Z_1 a = KP$:

$$C = \frac{KP + (KP)^2 R_1 + \cdots + \frac{(KP)^m}{(m-1)!} R_m}{1 + KP + \frac{1}{2!}(KP)^2 R_1 + \cdots + \frac{(KP)^m}{m!} R_m} \qquad (D\text{-}37)$$

The isotherm Eq. (D -37) is readily extended to mixtures. For a cage containing i molecules of A and j molecules of B, $i + j = s$. The configuration integral is given by (Yang, 1987):

$$Z_{ij} a_A^i a_B^j = \frac{(K_A P_A)^i (K_B P_B)^j}{i!\, j!} \left(R_{As}^i R_{Bs}^j\right)^{\frac{1}{i+j}} \qquad (D\text{-}38)$$

Eq. (D -38) works well for molecules of similar size and with weak interactions. The isotherm for the SSTM is hence given by (Yang, 1987):

$$C_A = \frac{K_A P_A + \sum_j \sum_i \frac{(K_A P_A)^i (K_B P_B)^j}{(1-i)!\,j!} \left(R_{As}^i R_{Bs}^j\right)^{\frac{1}{i+j}}}{1 + K_A P_A + K_B P_B + \sum_j \sum_i \frac{(K_A P_A)^i (K_B P_B)^j}{i!\,j!} \left(R_{As}^i R_{Bs}^j\right)^{\frac{1}{i+j}}} \qquad (D\text{-}39)$$

C_B is given by the corresponding equation for species *B*. the following relation must hold:

$$i + j \leq s \qquad (D\text{-}40)$$

The SSTM has been tested for a number of binary mixtures on zeolites and good agreement was obtained. The model is best suited for large, non-polar molecules of similar size (Yang, 1987).

Appendix E: Review of Apparatus used in Adsorption Measurement

The Volumetric Apparatus of Kaul (1987)

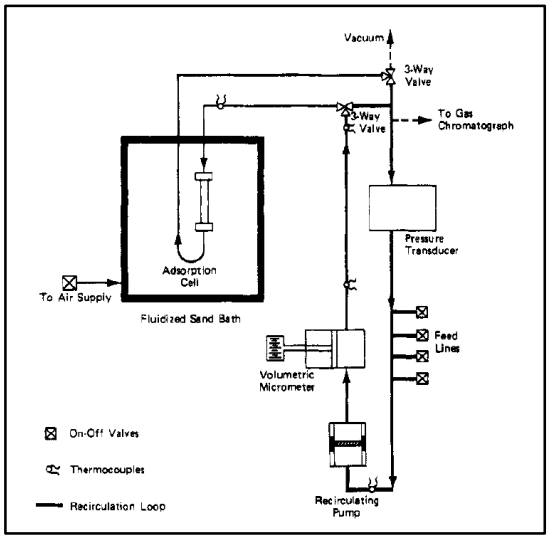

Figure E - 1: The volumetric apparatus of Kaul (1987).

The apparatus of Kaul (1987) introduced an improvement to the existing volumetric apparatus at the time. Conventional volumetric apparatus involved manipulating pressure by changing the number of moles of gas present in the adsorption cell. The apparatus of Kaul (1987) uses a volumetric micrometer to manipulate pressure. The number of moles of gas in the system is kept constant and pressure is manipulated by changing the volume. Using this technique, pressure can be changed rapidly without introducing additional gas when measuring pure gas isotherms. Kaul (1987) verified his new experimental technique and his results compared favourably to those of literature (Danner and Choi, 1978). A fluidized sand bath was used to maintain isothermal conditions in the adsorption cell. Kaul used a recirculation pump to achieve equilibrium faster. Gas composition analysis was done online.

The volumetric apparatus of Abdul-Rehman et al. (1990)

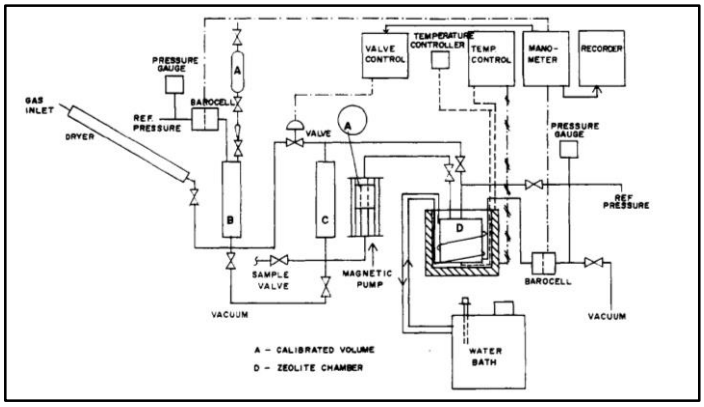

Figure E - 2: The volumetric apparatus of Abdul-Rehman et al. (1990) consists of 3 cells: a gas loading chamber (B), mixing chamber (C) and adsorption chamber (D).

The volumetric apparatus of Ghosh et al. (1993)

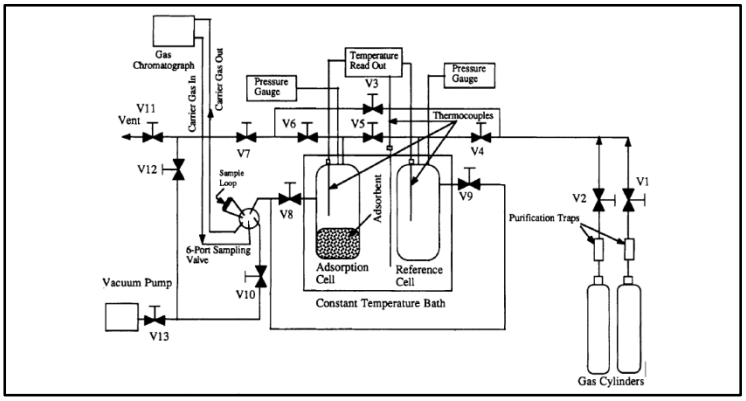

Figure E - 3: The volumetric apparatus of Ghosh et al. (1993).

The apparatus of Ghosh et al. (1993) uses a 6-port valve to remove a sample from the equilibrium at high pressure and send to the GC. GC specifications are provided in Table 2-2. For pure component measurements, equilibrium was achieved when the pressure remained constant over a period of time. For binary mixtures, samples were periodically measured to determine if equilibrium had been achieved. Equilibrium was typically established after 4 hours. Ghosh et al. (1993) did not use a recirculation pump in their study.

The volumetric apparatus of Keller et al. (1999)

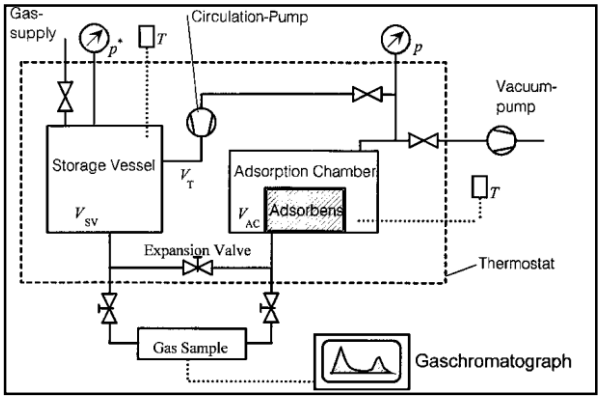

Figure E - 4: The volumetric apparatus of Keller et al. (1999).

Keller et al. (1999) used the traditional volumetric technique. A storage vessel is used and maintained under isothermal conditions. Equilibrium was determined when the pressure in the adsorption chamber stabilised. A re-circulation pump was used to aid the achievement of equilibrium. It is not clear if gas samples were removed and then injected into the GC or on-line GC analysis was done.

The volumetric apparatus of Pakseresht et al. (2002)

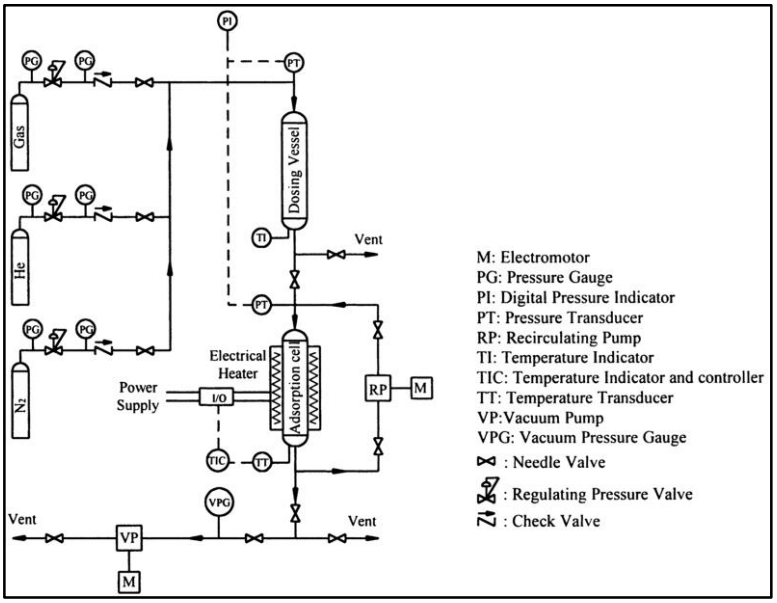

Figure E - 5: The volumetric apparatus of Pakseresht et al. (2002).

The apparatus of Pakseresht et al. (2002) is similar to that of Keller et al. (1999). A dosing vessel is used to prepare gas for expansion in the adsorption cell. An oven was used to maintain isothermal conditions as opposed to a bath. This allowed isotherms to be measured up to temperatures of 300°C. A recirculating pump is used. It is not clear how it was determined when equilibrium was achieved.

The volumetric apparatus of Yun et al. (2002)

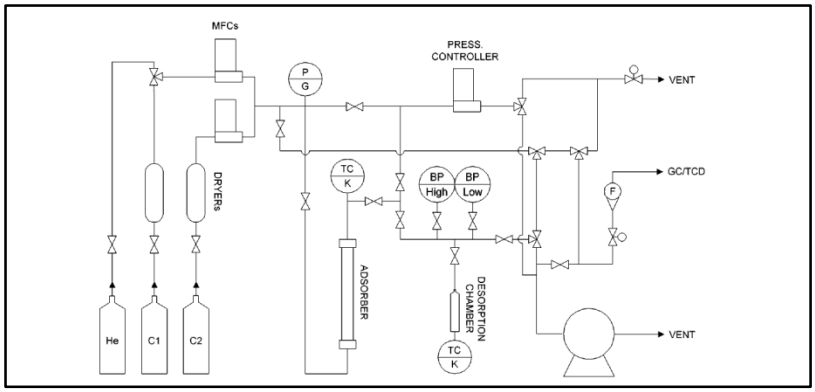

Figure E - 6: The volumetric apparatus of Yun et al. (2002).

Yun et al. (2002) used a flow through method to measure gas-solid adsorption isotherms. Most researchers use a fixed volume of gas, measuring adsorption using a static approach. The flow rate of gas and in cases of binary mixtures, the composition, was kept constant using mass flow controllers (MFC's). Equilibrium was determined by measuring the composition of the inlet and outlet gas of the adsorption cell. Upon the achievement of equilibrium, the gas was desorbed by raising the temperature in the adsorption cell.

The volumetric apparatus of Choi et al. (2003)

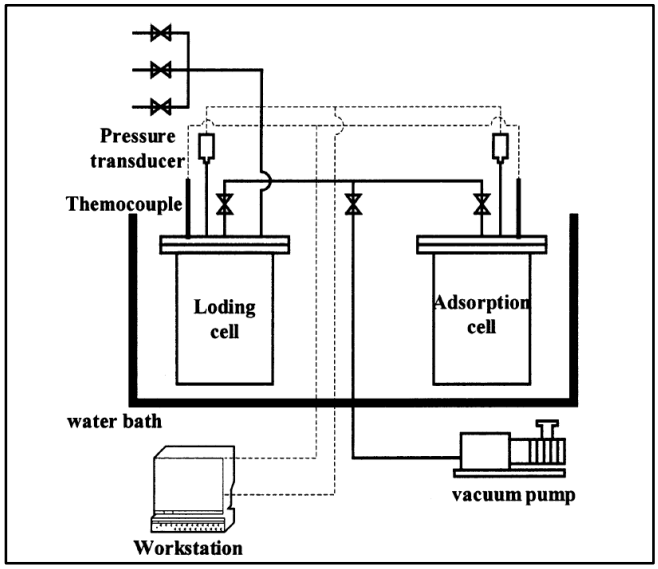

Figure E - 7: The volumetric apparatus of Choi et al. (2003).

Choi et al. (2003) used a static volumetric technique. Equilibrium was determined by monitoring the temperature and pressure of both the loading cell and the equilibrium cell. A recirculation pump was not used to aid the achievement of equilibrium. Choi et al. (2003) measured only pure component isotherms. A GC was not required for gas analysis.

The volumetric apparatus of Al-Muhtaseb et al. (2007)

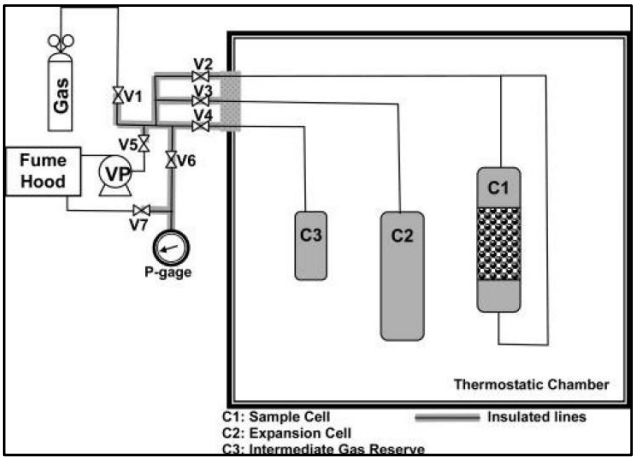

Figure E - 8: The volumetric apparatus of Al-Muhtaseb et al. (2007).

The apparatus of Al-Muhtaseb et al. (2007) introduces a variation to the typical static volumetric technique. In this apparatus, an additional preparation vessel is used. All three cells were placed inside an oven to maintain isothermal conditions. Equilibrium was achieved when the pressure in the adsorption cell (C1) stabilised for 30 minutes.

The volumetric apparatus of Ahmed et al. (2012)

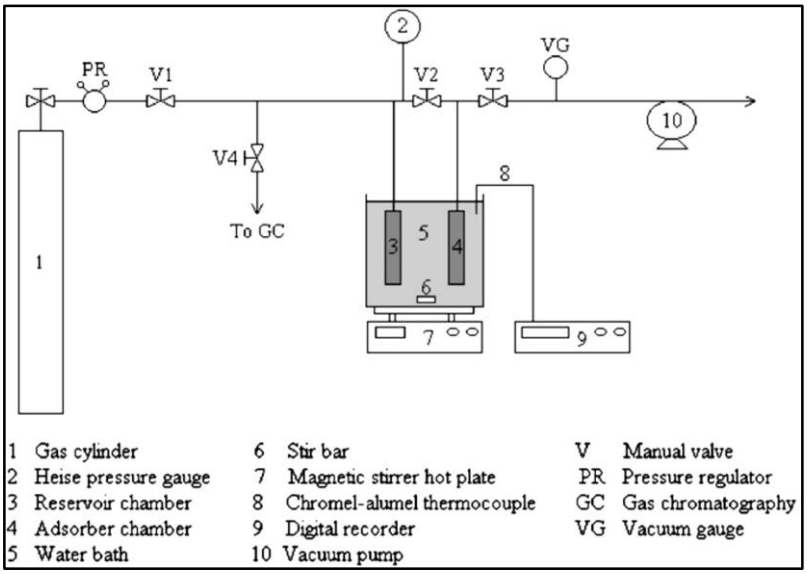

Figure E - 9: The volumetric apparatus of Ahmed et al. (2012).

The apparatus of Ahmed et al. (2012) used a magnetic stirrer and hot plate to maintain isothermal conditions in the bath. Typically a heating coil or an oven is used.

The gravimetric apparatus of Keller et al. (1999)

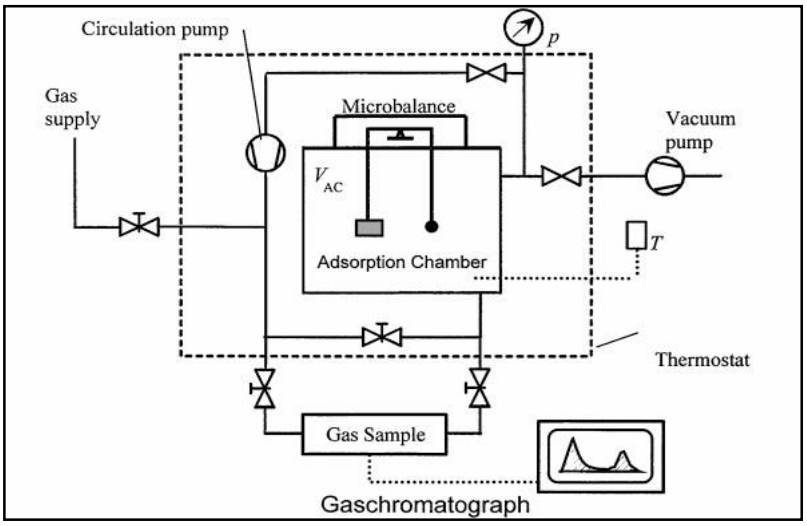

Figure E - 10: The gravimetric apparatus of Keller et al. (1999).

The apparatus consists of a microbalance holding a sample of adsorbent and a weight inside an adsorption chamber. For pure component isotherms, gas is expanded into the adsorption chamber where it is partly adsorbed. Upon the establishment of equilibrium, pressure and the change in mass of the adsorbent are recorded. The amount of gas adsorbed is thus calculated.

For multi-component adsorption, a known mass of gas is expanded into the equilibrium chamber. The mass of each component is required to completely specify the system mass balance. In addition to measuring the pressure and change in mass of adsorbent at equilibrium, a sample of the adsorptive is analysed using a GC. The molar concentrations at equilibrium are thus obtained, and the amount of each species adsorbed may be calculated.

The gravimetric apparatus of Dreisbach et al. (2002)

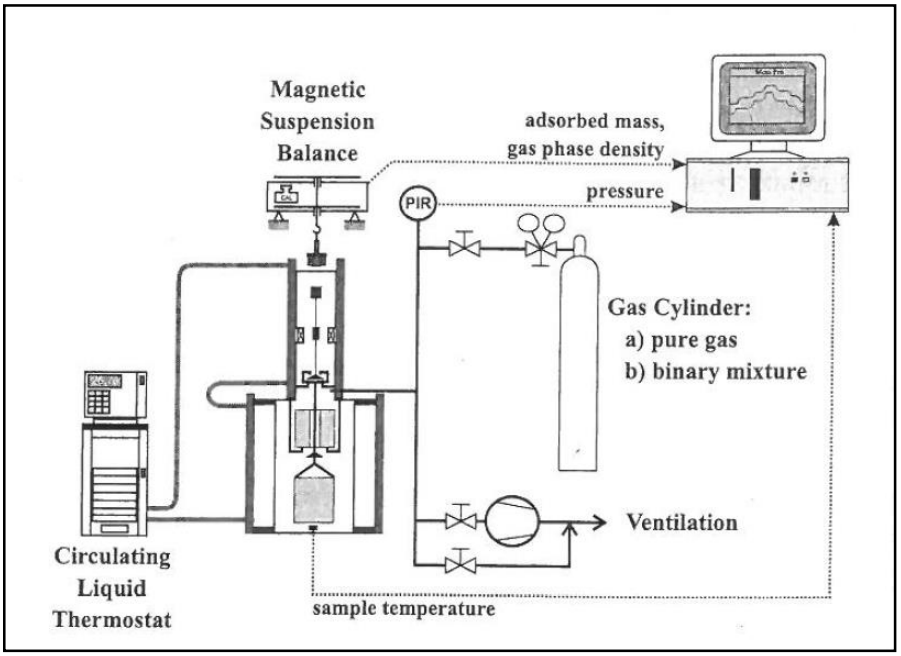

Figure E - 11: The gravimetric apparatus of Dreisbach et al. (2002).

Dreisbach et al. (2002) developed a gravimetric technique that does not require a GC for gas analysis. The technique improved upon the existing apparatus and techniques used for gravimetric analysis. The new apparatus overcomes the limitations of working at low pressures and small temperature ranges as was the case with older instruments for gravimetric measurement. This is made possible by the use of a *Magnetic Suspension Balance (MSB).* The MSB overcomes the limitations mentioned by separating the balance from the sample.

As opposed to using a GC for composition analysis, Dreisbach et al. (2002) used the relationship between gas density and gas composition. Using the MSB the densities of gas mixtures of known compositions were determined and a relationship determined.

Appendix F: Sample Calculations

The working equations used to generate the isotherms presented in Chapter 7 are provided in detail in Chapter 4. Calculations for the amount adsorbed, *q*, using the volumetric technique are presented. The IGA programme undertakes outputs adsorption data in the desired units mmol/g. no further data processing was required.

Zone 1 and Zone 2 have volumes of approximately 987 cm^3 and 18 cm^3 respectively. The experimental procedure followed is described in Chapter 5. The volume of the equilibrium space (zone 3) was determined to be 290 cm^3 with an adsorbent sample of 94.90 g using helium expansion. The equilibrium volume calculated accounted for the specific volume of the adsorbent.

Pure Component Measurements

A sample calculation for the adsorption of ethane at 0.194 bar and 298 K is shown. See Table 6-5 and Figure 6-19.

The storage cell (used for the pure component measurements) was maintained at 303 K using a water bath. A temperature of 298 K could not be achieved in the summer without the use of an additional chiller unit. The detailed procedure provided in Chapter 5 is summarised and presented in this Appendix for convenience.

1. The equilibrium bath was set to 298 K; the bath for the storage cell was set at 303 K.
2. The storage cell was charged with ethane.
3. The temperature (T^i_1) and pressure (P^i_1) of the storage cell as well as the temperature (T^i_2, T^i_3) and pressure (P^i_2) of the equilibrium cell was recorded.
4. The equilibrium cell was charged with ethane to the desired pressure P_2.
5. Equilibrium was achieved in two hours – indicated by a constant pressure reading in the equilibrium cell.
6. The temperature (T^f_1) and pressure (P^f_1) of the storage cell as well as the temperature (T^f_2, T^f_3) and pressure (P^f_2) of the equilibrium cell was recorded.

Table F - 1: Experimental measurements for sample calculation.

Initial		**Final**	
Storage Cell		*Storage Cell*	
T^i_1 (K)	303.42	T^f_1 (K)	303.42
P^i_1 (bar)	5.97	P^f_1 (bar)	3.54
Equilibrium Cell		*Equilibrium Cell*	
T^i_2 (K)	298.15	T^f_2 (K)	298.15
T^i_3 (K)	298.10	T^f_3 (K)	298.10
P^i_2 (bar)	0	P^f_2 (bar)	0.194

Initial

Storage Cell

The compressibility of ethane at 303.42 K and 5.97 bar was calculated using the PREoS as follows:

$$a(T_c) = 0.457235\frac{(RT_c)^2}{P_c} = 0.457235\frac{(0.08315 \times 305.32)^2}{48.72} = 6.048 \quad (4\text{-}20)$$

$$\kappa = 0.37464 + 1.54226\omega - 0.26992\omega^2 = 0.5262 \quad (4\text{-}22)$$

$$\alpha(T) = \left[1 + \kappa\left(1 - \sqrt{\frac{T}{T_c}}\right)\right]^2 = \left[1 + 0.5262\left(1 - \sqrt{\frac{303.42K}{305.32K}}\right)\right]^2 = 1.0032 \quad (4\text{-}21)$$

$$a(T) = a(T_c)\alpha(T) = 6.0480 \times 1.0032 = 6.068 \quad (4\text{-}19)$$

$$b = 0.077796\frac{RT_c}{P_c} = 0.0405 \quad (4\text{-}23)$$

$$A = \frac{aP}{R^2T^2} = \frac{6.0676 \times 5.97}{0.08315^{2\times}303.42^2} = 0.0569 \quad (4\text{-}25)$$

$$B = \frac{bP}{RT} = \frac{0.0405 \times 5.97}{0.08315 \times 303.42} = 0.0096 \quad (4\text{-}26)$$

$$Z^3 - (1 - B)Z^2 + (A - 3B - 2B^2)\mathrm{Z} - (AB - B^2 - B^3) = 0.962 \quad (4\text{-}24)$$

Using the PREoS the number of moles present in the storage cell was calculated:

$$n^i = \frac{P_1^i V_1}{ZRT_1^i} = \frac{5.97 \times 0.987}{0.962 \times 0.08315 \times 303.42} = 0.243\ mol \quad (A\text{-}1)$$

Equilibrium Cell

The equilibrium cell was evacuated prior to commencing with the run. The above calculation was hence not required.

Final

Storage Cell

Upon charging the equilibrium cell, the same calculations shown above were undertaken for ethane in the storage cell. The number of moles present was:

$$n^f = 0.144\, mol$$

The number of moles charged to the equilibrium cell was calculated by difference:

$$n^{charged} = n^i - n^f = 0.099\, mol$$

The total amount of gas in equilibrium was thus:

$$m^t = 0.099 mol \times 30.07 \frac{g}{mol} = 2.966 g$$

Upon achieving equilibrium, the amount of gas present in the adsorptive phase was calculated. The compressibility was calculated to be 0.999 using the PREoS. The density of the adsorptive phase was calculated using Eq. (4.16). The temperature of equilibrium gas was determined by taking the average of T_2 and T_3

$$\rho^g = \frac{PM^g}{ZRT} = \frac{0.194 \times 30.07}{0.999 \times 0.08315 \times 298.13} = 0.236 \frac{g}{L} \qquad (4\text{-}16)$$

The volume of adsorptive gas was calculated using helium displacement, viz:

$$V^t - V_{He}^{ad} = 0.290 L$$

The mass of gas adsorbed is given by Eq. (4.31)

$$m_i^a = m_i^t - \rho_i^g \left[V^t - V_{He}^{ad} - \sum_k^N \frac{m_k^a}{\rho_{k_0}^L} \right] \qquad (4\text{-}31)$$

Rewritten for a pure component system:

$$m^a = \frac{m^t - \rho^g \left(V^t - V_{He}^{ad} \right)}{1 - \frac{\rho^g}{\rho_0^L}} \qquad (A\text{-}2)$$

The liquid density of ethane at its normal boiling point – 184.57 K was used as ρ^{L_0} (Younglove and Ely, 1987).

$$m^a = \frac{2.966 - 0.236(0.290)}{1 - \frac{0.236}{544.9}} = 2.90 g_{ethane} = 0.096 mol_{ethane}$$

$$q = \frac{m^a}{MM_{ethane} \times mass_{13X}} = 1.02 \frac{mmol_{ethane}}{g_{13X}}$$

The data presented in Chapter 6 is presented in units of mol/$g_{13X.}$ The same calculation procedure was followed for ethylene. The liquid density of ethylene at its normal boiling point (169.45 K), 566 kg/m^3 was used as $\rho^L{}_0$ (Airgas, 2011).

Binary Isotherms

The calculation procedure followed to determine the binary isotherms were similar to the pure component isotherms with the following differences:

- Van der Waals mixing rules were used in conjunction with the PREoS to determine compressibility, Z_m of the ethane/ethylene mixture.
- The density of the binary mixture was calculated using Z_m.
  Mole fractions of the ethane and ethylene were determined using gas chromatography. The compositions used with mole fractions enabled the calculation of a separation factor.

Appendix G: Uncertainty in Measurements

The result of a measurement is only an approximation of the value of the quantity measured, referred to as the measurand. The result is only complete when the measurand is accompanied with its uncertainty. The uncertainty is quantified as an interval within which the true value of measurement has a high probability of residing. Uncertainty estimates can only apply to sound experimental data and in no way accounts for poor experimental technique.

In this study, the methods outlined by NIST will be used in uncertainty determination (Taylor and Kuyatt, 1994). The combined standard uncertainty (u_c) and the combined expanded uncertainty (U_c) are the most comprehensive expressions for uncertainty. The combined standard uncertainty is expressed as (Dong et al., 2005):

$$u_c(\theta) = \pm \sqrt{\sum_i u_i(\theta)^2} \qquad \textit{(G - 1)}$$

where u_i could be any source of uncertainty. The source could be the result of using a calibration equation, temperature gradients, standard deviations etc. The advantage of adding the uncertainties in quadrature is that it puts more weight on the larger uncertainty (Ellison et al., 1997). It is thus important to obtain good values for the larger uncertainties. The components that contribute the combined standard uncertainty are grouped into two categories: type A uncertainty and type B uncertainty.

Type A uncertainties are evaluated using statistical methods. Examples include determining uncertainty from the standard deviation of the mean of a series of independent observations or from undertaking an analysis of variance. Type A uncertainties may be determined from:

$$u_i(\theta) = \frac{\delta}{\sqrt{N_{repated\ points}}} \qquad \textit{(G - 2)}$$

Type B uncertainties are evaluated using scientific judgement based on the available information. One method of evaluating type B uncertainties is assuming a measured quantity; b has a 100% probability – for all practical purposes - of lying between the limits b_+ and b_-. In the absence of contradictory information, it is assumed that b has an equal probability of lying anywhere within the specified range. For a rectangular distribution, the uncertainty is given by:

$$u_i(\theta) = \frac{b}{\sqrt{3}} \qquad \textit{(G - 3)}$$

The rectangular distribution is a reasonable default model in the absence of additional data.

Temperature and Pressure

The combined uncertainty in temperature is given by:

$$u_c(T) = \pm\sqrt{u_{rep}(T)^2 + u_{calib}(T)^2 + u_{grad}(T)^2} \qquad (G - 4)$$

where:

$$u_{calib}(T) = \pm\sqrt{u_{poly}(T)^2 + u_{st}(T)^2} \qquad (G - 5)$$

where $u_{rep}(T)$ is the standard uncertainty due to measurement repeatability of temperature (Type A), $u_{poly}(T)$ is the uncertainty that arises from using a calibration polynomial (Type B), $u_{st}(T)$ is the uncertainty of the standard used for calibration (Type B) and $u_{grad}(T)$ is the uncertainty that results from the temperature gradient present in the equilibrium cell, taken as the difference in temperature measurement at the top and bottom of the equilibrium cell (Type B).

Similarly the uncertainty in pressure is given by:

$$u_c(P) = \pm\sqrt{u_{rep}(P)^2 + u_{calib}(P)^2 + u_{baro}(P)^2} \qquad (G - 6)$$

where:

$$u_{calib}(P) = \pm\sqrt{u_{poly}(P)^2 + u_{st}(P)^2} \qquad (G - 7)$$

where $u_{rep}(P)$ is the standard uncertainty due to measurement repeatability of temperature (Type A), $u_{poly}(P)$ is the uncertainty that arises from using a calibration polynomial (Type B), $u_{st}(P)$ is the uncertainty of the standard used for calibration (Type B) and $u_{baro}(P)$ is the uncertainty that results from the barometer(Type B).

Composition

Determining the uncertainty in the molar composition is more complicated than both temperature and pressure as the composition is derived as a function of a variety of measured variables.

There are several sources of uncertainty inherent with the phase composition determination method of Raal and Mühlbauer (1998):

- The correlation/polynomial relating FID areas to composition.
- The uncertainty in the measured mass of gas introduced by the precision of the balance.
- The repeatability of samples withdrawn at equilibrium.

In addition, the experimental technique used in this study requires the calculation of the composition of the adsorbed phase as this is not directly measureable. Uncertainties in temperature, pressure and volume at equilibrium thus contribute to uncertainty of the adsorbed phase

Gas phase:

As a starting point, the uncertainty of the gas phase composition is discussed. The uncertainty is split into two categories: the standard uncertainty due to calibration $u_{calib}(y_i)$ and the uncertainty due to sample repeatability at equilibrium $u_{rep}(y_i)$.

$$u_c(y_i) = \pm\sqrt{u_{rep}(y_i)^2 + u_{calib}(y_i)^2} \qquad (G - 8)$$

where, for the standard solution method (Raal and Mühlbauer, 1998):

$$u_{calib}(y_i) = \pm\sqrt{u_{poly}(y_i)^2 + u_{bal}(y_i)^2} \qquad (G - 9)$$

where $u_{poly}(y_i)$ and $u_{bal}(y_i)$ are standard uncertainties due to the composition calibration polynomial and the precision of the balance (0.07g) respectively. The masses measured for component *i* and *j* (m_i and m_j) are related to mole fractions y_i and y_j by their molar masses, MM_i *and* MM_j. Applying the root-sum-of-squares (RSS) method:

$$u_{bal}(y_i) = \pm\sqrt{\left[\left(\frac{\partial y_i}{\partial m_i}\right)u(m_i)\right]^2 + \left[\left(\frac{\partial y_j}{\partial m_j}\right)u(m_j)\right]^2} \qquad (G - 10)$$

where $u(m_i)$ is the standard uncertainty in mass for component *i* induced by the mass balance. Knowing that:

$$y_i = \frac{n_i}{n_i + n_j} \qquad (G - 11)$$

$$n_i = \frac{m_i}{MM_i} \qquad (G - 12)$$

Eqn. (G - 10) is simplified to:

$$u_{bal}(y_i) = \pm x_i x_j\sqrt{\left(\frac{u(m_i)}{m_i}\right)^2 + \left(\frac{u(m_j)}{m_j}\right)^2} \qquad (G - 13)$$

Vapour Pressure

Often the value of a result, θ, depends on other measured quantities (α_i).

$$\theta = f(\alpha_1, \alpha_2, \dots, \alpha_n) \qquad \textit{(G - 14)}$$

In this case, $u_c(\theta)$ is evaluated using the *Law of Propagation of Uncertainty*. Using the root-sum-squares (RSS) method, the uncertainty is expressed as (Taylor and Kuwatt, 1994):

$$u_c(\theta) = \pm\sqrt{\left[\left(\frac{\partial\theta}{\partial\alpha_i}\right)_{\alpha_{i\neq1}} u(\alpha_1)\right]^2 + \left[\left(\frac{\partial\theta}{\partial\alpha_i}\right)_{\alpha_{i\neq2}} u(\alpha_2)\right]^2 + \cdots + \left[\left(\frac{\partial\theta}{\partial\alpha_i}\right)_{\alpha_{i\neq n}} u(\alpha_n)\right]^2} \qquad \textit{(G - 15)}$$

The method of Shi et al. (2007) is used to determine the uncertainty in the vapour pressure measurement. The uncertainty in pressure as a result of the uncertainty in temperature is calculated using the RSS method. A function that relates pressure to temperature is required. A number of models are available in the literature that describes vapour pressure as a function of temperature (Polling et al., 2001). The *Extended Antoine Equation* is used here. Eq. (5 - 8) is re-written as:

$$P_{vap} = 10^{f(T)} \qquad \textit{(G - 16)}$$

where

$$f(T) = A - \frac{B}{T + C - 273.15} + 0.43429x^n + Ex^8 + Fx^{12} \qquad \textit{(G - 17)}$$

where

$$x = \frac{T - t_0 - 273.15}{T_c} \qquad \textit{(G - 18)}$$

Applying the RSS method and solving for the partial differential, the following is obtained:

$$\frac{\partial f}{\partial T} = \frac{df}{dT} = \frac{1}{T_c}\left[\frac{BT_c}{(T + C)^2} + 0.43429nx^{n-1} + 8Ex^7 + 12Fx^{11}\right] \qquad \textit{(G - 19)}$$

Using Eqs. (G - 15) and (G - 19),

$$u_f(T) = \pm\sqrt{\left[\frac{1}{T_c}\left(\frac{BT_c}{(T + C)^2} + 0.43429nx^{n-1} + 8Ex^7 + 12Fx^{11}\right) \times u_c(T)\right]^2} \qquad \textit{(G - 20)}$$

Applying Eq. (G - 15) once more:

$$u_{P_{sat}}(P) = \pm\sqrt{\left[10^{f(T)}u_f(T)\right]^2 + [u_c(P)]^2} \qquad \textit{(G - 21)}$$

Adsorption

The mass of pure gas adsorbed is given by:

$$m^a = \frac{m^t - \rho^g\left(V^t - V_{He}^{ad}\right)}{1 - \frac{\rho^g}{\rho_0^L}} \qquad \textit{(G - 22)}$$

where:

$$m^t = n_{charged} \times MM = \left(\frac{P_1^i V_1}{Z_1^i R T_1^i} - \frac{P_1^f V_1}{Z_1^f R T_1^f}\right) \times MM \qquad \textit{(G - 23)}$$

The methods used to determine uncertainties in temperature and pressure have been discussed. What remains is to determine the uncertainty in the amount adsorbed, *q*, using the *Law of Propagation of Uncertainty*. As a prerequisite however, the uncertainty in total amount of gas charged, m^t as well as the uncertainty in the amount of gas present in the equilibrium cell, $u_{n_{eq}}$denoted by the term $\rho^g\left(V^t - V_{He}^{ad}\right)$ must first be determined.

Following the methods of Taylor and Kuyatt (1994), the following relations are used to determine the aforementioned uncertainties.

The amount charged to the equilibrium cell is determined from the difference in the number of moles present in the storage/mixing cell before and after the charging step, Eq.***(G - 23)***. The uncertainty is thus:

$$u_{n_{charged}} = \sqrt{\left(u_{n_i}\right)^2 + \left(u_{n_f}\right)^2} \qquad \textit{(G - 24)}$$

where

$$u_{n_i} = \sqrt{\left(\frac{u_{T_i}}{T_i}\right)^2 + \left(\frac{u_{P_i}}{P_i}\right)^2 + \left(\frac{u_V}{V}\right)^2} \qquad \textit{(G - 25)}$$

Similarly, u_{n_f} and $u_{n_{eq}}$ are determined. The uncertainty in the amount adsorbed, $u_{adsorbed}$ *is given by:*

$$u_{n_{adsorbed}} = \sqrt{\left(u_{n_{charged}}\right)^2 + \left(u_{n_{eq}}\right)^2} \qquad \textit{(G - 26)}$$

The uncertainty in moles adsorbed per unit mass 13X is given by:

$$u_q = \sqrt{\left(\frac{u_{n_{adsorbed}}}{n_{adsorbed}}\right)^2 + \left(\frac{u_{m_{adsorbent}}}{m_{adsorbent}}\right)^2} \qquad (G - 27)$$

The uncertainties are calculated on a molar basis (in contrast to the mass basis adopted in Chapter 4) as the results of this study are reported on a mole basis.

Worked Examples

To illustrate the approach taken in this study towards quantifying experimental uncertainty, a detailed calculation procedure for the uncertainty in vapour pressure data are shown. Uncertainty in the measurement of the vapour pressure of propylene at 303 K is shown.

Vapour Pressure

Temperature uncertainty

From Eq. (G - 4), the uncertainty in temperature has 3 contributions. In this study, the standard deviation was used as an indication of the repeatability. Upon achieving equilibrium, temperature and pressure readings were recorded for two minutes in one second intervals. The readings for temperature (T_2, T_3) and pressure (P_2) are provided below.

P_2	T_2	T_3	P_2	T_2	T_3	P_2	T_2	T_3	P_2	T_2	T_3
bar	K	K	bar	K	K	bar	K	K	bar	K	K
13.106	303.27	303.27	13.106	303.26	303.27	13.106	303.26	303.28	13.105	303.27	303.27
13.106	303.27	303.27	13.106	303.26	303.27	13.106	303.27	303.28	13.105	303.27	303.27
13.106	303.27	303.27	13.106	303.26	303.27	13.106	303.27	303.28	13.105	303.27	303.27
13.106	303.27	303.27	13.106	303.26	303.27	13.106	303.27	303.28	13.106	303.27	303.27
13.106	303.27	303.27	13.106	303.26	303.27	13.106	303.27	303.28	13.105	303.27	303.27
13.105	303.27	303.27	13.106	303.26	303.27	13.106	303.26	303.28	13.106	303.27	303.27
13.105	303.27	303.27	13.106	303.26	303.27	13.106	303.26	303.28	13.105	303.27	303.27
13.105	303.27	303.27	13.106	303.26	303.27	13.106	303.27	303.28	13.105	303.26	303.27
13.106	303.27	303.27	13.106	303.26	303.27	13.106	303.27	303.28	13.106	303.26	303.27
13.106	303.27	303.27	13.106	303.26	303.27	13.106	303.27	303.28	13.106	303.26	303.27
13.106	303.27	303.27	13.106	303.26	303.27	13.106	303.27	303.28	13.106	303.26	303.27
13.105	303.27	303.27	13.106	303.26	303.27	13.106	303.27	303.28	13.106	303.26	303.27
13.105	303.27	303.27	13.106	303.26	303.27	13.106	303.27	303.28	13.106	303.26	303.27

13.106	303.27	303.27	13.106	303.26	303.27	13.106	303.27	303.28	13.106	303.26	303.27
13.105	303.27	303.27	13.106	303.26	303.27	13.106	303.27	303.28	13.105	303.26	303.27
13.105	303.27	303.27	13.106	303.26	303.27	13.106	303.27	303.28	13.105	303.26	303.27
13.106	303.27	303.27	13.106	303.26	303.28	13.105	303.27	303.28	13.105	303.26	303.27
13.106	303.27	303.27	13.105	303.26	303.28	13.106	303.27	303.28	13.105	303.26	303.27
13.106	303.27	303.27	13.106	303.26	303.28	13.106	303.27	303.28	13.105	303.26	303.27
13.106	303.27	303.27	13.106	303.26	303.28	13.106	303.27	303.28	13.105	303.26	303.27
13.106	303.26	303.27	13.106	303.26	303.28	13.106	303.27	303.28	13.105	303.26	303.27
13.106	303.26	303.27	13.105	303.26	303.28	13.106	303.27	303.28	13.105	303.26	303.27
13.106	303.26	303.27	13.106	303.26	303.28	13.105	303.27	303.27	13.105	303.26	303.27
13.106	303.26	303.27	13.106	303.27	303.28	13.106	303.27	303.27	13.105	303.26	303.27
13.106	303.26	303.27	13.106	303.27	303.28	13.106	303.27	303.27	13.105	303.26	303.27
13.106	303.26	303.27	13.106	303.27	303.28	13.105	303.27	303.27	13.105	303.26	303.27
13.106	303.26	303.27	13.106	303.27	303.28	13.105	303.27	303.27	13.104	303.26	303.27
13.106	303.26	303.27	13.106	303.26	303.28	13.105	303.27	303.27	13.105	303.26	303.27
13.106	303.26	303.27	13.106	303.26	303.28	13.105	303.27	303.27	13.105	303.26	303.26
13.106	303.26	303.27	13.106	303.26	303.28	13.105	303.27	303.27	13.105	303.26	303.26

Applying Eq. (G - 2)

$$u_{rep}(T_2) = \frac{5.02 \times 10^{-3}}{\sqrt{120}} = 4.58 \times 10^{-4}\ K \qquad \textit{(G - 28)}$$

$$u_{rep}(T_3) = \frac{4.88 \times 10^{-3}}{\sqrt{120}} = 4.46 \times 10^{-4}\ K \qquad \textit{(G - 29)}$$

The higher of these two values was used in subsequent calculations.

The calibration contribution to the uncertainty has two parts. The first contribution u_{poly} was determined from the residual plots presented in Chapter 6. A maximum value of 0.04 K was determined. The standard has an uncertainty of 0.03 K. Using a rectangular distribution:

$$u_{poly} = \frac{0.04}{\sqrt{3}} = 0.02\ K \qquad \textit{(G - 30)}$$

$$u_{st} = \frac{0.03}{\sqrt{3}} = 0.02\ K \qquad \textit{(G - 31)}$$

Applying Eq. (G - 5):

$$u_{calib}(T) = \pm\sqrt{0.02^2 + 0.02^2} = 0.03\ K \qquad (G - 32)$$

Applying Eq. (G - 3*)* and a gradient of 0.02 K – the maximum difference between T_2 and T_3:

$$u_{grad}(T) = \frac{0.02}{\sqrt{3}} = 0.01\ K \qquad (G - 33)$$

The combined standard uncertainty in temperature is given by:

$$u_c(T) = \pm\sqrt{4.58 \times 10^{-4^2} + 0.03^2 + 0.01^2} = 0.03\ K \qquad (G - 34)$$

Pressure uncertainty

Similarly to the temperature uncertainty, the pressure uncertainty has repeatability, calibration and barometer contributions. For the 0 – 15 bar range, the repeatability uncertainty is given by:

$$u_{rep} = \frac{4.88 \times 10^{-4}}{\sqrt{120}} = 4.45 \times 10^{-5} \qquad (G - 35)$$

Rectangular distributions have been assumed for the polynomial and standard uncertainty. From the calibration plots in chapter 6, the maximum residual is 0.003 bar. The standard has an uncertainty of 0.002 bar.

$$u_{poly} = \frac{0.003}{\sqrt{3}} = 0.002\ bar \qquad (G - 36)$$

$$u_{st} = \frac{0.002}{\sqrt{3}} = 0.001\ bar \qquad (G - 37)$$

$$u_{calib}(P) = \pm\sqrt{0.002^2 + 0.001^2} = 0.002\ bar \qquad (G - 38)$$

The barometer used in this study has an uncertainty of 0.0025 bar. Assuming a rectangular distribution:

$$u_{baro} = \frac{0.0025}{\sqrt{3}} = 0.001\ bar \qquad (G - 39)$$

Applying Eq. (G - 6) the combined standard uncertainty is given by:

$$u_c(P) = \pm\sqrt{4.45 \times 10^{-4^2} + 0.002^2 + 0.001^2} = 0.002\ bar \qquad (G - 40)$$

Vapour Pressure Uncertainty

The uncertainty in temperature and pressure has been calculated and will be used in these calculations. For propylene, Eq. (G - 17) becomes:

$$f(T) = 3.95606 - \frac{789.62}{T - 25.57} + 0.43429x^{2.67417} + 22.13x^{8} - 199.34x^{12} \qquad \textit{(G - 41)}$$

where:

$$x = \frac{T - 232.15}{365.57} \qquad \textit{(G - 42)}$$

Combining Eqs. (G - 41)and (G - 42), at 303 K: $x = 0.1945$ and $f(T) = 1.118$

From Eq. (G - 16)

$$P_{vap} = 10^{f(T)} = 10^{1.118} = 13.124\ bar \qquad \textit{(G - 43)}$$

Eq. (G - 19) becomes:

$$\frac{df}{dT} = \frac{1}{365.57}\left[\frac{288661.38}{(T + 247.58)^2} + 1.16137x^{1.67417} + 177.04x^{7} - 2392.08x^{11}\right] \qquad \textit{(G - 44)}$$

At 303 K, $df/dt = 0.01045$. Recalling that $u_c(T) = 0.03\ K$, Eq. (G - 20) becomes:

$$u_f(T) = \pm\sqrt{[0.01045 \times 0.03]^2} = 3.25 \times 10^{-4} \qquad \textit{(G - 45)}$$

Recalling that $u_c(P) = 0.002$ bar, Eq. (G - 21) becomes:

$$u_{P_{sat}}(P,T) = \pm\sqrt{\left[10^{f(T)}u_f(T)\right]^2 + [u_c(P)]^2}$$
$$u_{P_{sat}}(P,T) = \pm\sqrt{[13.124 \times 3.25 \times 10^{-4}]^2 + [0.002]^2} = 0.005\ bar \qquad \textit{(G - 46)}$$

Pure Component Adsorption

Volumetric Technique

From Eq. (G - 4), the uncertainty in temperature has 3 contributions. As mentioned previously, the standard deviation was used as an indication of the repeatability.

As an illustration, the uncertainty calculations for the adsorption of ethane at 0.194 bar and 298 K is shown.

The measurements for both the storage cell and mixing would prove too cluttered to be presented here. Instead, the standard deviation, δ calculated using 120 readings per variable is presented below.

Table G - 1: Experimental measurements for uncertainty sample calculations.

Initial			**Final**		
Storage Cell			*Storage Cell*		
Variable	*Measurand*	δ	*Variable*	*Measurand*	δ
T^i_1 (K)	303.42	9.70×10^{-13}	T^f_1 (K)	303.42	9.70×10^{-13}
P^i_1 (bar)	5.97	3.95×10^{-3}	P^f_1 (bar)	3.54	5.021×10^{-3}
Equilibrium Cell			*Equilibrium Cell*		
T^i_2 (K)	298.15	6.85×10^{-13}	T^f_2 (K)	298.15	6.85×10^{-13}
T^i_3 (K)	298.10	4.95×10^{-3}	T^f_3 (K)	298.10	2.78×10^{-3}
P^i_2 (bar)	0	1.78×10^{-15}	P^f_2 (bar)	0.194	2.5×10^{-4}

Initial

Storage Cell

Applying Eq. ***(G - 2)*** for temperature

$$u_{rep}\left(T_1^i\right) = \frac{9.70 \times 10^{-13}}{\sqrt{120}} = 8.86 \times 10^{-14}\ K \qquad (G - 47)$$

The calibration contribution to the uncertainty of temperature has two parts.

For temperature, the first contribution u_{poly} was determined from the residual plots presented in Chapter 6. A maximum value of 0.02K was determined for the first pt100. The standard has an uncertainty of 0.03 K. Using a rectangular distribution:

$$u_{poly} = \frac{0.02}{\sqrt{3}} = 0.01\ K \qquad (G - 48)$$

$$u_{st} = \frac{0.03}{\sqrt{3}} = 0.02\ K \qquad (G - 49)$$

Applying Eq. (G - 5)

$$u_{calib}\left(T_1^i\right) = \pm\sqrt{0.01^2 + 0.02^2} = 0.02\ K \qquad (G - 50)$$

The combined standard uncertainty in temperature is given by:

$$u_c\left(T_1^i\right) = \pm\sqrt{8.86 \times 10^{-14^2} + 0.02^2} = 0.02K \qquad (G - 51)$$

Applying Eq. (G - 2) for pressure

$$u_{rep}\left(P_1^i\right) = \frac{3.95 \times 10^{-3}}{\sqrt{120}} = 3.61 \times 10^{-4}\ K \qquad (G - 52)$$

Rectangular distributions have been assumed for the polynomial and standard uncertainty. From the calibration plots in chapter 6, the maximum residual for P_1 is 0.01 bar. The standard has an uncertainty of 0.02 bar.

$$u_{poly} = \frac{0.01}{\sqrt{3}} = 0.01\ bar \qquad (G - 53)$$

$$u_{st} = \frac{0.02}{\sqrt{3}} = 0.01\ bar \qquad (G - 54)$$

$$u_{calib}(P) = \pm\sqrt{0.01^2 + 0.01^2} = 0.01\ bar \qquad (G - 55)$$

The barometer used in this study has an uncertainty of 0.0025 bar. Assuming a rectangular distribution:

$$u_{baro} = \frac{0.0025}{\sqrt{3}} = 0.001\ bar \qquad (G - 56)$$

Applying Eq. (G - 6) the combined standard uncertainty is given by:

$$u_c(P) = \pm\sqrt{3.61 \times 10^{-4^2} + 0.01^2 + 0.001^2} = 0.01\ bar \qquad (G - 57)$$

The uncertainty in the compressibility factor, Z was not calculated as the uncertainty in temperature and pressure (inputs in the PREOS) have already been calculated on their own. To determine uncertainty in Z using the *Law of Propagation of Uncertainty* would be a redundant exercise with little effect on the overall uncertainty.

Applying the *Law of Propagation of Uncertainty*, the uncertainty in the number of moles initially present in the storage cell is given by:

$$u_{n_i} = \sqrt{\left(\frac{0.02}{303.42}\right)^2 + \left(\frac{0.01}{5.97}\right)^2 + \left(\frac{0.001}{0.987}\right)^2} = 0.002\ mol \qquad (G - 58)$$

Equilibrium Cell

The equilibrium cell was evacuated prior to commencing with the run. The above calculation was hence not required.

Final

Storage Cell

Upon charging the equilibrium cell, the same calculations shown above were undertaken for the uncertainty in the number of moles present in the storage cell after charging.

$$u_{n_f} = 0.002\ mol \qquad \textit{(G - 59)}$$

The uncertainty in the number of moles charged to the equilibrium cell was calculated as follows:

$$u_{n_{charged}} = \sqrt{(0.002)^2 + (0.002)^2} = 0.002\ mol \qquad \textit{(G - 60)}$$

Equilibrium Cell

Applying Eq. (G - 2)

$$u_{rep}\left(T_2^f\right) = \frac{6.85 \times 10^{-13}}{\sqrt{120}} = 6.25 \times 10^{-14}\ K \qquad \textit{(G - 61)}$$

$$u_{rep}\left(T_3^f\right) = \frac{2.78 \times 10^{-3}}{\sqrt{120}} = 2.53 \times 10^{-4}\ K \qquad \textit{(G - 62)}$$

The calibration contribution to the uncertainty of temperature has two parts.

For temperature, the first contribution u_{poly} was determined from the residual plots presented in Chapter 6. A maximum value of 0.02K was determined from the plots for T_2 and T_3. The standard has an uncertainty of 0.03 K. Using a rectangular distribution:

$$u_{poly} = \frac{0.04}{\sqrt{3}} = 0.02\ K \qquad \textit{(G - 63)}$$

$$u_{st} = \frac{0.03}{\sqrt{3}} = 0.02\ K \qquad \textit{(G - 64)}$$

Applying Eq. (G - 5)

$$u_{calib}\left(T_1^i\right) = \pm\sqrt{0.01^2 + 0.02^2} = 0.03\ K \qquad \textit{(G - 65)}$$

Applying Eq. (G - 3) and a gradient of 0.05 K – the maximum difference between T_2 and T_3:

$$u_{grad}(T) = \frac{0.05}{\sqrt{3}} = 0.03\ K \qquad \textit{(G - 66)}$$

The combined standard uncertainty, using the larger of the two repeatability uncertainties, in temperature is given by:

$$u_c(T) = \pm\sqrt{2.53 \times 10^{-4^2} + 0.03^2 + 0.02^2} = 0.03\ K \qquad \textit{(G - 67)}$$

Applying Eq. (G - 2)

$$u_{rep}\left(P_2^f\right) = \frac{2.5 \times 10^{-4}}{\sqrt{120}} = 2.29 \times 10^{-5}\ K \qquad \textit{(G - 68)}$$

Rectangular distributions have been assumed for the polynomial and standard uncertainty. From the calibration plots in chapter 6, the maximum residual for P_2 is 0.003 bar. The standard has an uncertainty of 0.002 bar.

$$u_{poly} = \frac{0.003}{\sqrt{3}} = 0.002\ bar \qquad \textit{(G - 69)}$$

$$u_{st} = \frac{0.002}{\sqrt{3}} = 0.001\ bar \qquad \textit{(G - 70)}$$

$$u_{calib}(P_2) = \pm\sqrt{0.002^2 + 0.001^2} = 0.002\ bar \qquad \textit{(G - 71)}$$

The barometer used in this study has an uncertainty of 0.0025 bar. Assuming a rectangular distribution:

$$u_{baro} = \frac{0.0025}{\sqrt{3}} = 0.001\ bar \qquad \textit{(G - 72)}$$

Applying Eq. (G - 6) the combined standard uncertainty is given by:

$$u_c(P_2) = \pm\sqrt{0.001^2 + 0.002^2 + 0.001^2} = 0.002\ bar \qquad \textit{(G - 73)}$$

Applying the *Law of Propagation of Uncertainty*, the uncertainty in the number of moles in equilibrium:

$$u_{n_{eq}} = \sqrt{\left(\frac{0.03}{298.13}\right)^2 + \left(\frac{0.002}{0.194}\right)^2 + \left(\frac{0.001}{0.290}\right)^2} = 0.006\ mol \qquad \textit{(G - 74)}$$

The uncertainty in the amount adsorbed, $u_{adsorbed}$ is given by*:*

$$u_{n_{adsorbed}} = \sqrt{(0.002)^2 + (0.006)^2} = 0.006 mol \qquad \textit{(G - 75)}$$

The uncertainty in moles adsorbed per unit mass 13X is given by:

$$u_q = \sqrt{\left(\frac{0.006}{0.096}\right)^2 + \left(\frac{0.07}{94.9}\right)^2} = 0.07 \frac{mmol_{ethane}}{g_{13X}} \qquad (G-76)$$

The mas balance used to determine the sample size of 13X charged to the equilibrium cell (94.9g) has an uncertainty of 0.07g.

Gravimetric Technique

The IGA directly measures the mass of gas adsorbed. The uncertainty in q is thus a function of the uncertainties in the mass measurement. The high precision balance has an uncertainty of $u_c = 1\times10^{-3}\ mg$.

The mass of ethane adsorbed on 78.25 mg of 13X at 298K and 0.198 bar is 3.02 mg or 1.00 mmol (presented as $q = 1.28\ mmol/g$ in Chapter 7). For ethane, an uncertainty in mass of 1×10^{-3} mg translates to:

$$u_{n_{adsorbed}} = \frac{1\times10^{-3} mg}{30.07 \frac{mg}{mmol}} = 3.33\times10^{-5} mmol \qquad (G-77)$$

The uncertainty in q is thus:

$$u_q = \sqrt{\left(\frac{3.33\times10^{-5} mmol}{1.00\ mmol}\right)^2 + \left(\frac{1\times10^{-3}\ mg}{78.25\ mg}\right)^2} = 3.57\times10^{-5} \frac{mmol_{ethane}}{g_{13X}} \qquad (G-78)$$

The gravimetric technique results in significantly smaller uncertainties, a hallmark of the IGA technology.